

Dissertation zur Erlangung des Doktorgrades
der Fakultät für Chemie und Pharmazie
der Ludwig-Maximilians-Universität München

Theoretical Investigations of Lewis Pairs

Von

Cong Zhang

Aus

Xuchang, Henan, China

2014

Erklärung

Diese Dissertation wurde im Sinne von § 7 der Promotionsordnung vom 28. November 2011 von Herrn Prof. Dr. H. Zipse betreut.

Eidesstattliche Versicherung

Diese Dissertation wurde eigenständig und ohne unerlaubte Hilfe erarbeitet.
München

CONG ZHANG

Dissertation eingereicht am 11.09.2014

1. Gutachter: Prof. Dr. Hendrik Zipse
2. Gutachter: Prof. Dr. Hans-Ullrich Siehl

Mündliche Prüfung am 07.10.2014

Acknowledgments

This work was carried out from 10. 2010 to 09. 2014 under the guidance of Prof. Dr. Hendrik Zipse at Department of Chemie und Biochemie, Ludwig-Maximilians-Universität München.

The work for this thesis was encouraged and supported by a number of people to whom I would like to express my gratitude at this point.

My main deep and sincere gratitude belongs to my supervisor and Doktorvater Prof. Dr. Hendrik Zipse for giving me this opportunity to work and study in his research group. I thank him for all the constructive discussion and critical comments on this subject, especially for the great degree of independence and freedom to explore. Also I am grateful for his kind help for my stay in Munich.

I would like to thank Prof. Dr. Hans Ullrich Siehl for acting as my “Zweitgutachter” and assessing this work. Thanks also to other referees Prof. Dr. Herbert Mayr, Prof. Dr. Konstantin Karaghiosoff, Prof. Dr. Sonja Herres-Pawlis and Prof. Dr. Manfred Heuschmann, for the interest shown in the present manuscript by accepting to be referees.

Special thank to Florian Achrainer for careful and patient reading and correcting this thesis. I am especially indebted to Dr. Johnny Hioe and Dr. Boris Maryasin, Pascal Patschinski, Dr. Christoph Lindner, Dr. Yinghao Liu, Sven Österling, Harish. Dr. Raman Tandon, Florian Barth, and all my friends in Germany. It was you people who made my stay in Germany a great time.

I acknowledge the China Scholarship Council and Ludwig-Maximilians-Universität München for financial support, and the international office of LMU for their kind help since my first arrival to Munich.

Words of special gratitude are addressed to my family for their unconditional love and encouragement during my life. The last and special thank goes to my fiance Dr. Huaiqiu Wang for his love, support and company in these years. Thank you so much.

Cong Zhang

09. 09. 2014

Parts of this Ph.D. Thesis have been published

1 C. Zhang, P. Patschinski, D. S. Stephenson, R. Panisch, J. Wender, M. Holthausen and H. Zipse, *Phys. Chem. Chem. Phys.* 2014, **16**, 16642-16650.

2 P. Patschinski, C. Zhang and H. Zipse , *J. Org. Chem.* ASAP. DOI: 10.1021/jo5016568.

3 S. Seel, T. Thaler, K. Takatsu, C. Zhang, H. Zipse, B. F. Straub, P. Mayer, P. Knochel, *J. Am. Chem. Soc.* 2011, **133**, 4774 – 4777.

Table of Contents

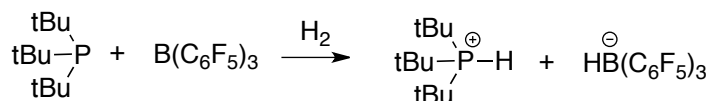
1 General Introduction	1
References	3
2 Binding Energies and Geometrical Characteristics of Lewis Pair Systems – A Methodological Survey	4
2.1 Introduction	4
2.2 Results and Discussions	4
2.2.1 Geometry Optimization of Lewis Pairs	4
2.2.2 Equilibrium Structures of PH ₃ -BF ₃	6
2.2.3 Investigation of Two Minima for PH ₃ -BF ₃	9
2.2.4 Extrapolation of Complexation Energy	11
2.2.5 NBO Analysis of Strongly and Weakly Bound Systems	13
2.2.6 EDA Analysis of Strongly and Weakly Bound Systems	14
2.2.7 Complexation Energy of Lewis Pair	15
2.2.8 The Impact of Structure Parameters on the Complexation Energy	16
2.3 Conclusions	23
References	23
3 The Reactivity of Lewis Pairs for Hydrogen Activation	25
3.1 Introduction	25
3.2 Results and Discussions	25
3.2.1 Strongly Bound Lewis Pair	26
3.2.2 Weakly Bound Lewis Pair	29
3.2.3 PMe ₃ -BF ₃	32
3.2.4 The Connection between Activation Energy and Structural Properties	36
3.3 Conclusions	41
References	41

4 Theoretical Studies on the Regioselective Functionalization of Pyrimidines	43
4.1 Introduction	43
4.2 Results and Discussions	43
4.2.1 The Relative Stability of Metalated Pyrimidines	43
4.2.2 Reaction System without the Lewis Acid $\text{BF}_3\cdot\text{OEt}_2$	46
4.2.3 Reaction System with the Lewis Acid $\text{BF}_3\cdot\text{OEt}_2$	51
4.3 Conclusions	57
References	57
5 The Calculation of ^{29}Si NMR Chemical Shifts of Tetracoordinated Silicon Compounds in the Gas Phase and in Solution	59
5.1 Introduction	59
5.2 Results and Discussions	59
5.2.1 The Effects of Geometry Optimization	59
5.2.2 Theoretical Methods for Chemical Shift Calculations	61
5.2.3 Solvent Effect	61
5.2.4 Spin-Orbit Corrections for Chlorosilanes	63
5.2.5 ^{29}Si Chemical Shifts for Larger Molecular Systems	64
5.2.6 Chemical Shifts for Ion Pairs	65
5.3 Conclusions	69
References	69
6 General Conclusions	72
7 Appendix	78
7.1 General Details	78
7.2 Calculated Data for Chapter 2	78
7.3 Calculated Data for Chapter 3	104
7.4 Calculated Data for Chapter 4	107
7.5 Calculated Data for Chapter 5	112

1 General Introduction

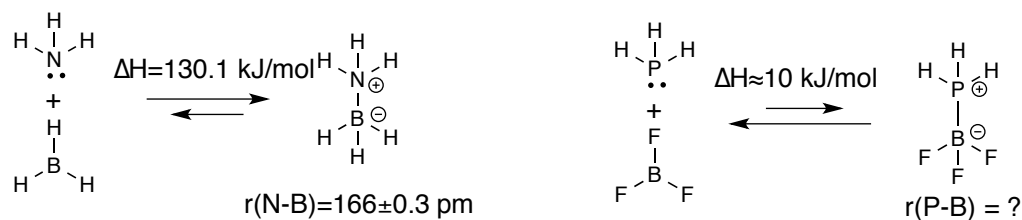
The definition of Lewis acids was raised by Gilbert N. Lewis for the first time in 1923.¹ According to the IUPAC,² Lewis acids are electron pair acceptors and therefore able to react with Lewis bases to form adducts by sharing the electron pair furnished by the Lewis base.³ The formation of a Lewis pair will thus lead to a transfer of electron density from the donor to the acceptor fragment of the newly formed adducts. Usually the Lewis adducts have completed electron octets through the formation of a dative bond, which leads to thermodynamic stability and as a consequence, it is expected that the reactivity will decrease because of the strong dative bond.

As catalysts, the roles of Lewis acids and Lewis bases are systematically different. Lewis acid activation leads to net transfer of electron density away from the substrate, whereas Lewis base activation leads to net transfer of electron density toward the substrate.⁴ Recently frustrated Lewis pair (FLP) systems attract lots of attention because of their ability to activate hydrogen (Scheme 1.1).^{5, 6}



Scheme 1.1. Heterolytic activation of H₂ by a frustrated Lewis pair.

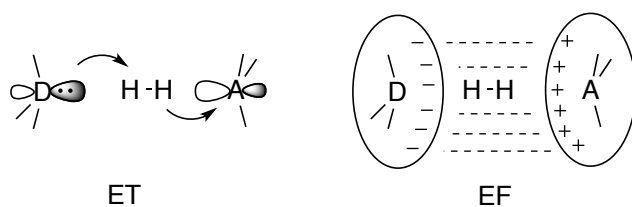
Frustrated Lewis pairs have bulky substituents on the acid and the base center to inhibit the connection between Lewis acid and Lewis base, and this unquenched reactivity makes hydrogen activation possible. The weak interaction between Lewis acid and Lewis base is the key issue in the FLP concept. As a typical weakly bonded Lewis pair, metal-free FLP shows great potential in biologically inspired and industrial processes. Strongly bonded Lewis pairs and weakly bonded Lewis pairs show totally different chemical behaviors. NH₃·BH₃ is known as a Lewis pair whose complexation energy is 130.1 kJ/mol⁷ and the strong dative bond reduces its reactivity (Scheme 1.2).



Scheme 1.2. Lewis acid–base adducts NH₃·BH₃ and PH₃·BF₃.

Hence, finding a reliable theoretical method to cover the full range of electronic and steric effects, but with high accuracy and low cost is a challenging question. Here we conducted a methodological survey of selected Lewis pair systems with particular emphasis on the comparison of strongly and weakly bonded systems.

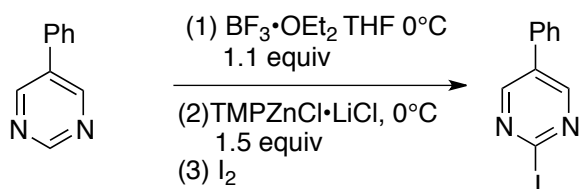
There have been two different mechanisms proposed for the activation of hydrogen by FLPs (Scheme 1.3).⁸



Scheme 1.3. Electron-transfer (ET) model and electric field (EF) model for hydrogen cleavage by frustrated Lewis pairs.

In the electron transfer (ET)⁹ model, charge is transferred first from the lone pair of the Lewis base to $\sigma^*(\text{H}_2)$ and then from $\sigma(\text{H}_2)$ to the empty orbital on the Lewis acid, leading to weakened H-H bond strength and, ultimately, to heterolytic cleavage of the H-H bond. The electric field (EF) model^{10, 11} suggests that the heterolytic bond cleavage occurs as a result of polarization by the strong EF present in the cavity of the reactive intermediates. Based on the different chemical behaviors of strongly and weakly bonded Lewis pairs, the mechanistic study will help to interrogate catalyst design.

Besides the main group Lewis pairs, metal-ligand compounds are the most used catalysts in chemical reactions. The use of Lewis basic ligands in substoichiometric amounts is a powerful method for tuning the reactivity or inducing stereoselectivity in metal-containing systems.¹² Knochel's group has reported that hindered metal amides display an exceptional kinetic basicity and tolerate a broad range of functional groups.¹³⁻¹⁶ In this reaction system, the regioselective metalation of pyrimidines with TMP was triggered by $\text{BF}_3\cdot\text{OEt}_2$ and the hindered metal amide base gives a highly regioselective metalation of various substituted pyrimidines and their derivatives. The overall reaction is shown in Scheme 1.4.



Scheme 1.4. Regioselective metalation of pyrimidines.

For this complicate reaction system, DFT calculations have been performed to clarify the roles of Lewis acid $\text{BF}_3\cdot\text{OEt}_2$ as well as the metal base in the reaction mechanism. In the mechanistic study, the reason for the high regioselective metalation is explored by examining energy profiles.

Theoretic methods are not only used for energy calculations, but also represent a powerful tool for chemical property prediction. The silylation of hydroxyl groups can be considered as one of the most important protecting-group strategies in the manipulation of polyfunctional molecules.^{17, 18} Usually the combination of theoretically predicted and experimentally measured ^{29}Si NMR chemical shifts is a

particularly helpful tool to establish the mechanism of a reaction, and the combination of theoretical calculations of chemical shifts with experimental data is very favorable for detecting the reaction.^{19, 20} Because of the appearance of a number of silicon-based species with rather similar chemical shifts in the solution-phase ²⁹Si NMR spectra,²¹ in order to obtain an accurate theoretical prediction of the respective chemical shifts, various theoretical methods including DFT and MP2 have been tested for NMR calculations.

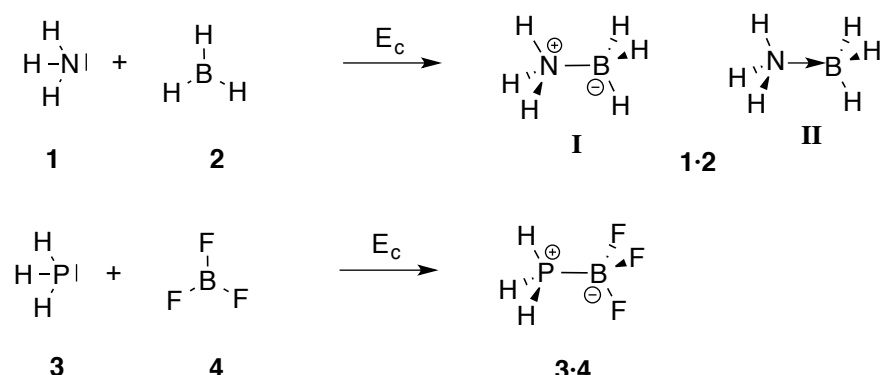
References

1. G. N. Lewis, *Valence and The Structure of Atoms and Molecules, Chemical Catalog*, New York, 1923.
2. Gold Book, <http://goldbook.iupac.org>.
3. H. C. Brown, H. Bartholomay and M. D. Taylor, *J. Am. Chem. Soc.*, 1944, **66**, 435-442.
4. S. E. Denmark and G. L. Beutner, *Angew. Chem. Int. Ed.*, 2008, **47**, 1560-1638.
5. D. W. Stephan and G. Erker, *Angew. Chem. Int. Ed.*, 2010, **49**, 46-76.
6. G. C. Welch, R. R. S. Juan, J. D. Masuda and D. W. Stephan, *Science*, 2006, **314**, 1124-1126.
7. A. Haaland, *Angew. Chem. Int. Ed.*, 1989, **28**, 992-1007.
8. T. A. Rokob, I. Bako, A. Stirling, A. Hamza and I. Papai, *J. Am. Chem. Soc.*, 2013, **135**, 4425-4437.
9. I. Bako, A. Stirling, S. Balint and I. Papai, *Dalton Trans.*, 2012, **41**, 9023-9025.
10. S. Grimme, H. Kruse, L. Goerigk and G. Erker, *Angew. Chem. Int. Ed.*, 2010, **49**, 1402-1405.
11. B. Schirmer and S. Grimme, *Chem. Commun.*, 2010, **46**, 7942-7944.
12. P. W. N. M. van Leeuwen, P. C. J. Kamer, J. N. H. Reek and P. Dierkes, *Chem. Rev.*, 2000, **100**, 2741-2770.
13. S. M. Manolikakes, M. Jaric, K. Karaghiosoff and P. Knochel, *Chem. Commun.*, 2013, **49**, 2124.
14. S. Duez, A. K. Steib, S. M. Manolikakes and P. Knochel, *Angew. Chem. Int. Ed.*, 2011, **50**, 7686-7690.
15. M. Jaric, B. A. Haag, A. Unsinn, K. Karaghiosoff and P. Knochel, *Angew. Chem. Int. Ed.*, 2010, **49**, 5451-5455.
16. K. Groll, S. M. Manolikakes, J. X. M. du, M. Jaric, A. Bredikhin, K. Karaghiosoff, T. Carell and P. Knochel, *Angew. Chem., Int. Ed.*, 2013, **52**, 6776-6780.
17. T. W. G. Peter G. M. Wuts, *Greene's Protective Groups in Organic Synthesis*, 4th Edition, John Wiley & Sons, Inc, 2006.
18. R. D. Crouch, *Synth. Commun.*, 2013, **43**, 2265-2279.
19. M. Karni, Y. Apeloig, N. Takagi and S. Nagase, *Organometallics*, 2005, **24**, 6319-6330.
20. A. I. Poblador-Bahamonde, R. Poteau, C. Raynaud and O. Eisenstein, *Dalton Trans.*, 2011, **40**, 11321-11326.
21. P. Patschinski, C. Zhang and H. Zipse, *J. Org. Chem.*, 2014, DOI: 10.1021/jo5016568.

2 Binding Energies and Geometrical Characteristics of Lewis Pair Systems - A Methodological Survey

2.1 Introduction

The properties of Lewis pairs formed through the reaction of a Lewis acid and a Lewis base have recently received considerable attention in the context of Frustrated Lewis Pair (FLP) chemistry.¹ According to the IUPAC definition, Lewis acids are electron pair acceptors and therefore able to react with Lewis bases to form Lewis adducts by sharing the electron pair furnished by the Lewis base.² The formation of Lewis pair will thus lead to a transfer of electron density from the donor to the acceptor fragment of the newly formed adduct. A stereotypical example for this type of system is ammonia borane (NH_3BH_3 , **1•2**), where ammonia (**1**) acts as electron pair donor and borane (**2**) as acceptor. In this strongly bound system, the donor and acceptor centers can interact freely, leading to a comparatively short N-B distance of $r(\text{N-B}) = 166 \pm 0.3 \text{ pm}$ ³ and a comparatively high complexation energy of $E_c(\mathbf{1} \bullet \mathbf{2}) = -130.1 \text{ kJ/mol}$.⁴ The bonding situation in this system may either be described by the zwitterionic Lewis structure **1•2I** or by an electron pair donor bond as in the structure **1•2II** (Scheme 2.1).



Scheme 2.1. Lewis complexes (**1•2**), and (**3•4**) formed from their respective Lewis base and Lewis acid components

The Lewis pair **1•2** is known as a strong Lewis pair because of the electrostatic interaction between Lewis acid and Lewis base. However, weakly bound Lewis pairs may also result from interactions between (electronically) weak Lewis acids and Lewis bases. An example for this latter case is PH_3BF_3 (**3•4**), whose complexation energy has not yet been determined reliably due to the rather weakly interacting components PH_3 (**3**) and BF_3 (**4**). From these two examples it is clear that Lewis pair chemistry can be rather complex and the question what type of theoretical methods are suited to cover the full range of electronic and steric effects, is more difficult to answer than expected. Therefore we provide herein a methodological survey of selected Lewis pair systems with particular emphasis on the comparison of strongly and weakly bound systems.

2.2 Results and Discussions

2.2.1 Geometry Optimization of Lewis Pairs

In order to identify a reliable approach for geometry optimization, HF, DFT and *ab initio* methods have been applied for the calculation and the results for some selected Lewis pairs are summarized in Table 2.1.

Table 2.1. Bond length between acid and base in selected Lewis pairs (in pm) (all the geometries here are staggered).

Methods	NH ₃ -BH ₃	PF ₃ -BH ₃	PMe ₃ -BH ₃	PH ₃ -BH ₃	MUE ^a	PH ₃ -BF ₃
EXP	166 ± 0.3 ^[3]	183.6 ^[5, 6]	190.1 ^[7]	193.7 ^[8]	–	192.1 ^[9]
HF/6-31+G(d)	168.6	193.3	196.6	202.1	6.8	346.9
B3LYP/6-31G(d)	166.9	187.5	193.3	196.0	2.6	317.2
B97D/6-31+G(d)	170.7	189.9	193.9	197.0	4.5	323.7
B98/6-31G(d)	166.1	188.1	193.9	196.6	2.8	314.4
MPW1K/6-31G(d)	164.4	185.1	191.3	193.6	1.1	303.8
MPW1K/6-31+G(d)	164.4	185.6	191.3	193.6	1.2	228.7/288.6
M05-2X/6-31G(d)	167.2	186.2	192.0	195.8	2.0	295.0
M05-2X /6-31+G(d)	167.3	187.1	192.1	195.6	2.2	290.5
M06-2X/6-31+G(d)	166.1	187.5	192.4	195.9	2.1	296.6
M06-2X/6-31+G(d,p)	166.0	187.3	192.4	195.9	2.1	296.9
ωB97XD/6-31G(d)	165.8	186.7	192.2	195.4	1.8	314.5
ωB97XD/6-31+G(d)	165.7	187.7	192.2	195.5	2.1	311.5
ωB97XD/def2-TZVP	164.9	184.9	190.3	192.7	0.9	317.2
ωB97XD/						
def2-TZVPP	164.8	184.8	190.2	192.7	0.9	317.0
ωB97XD/cc-pVTZ	164.8	185.8	191.1	193.7	1.1	315.9
MP2(FC)/						
aug-cc-pVDZ	166.7	188.8	193.3	195.9	2.8	226.1/303.4
MP2(FC)/cc-pVTZ	164.9	185.4	191.1	193.5	1.0	311.7
MP2(FULL)/						
aug-cc-pVDZ	166.3	188.1	192.8	195.8	2.4	223.6/300.1
SCS-MP2/cc-pVTZ	165.9	186.8	192.3	195.0	1.7	320.5
DF-SCS-LMP2/						
cc-pVTZ	166.3	187.9	193.1	195.8	2.4	334.7
CCSD(T)/cc-pVDZ	166.4	188.8	194.1	197.8	3.4	317.0
CCSD(T)/cc-pVTZ	165.5	186.4	191.9	194.9	1.6	313.9
CCSD(T)/cc-pVQZ	165.1	185.6	185.6	193.7	1.9	312.9

^aMean unsigned error(MUE)=(1/n)Σ|X_{cal}-X_{exp}| is calculated without PH₃-BF₃ molecule.

The accuracy of theoretical bond distances in Table 2.1 is measured by mean unsigned error (MUE). Lacking of correlation energy, the biggest MUE (6.8 pm) is given by the HF method. The B97D¹⁰ functional includes empirical dispersion correction, but the MUE of bond distances is bigger than for other DFT methods. The B3LYP and B98¹¹ hybrid functional with Pople basis sets give similar results. Recently M05-2X¹² and M06-2X¹³ are commonly used in quantum chemistry. The results of M05-2X and M06-2X level with

different basis sets are similar and the MUE is around 2.0 pm. MPW1K¹⁴ with 6-31G(d) and 6-31+G(d) give shorter bond distances and smaller MUEs than other DFT methods with the same basis sets. ω B97XD¹⁵ is a modified B97 functional including empirical dispersion corrections.¹⁰ Compared with experiment value, the best prediction is given by ω B97XD/def2-TZVPP with a mean unsigned deviation (MUE) of 0.9 pm. MP2 optimizations with double zeta basis sets yield longer bonds than MP2 in combination with triple zeta basis sets. MP2 is known for overestimating dispersion interactions. Therefore the spin-component scaling MP2 (SCS-MP2) theory is applied for geometry optimization.¹⁶ Bond distances at SCS-MP2/cc-pVTZ are rather close to the results at CCSD(T)/cc-pVTZ level. Compared with SCS-MP2, density fitting local MP2 (DF-SCS-LMP2) has much longer bond distances. In the case for CCSD(T), Dunning's cc-pVDZ basis set gives longer bond distances than cc-pVTZ or cc-pVQZ. For quadruple zeta basis set cc-pVQZ the MUE of the bond distance is 1.9 pm, which means that the bond distances predicted by coupled cluster methods are ordinarily 1.9 pm longer than experimental measurements.

To conclude, the geometries obtained with ω B97XD/def2-TZVP are most close to experimental measurements. The bond distances predicted by the most expensive method CCSD(T)/cc-pVQZ are longer than experimental results, and ω B97XD with small Pople basis sets 6-31G(d) provides almost identical results compared with CCSD(T)/cc-pVQZ.

2.2.2 Equilibrium structures of PH₃-BF₃

For PH₃-BF₃, most theories confirmes that there is only one minimum, which characterizes PH₃-BF₃ as a weak Lewis complex with r(P-B) longer than 310 pm. However at MPW1K and MP2 level, two minima can be identified at the same time. Minimum 1 has a bond distance at around 230 pm and minimum 2 at 300 pm. These results have already been shortly dealt within Dr. Maryasin's Ph.D. thesis.¹⁷ In order to probe into the detail of minimum 1 and minimum 2, more calculations have been carried out and discussed in the following paragraph.

According to experimental data the r(P-B) in PH₃-BF₃ has been estimated to be 192.1 pm, which is evaluated by measuring bond rotation constants at -70 °C in microwave spectra.⁹ Before this study, there were several theoretical data available for r(P-B). The first theoretical value is obtained at HF/3-21G level, and the bond distance is 218.5 pm.¹⁸ Later, Ahlrich used HF/TZP and MP2/TZP for PH₃-BF₃ and the bond distances are 349.5 pm and 322.0 pm, respectively.¹⁹ After that, MP2(FULL)/6-31G(d) is also used for bond distance calculation, which provides bond distance as 308.9 pm. However, the latest bond distance calculation is 307.5 pm at MP2(FC)/6-311++G(d,p) level.²⁰ All the theory data are longer than experimental value and there is only one minimum existed for PH₃-BF₃ according to these previous studies.

From Table 2.1, we can see that two minima only exist with MPW1K and MP2 theories, therefore various basis sets have been tested for these two methods and the results are summarized in Table 2.2. MPW1K is the acronym for modified Perdew-Wang 1 parameter model for kinetics and represents an example for hybrid functional.¹⁴ The difference between MP2(FC) and MP2(Full) is that correlation energies of core electrons are not calculated for MP2(FC), because the core orbitals are not responsible for the chemical valence and bonding and therefore not sensitive to the environment. SCS-MP2 is the spin-component-scaled MP2 method and can correct the overestimation of dispersion interaction.^{16, 21} Because of the high accuracy performance, CCSD(T) is usually considered as the benchmark method.

Table 2.2. Central bond distances r(P-B) (pm) and complexation enthalpy (kJ/mol) of $\text{PH}_3\text{-BF}_3$. For the calculation of ΔH_{298} , separated acid and base are taken as the references.

	Minimum 1		Minimum 2	
	r(P-B) (pm)	ΔH_{298} (kJ/mol)	r(P-B) (pm)	ΔH_{298} (kJ/mol)
MPW1K/6-31+G(d)	229.1	-8.11	288.6	-7.89
MPW1K/6-31+G(d,p)	228.8	-7.86	289.6	-7.61
MPW1K/6-311+G(d,p)	226.6	-10.59	-	-
MPW1K/6-311++G(2d,2p)	-	-	288.9	-7.97
MPW1K/cc-pVDZ	-	-	277.5	-9.16
MPW1K/cc-pVTZ	-	-	299.5	-6.74
MPW1K/cc-pVQZ	-	-	303.5	-5.41
MPW1K/aug-cc-pVDZ	223.8	-11.44	-	-
MPW1K/aug-cc-pVTZ	-	-	298.2	-6.40
MPW1K/aug-cc-pVQZ	-	-	302.9	-5.32
MP2(FC)/6-31+G(d)	220.3	-12.95	298.4	-16.59
MP2(FC)/6-31+G(d,p)	221.9	-10.51	301.8	-13.09
MP2(FC)/6-31+G(2d,2p)	-	-	308.9	-9.78
MP2(FC)/6-311++G(d,p)	-	-	307.5	-12.71
MP2(FC)/6-311++G(2d,2p)	-	-	308.1	-10.43
MP2(FC)/cc-pVDZ	-	-	316.9	-7.71
MP2(FC)/cc-pVTZ	-	-	309.0	-10.79
MP2(FC)/cc-pVQZ	-	-	308.7	-8.31
MP2(FC)/aug-cc-pVDZ	227.2	-8.81	304.1	-12.12
MP2(FC)/aug-cc-pVTZ	-	-	305.6	-10.53
MP2(Full)/6-31+G(d)	219.6	-14.70	296.3	-15.33
MP2(Full)/6-31+G(d,p)	220.8	-12.32	299.2	-14.16
MP2(Full)/6-311++G(d,p)	228.8	-9.13	306.4	-13.13
MP2(Full)/6-311++G(2d,2p)	-	-	306.4	-11.05
MP2(Full)/cc-pVDZ	-	-	315.5	-8.30
MP2(Full)/cc-pVTZ	-	-	305.9	-11.56
MP2(Full)/cc-pVQZ	-	-	308.3	-8.83
MP2(Full)/aug-cc-pVDZ	224.7	-11.54	300.1	-13.90
MP2(Full)/aug-cc-pVTZ	-	-	294.7	-17.16
MP2(Full)/aug-cc-pVQZ	-	-	302.7	-10.36
SCS-MP2(FC)/6-31+G(d)	223.2	-6.68	308.3	-13.71
SCS-MP2(FC)/6-31+G(d,p)	224.8	-4.92	310.6	-12.94
SCS-MP2(FC)/cc-pVTZ	-	-	320.5	-6.37
SCS-MP2(FC)/	-	-	313.6	-9.81

aug-cc-pVDZ				
SCS-MP2(FC)/def2-SVP	–	–	324.6	–5.58
SCS-MP2(FC)/def2-TZVP	–	–	318.3	–6.55
SCS-MP2(FC)/def2-QZVP	–	–	318.9	–6.84
SCS-MP2(FULL)/6-31+G(d)	221.9	–8.20	307.1	–14.85
SCS-MP2(FULL)/				
6-31+G(d,p)	223.1	–5.91	309.4	–13.52
SCS-MP2(FULL)/cc-pVTZ	–	–	313.7	–9.69
SCS-MP2(FULL)/				
aug-cc-pVDZ	–	–	309.9	–11.35
CCSD(T)/ cc-pVDZ	–	–	317.0	–7.21
CCSD(T)/ cc-pVTZ	–	–	313.9	–10.45
CCSD(T)/ cc-pVQZ	–	–	312.9	–10.54

Pople basis sets, correlation consistent as well as split valence basis sets have been used for geometry optimization and complexation energy calculations. From Table 2.2, there is no clear and straightforward rule for this two minima phenomenon. But for basis set 6-31+G(d) with MPW1K and MP2, we can always find the global minimum at the short distance range. From the selected basis sets in Table 2.2, MPW1K with aug-cc-pVDZ and 6-311+G(d,p) can only find minimum 1 located in a short bond distance range of 223 to 226 pm. Except for these two basis sets, other basis sets always find minimum 2, which is located at long range distance around 310 pm. Most of Pople-type basis sets find both minima at the same time and double zeta and triple zeta sets produce similar bond distances. Diffuse and polarization functions have no big influence on the minima location. For correlation consistent basis sets, like aug-cc-pVDZ, it can always identify minimum 1. But triple zeta and quadruple zeta sets are fixed to minimum 2. Meanwhile, Ahlrich's basis sets^{22, 23} locate only minimum 2 with an r(P-B) of about 320 pm. For these three different types of basis sets, triple zeta and quadruple zeta results are more consistent with each other.

At MPW1K level, r(P-B) of minimum 2 is apparently shorter than the bond distance at MP2 and CCSD(T) level. For the MP2 method, frozen core and full correlation make no difference for the minima location. The dispersion interaction is important for the weakly bound complex, SCS-MP2 is also considered here.¹⁶ SCS-MP2 with Pople basis sets detects both minima. But SCS-MP2 with Dunning's correlation consistent basis set and Ahlrich's basis sets, only provide minimum 2 which is near 320 pm. For CCSD(T), there is only minimum 2 with correlation consistent basis sets. At CCSD(T)/cc-pVQZ level, r(P-B) is 312.9 pm, which is taken as benchmark result.

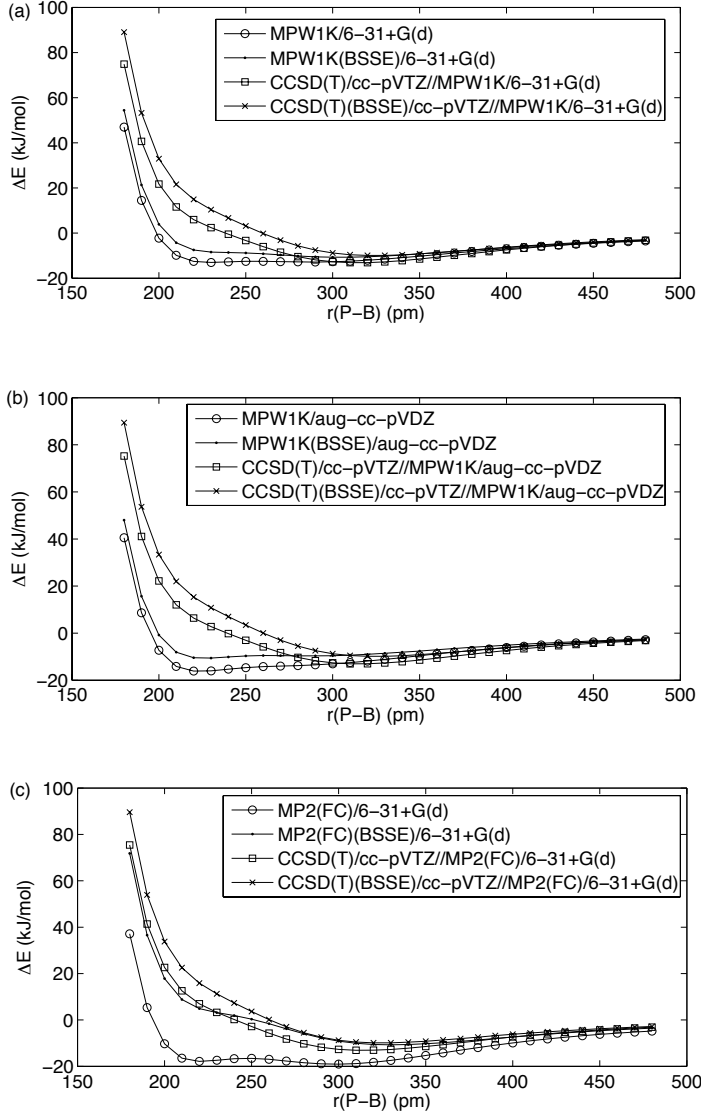
From Table 2.2, we find that the complexation energy for $\text{PH}_3\text{-BF}_3$ is around 10 kJ/mol. Compared with strong Lewis pairs, the complexation energy of $\text{PH}_3\text{-BF}_3$ is thus rather small. For MPW1K method, minimum 1 is always more stable than minimum 2, but the energy difference between the two minima is negligible with a value of less than 1 kJ/mol.

For MP2 methods, the global minimum shifts to minimum 2 and complexation energies increase. But still, energy differences between frozen core and full correlation are close, which is less than 3 kJ/mol. After spin-component scaled correction, the difference of two minima increases to around 7 kJ/mol with the largest value of 7.03 kJ/mol at SCS-MP2/6-31+G(d,p) level. The largest complexation energy is –17.16 kJ/mol at MP2(Full)/aug-cc-pVTZ level. At CCSD(T) level, complexation energies converges closely to –10.5 kJ/mol.

Generally the small basis set with diffuse function like 6-31+G(d) and aug-cc-pVDZ can locate both minimum 1. But for Ahlrich's basis set def2-SVP, only minimum 2 is located. Increasing the basis sets to triple zeta and quadruple zeta basis set, the only minimum is located as minimum 2.

2.2.3 Investigation of Two Minima for $\text{PH}_3\text{-BF}_3$

In order to observe the variation of two minima, relaxed scans have been carried out for $\text{PH}_3\text{-BF}_3$. Herein, E_{tot} of $\text{PH}_3\text{-BF}_3$ is relative to the sum of $E_{\text{tot}}(\text{PH}_3)$ and $E_{\text{tot}}(\text{BF}_3)$ in kJ/mol.



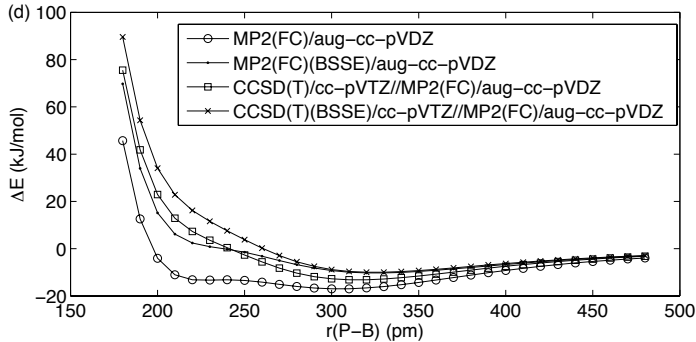


Figure 2.1. Relaxed scan of $r(\text{P-B})$ in $\text{PH}_3\text{-BF}_3$ at different theory levels.

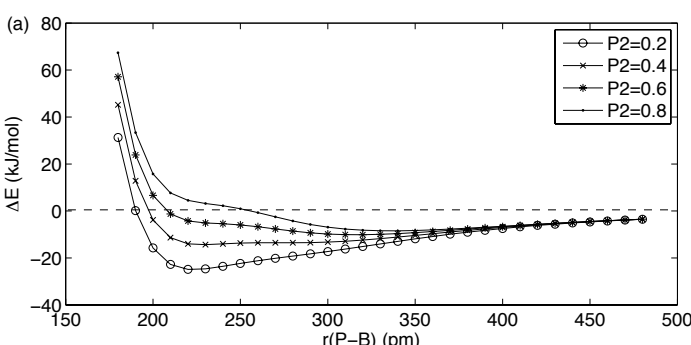
Basis set super position error (BSSE) is caused by the monomer of the complex borrowing basis set functions from neighboring component, and the BSSE can over stabilize the complex. Usually BSSE can be eliminated by the counterpoise method. The steps are summarized as follows:

- (1) Optimize and calculate the energy of complex and individual monomer to obtain the ordinary complexation energy of complex, E_{12} .
 - (2) Calculate each monomer on their own, using the same geometry as they are in the complex. This results in values E_1 and E_2 .
 - (3) Recalculate each monomer in the complex, but keep the basis set of other monomer to obtain additional functions. This results in energies E_1^* and E_2^*
- The corrected interaction energy is calculated using eqn. (1):

$$\Delta E(\text{BSSE}) = E_{12} + E_1 + E_2 - E_1^* - E_2^* \quad (1)$$

Figure 2.1 shows that the complexation energy potential is very flat at all levels considered here. After correction, the energy potential of MPW1K/6-31+G(d) gets even more flat and minimum 1 vanishes. But for MPW1K/aug-cc-pVDZ, both minima still exist. For MP2 methods, BSSE changes the energy potential seriously, coming across with minimum 1 as shoulder. These results indicate that the BSSE is not the reason for the two minima phenomenon.

The single point calculations for the geometries laying on the relaxed scan curve are calculated at CCSD(T)/cc-pVTZ level to get more accurate results. After single point correction at CCSD(T)/cc-pVTZ level, only minimum 2 occurs. BSSE effects only reduce the complexation energy at CCSD(T)/cc-pVTZ level and have no influence on the global minimum location.



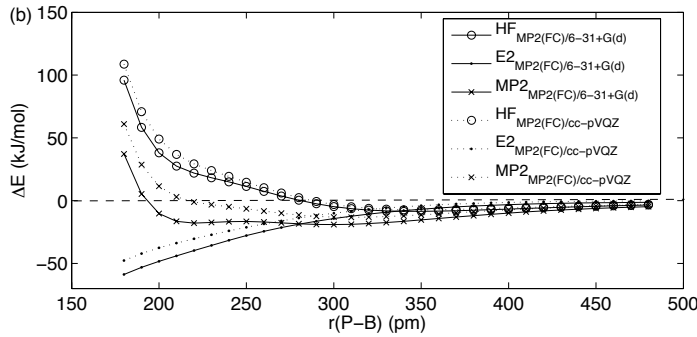


Figure 2.2. Relaxed scan of $r(\text{P-B})$ in $\text{PH}_3\text{-BF}_3$, $\Delta E = E_{\text{tot}}(\text{PH}_3\text{-BF}_3) - E_{\text{tot}}(\text{PH}_3) - E_{\text{tot}}(\text{BF}_3)$ (a) Variation of HF exchange energy in MPW1K/6-31+G(d) level with $P_1=1$, $P_2+P_4=1$, $P_3=0.527$, $P_5=P_6=1$. (b) Energy contributions for MP2(FC)/6-31+G(d) and MP2(FC)/cc-pVQZ.

For hybrid functional theory, the exchange-correlation function incorporates a portion of exact exchange from HF theory. The exchange- correlation energy is defined as follows:

$$P_2 E_X^{\text{HF}} + P_1 (P_4 E_X^{\text{Slater}} + P_3 \Delta E_X^{\text{non-local}}) + P_6 E_C^{\text{local}} + P_5 \Delta E_C^{\text{non-local}} \quad (2)$$

In MPW1K, the coefficients are $P_1=1.0$, $P_2=0.428$ $P_3=0.572$, $P_4=0.572$, $P_5=1.0$ $P_6=1.0$. Increasing coefficient P_2 will change the HF exchange contribution in hybrid DFT. Figure 2.2 (a) shows clearly that $r(\text{P-B})$ of the respective minimum varies from 230 pm to 350 pm if coefficient P_2 is changed from 0.2 to 0.8. It is noteworthy that only one minimum is found if $P_2=0.2$. On the other hand when P_4 has the value of 0.4, two minima are defined and the global minimum is located at a P-B distance more than 240 pm. According to the definition of MPW1K, increasing P_2 to 0.6 continuously, only one minimum exists with $r(\text{P-B})=310$ pm. The energy surface with $r(\text{P-B})$ more than 230 pm is rather flat. $P_2=0.8$ means, HF exchange energy has its major contribution, and minimum 2 apparently forms the global minimum. The coefficient P_4 reflects the exchange contribution from the Perdew-Wang functional at MPW1K/6-31+G(d) level. Therefore, P_2 not only influences the bond distance but also the complexation energy. The complexation energy is reduced to half when P_2 changes from 0.2 to 0.8.

For MP2, the energy can be decomposed as

$$E_{\text{MP2}} = E_{\text{HF}} + E_2 \quad (3)$$

Therefore MP2 energy has been analyzed separately in Figure 2.2 (b). E_{HF} is the Hartree-Fock energy and E_2 is the correlation energy at the same level. At MP2(FC)/6-31+G(d) level, the global minimum is found at a distance $r(\text{P-B})=298.4$ pm and the respective global minimum at $r(\text{P-B})=220.3$ pm. At MP2(FC)/cc-pVQZ level, only the long range minimum has been found with $r(\text{P-B})=308.7$ pm. Closer investigations of MP2 energy components shows that close to minimum 1, E_2 at MP2(FC)/6-31+G(d) level is much lower than at MP2(FC)/cc-pVQZ and E_{HF} at MP2(FC)/6-31+G(d) is close to E_{HF} at MP2(FC)/ cc-pVQZ level. The above discussion indicates that the mixture of HF exchange and correlation energy is the main factor that influences the bond distance between PH_3 and BF_3 .

2.2.4 Extrapolation of Complexation Energy

Table 2.2 shows that the complexation energy of $\text{PH}_3\text{-BF}_3$ can vary considerably. In order to get converged complexation energy and bond distance, the two points extrapolation method²⁴ is used to approach the complexation energy and bond distance limit by eqn. (4)

$$E(L) = E(L)_{\infty} + \frac{A}{(L + 0.5)^4} \quad (4)$$

L is the maximum angular momentum present in the basis set, A represents the coefficient. $E(L)$ represents the bond distance or energy with the angular momentum of L , $E(L)_{\infty}$ is the limit convergence of bond distance or energy. All results are shown in Figure 2.3.

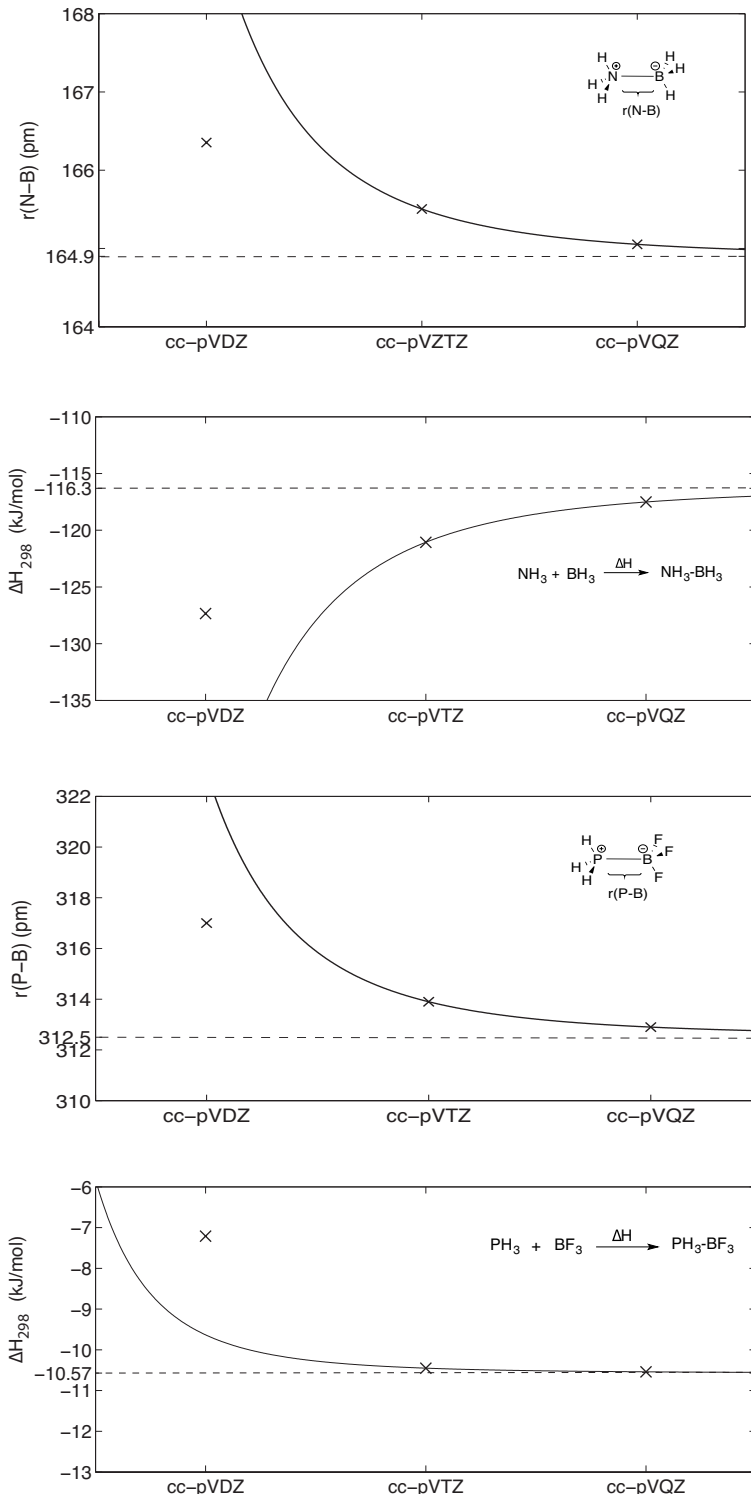


Figure 2.3. Extrapolation results of $\text{NH}_3\text{-BH}_3$ and $\text{PH}_3\text{-BF}_3$ at CCSD(T) level.

The extrapolation method predicts a bond distance of 164.9 ppm and a complexation energy of -116.3 kJ/mol for $\text{NH}_3\text{-BH}_3$. For the weakly bonded Lewis pair $\text{PH}_3\text{-BF}_3$ the extrapolated values are $r(\text{P-B})=312.6 \text{ pm}$ and $\Delta H_{298}=-10.57 \text{ kJ/mol}$.

2.2.5 NBO Analysis of Strongly and Weakly Bound Systems

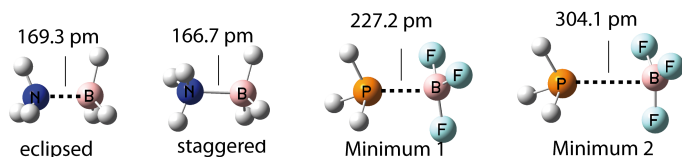


Figure 2.4. Geometry parameters of $\text{NH}_3\text{-BH}_3$ (**1•2**) and $\text{PH}_3\text{-BF}_3$ (**3•4**) at MP2(FC)/aug-cc-pVDZ level

For the Lewis pairs, there are usually two different conformations: staggered and eclipsed conformation and eclipsed conformation is normally a conformational energy maximum. For $\text{NH}_3\text{-BH}_3$, the staggered and eclipsed conformation at MP2(FC)/aug-cc-pVDZ level are shown in Figure 2.4. Because of hyperconjugation between hydrogen atoms, eclipsed conformation is not a minimum and $r(\text{N-B})$ is 2.6 pm longer than in its staggered conformation. The complexation energies of strong Lewis pairs and weak Lewis pairs are very different. In order to analyze the difference between strongly and weakly bound Lewis pairs, Natural bond orbital (NBO) analysis has been applied.

Table 2.3. NBO analysis of $\text{NH}_3\text{-BH}_3$ and $\text{PH}_3\text{-BF}_3$ at MP2(FC)/aug-cc-pVDZ level. (BO: bond order)

	$\text{NH}_3\text{-BH}_3$		$\text{PH}_3\text{-BF}_3$	
	Eclipsed	Staggered	Minimum1	Minimum 2
$r(\text{P-B}) \text{ (pm)}$	169.3	166.7	227.2	304.1
BO^{tot}	0.992	1.003	0.925	0.015
BO^{cov}	0.308	0.316	0.315	0.000
BO^{ion}	0.684	0.687	0.610	0.015
$q(\text{PH}_3)$	0.307	0.310	0.318	0.032
$q(\text{BF}_3)$	-0.307	-0.310	-0.318	-0.032

For both strong Lewis pair $\text{NH}_3\text{-BH}_3$ and weak Lewis pair $\text{PH}_3\text{-BF}_3$, ionic bond order has bigger contribution than covalent bond order. For staggered conformation of $\text{NH}_3\text{-BH}_3$, the total bond order is slightly bigger than that of eclipsed bond order. The contribution of ionic bond is twice as large as the contribution from covalent bond. For $\text{PH}_3\text{-BF}_3$, the BO^{tot} of minimum 1 is 0.891, which indicates the bind between PH_3 and BF_3 is a strong bond, and the main contribution is made by ionic bond. But for minimum 2, the BO^{tot} is close to zero, and Lewis acid and Lewis base are complexed by electrostatic interaction. The charge separation of $\text{PH}_3\text{-BF}_3$ in minimum 2 is almost zero. Further exploration about interaction between Lewis acid and Lewis base, the EDA (energy decomposition analysis) has been calculated with GAMESS using LMO-EDA.

2.2.6 EDA Analysis of Strongly and Weakly Bound Systems

Energy decomposition analysis (EDA) is a powerful tool to understand the interaction between two fragments.²⁵⁻³¹ Complexation energy contains bond energies between two fragments and also the energy arising from the fragments preparation energy, which includes the process of geometry and charge transformation from fragments to equilibrium.³²⁻³⁴ According to the definition, the complexation energy is defined as:

$$E_{\text{dcomp}} = E^{\text{ES}} + E^{\text{EX}} + E^{\text{REP}} + E^{\text{POL}} + E^{\text{DISP}} \quad (5)$$

$$E_{\text{comp}} = E_{\text{dcomp}} + \Delta E^{\text{DEF}} \quad (6)$$

The electrostatic energy term (E^{ES}) can be defined as the interaction between the static charge densities of each monomer within the complex. This term includes the attractive Coulomb interactions between the nuclei of one monomer with the electrons of the other monomer, the repulsive Coulomb interactions between the nuclei of each monomer and the electrons of each monomer. The total electrostatic interaction is attractive under the normal conditions. The Pauli term contains the exchange (E^{EX}) and repulsion (E^{REP}) energies, which cause the stabilization and destabilization, respectively. E^{EX} reflects the interaction between occupied molecule orbitals. E^{REP} is the repulsion between filled molecule orbitals.

The exchange interaction arises due to the antisymmetric nature of the wave function that allows electrons to exchange between monomers. Polarization (E^{POL}) is a stabilizing effect that is caused by relaxation of the complex wave function. This is also known as the orbital relaxation energy and is always attractive. The term is a major indicator of the covalent nature of a bonding interaction. The dispersion term (E^{DISP}) computed in the LMOEDA³⁵ method is an attractive term, which arises due to electron correlation. Deformation energy (E^{DEF}) is the geometrical distortions of the donor and acceptor subunits that occur upon complex formation, which in this case is dominated by the pyramidalization.

Table 2.4. LMO-EDA analysis at MP2 (FC)/aug-cc-pVDZ level (kJ/mol).

	NH ₃ -BH ₃			PH ₃ -BF ₃		
	staggered	eclipsed	Δ	Minimum 1	Minimum 2	Δ
r(N-B) (pm)	166.7	169.3	-2.6	227.2	304.1	-76.9
E ^{ES}	-335.2	-316.9	-18.3	-203.9	-42.7	-161.2
E ^{EX}	-501.2	-473.9	-27.3	-304.1	-58.4	-245.7
E ^{REP}	966.3	909.5	56.8	618.2	109.1	509.1
E ^{POL}	-270.2	-252.6	-17.6	-173.9	-14.5	-159.4
E ^{DISP}	-30.6	-30.7	0.1	-2.2	-5.7	3.5
E ^{DEF}	53.9	55.5	-1.6	67.5	3.1	64.4
E _{comp}	-117.0	-109.1	-7.9	1.6	-9.1	10.7

In NH₃-BH₃, because of the steric hindrance of eclipsed conformer has a longer r(N-B) than staggered. The biggest contribution comes from Pauli repulsion for both staggered and eclipsed conformation. But because of the r(N-B) difference, ΔE^{REP} in staggered conformation is 56.8 kJ/mol higher than that in eclipsed conformation. The following contributions are exchange (ΔE^{EX}), polarization (ΔE^{POL}) as well as electrostatic interaction (ΔE^{ES}), and these interactions stabilize the complex. For staggered conformation, these

interactions are bigger than that in eclipsed conformation. Compared with other interactions, deformation and dispersion energies for both conformations are similar, and these two interactions are rather weak.

For $\text{PH}_3\text{-BF}_3$ at MP2(FC)/aug-cc-pVDZ level, $r(\text{P-B})$ in minimum 2 is 76.9 pm bigger than that in minimum 1. Destabilization energy E^{REP} in minimum 2 is 509.1 kJ/mol smaller than that in minimum 1 and this energy difference helps to stabilize minimum 2. For stabilization factor, ΔE^{ES} , ΔE^{EX} and ΔE^{POL} in minimum 2 are bigger than that in minimum 1, respectively. Deformation energy, which will destabilize complex, is 64.4 kJ/mol higher in minimum 1 than that in minimum 2. For both minima, the dispersion energies are negligible.

The data in Table 2.4 clearly show that for both $\text{NH}_3\text{-BH}_3$ and $\text{PH}_3\text{-BF}_3$, the biggest energy difference between different conformations comes from repulsion energy, which is very sensitive to bond distance. Especially for $\text{PH}_3\text{-BF}_3$, the deformation energy plays a big role in stabilizing minimum 2.³⁶

2.2.7 Complexation Energy of Lewis Pairs

The straightforward evidence for distinguishing strong and weak Lewis pairs is the complexation energy. Therefore, an effort has been made to identify the theoretical method for evaluating a complexation energy, which is accurate and economic. Plenty of methods are tested and the information is summarized in Table 2.5.

Table 2.5. Complexation energies (ΔH_{298}) of Lewis pair systems (in kJ/mol).

	$\text{PM}_{\text{e}}\text{BMe}_3$	NMe_3BMe_3	$\text{PM}_{\text{e}}\text{BF}_3$	PF_3BH_3	NH_3BH_3	$\text{PM}_{\text{e}}\text{BH}_3$	MUE
EXP	-69.2 ^[37]	-74.0 ^[2]	-94.9 ^[22]	-102.5 ^[5, 38]	130.1 ± 4.2 ^[4]	-178.5 ^[7]	-
			-79.1 ^[24]				
HF/6-31+G(d)	+3.34	+6.48	-31.29	-22.81	-73.89	-89.57	-71.05
B3LYP/6-31G(d)	-25.7	-24.76	-44.65	-96.46	-120.48	-133.92	-31.35
B97D/6-31+G(d)	-54.24	-64.04	-59.08	-71.85	-109.88	-139.85	-22.52
B98/6-31G(d)	-39.28	-38.38	-48.87	-104.55	-128.69	-142.45	-22.42
MPW1K/6-31G(d)	-53.53	-50.43	-61.68	-116.68	-136.73	-159.56	-15.95
MPW1K/6-31+G(d)	-53.21	-45.19	-70.26	-96.72	-128.47	-159.58	-13.44
M05-2X/6-31G(d)	-62.24	-77.94	-60.64	-99.5	-118.18	-142.77	-13.45
M05-2X/6-31+G(d)	-61.86	-73.95	-69.24	-84.49	-127.27	-151.09	-11.03
M06-2X/6-31+G(d)	-64.53	-81.81	-61.88	-82.83	-125.77	-146.38	-14.41
M06-2X/6-31+G(d,p)	-63.61	-80.74	-62.59	-83.27	-121.82	-146.72	-14.80
ω B97XD/6-31G(d)	-68.27	-75.50	-63.49	-106.58	-129.94	-155.29	-7.46
ω B97XD/6-31+G(d)	-67.39	-66.69	-73.51	-83.02	-120.29	-155.36	-11.3
ω B97XD/def2-TZVP	-61.54	-63.05	-65.06	-108.28	-118.28	-165.67	-10.39
ω B97XD/def2-TZVPP	-70.74	-62.72	-65.34	-108.8	-117.54	-165.58	-9.62
ω B97XD/cc-pVTZ	-67.14	-64.28	-62.86	-101.7	-121.5	-161.13	-9.24
MP2(FC)/cc-pVDZ	-78.76	-93.54	-53.47	-89.05	-132.66	-151.47	-16.42
MP2(FC)/cc-pVTZ	-86.34	-96.02	-55.64	-108.18	-124.96	-161.6	-14.95
ω B97XD/cc-pVTZ							
// ω B97XD/6-31G(d)	-66.74	-70.1	-62.38	-100.66	-121.5	-160.48	-8.7

ω B97XD/def2-TZVP							
// ω B97XD/6-31G(d)	-71.01	-68.33	-64.91	-106.16	-118.19	-165.16	-8.32
RI-SCS-MP2/cc-pVTZ							
// ω B97XD/6-31G(d)	-67.27	-81.02	-48.06	-86.35	-113.41	-143.73	-18.04
RI-SCS-MP2/def2-TZVP							
// ω B97XD/6-31G(d)	-71.67	-78.55	-54.44	-89.77	-110.22	-148.15	-15.9
CCSD(T)/CBS							
// ω B97XD/6-31G(d)	-75.46	-83.29	-59.37	-100.45	-116.1	-158.9	-11.95

Compared with gas phase experimental data, HF results have the largest MUE value, which is 71.05 kJ/mol. B3LYP/6-31G(d) gives a slightly better energy description (MUE=31.35 kJ/mol). Complexation energies predicted at B97D/6-31+G(d) and B98/6-31G(d) are similar. For DFT methods like MPW1K, M05-2X and M06-2X with small Pople style basis sets the results are very close, and the MUE values are around -14 kJ/mol. From Table 2.1, we already found that ω B97XD with the small basis set 6-31G(d) can provide geometries, which are rather close to CCSD(T)/cc-pVQZ level. Unexpectedly, for energy calculation, ω B97XD/6-31G(d) can give the smallest deviation compared to other methods by using the geometry at the same level, and the MUE is -7.46 kJ/mol at ω B97XD/6-31G(d) level. Split valence basis sets are tested for complexation calculations in combination with the ω B97XD functional. The performances of def2-TZVP and def2-TZVPP with ω B97XD are quite close to ω B97XD/cc-pVTZ. By using geometries obtained at ω B97XD/6-31G(d) level of theory, complexation energies have been corrected with higher level methods. Using the same geometry at ω B97XD/6-31G(d) level, ω B97XD/cc-pVTZ and ω B97XD/def2-TZVP yield almost identical results as the geometries optimized at ω B97XD/def2-TZVP and ω B97XD/cc-pVTZ level. RI-SCS-MP2/cc-pVTZ and RI-SCS-MP2/def2-TZVP have slightly higher MUE values than DFT methods using the ω B97XD/6-31G(d) geometry. Taken together, ω B97XD/6-31G(d) provides satisfying results with economic cost.

2.2.8 The Impact of Structural Parameters on the Complexation Energy

The steric hindrance can be evaluated by measuring the dihedral angle of Lewis base and Lewis acid as shown in Figure 2.5.

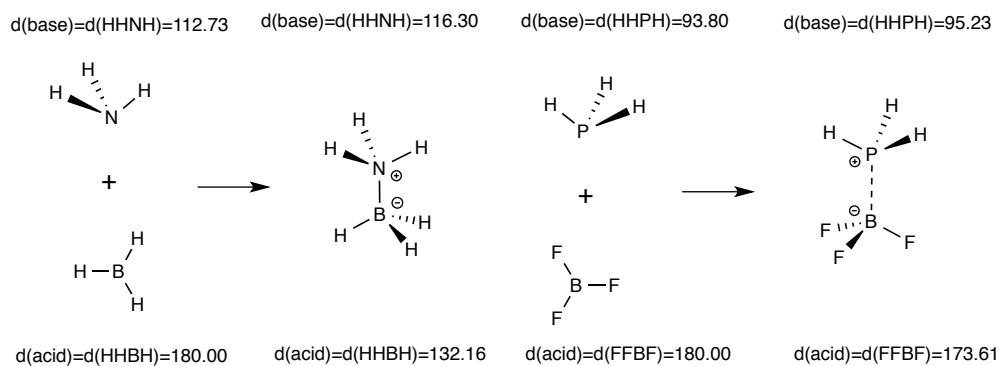


Figure 2.5. Dihedral angle of Lewis acid and Lewis base at MP2(FC)/aug-cc-pVDZ level.

The substituent has perceptible effects on the complexation energy of Lewis pairs. Interaction between Lewis acid and Lewis base is based on the charge distribution and the distance between acid and base. The substituent effect not only impacts the charge

distribution of the Lewis pair, but also has an influence on distance. Dihedral angle of d(base) in monomeric NH_3 is 112.73° and d(acid) in monomeric BH_3 is 180° as a result of hybridization. In $\text{NH}_3\text{-BH}_3$, because the NH_3 donates a lone pair to BH_3 , BH_3 is not planar anymore and d(acid) is 132.16° . Because monomeric NH_3 is already pyramidal, the change of d(base) is small. The distance between phosphorous and boron in $\text{PH}_3\text{-BF}_3$ is 304.1 pm at MP2(FC)/aug-cc-pVDZ level and again the dihedral angle changes are small. More Lewis pairs are discussed in Table 2.6.

Table 2.6. Properties of selected Lewis pairs calculated at $\omega\text{B97XD}/6-31\text{G(d)}$ level.

		ΔH_{exp} (kJ/mol)	$\Delta H_{298}^{\text{opt a}}$ (kJ/mol)	r(N-B) (pm)	d(acid)	d(base)	q(base)
S_1		-130.1 ^[4]	-130.0	165.8	132.5	116.7	0.35
S_2		-57.6 ^[2]	-73.7	169.2	133.7	116.8	0.34
S_3		-73.9 ^[2]	-85.9	168.8	131.5	117.0	0.33
S_4		-80.6 ^[2]	-85.3	170.8	128.4	117.6	0.32
S_5		-73.8 ^[2]	-73.2	175.0	126.0	117.5	0.30
S_6		-75.4 ^[39]	-80.1	169.1	130.7	117.5	0.33
S_7		-68.3 ^[39]	-77.0	170.5	128.3	118.2	0.32
S_8		-41.9 ^[39]	-48.9	179.8	123.9	122.5	0.30

^a The complexation energy is calculated at $\omega\text{B97XD}/6-31\text{G(d)}$ level.

Structure properties of selected Lewis pairs are shown in Table 2.6. Changing substituent on the Lewis center has a big impact on the complexation energy. However, the influence on NBO charge distributions is negligible under the same condition.

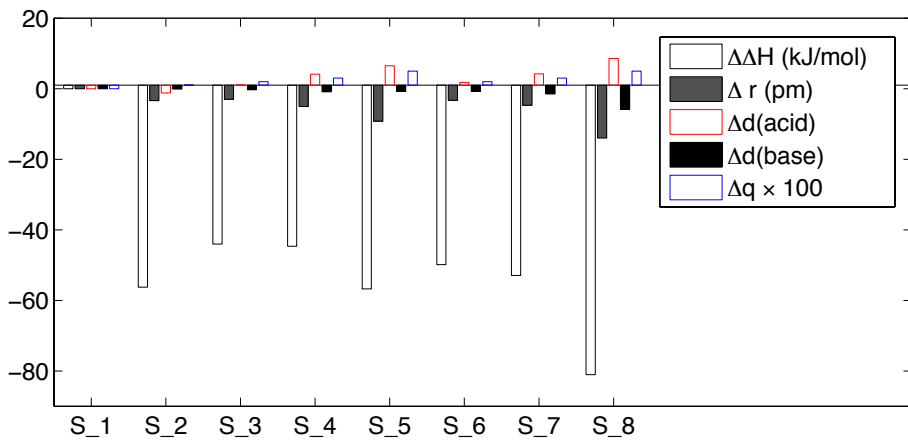


Figure 2.6. Properties of selected Lewis pairs relative to $\text{S}_1(\text{NH}_3\text{-BH}_3)$ calculated at $\omega\text{B97XD}/6\text{-}31\text{G(d)}$ level. The charge Δq (base) is magnified 100 times.

In order to compare the changes in structural properties and energies by varying the substituent, all the data is relative to $\text{NH}_3\text{-BH}_3$ and shown in Figure 2.6. By expanding the number of methyl or ethyl groups on the nitrogen center, the complexation energy is dramatically reduced in the fully substituted Lewis base. For instance the $\Delta\Delta H$ of S_3 and S_4 are comparable, but $\Delta\Delta H$ of S_5 is roughly 12 kJ/mol lower than S_3 and S_4 at $\omega\text{B97XD}/6\text{-}31\text{G(d)}$ level, $\Delta\Delta H$ of S_6 and S_7 are almost identical meanwhile, $\Delta\Delta H$ of S_8 are roughly -30 kJ/mol lower than S_6 and S_7 . As expected, increasing the steric hindrance, distances between Lewis acid and base will be extended systematically. In substrates S_3 to S_5 , by adding methyl group on the nitrogen center from zero to three, $r(\text{N-B})$ increases from 168.8 pm to 175.0 pm accordingly. This trend can be confirmed by replacing methyl with ethyl groups. $r(\text{N-B})$ is 169.1 pm in S_7 with one ethyl group, but in S_8 with three ethyl groups, $r(\text{N-B})$ is 180.2 pm. Steric effects not only have an influence on the complexation energy and bond distances but also have big impact on the dihedral angle. The expansion of methyl and ethyl groups on the Lewis base extrudes the dihedral angle of the Lewis base. The red color bar shows that from S_3 to S_5 , d (base) keeps on minishing. For the sterically more demanding ethyl group, d (base) decreases from S_6 to S_8 . The NBO charge is less affected by the substituent, which is described in Table 2.6.

Figure 2.6 illustrates the substituent effects on geometry properties, such as bond distance, NBO charge distribution and dihedral angle changes. In order to identify the reasons for the substantial differences in the structural and energetic properties of the Lewis pairs, energy decomposition analyses (EDA)^{28, 35, 40} is conducted on these systems, and the results are shown in Table 2.7.

Table 2.7. Energy decomposition analysis of Lewis pairs calculated at MP2(FC)/aug-cc-pVDZ// $\omega\text{B97XD}/6\text{-}31\text{G(d)}$ level (in kJ/mol).

	E^{ES}	E^{EX}	E^{REP}	E^{POL}	E^{DISP}	E_{decomp}	E^{DEF} (base)	E^{DEF} (acid)	E_{comp}
S_1		-341.4	-510.3	985.4	-274.9	-30.6	-171.7	0.30	54.60 -116.84
S_2		-350.6	-566.2	1085.3	-255.4	-38.3	-125.1	0.33	62.16 -62.65
S_3		-373.2	-589.4	1126.9	-265.5	-50.5	-151.6	1.20	68.49 -81.87
S_4		-370.2	-586.4	1111.1	-259.2	-62.9	-167.6	2.31	76.94 -88.38

S_5	<chem>[CH3][B+]([CH3])[N+]([CH3])C(C)C</chem>	-353.4	-568.3	1054.8	-232.9	-49.4	-149.1	4.45	84.09	-60.55
S_6	<chem>[CH3][B+]([CH3])N([CH3])C(C)C</chem>	-371.2	-595.0	1133.1	-266.4	-54.0	-153.5	6.68	70.48	-76.37
S_7	<chem>[CH3][B+]([CH3])N([CH3])C(C)CC</chem>	-375.5	-601.8	1136.0	-265.0	-68.6	-175.0	18.50	78.59	-77.87
S_8	<chem>[CH3][B+]([CH3])N([CH3])C(C)CC</chem>	-330.0	-562.6	1031.6	-223.8	-89.2	-174.0	15.07	92.45	-66.48

It is noticeable that from **S_1** to **S_8**, E^{DEF} terms differ quite significantly across the series, being largest in the case of **S_8** and smallest in the case of **S_1**. Keeping the Lewis acid as constant and increasing the number of same type of substituents lead to the systematically increasing of E^{DEF} . For instance, from **S_2** to **S_5**, the E^{DEF} increases from 62.49 kJ/mol to 88.54 kJ/mol. From **S_6** to **S_8**, the deformation energy changes from 77.16 kJ/mol to 107.52 kJ/mol. This data indicates that the deformation energies not only depend on the type of substituent (methyl or ethyl), but also depend on the number of substituent attached on the Lewis center. The different contributions from E^{ES} , E^{EX} , E^{REP} , E^{POL} , and E^{DISP} are graphically demonstrated in Figure 2.7.

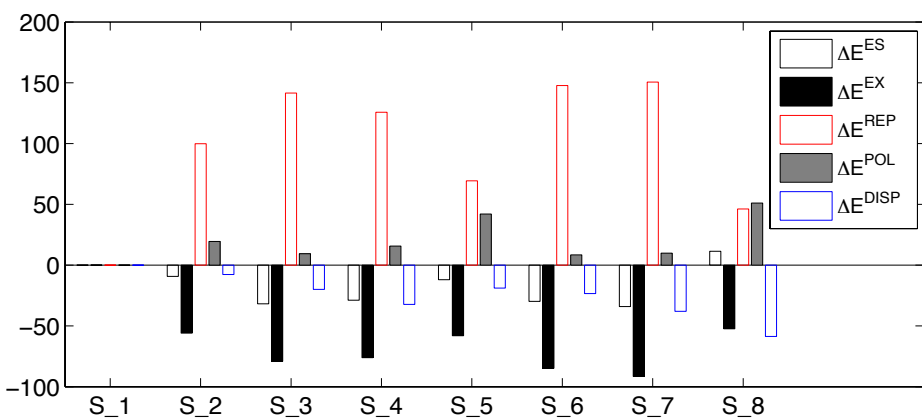


Figure 2.7. Energy decomposition parameters relative to **S_1** for Lewis pairs **S_2** to **S_8**.

The biggest energy contribution is made by the repulsion energy, which destabilizes the Lewis pairs. E^{REP} represents the repulsion energy between the electrons of Lewis acid and Lewis base with the same spin. It is unexpected that by adding methyl group on the base center from zero to three, the energy gap of E^{REP} is narrow and it is confirmed by the variation of ethyl group on Lewis base center. The absolute value of stabilized energy E^{POL} and destabilized energy E^{DISP} both increase by adding substituent on Lewis base. But E^{ES} and E^{EX} show the different trend, E^{ES} and E^{EX} in trisubstituted ammonia are significant smaller than disubstituted and monosubstituted ammonia. For example, E^{ES} of **S_5** is 16.8 kJ/mol smaller than that of **S_4**, E^{EX} of **S_4** is 18.1 kJ/mol smaller than that of **S_5**. The energy differences are enhanced by ethyl group, comparing **S_8** and **S_7**, ΔE^{ES} is 45.5 kJ/mol and ΔE^{EX} is 39.2 kJ/mol.

Table 2.8. Properties of selected Lewis pairs using geometries obtained at ωB97XD/6-31G(d) level.

		ΔH _{exp} (kJ/mol)	r ^a (pm)	^b ΔH ₂₉₈ ^{opt} (kJ/mol)	^c ΔH ₂₉₈ ^{sp} (kJ/mol)	q(base)	d(acid)	d(base)
S_1		-130.1 ^[4]	165.8	-129.95	-106.36	0.35	132.5	116.7
S_2		-57.6 ^[2]	169.2	-73.7	-63.8	0.34	133.7	116.8
S_3		-73.9 ^[2]	168.8	-85.9	-84.1	0.33	131.5	117.0
S_4		-80.6 ^[2]	170.8	-85.3	-92.2	0.32	128.4	117.6
S_5		-73.8 ^[2]	175.0	-73.2	-87.3	0.30	126.0	117.5
S_6		-75.4 ^[39]	169.1	-80.1	-79.1	0.33	130.7	117.5
S_7		-68.3 ^[39]	170.5	-77.0	-79.0	0.32	128.3	118.2
S_8		-41.9 ^[39]	179.8	-48.9	-63.52	0.30	123.9	122.5
S_9		-4.6 ^[41]	211.7	-40.52	-45.44	-0.43	136.7	106.8
S_10		-10.1 ^[41]	212.6	-36.84	-40.21	0.43	137.1	104.7
S_11		-13.0 ^[41]	/200.3	/-49.05	/-67.00	/0.66	131.0	105.3
S_12		-36.6 ^[41]	200.5	-46.3	-61.7	0.65	131.3	103.7
S_13		-39.6 ^[42, 43]	206.6	-78.1	-73.9	0.50	132.6	113.5
S_14		-102.5 ^[5]	186.7	-106.58	-83.76	0.71	136.6	102.2
S_15		-54.8 ^[44]	171.5	-73.7	-69.2	0.33	128.6	113.7
S_16		-61.6 ^[42, 43]	200.2	-49.4	-67.2	0.67	130.9	107.5
S_17		-69.0 ^[42, 43]	199.2	-68.3	-84.5	0.69	129.7	109.1
S_18		-72.3 ^[43, 44]	169.1	-83.7	-80.0	0.33	130.8	117.5

S_19		-72.9 ^[44]	169.3	-82.7	-81.1	0.33	128.7	114.4
S_20		-73.6 ^[45]	167.2	-83.5	-86.7	0.32	128.4	92.1
S_21		-75.9 ^[46]	169.9	-85.7	-84.8	0.33	131.2	117.4
S_22		-77.1 ^[46]	168.7	-87.6	-85.2	0.33	131.4	117.3
S_23		-78.3 ^[46]	168.7	-86.9	-84.1	0.33	131.2	117.4
S_24		-77.6 ^[46]	168.4	-87.4	-85.1	0.33	131.1	117.3
S_25		-79.1 ^[42, 43]	207.1	-63.5	-67.2	0.49	134.3	111.9
S_26		-82.3 ^[45]	170.2	-89.6	-97.7	0.32	128.0	117.3
S_27		-83.5 ^[47]	172.7	-87.4	-105.1	0.30	125.1	116.5
S_28		-85.4 ^[45]	168.5	-93.9	-100.0	0.32	129.0	114.0
S_29		-94.1 ^[45]	167.5	-115.5	-120.2	0.32	130.0	110.5
S_30		-178.36 ^[7]	192.2	-155.3	-153.1	0.70	131.5	109.1

^a r represents the bond distance between Lewis acid and Lewis base. ^b ωB97XD/6-31G(d) ^c MP2(FC)/6-31+G(2d,p)//ωB97XD/6-31G(d)

It is noteworthy that, the experimental complexation energy measurement for **S_9** is only 4.61 kJ/mol, the complexation energies of **S_10** and **S_11** are approximately 10 kJ/mol. The small complexation energy shows these Lewis pairs are weakly bonded. By looking into these weakly bound Lewis pairs, it is found that there are two types of complexation forms, the strongly bound system and weakly bound system (Figure 2.8). In the strongly bound system, the Lewis acid center (boron atom) directly connects with Lewis base center (phosphorus atom), but in the weakly bound systems, the Lewis acid and Lewis base are weakly bunched with each other by the Van-der-Waal's interaction.

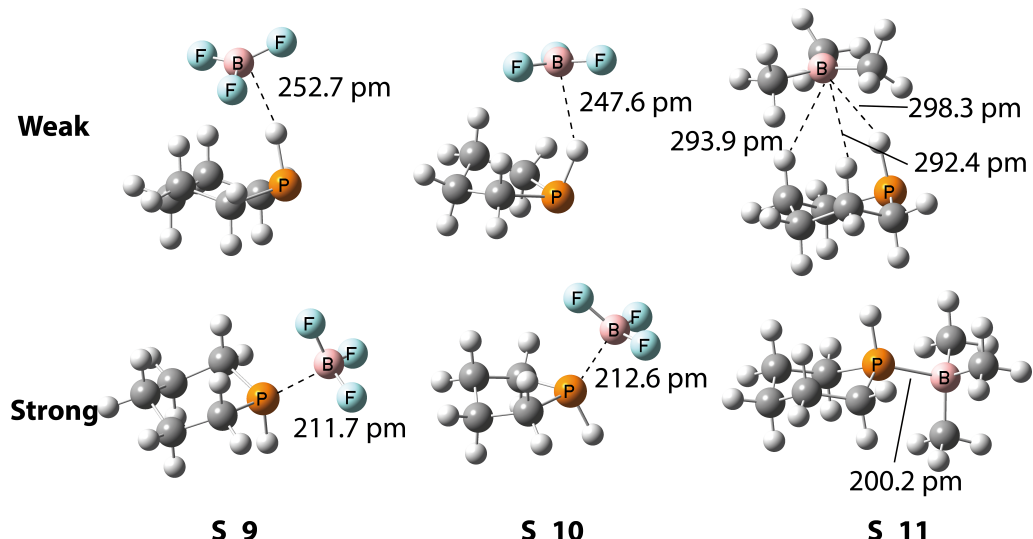


Figure 2.8. Structures of selective Lewis pairs at ω B97XD/6-31G(d) level.

For the weakly bound Lewis pairs **S₉**, **S₁₀** and **S₁₁**, the complexation energies are calculated as 9.67 kJ/mol, 11.05 kJ/mol and 14.78 kJ/mol, separately. But the complexation energies of strongly bound system **S₉**, **S₁₀** and **S₁₁** are 40.52 kJ/mol, 36.84 kJ/mol and 49.05 kJ/mol in the gas phase, respectively. The calculation results of weakly bound Lewis pairs fit the experimental data quite well. These indicate that the ω B97XD method with 6-31G(d) basis set can provide satisfactory thermochemical data for the Lewis pairs, especially for the weakly bound systems, which is very important for the Frustrated Lewis pairs.

Complexation energies of Lewis pairs in Table 2.8 are graphically shown in Figure 2.9.

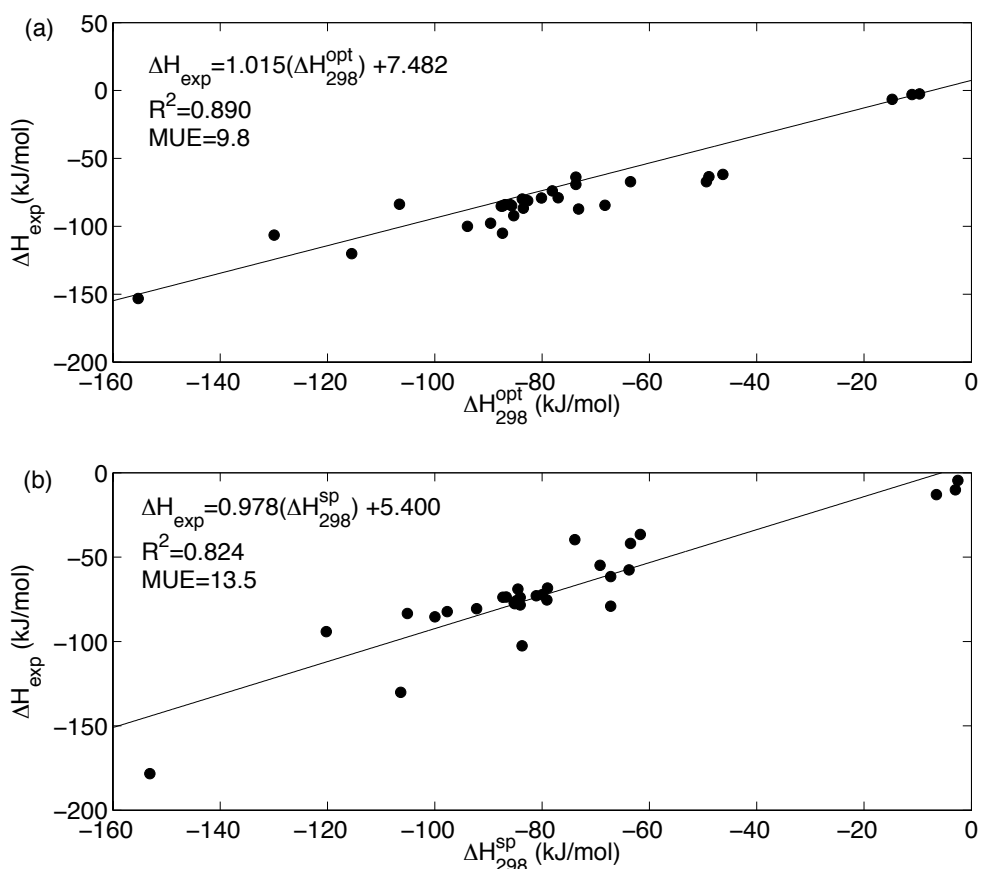


Figure 2.9. Calculated complexation energy correlated with experiment value. (a) $\Delta H_{298}^{\text{opt}}$ is calculated at $\omega\text{B97XD}/6-31\text{G(d)}$ level. (b) $\Delta H_{298}^{\text{sp}}$ is obtained at MP2 (FC)/6-31+G(2d,p)// $\omega\text{B97XD}/6-31\text{G(d)}$ level.

Figure 2.9 shows that the DFT method ωB97XD with small basis set 6-31G(d) yields satisfying results compared with experimental value ($R^2=0.890$). Mean unsigned deviation of complexation energy at same level is 9.8 kJ/mol. Mean unsigned error (MUE) at MP2(FC)/6-31+G(2d,p)// $\omega\text{B97XD}/6-31\text{G(d)}$ level is 13.5 and $R^2=0.824$. From previous discussion, for Lewis pairs, geometry and complexation energy at $\omega\text{B97XD}/6-31\text{G(d)}$ is close to experimental results.

2.3 Conclusions

Compared with experimental values, $\omega\text{B97XD}/6-31\text{G(d)}$ is recommended for the calculations of Lewis pairs, because of its outstanding performance in geometry optimizations and energy evaluations. The results obtained at $\omega\text{B97XD}/6-31\text{G(d)}$ level are comparable with those obtained from CCSD(T)/CBS. For $\text{PH}_3\text{-BF}_3$, the energy surface is very flat so that it is hard to evaluate accurately the complexation energy by theoretical methods. MPW1K and MP2 with specific basis sets predict two minima, a short minimum with $r(\text{P-B})$ around 230 pm, and minimum 2 with $r(\text{P-B})$ near 300 pm. The portion of the mixture of HF exchange and the correlation energy is the main factor that influences the bond distance between PH_3 and BF_3 . By using the extrapolation method, the complexation energy of $\text{PH}_3\text{-BF}_3$ is -10.57 kJ/mol with $r(\text{P-B})$ as 312.5 pm. By analyzing the complexation energy components, the opposite sign of electrostatic energy and polarization energy have the biggest contribution to the complexation energy. Increasing the steric hindrance, deformation energy and repulsion energy will dramatically increase, while the exchange energy and dispersion energy will be reduced.

References

1. D. W. Stephan and G. Erker, *Angew. Chem. Int. Ed.*, 2010, **49**, 46-76.
2. H. C. Brown, H. Bartholomay and M. D. Taylor, *J. Am. Chem. Soc.*, 1944, **66**, 435-442.
3. R. D. Suenram and L. R. Thorne, *Chem. Phys. Lett.*, 1981, **78**, 157-160.
4. A. Haaland, *Angew. Chem. Int. Ed.*, 1989, **28**, 992-1007.
5. R. L. Kuczowski, *J. Chem. Phys.*, 1967, **46**, 357.
6. J. R. Durig, S. Riethmiller, V. F. Kalasinsky and J. D. Odom, *Inorg. Chem.*, 1974, **13**, 2729-2735.
7. P. S. Bryan and R. L. Kuczowski, *Inorg. Chem.*, 1972, **11**, 553-559.
8. J. R. Durig, Y. S. Li, I. A. Carreira and J. D. Odom, *J. Am. Chem. Soc.*, 1973, **95**, 2491-2496.
9. J. D. Odom, V. F. Kalasinsky and J. R. Durig, *Inorg. Chem.*, 1975, **14**, 2837-2839.
10. S. Grimme, *J. Comput. Chem.*, 2006, **27**, 1787-1799.
11. H. L. Schmid and A. D. Becke, *J. Chem. Phys.*, 1998, **108**, 9624-9631.
12. Y. Zhao, N. E. Schultz and D. G. Truhlar, *J. Chem. Theory Comput.*, 2006, **2**, 364-382.
13. Y. Zhao and D. G. Truhlar, *Theor. Chem. Acc.*, 2007, **120**, 215-241.
14. B. J. Lynch, P. L. Fast, M. Harris and D. G. Truhlar, *J. Phys. Chem. A*, 2000, **104**, 4811-4815.
15. J. D. Chai and M. Head-Gordon, *Phys. Chem. Chem. Phys.*, 2008, **10**, 6615-6620.
16. S. Grimme, *J. Chem. Phys.*, 2003, **118**, 9095.
17. B. Maryasin, *Theoretical Investigations in Nucleophilic Organocatalysis*, 2011, Ludwig-Maximilians-Universität München.
18. F. Hirota, K. Miyata and S. Shibata, *J. Mol. Struct. THEOCHEM*, 1989, **201**, 99-111.
19. R. Ahlrichs, M. R. Bar, M. Haser and E. Sattler, *Chem. Phys. Lett.*, 1991, **184**, 353-358.
20. T. A. Ford, *J. Phys. Chem. A*, 2008, **112**, 7296-7302.
21. S. Grimme, *J. Comput. Chem.*, 2006, **27**, 1787-1799.
22. F. Weigend and R. Ahlrichs, *Phys. Chem. Chem. Phys.*, 2005, **7**, 3297-3305.
23. F. Weigend, *Phys. Chem. Chem. Phys.*, 2006, **8**, 1057-1065.

24. J. M. L. Martin and P. R. Taylor, *J. Chem. Phys.*, 1997, **106**, 8620-8623.
25. K. Kitaura and K. Morokuma, *Int. J. Quantum Chem.*, 1976, **10**, 325-340.
26. F. Bessac and G. Frenking, *Inorg. Chem.*, 2006, **45**, 6956-6964.
27. N. Thellamurege and H. Hirao, *Molecules*, 2013, **18**, 6782-6791.
28. M. v. Hopffgarten and G. Frenking, *Wiley Interdisciplinary Reviews: Computational Molecular Science*, 2012, **2**, 43-62.
29. E. D. Glendening and A. Streitwieser, *J. Chem. Phys.*, 1994, **100**, 2900.
30. M. Lein, A. Szabo, A. Kovacs and G. Frenking, *Faraday Discuss.*, 2003, **124**, 365.
31. E. A. Cobar, P. R. Horn, R. G. Bergman and M. Head-Gordon, *Phys. Chem. Chem. Phys.*, 2012, **14**, 15328.
32. Y. Chen and H. Li, *J. Phys. Chem. A*, 2010, **114**, 11719-11724.
33. E. L. Smith, D. Sadowsky, C. J. Cramer and J. A. Phillips, *J. Phys. Chem. A*, 2011, **115**, 1955-1963.
34. G. Cavigliasso, R. Stranger and B. F. Yates, *Dalton Trans.*, 2012, **41**, 13948.
35. P. Su and H. Li, *J. Chem. Phys.*, 2009, **131**, 014102.
36. J. P. Wrass, D. Sadowsky, K. M. Bloomgren, C. J. Cramer and J. A. Phillips, *Phys. Chem. Chem. Phys.*, 2014, **16**, 16480.
37. H. D. Kaesz and F. G. A. Stone, *J. Am. Chem. Soc.*, 1960, **82**, 6213-6218.
38. J. D. Odom, S. Riethmil, S. J. Meischen and J. R. Durig, *J. Mol. Struct.*, 1974, **20**, 471-485.
39. H. C. Brown and M. D. Taylor, *J. Am. Chem. Soc.*, 1947, **69**, 1332-1336.
40. D. M. Camaioni, B. Ginovska-Pangovska, G. K. Schenter, S. M. Kathmann and T. Autrey, *J. Phys. Chem. A*, 2012, **116**, 7228-7237.
41. H. L. Morris, M. Tamres and S. Searles, *Inorg. Chem.*, 1966, **5**, 2156-2160.
42. E. A. Fletcher, *A Study of the Steric Consequences of Planer Boron. The Base Strength of the Methyl Phosphines*, 1952, Purdue.
43. H. C. Brown, *J. Chem. Soc.*, 1956, 1248-1268.
44. H. C. Brown and G. K. Barbaras, *J. Am. Chem. Soc.*, 1953, **75**, 6-9.
45. H. C. Brown and M. Gerstein, *J. Am. Chem. Soc.*, 1950, **72**, 2926-2933.
46. H. C. Brown, M. D. Taylor and S. Sujishi, *J. Am. Chem. Soc.*, 1951, **73**, 2464-2467.
47. H. C. Brown and S. Sujishi, *J. Am. Chem. Soc.*, 1948, **70**, 2878-2881.

3 The Reactivity of Lewis Pairs for Hydrogen Activation

3.1 Introduction

Recently the concept of Frustrated Lewis Pair (FLP) has been raised by Douglas Stephan.¹⁻⁴ These Lewis pairs are able to activate small molecules such as H₂, or CO₂ reversibly at room temperature.⁵⁻¹⁵ It is known that Lewis acidic and basic centers connected to each other by a strong dative bond and this strong bond will reduce the activity of the Lewis pairs towards small molecule activation.¹⁶ In order to avoid that acids and bases form strong bonds, one can increase the steric hindrance of substituents to hinder the connection between Lewis acid and base. But the activity is still unquenched, acid and base are still weakly connected and this special Lewis adduct is called Frustrated Lewis Pair. The mechanisms of small molecule activation by FLP systems have been discussed for a long time since this concept has been invented.¹⁷⁻²¹

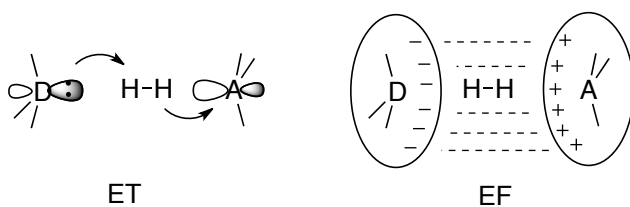


Figure 3.1. Electron-transfer (ET) and electric field (EF) model for heterolytic hydrogen cleavage by frustrated Lewis pairs.

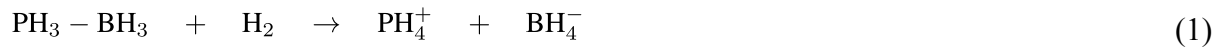
Until now two reaction mechanisms models for H₂ activation have been raised (Figure 3.1).^{22, 23} In the electron transfer (ET) model,²⁴ the hydrogen activation is associated with synergistic electron donation processes including the simultaneous involvement of active centers and the bridging hydrogen. The electric field (EF) model^{25, 26} suggests that the heterolytic bond cleavage occurs as a result of polarization by the strong EF present in the cavity in the reactive intermediates. This proposal is based on the fact that frustrated Lewis pairs possess significant electric fields (EF) in their interior. H-H bond splitting will follow a barrierless reaction pathway if the homogeneous EF is big enough. But later it has been shown that this type of electric field can only be found in spherical regions around the donor/acceptor atoms, and the EF in the reaction area is not big enough to overcome the hydrogen bond breaking barrier.^{22, 23} Besides that, it has also been verified that the location of the H-H bond in the transition states does not parallel to the electric field. Although there are quite some discussions about the mechanism of FLP activation of small molecules,^{17, 19} there are no comparisons about the different activation behaviors between FLPs and normal Lewis pairs as well as weakly bound Lewis pair. It will be helpful for understanding the connection of mechanism between strongly and weakly bound Lewis pairs. The frustrated Lewis pairs usually possess bulky groups and it is a challenge for theoretical simulations, hence finding a relationship between structure properties and reactivity is extremely helpful for the design of frustrated Lewis pairs.

3.2 Results and Discussions

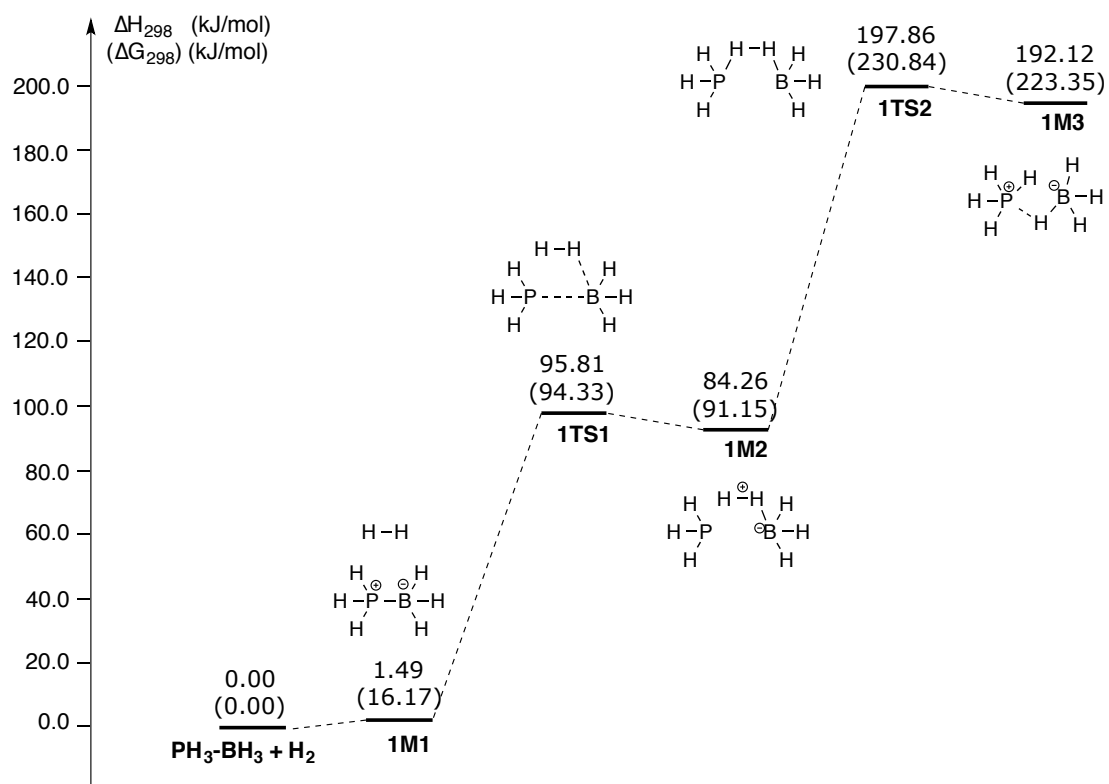
The hydrogen activation by frustrated Lewis pairs has been studied a lot experimentally. However, there are not many studies based on the difference of frustrated Lewis pairs and non-frustrated Lewis pairs, especially with the respect to the difference between the strongly and weakly bound Lewis pairs. But understanding those differences among different Lewis pairs will be greatly helpful for selection of catalysts and catalyst design. Therefore the efforts

will be put on the mechanism of hydrogen activated by strongly and weakly bound Lewis pairs.

3.2.1 Strongly Bound Lewis Pair



The complexation energy of $\text{PH}_3\text{-BH}_3$ is not available from experiment. Based on theoretical calculations, the complexation energy ΔH_{298} is -95.46 kJ/mol at MP2/cc-pVTZ level in the gas phase. Hence, $\text{PH}_3\text{-BH}_3$ is taken as a strongly bound Lewis pair model for mechanistic investigations.



Scheme 3.1. Reaction mechanism of H_2 activation by $\text{PH}_3\text{-BH}_3$, enthalpy and free energy are calculated at MP2/cc-PVTZ level in the gas phase and free energies are shown in parentheses.

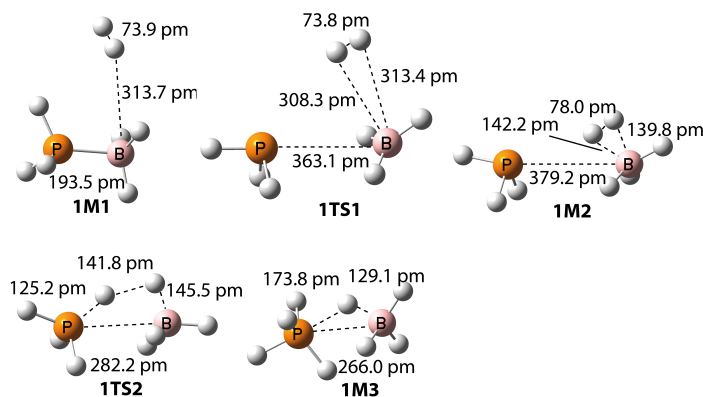
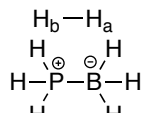


Figure 3.2. Structures of intermediates and transition states in the reaction of $\text{PH}_3\text{-BH}_3$ with H_2 in the gas phase at MP2/cc-pVTZ level.

As shown in Scheme 3.1, hydrogen activation begins with the complexation of H₂ with PH₃-BH₃, and intermediate **1M1** is formed via Van-der-Waals's interactions. The calculation results in Scheme 3.1 suggest that activation of H₂ by PH₃-BH₃ can be separated into two steps. In the first step, H₂ interacts with BH₃ and simultaneously, the bond between Lewis acid BH₃ and Lewis base PH₃ breaks. During the course, the activation enthalpy is 95.81 kJ/mol and activation free energy is 94.33 kJ/mol at MP2(FC)/cc-pVTZ level in the gas phase, respectively. In the intermediate **1M2**, with the distance of r(P-B)= 379.2 pm, there is hardly any interaction between Lewis base PH₃ and Lewis acid adduct H₂-BH₃. The second step is that PH₃ gets close to the complex involving H₂ and BH₃ and as a consequence P-H bond and B-H bonds are newly generated but the H-H bond is split. The free energy barrier of the second step is 230.84 kJ/mol, which includes two new generated bonds and heterolytic splitting of the H-H bond. As expected, the overall reaction is strongly endothermic and the rate-determining step is present in the H-H bond breaking which has a free energy barrier of 230.84 kJ/mol.

Table 3.1. Angles and dihedral angles of the intermediates and transition states at MP2(FC)/cc-pVTZ level.

 1M1	1TS1	1M2	1TS2	1M3
d(base) (°)	102.4	94.3	94.8	124.8
d(acid) (°)	135.9	178.4	145.6	111.6
∠H _a H _b P (°)	-	155.3	166.5	148.2
∠H _b H _a B (°)	154.6	-	-	93.0
q(BH ₃)	-0.630	-0.006	-0.374	-0.713
q(PH ₃)	0.630	0.006	0.010	0.670
q(H _b)	0.014	0.006	0.187	0.159
q(H _a)	-0.015	-0.006	0.177	-0.116
				-0.085

In complex **1M1**, H₂ is still far away from the reaction region, the distance between H₂ and BH₃ is 313.7 pm, and the distance between the acidic and basic center is 193.5 pm. From Table 3.1, we find that both PH₃ and BH₃ moieties are pyramidal, and the dihedral angle of d(base) and d(acid) are 102.4° and 135.9°, respectively. But in the transition state **1TS1**, d(acid) is expanded to 178.4° and d(base) to 94.3°. From **1M1** to **1TS1**, the BH₃ group changes from pyramidal to a planar conformation. In **1TS1**, PH₃ is released from BH₃, and the distance between H₂ and BH₃ is around 310 pm, which is close to **1M1**. Meanwhile the distance between PH₃ and BH₃ is elongated to 363.1 pm which is close to intermediate **1M2**. In **1M2**, r(P-B) equals 379.2 pm and there are barely interaction between BH₃ and PH₃. But when H₂ replaces PH₃ to complex with BH₃, the distances of two H atom and B atom are not the same, and one H atom is directed towards PH₃ moiety. It is noteworthy that in **1M2**, the d(acid) is 145.6°, which indicates BH₃ becomes pyramidal because of the complexation with H₂. For the last step, in **1TS2**, PH₃ takes one of the hydrogen atoms from the complex of H₂ and BH₃. It is unexpected that in transition state **1TS2**, the angle of HHP is 148.2° other than 180°. This result is conflicted with the conclusion of Rokob's previous work.^{27,28} In his work, he investigated the activation mechanism of the reaction of H₂ with P(*t*-Bu)₃ and B(C₆F₅)₃ with a linear transition states. But Grimme suspected that this linear four centered transition state is an artifact of the insufficient treatment of intramolecular London dispersion forces between the large substituents.²⁵ Interactions between PH₄ with BH₄ moieties reduce the distance between phosphorus and boron, and as a consequence, a trigonal bipyramidal configuration is formed for **1M3** with d(acid) = 137.0°.

Intrinsic reaction coordinate (IRC) calculation are carried out and shown in Figure 3.3.

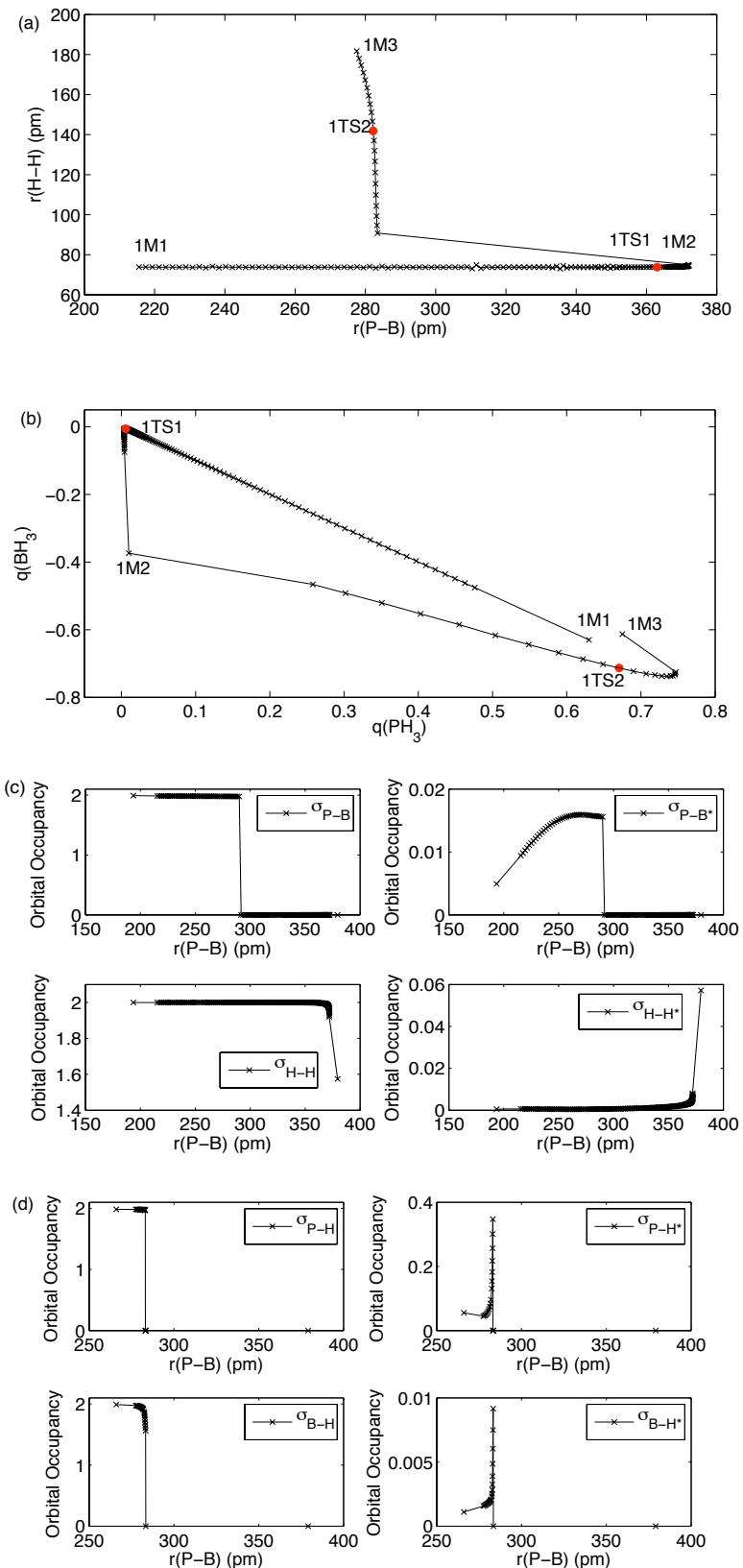


Figure 3.3. Reaction of H_2 with $\text{PH}_3\text{-BH}_3$. (a) $r(\text{P-B})$ vs $r(\text{H-H})$ along IRC pathway at MP2/cc-pVTZ level. (b) NBO analysis of PH_3 and BH_3 along IRC at MP2/cc-pVTZ level. (c) Orbital occupancy from NBO analysis along IRC from **1M1** to **1M2** through **1TS1** to **1M3** at MP2/cc-pVTZ level.

MP2/cc-pVTZ level. (d) Orbital occupancy from NBO analysis along IRC from **1M2** to **1M3** via **1TS2** at MP2/cc-pVTZ level.

Figure 3.3 (a) clearly shows that the distance between PH₃ and BH₃ is elongated first to prepare for the heterolytic hydrogen splitting. During the dative bond breaking, the hydrogen bond distance undergoes almost no change. After transition state **1TS1**, the distance between PH₃ and BH₃ is more than 370 pm and there are hardly any interactions. In **1M2** the distance between PH₃ and BH₃ is close to the typical distance between Lewis base and acid center, which is 396 pm in P(*t*-Bu)₃-B(C₆F₅)₃ calculated at B97-D/TZVP' level of theory.²⁵ For the next step on the reaction pathway, PH₃ shortens the distance between H₂ and BH₃, to heterolytically cleave the hydrogen bond. For the hydrogen bond splitting step, the behavior of normal Lewis pairs is the same as frustrated Lewis pairs.

Figure 3.3 (b) shows the charge transferred during the reaction. At the beginning of the reaction, because there is no interaction between Lewis acid and hydrogen, the absolute charges for PH₃ and BH₃ are identical. But with increasing the r(P-B) distance, the charge is transferred from BH₃ to PH₃. In transition state **1TS1**, the overall charges of BH₃ and PH₃ both are zero. But after **1TS1**, the amount of q(BH₃) is increased by the incoming H₂ molecule. In the hydrogen splitting step, PH₃ comes close to the H₂-BH₃ complex and the charge is transferred from PH₃ to BH₃ via the H-H bond.

Orbital occupancy from NBO analysis in Figure 2.3 (c) shows that before **1TS1**(r(P-B)=363.1 pm), a bond between phosphorus and boron cannot be detected. But after **1TS1**, occupancy of antibonding $\sigma^*_{(H-H)}$ keeps on increasing, which means H₂ is activated during the P-B bond breaking, even though the H-H bond distance undergoes almost no change. Along the reaction pathway from **1M2** to **1TS2**, and then to **1M3**, the distance between P and B is shortened. In the second step, according to the NBO analysis (Figure 3.4 (d)), the H-H bond vanishes, but the B-H and P-H bond start to be generated.

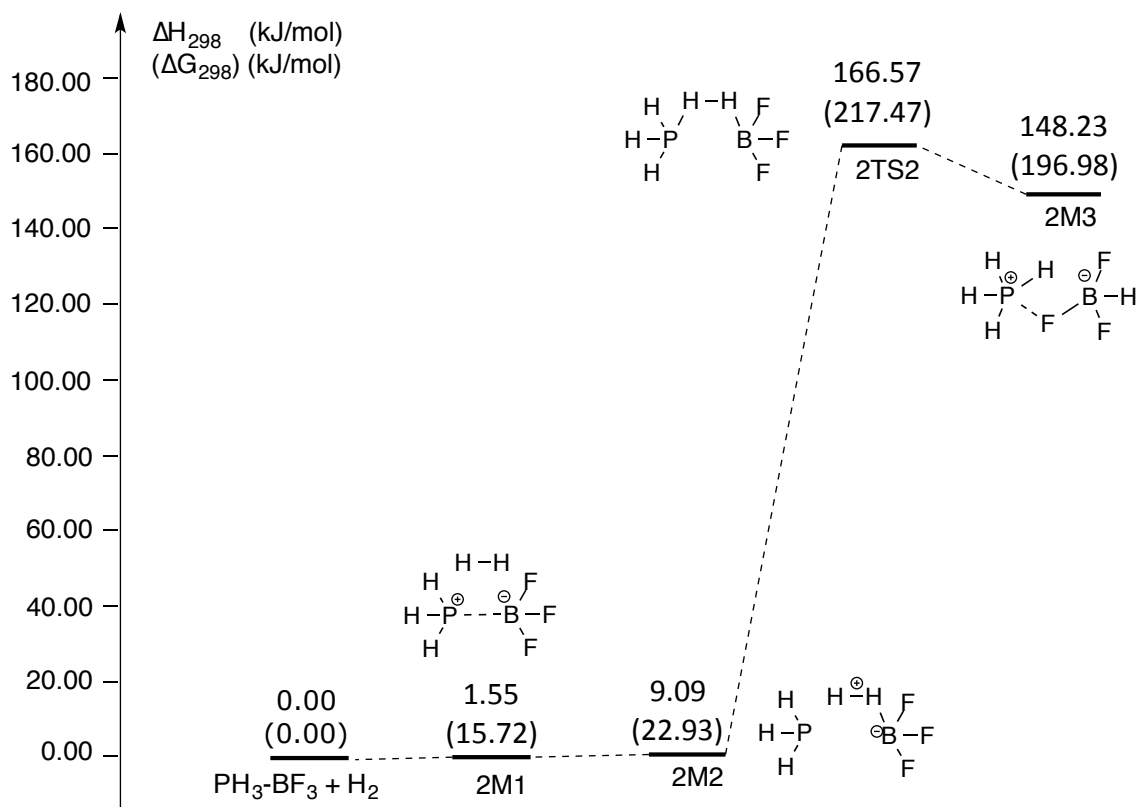
From the analysis above, the hydrogen activation by PH₃-BH₃ contains two steps, first, the dative bond breaks and the distance between Lewis acid and base elongates, and the conformation of BH₃ changes from pyramidal to planar. During this step, charge is transferred from Lewis acid to Lewis base. In the first step, the deformation is necessary for the complexation of H₂ and BH₃. The second step involves the hydrogen bond breaking and charge transfer from PH₃ to BH₃ through bridged H-H until reaching the equilibrium structure, and the second step is the rate-determining step for the whole reaction.

In intramolecular frustrated Lewis pairs, it is also found that the preorganization step is essential for reaction, and this preorganization reduces the energy gap between HOMO and LUMO of the components to form a “reactive pocket”, which is the active site of the frustrated complex and the key to their unique reactivity.²⁴ Because of the steric hindrance, the distance between Lewis acid and base can hardly be changed. In intramolecular phosphane–borane FLPs²¹, it has been found that before hydrogen cleavage, the bond between phosphane and borane breaks for the incoming H₂. The analysis of the PH₃-BH₃ activating hydrogen model shows that, for the strongly bound Lewis pairs, the interaction between Lewis acid and Lewis base should be broken first, so that H₂ can complex with the Lewis acid to prepare for the H-H bond splitting.

3.2.2 Weakly Bound Lewis Pair



Compared with PH₃-BH₃ ($\Delta H_{298} = -95.46$ kJ/mol, at MP2/cc-pVTZ level in the gas phase), PH₃-BF₃ is a weakly bound Lewis pair ($\Delta H_{298} = -8.13$ kJ/mol, at MP2/cc-pVTZ level in the gas phase).



Scheme 3.2. Hydrogen activation by $\text{PH}_3\text{-BF}_3$ at MP2(FC)/cc-pVTZ level in the gas phase. Free energies are shown in parentheses.

The overall reaction enthalpy and free energy show that the reaction of $\text{PH}_3\text{-BF}_3$ with H_2 is a strongly endothermic reaction (Scheme 3.2). But compared with the reaction of $\text{PH}_3\text{-BH}_3$ with H_2 , it is found that the first step for P-B bond breaking is barrierless. This is because the interaction between Lewis base PH_3 and Lewis acid BF_3 is rather weak, which is -8.13 kJ/mol at MP2(FC)/cc-pVTZ level. The distance between PH_3 and BF_3 is 310.4 pm in **2M1** (shown in Figure 3.4). The free energy difference between the intermediate **2M1** and **2M2** is 7.21 kJ/mol. In **2M2**, $r(\text{P-B})$ is 398.5 pm, which is in the suitable range of a FLP.²⁹ In second step involving hydrogen splitting, activation free energy is 217.47 kJ/mol in the gas phase. In the transition state **2TS2**, $r(\text{P-B})$ is reduced to 298.8 pm so that PH_3 can approach one hydrogen in the $\text{H}_2\text{-BF}_3$ complex. The final product is **2M3** with $r(\text{P-B}) = 299.8$ pm.

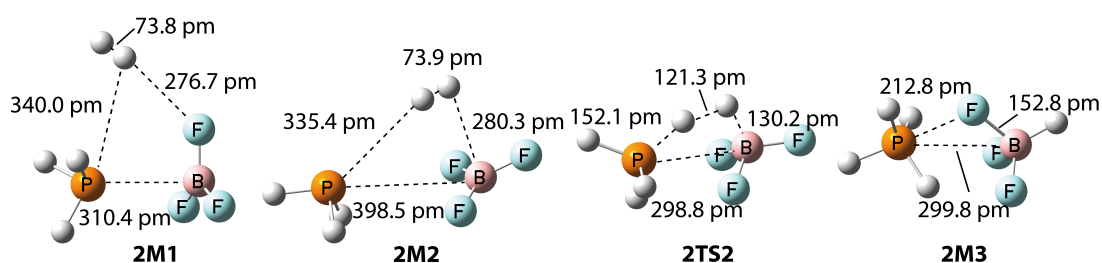
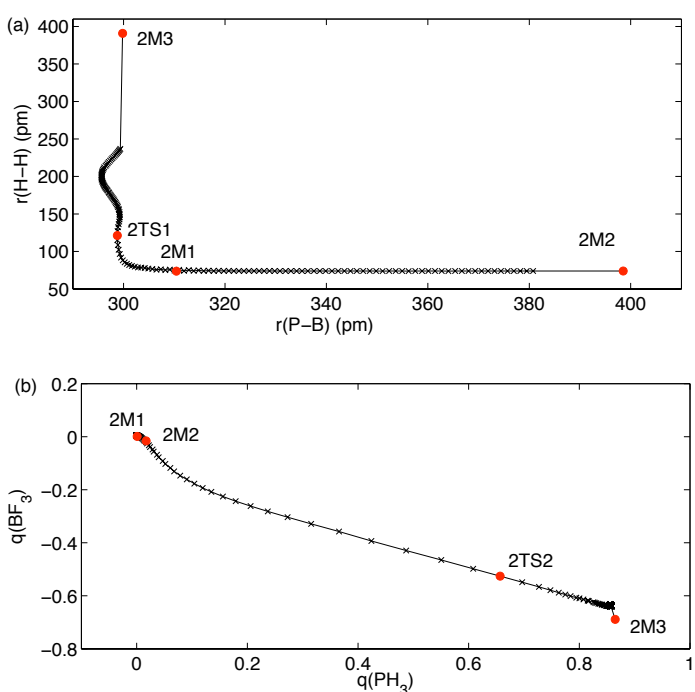


Figure 3.4. Structures of intermediates and transition states in the reaction of $\text{PH}_3\text{-BF}_3$ with H_2 in the gas phase at MP2/cc-pVTZ level.

Table 3.2. Structure parameters and NBO analysis of intermediates and transition states for the reaction of $\text{PH}_3\text{-BF}_3$ with H_2 at MP2/cc-pVTZ level in the gas phase.

$\text{H}_b\text{-H}_a$	$\text{H}_2\text{-P}^{\oplus}$	$\text{B}-\text{F}_7^{\ominus}$	2M1	2M2	2TS2	2M3
d(base) ($^{\circ}$)	95.5		94.4	109.5	119.7	
d(acid) ($^{\circ}$)	173.0		178.4	128.4	114.3	
$\angle \text{H}_a\text{H}_b\text{P}$ ($^{\circ}$)	—		161.9	158.7	—	
$\angle \text{H}_b\text{H}_a\text{B}$ ($^{\circ}$)	—		82.6	101.3	—	
q(BF_3)	0.017		0.001	-0.526	-0.689	
q(PH_3)	-0.016		0.001	0.657	0.865	
q(H_b)	0.008		0.008	0.130	0.040	
q(H_a)	-0.009		-0.009	-0.261	-0.216	

In the reaction of $\text{PH}_3\text{-BF}_3$ activating H_2 , even though the interaction between PH_3 and BF_3 is weak, but the first step is breaking the connection between Lewis acid and base, which is reorganized for hydrogen splitting in the next step. In the first step, the dihedral angles of PH_3 and BF_3 moieties in **2M1** are almost identical with that in **2M2**, and dihedral angles of the PH_3 and BF_3 in Table 3.2 show that there is no big change on geometry of Lewis acid and Lewis base moieties in the first step. But in the second step, the conformation of BF_3 changes from planar to pyramidal, and d(acid) changes from 178.4° in **2M2** to 114.3° in **2M3**. Because of the interactions between the fluorine in BF_3 and the hydrogen atoms in PH_3 moiety, d(base) in **2M3** is bigger than in **2M2**. In transition state **2TS2**, the angle of HHP is 158.7° , which is non-linear. More analysis are carried out and shown in Figure 3.5.



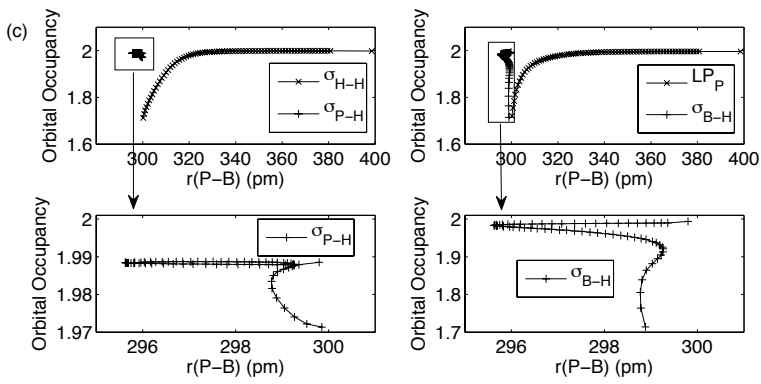


Figure 3.5. Reaction of $\text{PH}_3\text{-BF}_3$ with H_2 . (a) Correlation between $r(\text{P-B})$ and $r(\text{H-H})$ at MP2/cc-pVTZ level in the gas phase. (b) NBO charge of PH_3 vs BF_3 (c) Orbital occupancy from NBO analysis along IRC from **2M1** to **2M2** via **2TS2** at MP2/cc-pVTZ level of theory.

The results of NBO analysis for the reaction of $\text{PH}_3\text{-BF}_3$ with H_2 along the IRC determination at MP2/cc-pVTZ level are shown in Figure 3.5. Figure 3.5 (a) indicates that the reaction consists of two stages. The first step is from **2M1** to **2M2**, and the mainly difference is $r(\text{P-B})$ elongated, but $r(\text{H-H})$ possesses no change. The second stage is from **2M2** to **2M3** via **2TS2**. At the beginning of this step, $r(\text{P-B})$ is reduced so that PH_3 can interact with $\text{H}_2\text{-BF}_3$. When $r(\text{P-B})$ is reduced to 300 pm, the hydrogen bond begins to break. At the end of the reaction, the PH_3 and BF_3 moieties rotate to form the interactions between the fluoro substituents and the phosphorous center, which is shown as a curve in Figure 3.5 (a).

Details of charge transfer processes during the reaction are shown in Figure 3.5 (b). Because $r(\text{P-B})$ is 310.4 pm in **2M1**, there are hardly any interactions between PH_3 and BF_3 , and the charge on the PH_3 and BF_3 moieties are almost zero. From **2M2** to **2TS2**, the distance between PH_3 and BF_3 is reduced with subsequent H_2 activation and charge donation from PH_3 to BF_3 via the H-H bond.

Figure 3.5 (c) reflects the changing of orbital occupancy from **2M2** to **2M3**. NBO analysis indicates that before transition state **2TS2** no bond is formed between BF_3 and the hydrogen atom. But the occupancy of $\sigma^*(\text{H}_2)$ is increasing while the occupancy of lone pair orbital is decreasing. After the transition states, the H-P bond is formed early than the B-H bond and the charge is transferred to H_a atom first which is close to BF_3 to form a hydride ion. This unstable hydride ion connects with BF_3 rapidly and the new B-H bond is formed. After **2TS2**, the charge keeps on transferring from PH_4^+ to HBF_3^- , and the product **2M2** is formed.

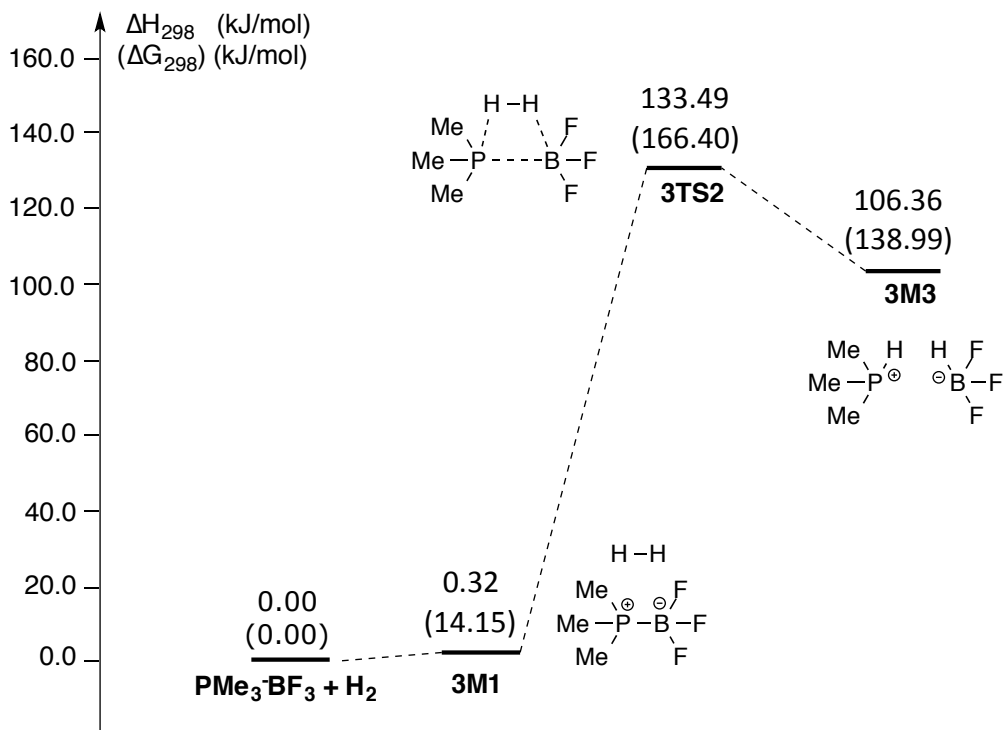
Comparing the hydrogen activation by $\text{PH}_3\text{-BH}_3$ and $\text{PH}_3\text{-BF}_3$, both reactions have two steps. Firstly the interaction between Lewis acid and base are cancelled by the Lewis acid donating the charge to Lewis base, and the distance between acid and base is elongated. The consequences are following: the hydrogen molecule can enter the cavity between the reaction center and complex with Lewis acid, which is essential for the next step. In the second step the Lewis base approaches the H_2 -Lewis acid complex and starts interacting. During this procedure, Lewis base donates the electron pair to Lewis acid through the H-H bond. The first step for $\text{PH}_3\text{-BF}_3$ reacting with H_2 is found to be barrierless, this is because PH_3 and BF_3 are weakly bonded with each other, and the $r(\text{P-B})$ in $\text{PH}_3\text{-BF}_3$ is much longer compared to $\text{PH}_3\text{-BH}_3$, furthermore the deformation energy is negligible for the PH_3 and BF_3 in $\text{PH}_3\text{-BF}_3$.

3.2.3 PMe₃-BF₃

The activation capabilities of FLP systems are greatly impacted by the substituent, which is usually a bulky group. Hereby, PMe₃-BF₃ is taken as a model to study the mechanism including substituent effects. The reaction (3) is as follows:



The complexation energy of $\text{PMe}_3\text{-BF}_3$ is -55.63 kJ/mol at MP2(FC)/cc-pVTZ level in the gas phase, which is 39.38 kJ/mol smaller than that of $\text{PH}_3\text{-BH}_3$. The mechanism of hydrogen activation is shown in Scheme 3.3.



Scheme 3.3. Mechanism and reaction profile of H_2 activation by $\text{PMe}_3\text{-BF}_3$ at MP2/cc-pVTZ level of theory in the gas phase, and free energies are shown in parentheses.

The reaction of $\text{PMe}_3\text{-BF}_3$ with H_2 proceeds through a single transition state **3TS2** to generate product complex **3M3** (Scheme 3.3) and the total reaction is endothermic by 106.36 kJ/mol. The activation free energy needed for the H_2 activation is 166.40 kJ/mol at MP2/cc-pVTZ level in the gas phase. Structures of intermediates and transition states are shown in Figure 3.6.

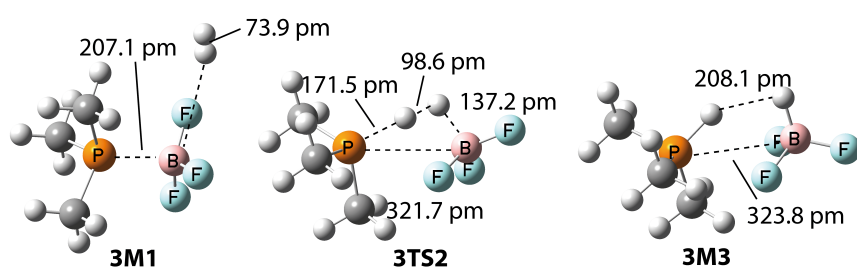


Figure 3.6. Intermediates and transition states for the reaction of H_2 activation by $\text{PMe}_3\text{-BF}_3$ at MP2/cc-pVTZ level in the gas phase.

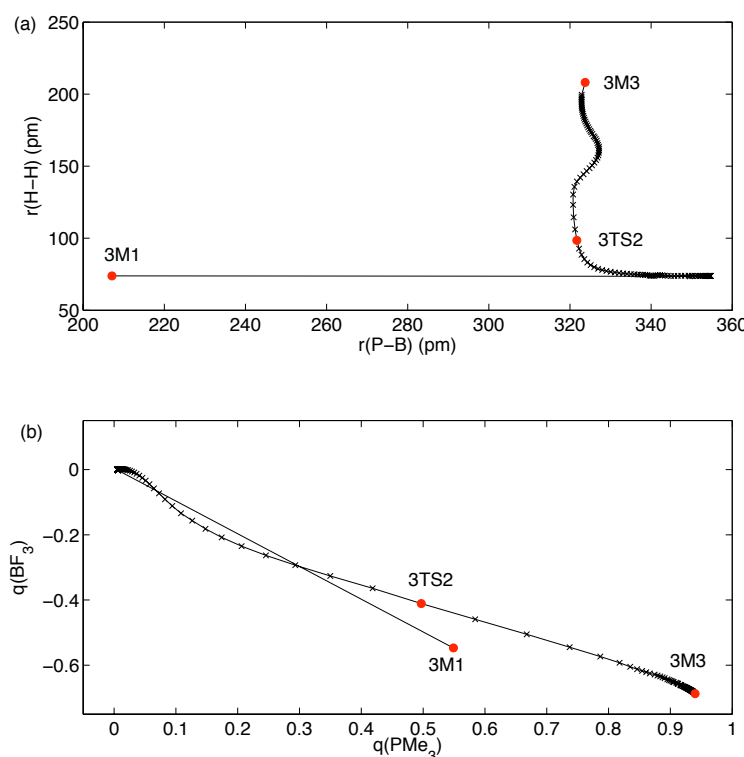
Because of the substituents on the Lewis center, the reaction procedure of $\text{PMe}_3\text{-BF}_3$ with H_2 is changed, and the P-B bond breaking and hydrogen bond splitting occur simultaneously.

Table 3.3. Structure parameters and NBO analysis of intermediates and transition states for the reaction of H₂ with PMe₃-BF₃ at MP2/cc-pVTZ level in the gas phase.

H _b -H _a	3M1	3TS2	3M3
d(base) (°)	112.4	110.2	117.7
d(acid) (°)	132.3	134.0	119.3
∠H _a H _b P (°)	-	172.2	143.0
∠H _b H _a B (°)	-	103.7	86.4
q(BF ₃)	-0.547	-0.411	-0.687
q(PMe ₃)	0.549	0.497	0.940
q(H _b)	0.026	0.146	0.027
q(H _a)	-0.028	-0.232	-0.281

Through the addition of the methyl substituents to the phosphorous center, the d(base) is expanded compared to d(base) in PH₃-BH₃, but d(acid) in PMe₃-BF₃ is much smaller than d(acid) in PH₃-BH₃. In the transition state **3TS2**, the angle of H_aH_bP is 172.2°, which is close to linear. Comparing the dihedral angles of the Lewis acidic and basic moiety in **3M1**, **3TS2** and **3M3**, d(acid) are almost identical and d(acid) in **3M3** is smaller than that in **3M1**.

NBO analysis has been carried out along the IRC pathway and the results are shown in Figure 3.7.



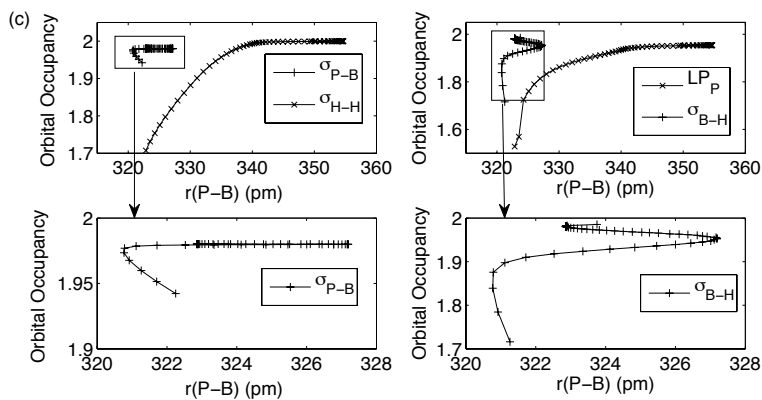
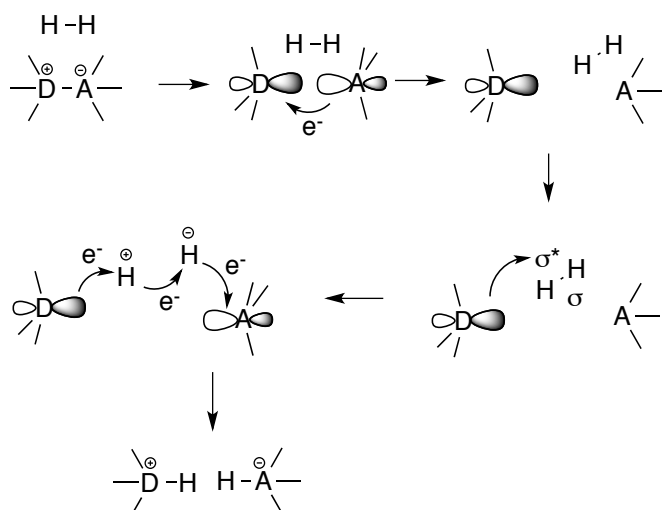


Figure 3.7. Reaction of H₂ with PMe₃-BF₃ (a) Correlation between r(P-B) and r(H-H) at MP2/cc-pVTZ level in the gas phase. (b) NBO charge of PMe₃ vs BF₃ (c) Orbital occupancy from NBO analysis along IRC from 3M1 to 3M3 via 3TS2 at MP2/cc-pVTZ level of theory.

The results of Figure 3.7 show that, during the reaction, r(P-B) is elongated without generating any intermediate. Even though, r(P-B) still shows the same trend as PH₃-BH₃ and PH₃-BF₃, that is, r(P-B) increases firstly, followed by a subsequent decrease. The minimum bond distance is obtained in transition states, which involves the breaking of the H-H bond by the Lewis base. Figure 3.7 (b) indicates that charge separation is an essential loop, and in this loop the charge initially is transferred from BF₃ to PMe₃ until both are neutral. After that, the charge is transferred back from PMe₃ to BF₃ via the H-H bond. It is noteworthy that the formation of the P-H_b bond is earlier than that of the B-H_a bond.

Compared with the reaction of PH₃-BF₃ with H₂, the reaction of PMe₃-BF₃ with H₂ has a similar characteristic. Although one step can achieve the same results, the activation free energy is quite different. The rate-determining step for PH₃-BF₃ has an energy barrier of 217.47 kJ/mol, while the activation free energy for PMe₃-BF₃ is 166.40 kJ/mol. The rate-determining step is closely related to the substituents attaching to the Lewis center. Increasing the Lewis basicity while the Lewis acid retains, the activation energy for the rate-determining step will be significantly reduced. From the three reaction models, the mechanism of hydrogen activation by Lewis pairs is summarized as Scheme 3.4.



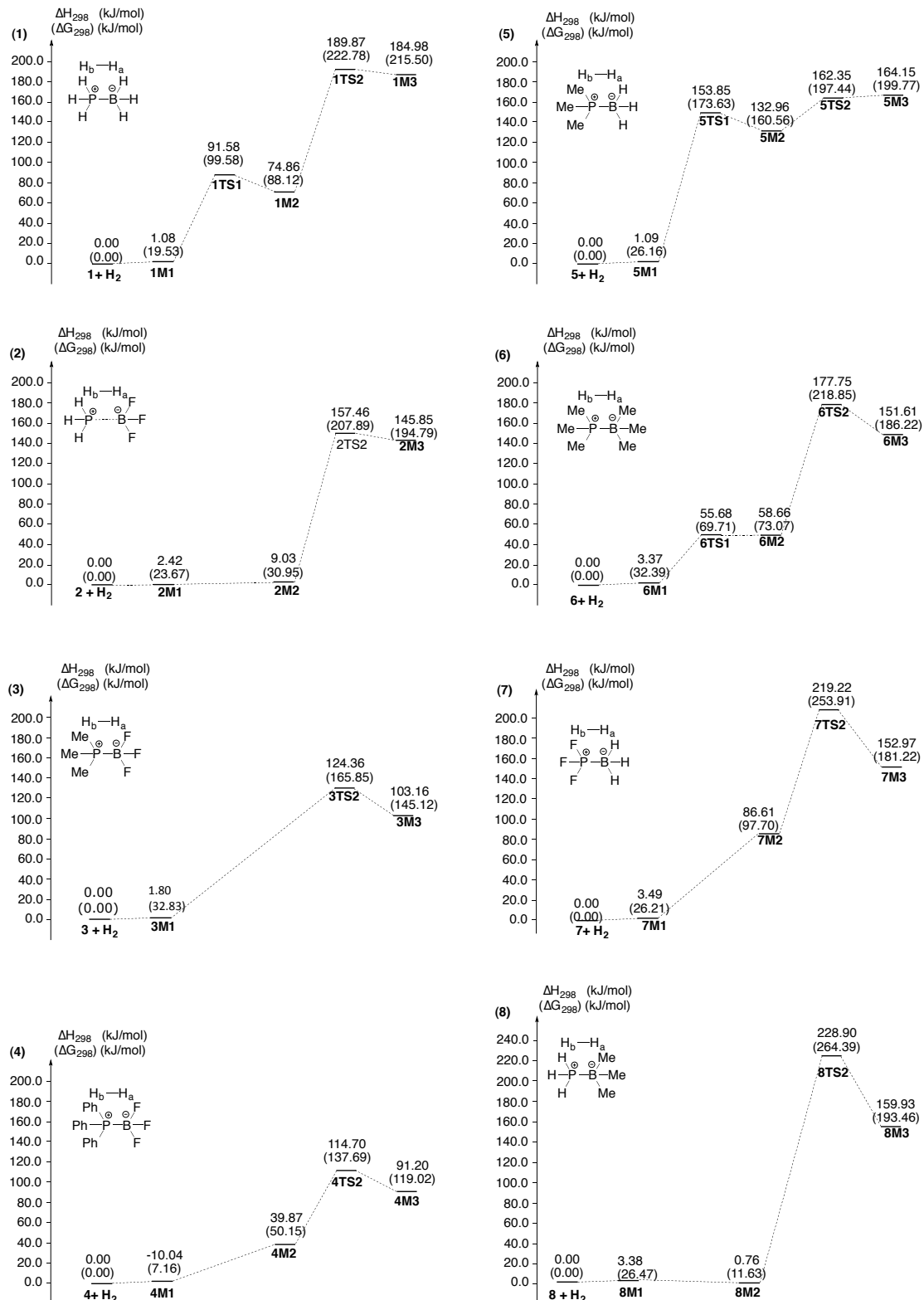
Scheme 3.4. General mechanism for hydrogen activation by Lewis pairs.

Based on the three models, it is found that for the reaction of normal Lewis pairs with H₂, a preorganization step must exist. In this step, the (P-B) bond distance is elongated and the

dative bond is broken by charge transferring from Lewis acid to Lewis base. This step will stop until moieties are neutral. At the end of this step, Lewis base is completely separated from the Lewis acid and H₂ is weakly bonded to the Lewis acid to form an adduct. Only under these circumstances, the hydrogen molecule is allowed to enter the reaction region. This is the so called preorganization. The second step starts with the Lewis base attaches the H₂-BF₃ adduct so that the base can interact with H₂ fragment. The Lewis base approaches the H₂ and at the same time the lone pair of the base is donating electron density into the anti-bonding σ*(H-H). The P-H_b bond is formed faster than the B-H_a bond. In the transition state for heterolytic cleavage of hydrogen, the four atoms P—H_b—H_a—B are not in the same line, and the angle of HHP is less than 180°. The energy profiles show that, for these three reaction mechanisms, the total reaction is strongly endothermic. The reaction energy of the first step is approximately the complexation energy of the Lewis pairs. The step for heterolytic cleavage of hydrogen is the rate-determining step, but the substituent connected to the Lewis center has a big impact on this activation energy. In the following studies, more reaction systems have been examined to find the relation between structure properties and activation energy.

3.2.4 The Connection between Activation Energy and Structural Properties

Structural properties of chemical species, such as bond distances, and bond angles, determine the reactivity of chemical intermediates. The relationship between structure properties and reactivity is a powerful tool for the prediction of product outcome as well as catalyst design.³⁰⁻³³ In order to illuminate the connection between structural properties and reactivity, more research on Lewis pair systems has been carried out. The DFT method ωB97XD with cc-pVTZ basis set is performed for the reaction of Lewis pairs with H₂, because of the economic cost and high accuracy.



Scheme 3.5. The energy profiles of hydrogen activation by different Lewis pairs at the ω B97XD/cc-pVTZ level in the gas phase.

In total eight Lewis pairs have been investigated for hydrogen activation and the energy profiles are displayed in Scheme 3.5. For the eight different systems, the activation free energies for hydrogen activation reactions are quite different, varying from 137.69 to 264 kJ/mol. This diversity mainly depends on the substitution pattern of the Lewis pairs. The

substituent effects have influences on both geometry and activation energy. The geometries of different transition states are shown in Figure 3.8.

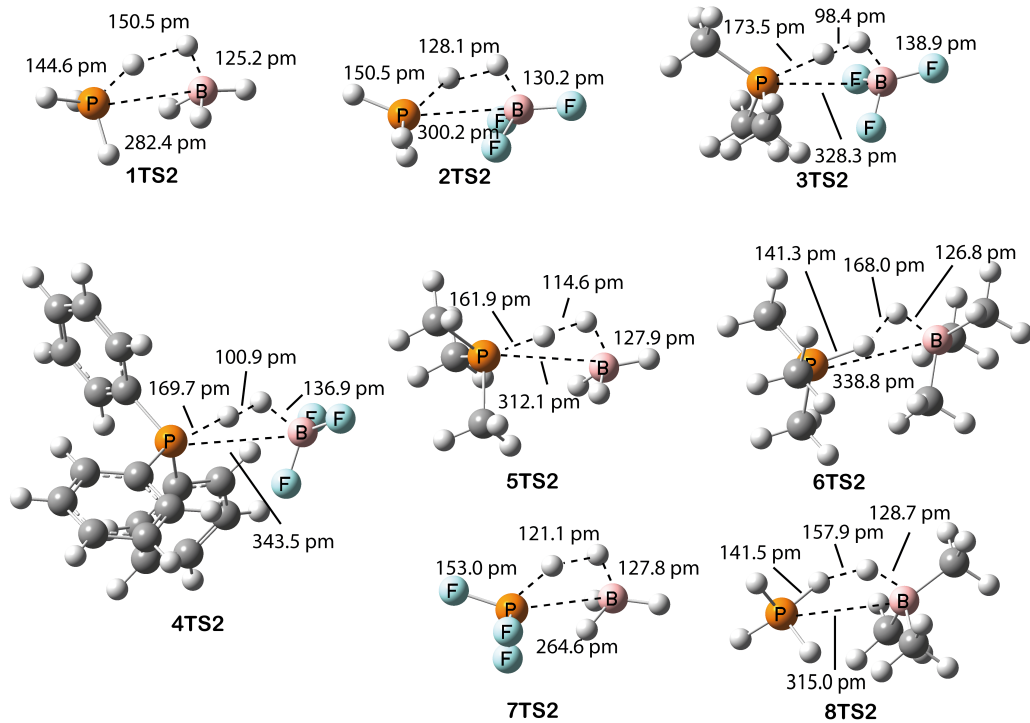


Figure 3.8. Structures of transition states of the hydrogen splitting step at ω B97XD/cc-pVTZ level in the gas phase.

Table 3.4. Structural information of intermediates and transition states for different Lewis pairs at ω B97XD/cc-pVTZ level in the gas phase.

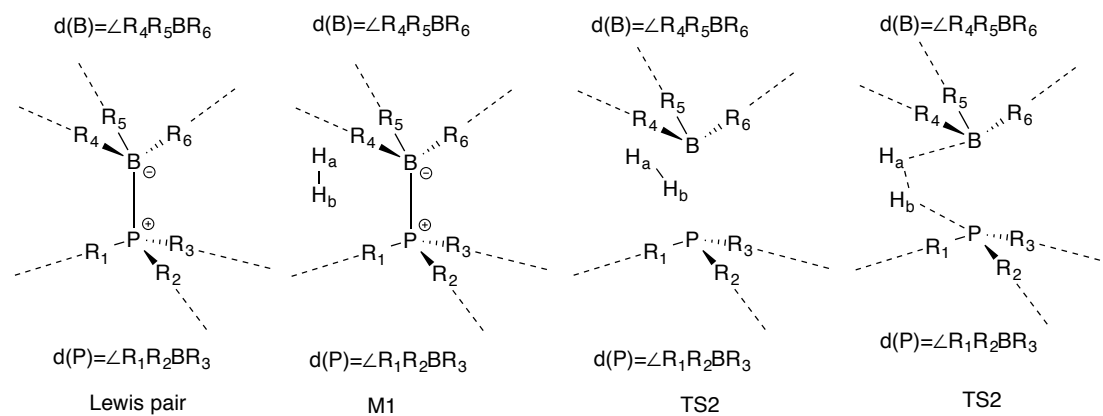
	1	2	3	4	5	6	7	8
r(P-B) (pm)	193.7	315.9	207.9	211.8	191.1	198.5	185.8	205.8
d(P) ($^{\circ}$)	102.1	95.4	112.9	113.2	109.6	109.6	102.2	101.5
d(B) ($^{\circ}$)	135.4	173.2	132.4	133.2	131.4	129.6	138.3	135.2
q(base)	0.597	0.015	0.525	0.475	0.700	0.672	0.705	0.521
q(acid)	-0.597	-0.015	-0.525	-0.475	-0.700	-0.672	-0.705	-0.521
	1M1	2M1	3M1	4M1	5M1	6M1	7M1	8M1
r(P-B) (pm)	193.7	315.9	207.9	211.8	191.1	198.5	185.8	205.8
d(P) ($^{\circ}$)	102.3	95.6	113.1	113.0	109.6	109.9	102.2	101.6
d(B) ($^{\circ}$)	135.1	172.6	132.1	132.5	131.0	129.2	138.1	134.5
q(base)	0.602	0.016	0.528	0.480	0.703	0.675	0.707	0.524
q(acid)	-0.601	-0.015	-0.524	-0.477	-0.700	-0.672	-0.706	-0.523
q(H _b)	0.010	0.006	0.021	-0.017	0.012	-0.001	0.000	-0.004
q(H _a)	-0.012	-0.006	-0.025	0.015	-0.015	-0.002	-0.001	0.003
	1M2	2M2	3M2	4M2	5M2	6M2	7M2	8M2
r(P-B) (pm)	384.1	399.5	—	399.4	363.7	424.9	362.2	419.7
d(P) ($^{\circ}$)	94.9	94.4	—	105.2	102.7	101.3	98.6	94.2
d(B) ($^{\circ}$)	145.7	178.0	—	177.4	142.6	178.2	144.8	178.9
\angle HHP ($^{\circ}$)	161.6	165.4	—	171.2	163.2	168.5	160.1	162.4
q(base)	0.011	0.002	—	0.004	0.035	0.011	0.009	0.002
q(acid)	-0.407	0.000	—	0.003	-0.429	-0.006	-0.399	-0.003
q(H _b)	0.201	0.004	—	0.002	0.217	-0.014	0.183	0.004
q(H _a)	0.195	-0.006	—	-0.009	0.178	0.009	0.207	-0.003

	1TS2	2TS2	3TS2	4TS2	5TS2	6TS2	7TS2	8TS2
r(P-B) (pm)	282.4	300.2	328.3	343.5	312.1	338.8	264.6	315.0
r(H _b -H _a) (pm)	150.5	128.1	98.4	100.9	114.6	168.0	121.1	157.9
r(P-H _b) (pm)	144.6	150.5	173.5	169.7	161.9	141.3	153.0	141.5
r(B-H _a) (pm)	125.2	130.1	138.9	136.9	127.9	126.8	127.8	128.7
d(P) (°)	108.0	109.9	110.7	114.0	112.3	119.4	99.8	113.9
d(B) (°)	122.9	127.4	133.9	132.8	129.6	122.9	125.4	125.1
∠HHP (°)	143.7	155.6	172.4	174.5	175.0	126.5	143.1	111.2
∠HHB (°)	93.0	101.8	105.6	108.8	93.9	90.9	92.1	105.9
q(base)	0.617	0.624	0.461	0.479	0.536	0.770	0.489	0.654
q(acid)	-0.728	-0.545	-0.412	-0.431	-0.671	-0.784	-0.549	-0.707
q(H _b)	0.168	0.123	0.120	0.124	0.165	0.144	0.099	0.187
q(H _a)	-0.057	-0.203	-0.169	-0.177	-0.030	-0.131	-0.039	-0.134
ΔG ₂₉₈ [#] (kJ/mol)	222.78	207.89	165.85	137.69	197.44	218.85	253.91	264.39

Substituent effects are the important issue for FLP, which include steric hindrance and electron static effects. With the increasing of steric hindrance, the distance between Lewis acid and Lewis base will apparently increase accordingly and this influence is not only reflected in intermediates, but also in transition states. Take Lewis pairs **2**, **3** and **4** as examples, which represent PH₃-BF₃, PMe₃-BF₃ and PPh₃-BF₃, respectively. Because Lewis pairs **2** is proved to be a weakly bound system, the r(P-B) in **2** is 315.9 pm. But for **3** and **4**, the substituents changes from methyl to phenyl group on Lewis base, the r(P-B) are increasing from 207.9 pm to 211.8 pm. The r(P-B) in **5** and **6** also proves bond distance correlates with steric hindrance. r(P-B) in **5** is 191.1 pm, but in trimethylphosphine-trimethylboron complex (**6**), r(P-B) is 198.5 pm. In the transition state **2TS2**, **3TS2** and **4TS2**, r(P-B) are 300.2 pm, 328.3 pm and 343.5 pm, respectively. These data indicate r(P-B) increases with steric hindrance in the transition states for the H-H bond breaking. For r(H_b-H_a), the order in **2**, **3** and **4** is r(H_b-H_a, **3TS2**) < r(H_b-H_a, **4TS2**) < r(H_b-H_a, **2TS2**). These data show r(H_b-H_a) has no directly relationship with steric hindrance.

Steric hindrance has also influences on NBO charge distribution. In Lewis base of **2**, **3** and **4**, charge distributions are shown as q(base, **2**) < q(base, **4**) < q(base, **3**) and q(acid, **3**) < q(acid, **4**) < q(acid, **2**). For the transition states, q(base, **3TS2**) < q(base, **4TS2**) < q(base, **2TS2**) and q(acid, **2TS2**) < q(acid, **4TS2**) < q(acid, **3TS2**). For **5** and **6**, which represent PMe₃-BH₃ and PMe₃-BMe₃, q(base, **5TS2**) < q(base, **6TS2**) and q(acid, **6TS2**) < q(acid, **5TS2**). All these results show that there is no direct connection between charge distribution and steric hindrance.

Steric hindrance impacts on the dihedral angles in Lewis pairs (Scheme 3.6).



Scheme 3.6. Dihedral angle of Lewis pairs, intermediates and transition states.

The monomer borane is a planar but the dihedral angle of the PH_3 monomer is 94.0° at $\omega\text{B97XD/cc-pVTZ}$ level. The dihedral angles are impacted by the steric hindrance. For instance, with the order of the sterice hindrance $2 < 3 < 4$, the orders of the dihedral angles are in the order of $d(\text{P}, 2) < d(\text{P}, 3) < d(\text{P}, 4)$ and $d(\text{B}, 3) < d(\text{B}, 4) < d(\text{B}, 2)$. The dihedral angles in transition states are in the order of $d(\text{P}, \text{2TS2}) < d(\text{P}, \text{3TS2}) < d(\text{P}, \text{4TS2})$ and $d(\text{B}, \text{2TS2}) < d(\text{B}, \text{4TS2}) < d(\text{B}, \text{3TS2})$. For the Lewis pairs **5** and **6**, the substituent on the Lewis acid is changed form hydrogen to methyl gourp, the dihedral angle changes in the order of $d(\text{P}, \text{5}) = d(\text{P}, \text{6})$ and $d(\text{B}, \text{6}) < d(\text{B}, \text{5})$. And in the transition states, the dihedral angle is in the order of $d(\text{P}, \text{5TS2}) < d(\text{P}, \text{6TS2})$ and $d(\text{B}, \text{6TS2}) < d(\text{B}, \text{5TS2})$. These data about dihedral angles also show that there is no simple linear correlation with steric hindrance.

The relationship between structural properties and reaction energy and activation energy is a very useful tool to predict the reactivity of the Lewis pair for hydrogen activation. Because there are not so much experimental thermochemistry data for Lewis pairs activating hydrogen, the theoretical calculation data is used for the quantitative description. And based on the theoretical calculation, the prediction values will be very helpful for selection of catalysts on the experiment.

From the data collected in Table 3.4, the correlation between bond distance and free activation energy is shown in Figure 3.9.

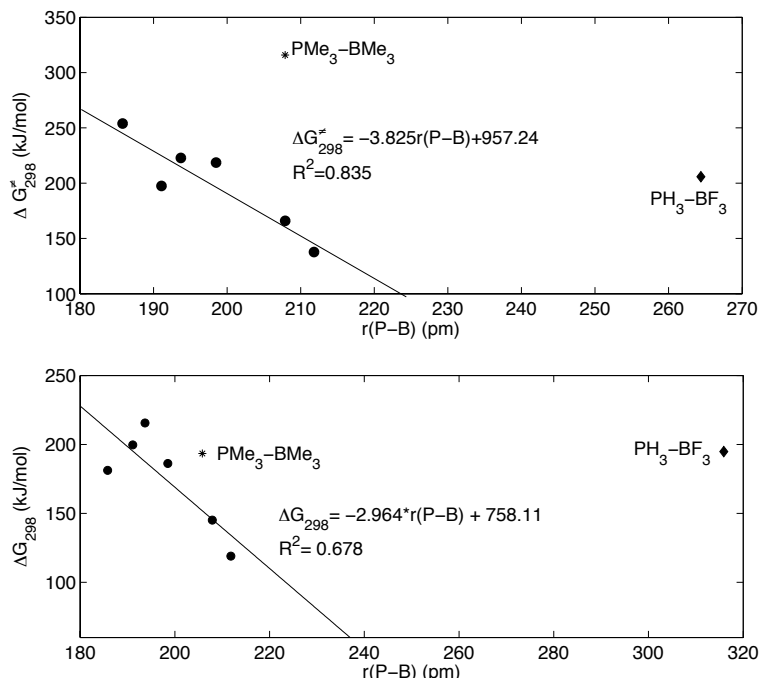


Figure 3.9. Correlation between bond distance and energy. (a) $r(\text{P-B})$ correlated with activation free energy (ΔG^{\ddagger}) at $\omega\text{B97XD/cc-pVTZ}$ level. $r(\text{P-B})$ is P-B bond distance in Lewis pairs without H_2 . (b) $r(\text{P-B})$ correlates with reaction free energy at $\omega\text{B97XD/cc-pVTZ}$ level in the gas phase. $r(\text{P-B})$ is P-B bond distance in Lewis pairs without H_2 . ΔG_{298} is the energy difference of products and reactants.

$\text{PH}_3\text{-BF}_3$ is weakly bound Lewis pair with $r(\text{P-B})$ as 315.9 pm which is much longer than that of other Lewis pairs, apparently $\text{PH}_3\text{-BF}_3$ is weakly bound Lewis pair, and $r(\text{P-B})$ is larger than the bond distance in other Lewis pairs. By analyzing the data, $\text{PH}_3\text{-BF}_3$ and $\text{PMe}_3\text{-BMe}_3$ are set as outliers. The correlation between activation energy and $r(\text{P-B})$ is $\Delta G_{298}^{\ddagger} = -3.8253 \times r(\text{P-B}) + 957.24$ with $R^2 = 0.835$ shown in Figure 3.9. This formula can be used for activation free energy prediction using P-B bond distance in the Lewis pairs. The correlation

$\Delta G_{298} = -2.946 \times r(P-B) + 758.11$ with $R^2 = 0.678$ is used for predicting the reaction free energy.

3.3 Conclusions

The mechanistic studies show that normal Lewis pairs are able to activate hydrogen molecule with high activation energies. The NBO analysis suggests that the reaction begins with the P-B bond breaking by elongating the distance between Lewis acid and Lewis base. During this step the charge transfers from Lewis acid to Lewis base. This procedure will stop once Lewis acid and Lewis base are neutral. The first step is preorganization for the next step, that is, the dative bond breaks and H₂ comes close to the reaction center. The second step is that Lewis base comes close to H₂ and takes one H atom. In this stage the charge transfers back from the Lewis base to the Lewis acid via the H-H bond. The P-H bond forms earlier than the B-H bond. During the course of the charge transfers from Lewis base to Lewis acid, the hydrogen bond will be activated. The investigations on more systems of Lewis pairs activating H₂ show that the steric hindrance will impact bond distances and the dihedral angles. The correlation between r(P-B) and activation energy is obtained as $\Delta G_{298}^\neq = -3.8253 \times r(P-B) + 957.24$, with $R^2=0.835$, which indicates that, with increasing of the bond distance the activation free energy will decrease accordingly. Considering this formula is obtained based on limited systems, in order to further prove this formula more systems need to be calculated and more experimental data should be obtained also.

References

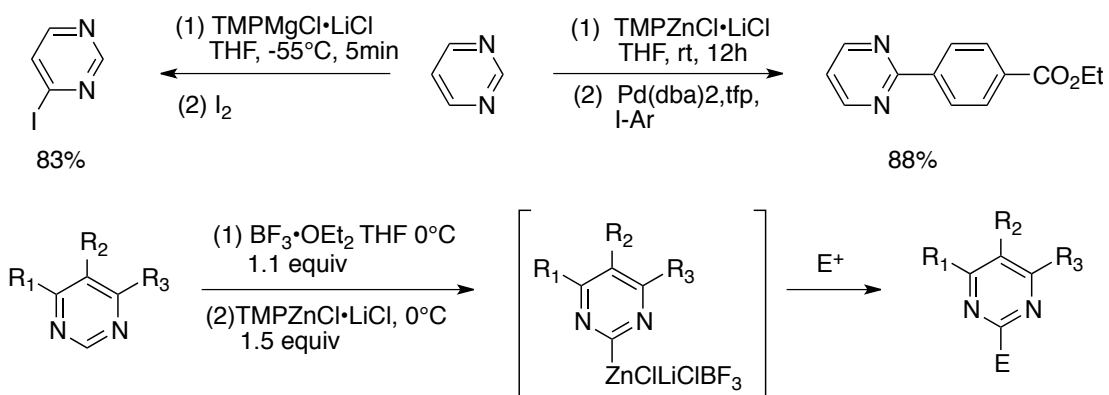
1. G. C. Welch, R. R. S. Juan, J. D. Masuda and D. W. Stephan, *Science*, 2006, **314**, 1124-1126.
2. D. W. Stephan and G. Erker, *Angew. Chem. Int. Ed.*, 2010, **49**, 46-76.
3. D. W. Stephan, *Org. Biomol. Chem.*, 2008, **6**, 1535-1539.
4. D. W. Stephan, *Org. Biomol. Chem.*, 2012, **10**, 5740-5746.
5. A. L. Kenward and W. E. Piers, *Angew. Chem., Int. Ed.*, 2008, **47**, 38-41.
6. D. W. Stephan, S. Greenberg, T. W. Graham, P. Chase, J. J. Hastie, S. J. Geier, J. M. Farrell, C. C. Brown, Z. M. Heiden, G. C. Welch and M. Ullrich, *Inorg. Chem.*, 2011, **50**, 12338-12348.
7. G. Erker, *C. R. Chim.*, 2011, **14**, 831-841.
8. T. Soos, *Pure Appl. Chem.*, 2011, **83**, 667-675.
9. G. Erker, *Organometallics*, 2011, **30**, 358-368.
10. A. Ramos, A. J. Lough and D. W. Stephan, *Chem. Commun.*, 2009, 1118-1120.
11. V. Sumerin, F. Schulz, M. Nieger, M. Leskela, T. Repo and B. Rieger, *Angew. Chem., Int. Ed.*, 2008, **47**, 6001-6003.
12. S. J. Geier and D. W. Stephan, *J. Am. Chem. Soc.*, 2009, **131**, 3476-3477.
13. P. Spies, S. Schwendemann, S. Lange, G. Kehr, R. Froehlich and G. Erker, *Angew. Chem., Int. Ed.*, 2008, **47**, 7543-7546.
14. V. Sumerin, F. Schulz, M. Atsumi, C. Wang, M. Nieger, M. Leskelä, T. Repo, P. Pyykkö and B. Rieger, *J. Am. Chem. Soc.*, 2008, **130**, 14117-14119.
15. H. Wang, R. Fröhlich, G. Kehr and G. Erker, *Chem. Commun.*, 2008, 5966-5968.
16. S. E. Denmark and J. Y. Choi, *J. Am. Chem. Soc.*, 1999, **121**, 5821-5822.
17. G. C. Welch and D. W. Stephan, *J. Am. Chem. Soc.*, 2007, **129**, 1880-1881.
18. S. J. Geier and D. W. Stephan, *J. Am. Chem. Soc.*, 2009, **131**, 3476-3477.
19. S. Gao, W. Wu and Y. Mo, *J. Phys. Chem. A*, 2009, **113**, 8108-8117.
20. M. Pu and T. Privalov, *J. Chem. Phys.*, 2013, **138**, 154305/154301-154305/154312.
21. P. Spies, G. Erker, G. Kehr, K. Bergander, R. Fröhlich, S. Grimme and D. W. Stephan, *Chem. Commun.*, 2007, 5072.
22. T. A. Rokob, I. Bako, A. Stirling, A. Hamza and I. Papai, *J. Am. Chem. Soc.*, 2013, **135**, 4425-4437.
23. R. Ponec and P. Beran, *J. Phys. Chem. A*, 2013, **117**, 2656-2663.
24. I. Bako, A. Stirling, S. Balint and I. Papai, *Dalton Trans.*, 2012, **41**, 9023-9025.

25. S. Grimme, H. Kruse, L. Goerigk and G. Erker, *Angew. Chem. Int. Edit.*, 2010, **49**, 1402-1405.
26. B. Schirmer and S. Grimme, *Chem. Commun.*, 2010, **46**, 7942-7944.
27. T. A. Rokob, A. Hamza, A. Stirling, T. Soos and I. Papai, *Angew. Chem., Int. Ed.*, 2008, **47**, 2435-2438.
28. W. Cui and B. B. Wayland, *J. Am. Chem. Soc.*, 2004, **126**, 8266-8274.
29. L. L. Zeonjuk, N. Vankova, A. Mavrandonakis, T. Heine, G.-V. Röschenthaler and J. Eicher, *Chem. Eur. J.*, 2013, **19**, 17413-17424.
30. C. Nantasesamat, C. Isarankura-Na-Ayudhya and V. Prachayasittikul, *Expert Opinion on Drug Discovery*, 2010, **5**, 633-654.
31. R. Tandon, T. Unzner, T. A. Nigst, N. De Rycke, P. Mayer, B. Wendt, O. R. P. David and H. Zipse, *Chem. Eur. J.*, 2013, **19**, 6435-6442.
32. T. A. Manz, J. M. Caruthers, S. Sharma, K. Phomphrai, K. T. Thomson, W. N. Delgass and M. M. Abu-Omar, *Organometallics*, 2012, **31**, 602-618.
33. T. A. Manz, K. Phomphrai, G. Medvedev, B. B. Krishnamurthy, S. Sharma, J. Haq, K. A. Novstrup, K. T. Thomson, W. N. Delgass, J. M. Caruthers and M. M. Abu-Omar, *J. Am. Chem. Soc.*, 2007, **129**, 3776-3777.

4 Theoretical Studies on the Regioselective Functionalization of Pyrimidines

4.1 Introduction

Heterocyclic and aromatic compounds are an integral part of many biologically active molecules due to their potential biological activities.¹⁻⁴ These structures are present in many pharmaceuticals or agrochemicals.⁵⁻⁷ Nowadays, among the many strategies for the construction of heterocyclic species, cross coupling reactions are powerful examples, especially for forming highly stereospecific carbon–heteroatom and carbon–carbon bonds.⁸⁻¹⁵ The preparation of metal-containing frustrated Lewis pairs as reagent for cross coupling reaction has been reported by Knochel's group.¹⁶⁻¹⁹ LiCl-solubilized 2,2,6,6-tetramethylpiperidyl (TMP) metal bases show highly kinetic basicity, such as $\text{TMPMgCl}\cdot\text{LiCl}$,^{20, 21} $\text{TMPZnCl}\cdot\text{LiCl}$,²² $\text{TMP}_2\text{Zn}\cdot 2\text{MgCl}_2\cdot 2\text{LiCl}$,¹⁸ and $\text{TMP}_3\text{Al}\cdot 3\text{LiCl}$.²³ These TMP–metal bases are compatible with strong Lewis acids, such as $\text{BF}_3\cdot\text{OEt}_2$,^{2, 24} and Et_3Al .²⁵ Thus, the reactivity of the sterically hindered TMP base is not annihilated by $\text{BF}_3\cdot\text{OEt}_2$, but on the contrary, a synergistic effect is observed. This effect allows a regioselective metalation of various substituted pyridines and their derivatives,^{21, 26, 27} which is not possible without the use of this Lewis pair combination. More specifically, mediated by TMP bases (TMPLi or $\text{TMPMgCl}\cdot\text{LiCl}$), the reaction of pyrimidine with iodine can afford 4-iodo-pyrimidine.²⁸ Recently it was discovered that metalation of pyrimidine with $\text{TMPZnCl}\cdot\text{LiCl}$ followed by Negishi cross-coupling²⁹⁻³² with $\text{Pd}(\text{dba})_2$, TFP and 4-iodoethylbenzoate could afford pyrimidine in high yield (shown in Scheme 4.1). This surprising regioselectivity shed light on different mechanistic pathways involving $\text{TMPMetX}\cdot\text{LiCl}$ bases (Met = Mg, Zn). Interestingly, it was observed that pretreatment of pyrimidine with the strong Lewis-acid $\text{BF}_3\cdot\text{OEt}_2$ accelerates significantly the metalation in presence of $\text{TMPZnCl}\cdot\text{LiCl}$. Although the experiment done by Sophia M. Manolikakes from the Knochel group shows that C-H bonds of 5-phenylpyrimidine at C2 and C4 position can be activated by $\text{TMPZnCl}(\text{THF})_2$ or $\text{TMPMgCl}(\text{THF})_2$, the addition of Lewis acid $\text{BF}_3\cdot\text{OEt}_2$ cooperates with TMP affording high regioselective metalation product is still not clarified. Hence theoretical investigations based on DFT method have been carried out in the following discussion.



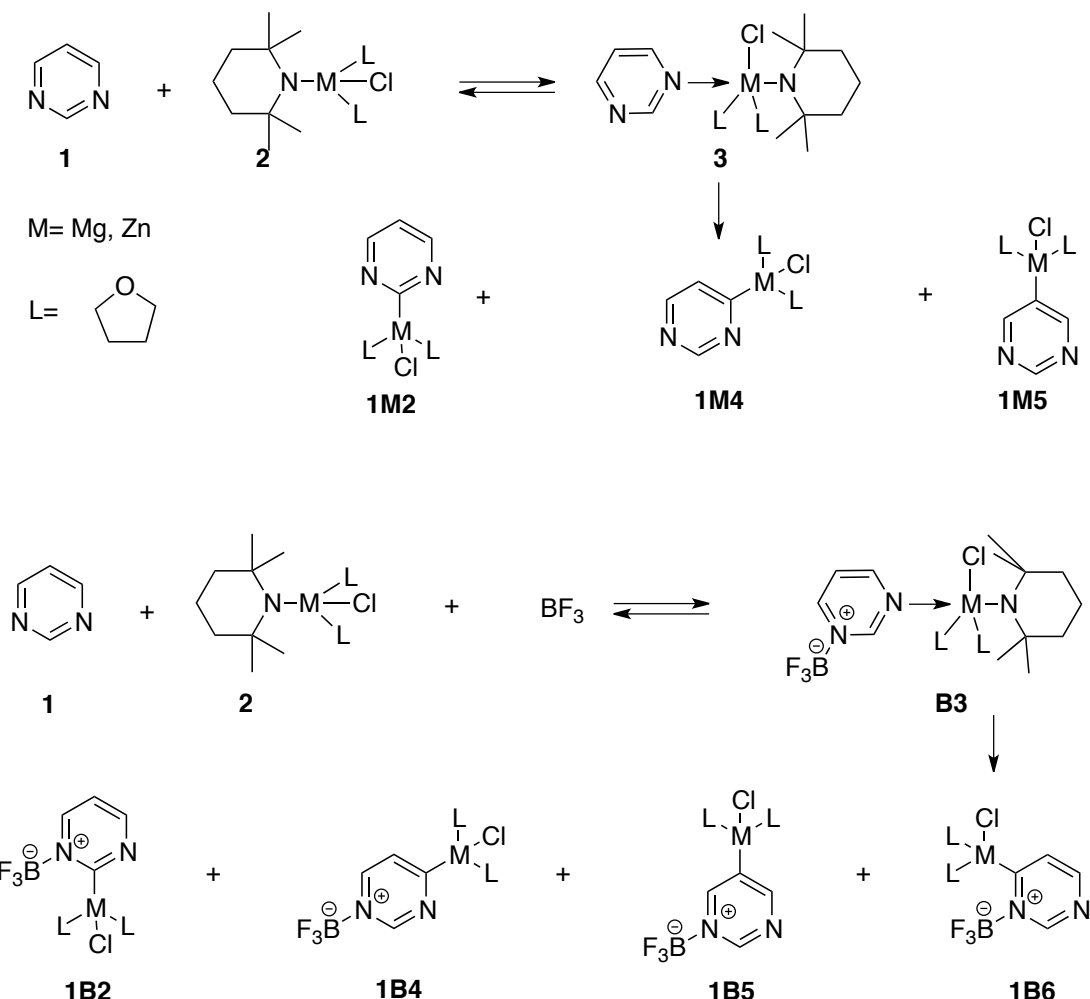
Scheme 4.1. Regioselective metalation of pyrimidines using $\text{TMPMetCl}\cdot\text{LiCl}$ (Met=Mg, Zn).

4.2 Results and Discussions

4.2.1 The Relative Stability of Metalated Pyrimidines

Pyrimidine reacts with sterically hindered metal TMP bases such as $\text{TMPZnCl}\cdot 2\text{THF}$ and $\text{TMPMgCl}\cdot 2\text{THF}$ lead through the initial formation of a Lewis acid/base complex **3** and

subsequent insertion into one of the pyrimidine C-H bonds at C2, C4 or C5 to the organometal species **1M2** to **1M5** (Scheme 4.2).



Scheme 4.2. Regioselective metalation of pyrimidine with or without BF_3 .

Formation of complex **3** is assumed here to involve a pentacoordinated Zn/Mg structure, but losing one of the THF ligands is equally conceivable. Gas phase calculations of the relative stability of intermediates **1M2 – 1M5** for organozinc and organomagnesium reagents have been performed at the B3LYP/631SVP level of theory used in previous studies on related organozinc complexes.^{2, 33-35} The basis set 631SVP includes the Ahlrich all-electron basis set def2-SVP for metal atoms (Zn and Mg) and Pople basis set 6-31G(d,p) for other non-metal atom. The relative enthalpies are shown in Table 4.1.

Table 4.1. Relative enthalpy (ΔH_{298}) of **1M2** to **1M5** at different theory levels (kJ/mol).

	B3LYP/631SVP ^a	B3LYP/631TZVP ^b	B3LYP/6311TZVP ^c
1M2_Mg	0.00	0.00	0.00
1M4_Mg	-3.48	-2.15	-3.43
1M5_Mg	7.01	4.46	8.69
1M2_Zn	0.00	0.00	0.00
1M4_Zn	-3.96	-4.03	-4.92
1M5_Zn	2.46	-1.39	-1.46

^aMetal atom is calculated with B3LYP/def2-SVP and non-metal atoms are calculated at B3LYP/6-31G(d,p) level. ^bMetal atom is evaluated with B3LYP/def2-SVP and non-metal atoms are evaluated at B3LYP/6-31G(d,p) level. ^cMetal atom is calculated with def2-TZVP and non-metal atoms are calculated with 6-311G(d,p).

The data in Table 4.1 shows that deprotonation at C4 position is slightly preferred over position C5 and C2 for both organozinc and organomagnesium species at B3LYP/631SVP level, but the energy differences are relatively small. In order to probe the influence of basis set selection on the calculated relative stabilities, the calculations have been repeated using the larger TZVP basis set on zinc and/or the larger 6-311G(d,p) basis set for all other elements. For both organomagnesium and organozinc systems, the C4 position is slightly energetically preferred over C2 and C5 position, and the energy difference is again rather small. For the organozinc, C5 position is slightly energetically favored than C2 position, while this is not for the organomagnesium systems.

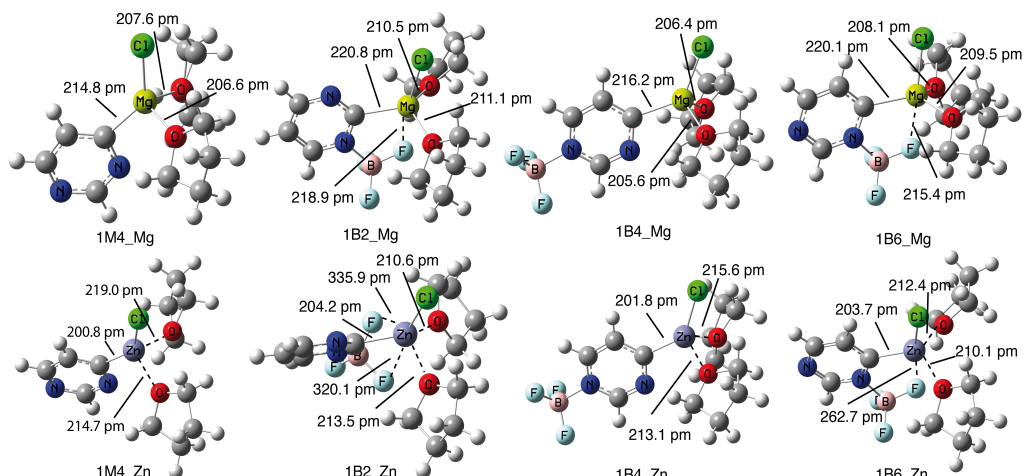


Figure 4.1. Geometries of pyrimidine complexes optimized at B3LYP/6311TZVP level of theory.

The complexation of the organometal species in Scheme 4.2 by BF_3 as Lewis acidic activator can, in principle, lead to the four complexes **1B2 - 1B6** shown in Scheme 4.2. These can, of course, equally well be generated through reaction of TMP base (2) with the preformed BF_3 -pyrimidine complex **B3**. These complexes differ not only in the regioselectivity of the deprotonation step, but also in the relation of the Lewis acid BF_3 and the zinc complex: while these two fragments occupy neighboring positions on the pyrimidine ring in the first two complexes **1B2** and **1B6**, more distant relationships exist in complexes **1B4** and **1B5**. The relative enthalpies are collected in Table 4.2.

Table 4.2. Relative enthalpies (ΔH_{298}) of metallated BF_3 -pyrimidine at B3LYP/ 631SVP and B3LYP/6311TZVP level. (in kJ/mol)

	B3LYP/631SVP ^a	B3LYP/6311TZVP ^b
1B2_Mg	0.00	0.00
1B4_Mg	56.71	44.49
1B5_Mg	56.21	44.55
1B6_Mg	-24.98	-25.92
1B2_Zn	0.00	0.00
1B4_Zn	20.36	20.14

1B5_Zn	16.27	16.61
1B6_Zn	-20.69	-13.27

^aMetal atom is calculated with B3LYP/def2-SVP while non-metal atoms are calculated with B3LYP/6-31G(d,p). ^bMetal atom is evaluated with B3LYP/def2-TZVP and the non-metal atoms are evaluated with B3LYP/6-311G(d,p).

Relative enthalpies in Table 4.2 clearly show that the C6 metalated complex **1B6** is the most energetically favored conformer for both organometallics. the most stable conformer of Mg-pyrimidines is the C6 position metalation product and the energy difference between **1B2_Mg** and **1B6_Mg** is -25.92 kJ/mol at B3LYP/6311TZVP level. C4 and C5 metalation products have similar energy. The relative energies of Mg-pyrimidines predict C6 position metallated pyrimidine is most stable conformer and this calculation results are consistent with experimental results well.

For organozinc complexes, the most stable complex is **1B6_Zn** with BF₃ and zinc TMP base in ortho-position. The energy difference between **1B6_Zn** and **1B2_Zn** is only -13.27 kJ/mol at B3LYP/6311TZVP level, and this energy gap is much smaller than that between **1B6_Mg** and **1B2_Mg**. **1B4_Zn** is the energetically least favored conformer (20.14 kJ/mol higher than **1B6_Zn** at B3LYP/6311TZVP level), which has BF₃ and zinc TMP base in the para-position. The energy difference between **1B6_Zn** and **1B2_Zn** is -13.27 kJ/mol, which is smaller than that of organomagnesium complex. From the relative energies we can see that BF₃ in the neighboring position of zinc can stabilized the complex, and this is also confirmed by calculated structures.

The structures of selected metalated-pyrimidine are shown in Figure 4.1. When BF₃ is in ortho-position to the metal atom, there is a large interaction between metal atom and at least one of the BF₃ fluorine atoms, which is readily seen in Figure 4.1. The coordination between metal base and BF₃ elongates the distance between metal and pyrimidine. This interaction is strong enough to transform the tetrahedral coordination sphere around metal atom center into trigonal bipyramidal in **1B6_Zn** and **1B6_Mg**.

Relative energy analysis results show that, for the reaction system without BF₃·OEt₂, the main product is the C4 metalated product. After adding the Lewis acid BF₃·OEt₂, BF₃ coordinates with the metal TMP. For magnesium pyrimidine complex, the most stable complex is the C6 position metalated pyrimidine, and for the zinc-pyrimidine complex, the energies of **1B6_Zn** and **1B2_Zn** are much more stable than **1B4_Zn** and **1B5_Zn**. More analysis will be carried out in the following mechanism studies.

Relative energies of products correlate with experimental results, but the details of the reaction mechanism haven't still been clearly understood, especially how the hydrogen transfer occurs to form finally the metallated intermediates. In the following discussions we will focus on energy profiles for different mechanisms with or without BF₃, respectively. To explore the reaction in detail the representative system 5-phenyl pyrimdine (**4**) and the respective metalated TMP base has been chosen.

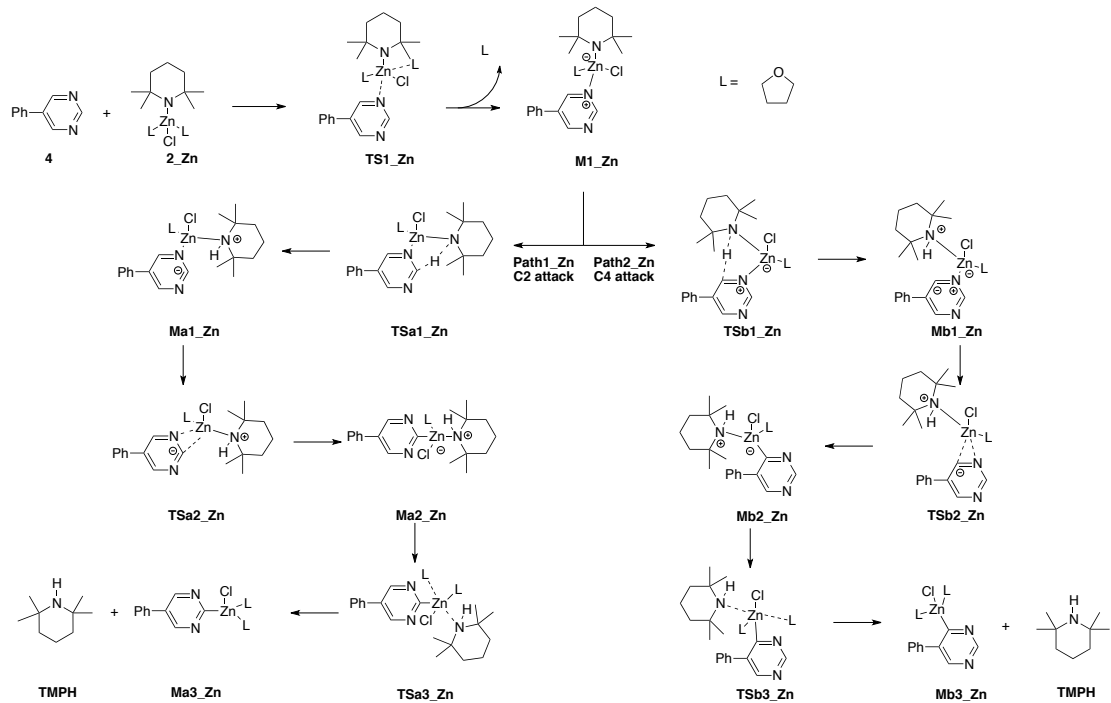
4.2.2 Reaction System Without Lewis Acid BF₃·OEt₂

Experiment records (Scheme 4.1) shows that pyrimidine reacts with metal-TMP bases (TMPMgCl(THF)₂ and TMPZnCl(THF)₂) to afford high yield and regioselective products. The reaction of 5-phenylpyrimidine (**4**) reacting with the metal TMP-base (**2_Zn** and **2_Mg**), are shown in Scheme 4.3 and in the following discussion the reaction pathways are called Path1 and 2. Path1 affords C2 position metalation of pyrimidine, but Path2 is metallated at C4 position. For the reaction involving zinc, Path1 and Path2 start with intermediate **M1_Zn** (shown in Figure 4.2, r(Zn-N)=219.1 pm), in which zinc attaches to the N atom of pyrimidine **4**. Starting from intermediates **M1_Zn**, deprotonations have two reaction channels (Scheme

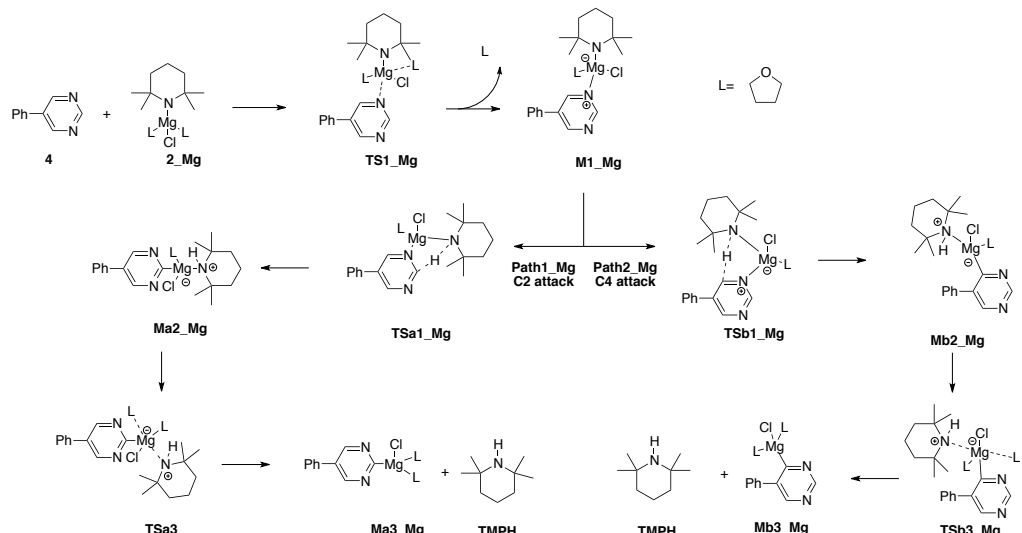
4.3). In Path1_Zn, the C2-H bond is activated and followed by the metalation of C2 position functionalization. Path2_Zn is C4-H activation and functionalization. In both pathways, the C-H extraction and metalation are separated and deprotonation step is followed by metalation step.

The reaction mechanisms involving magnesium TMP base are different with the mechanisms involving zinc. The reaction with the Mg complex starts with Mg attaching to the N atom in **4** (Scheme 4.3). Then the following reaction procedures are deprotonation in C2 position (Path1_Mg) or C-H activation in C4 position (Path2_Mg), which cause the metalation step. But in the reaction **4** with **2_Mg**, these two steps occur simultaneously and the reaction procedures are examined by intrinsic reaction coordinate (IRC) calculation.

5-phenylpyrimidine (4) reacts with TMPZnCl·2THF



5-phenylpyrimidine (4) reacts with TMPMgCl·2THF



Scheme 4.3. Theoretically examined metalation mechanism of 5-phenylpyrimidine (**4**) with TMPMetCl·THF (Met=Zn, Mg) in THF solution.

Reaction energies in Scheme 4.4 demonstrate the thermodynamic information of the reaction of **4** with TMP metal base and all the data is evaluated at SMD/B3LYP/631SVP//B3LYP/631SVP level. First comparing the relative energy of products, for the reaction energy profile involving organozinc, C2 position metalation of pyrimidine (**Ma3_Zn**) is -10.76 kJ/mol lower than reactants at B3LYP/631SVP level; C4 position matalated product (**Mb3_Zn**) is -18.31 kJ/mol lower than reactants. Thermo chemical data indicates that the reaction is slightly exothermic reaction. The stability of the two different products is close, and the energy difference is only 7.55 kJ/mol at SMD/B3LYP/631SVP//B3LYP/631SVP level.

The detailed energy profiles for the reactions are shown in Scheme 4.4. To afford the complexation intermediates **M1_Zn**, the energy barrier for **TS1_Zn** is 20.65 kJ/mol. After the formation of **M1_Zn**, the reaction has two possible ways to generate final products. In Path1_Zn, energy barrier of deprotonation at C2 position is 68.71 kJ/mol, and energy barrier for metalation is 85.95 kJ/mol. The last step is THF replaces TMPH with an energy barrier of 0.94 kJ/mol. For Path2_Zn, the energy barriers for C4-H activation, metalation and replacing step, are 59.13 kJ/mol, 76.80 kJ/mol and 4.60 kJ/mol, respectively. This implies that, the energy barriers for deprotonation and metalation in Path2_Zn are 9.58 kJ/mol and 9.15 kJ/mol lower than those in Path1_Zn.

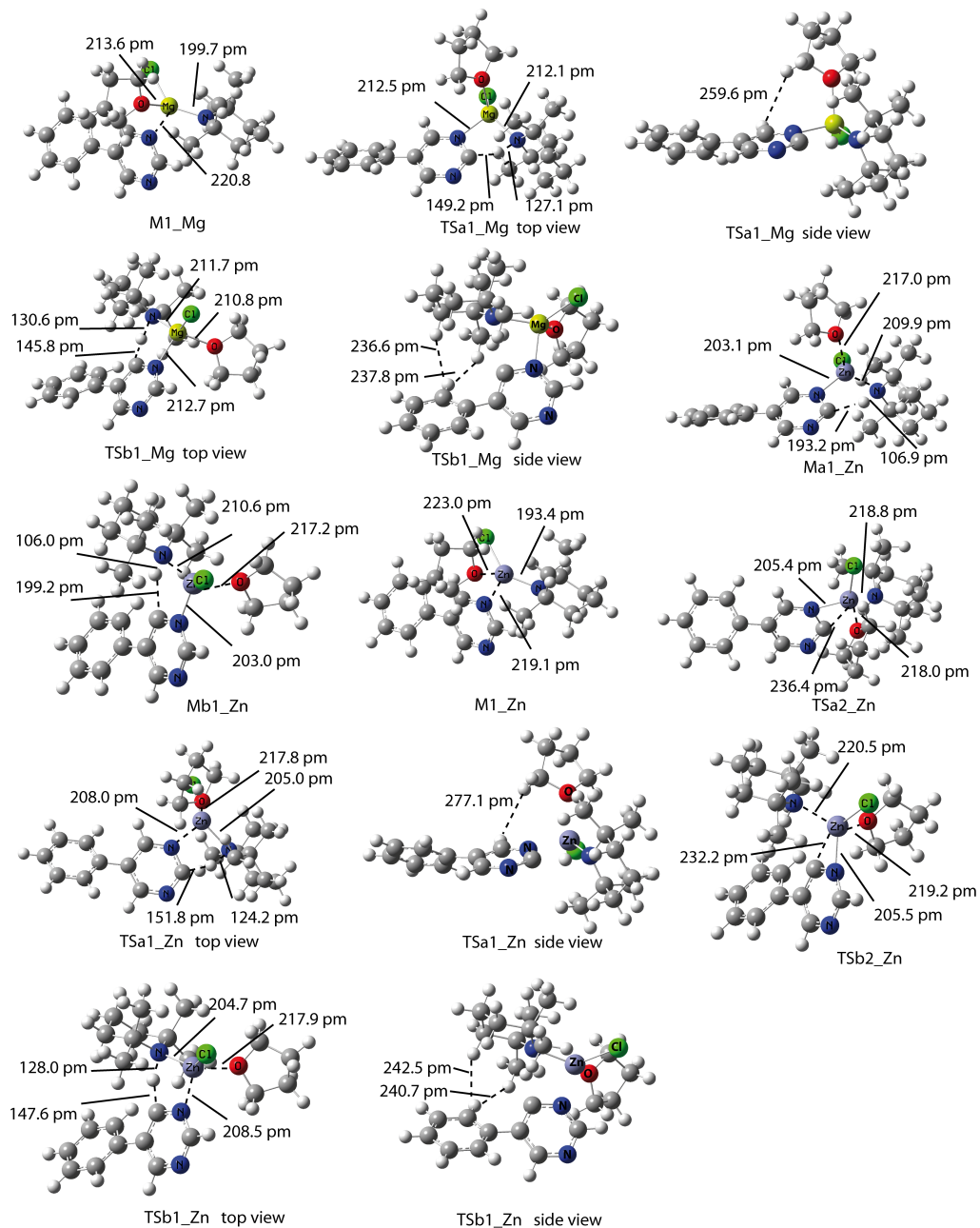
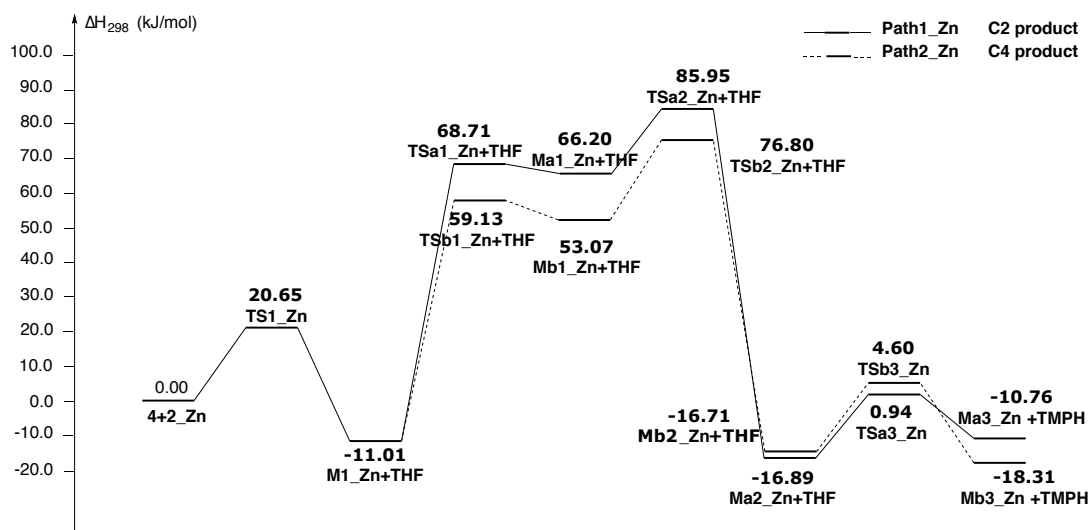
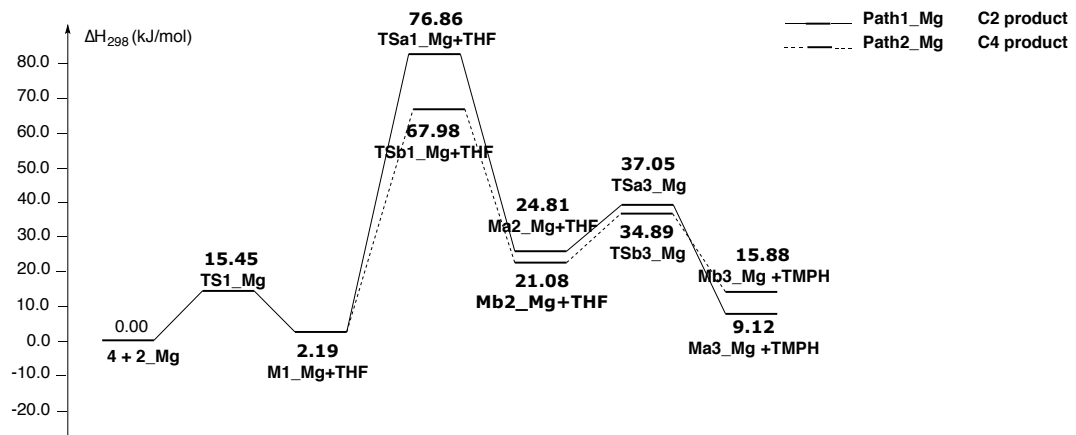


Figure 4.2. Structures of intermediates and transition states for the reaction of 5-phenylprimidine (**4**) with TMPMetCl·2THF (Met=Zn, Mg) calculated at B3LYP/631SVP level.

5-phenylpyrimidine (**4**) reacts with TMPZnCl·2THF



5-phenylpyrimidine (**4**) reacts with TMPPMgCl·2THF

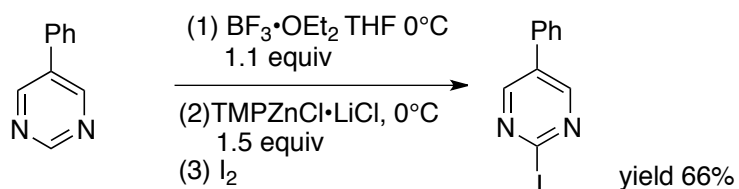


Scheme 4.4. Reaction energy profiles of 5-phenylpyrimidine (**4**) with TMPZnCl·2THF in THF solution at SMD/B3LYP/631SVP//B3LYP/631SVP level.

The reaction of 5-phenylpyrimidine (**4**) with TMPPMgCl·2THF is also explored and the mechanisms are shown in Scheme 4.2. Compared with TMPZnCl·2THF, TMPPMgCl·2THF reacts with 5-phenylpyrimidine (**4**) via a different reaction profile. The total reaction energy is defined as the energy difference between products and reactants. The data in Scheme 4.4 indicates that the reaction involving organomagnesium is slightly endothermic. Energy of C2 position metalation product is 9.12 kJ/mol higher than that of reactants. C4 position metalation product is 15.88 kJ/mol less stable than the reactants. Both Path1_Mg and Path2_Mg begin with intermediate **M1_Mg**, with $r(\text{Mg-N}) = 220.8 \text{ pm}$ (shown in Figure 3.2). For reaction Path1_Mg, C2-H activation and magnesium migration occur simultaneously, and the energy barrier is 76.68 kJ/mol. In the second step, TMPh is replaced by THF with barrier of 37.05 kJ/mol. In Path2_Mg, the energy barrier needed for hydrogen extraction as well as metalation is 67.98 kJ/mol. The energy barrier for replacing TMPh by THF is 34.89 kJ/mol. The rate-determining step for both reaction pathways is hydrogen transfer combined with Mg migration. Comparing Path1_Mg and Path2_Mg, Path2_Mg has a lower energy barrier, which means Path2_Mg is the main reaction pathway. For the reaction of **4** with **2_Mg**, the final product **Ma3_Mg** is preferred thermodynamically.

For the reactions involving $\text{TMPPMetCl}\cdot\text{2THF}$ ($\text{Met}=\text{Zn, Mg}$), the transition states for deprotonation and migration in Path2 are more stable than those in Path1. In order to identify the possible reason, the structures of the corresponding transition states are collected and shown in Figure 4.2. It is found that in Path2_Zn and Path2_Mg, even when the steric hindrance exists between metal base and 5-phenylpyrimidine, TMP can coordinate with phenyl group through π - σ interactions. This intramolecular interaction helps to hold the participants together and the transition states are stabilized by this interaction between TMP and the phenyl group. Lacking this type of interaction, **TSa1_Zn** and **TSa1_Mg** have higher energies and the reaction via Path1_Zn or Path1_Mg is energetically unfavorable.

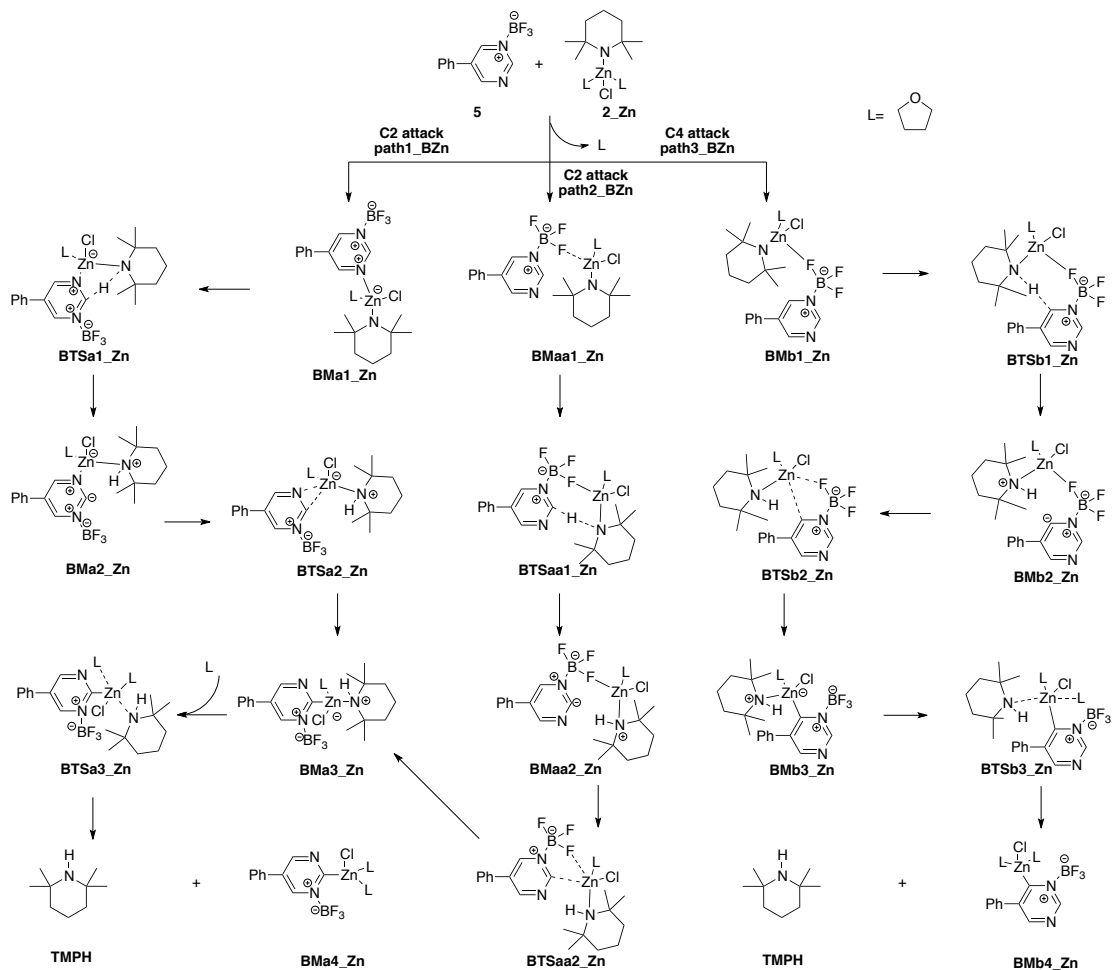
4.2.3 Reaction System With the Lewis Acid $\text{BF}_3\cdot\text{OEt}_2$



Scheme 4.5. 5-phenylpyrimidine reacts with $\text{TMPZnCl}\cdot\text{2THF}$ in the presence of $\text{BF}_3\cdot\text{OEt}_2$.

According to experiment (Scheme 4.5), the strong Lewis acid $\text{BF}_3\cdot\text{OEt}_2$ plays an important role in activating with metal TMP base. BF_3 not only accelerates the reaction speed but also increases the selectivity of reaction. The role of BF_3 in reaction has therefore been investigated in following work.

5-phenylpyrimidine (5) reacts with TMPZnCl·2THF



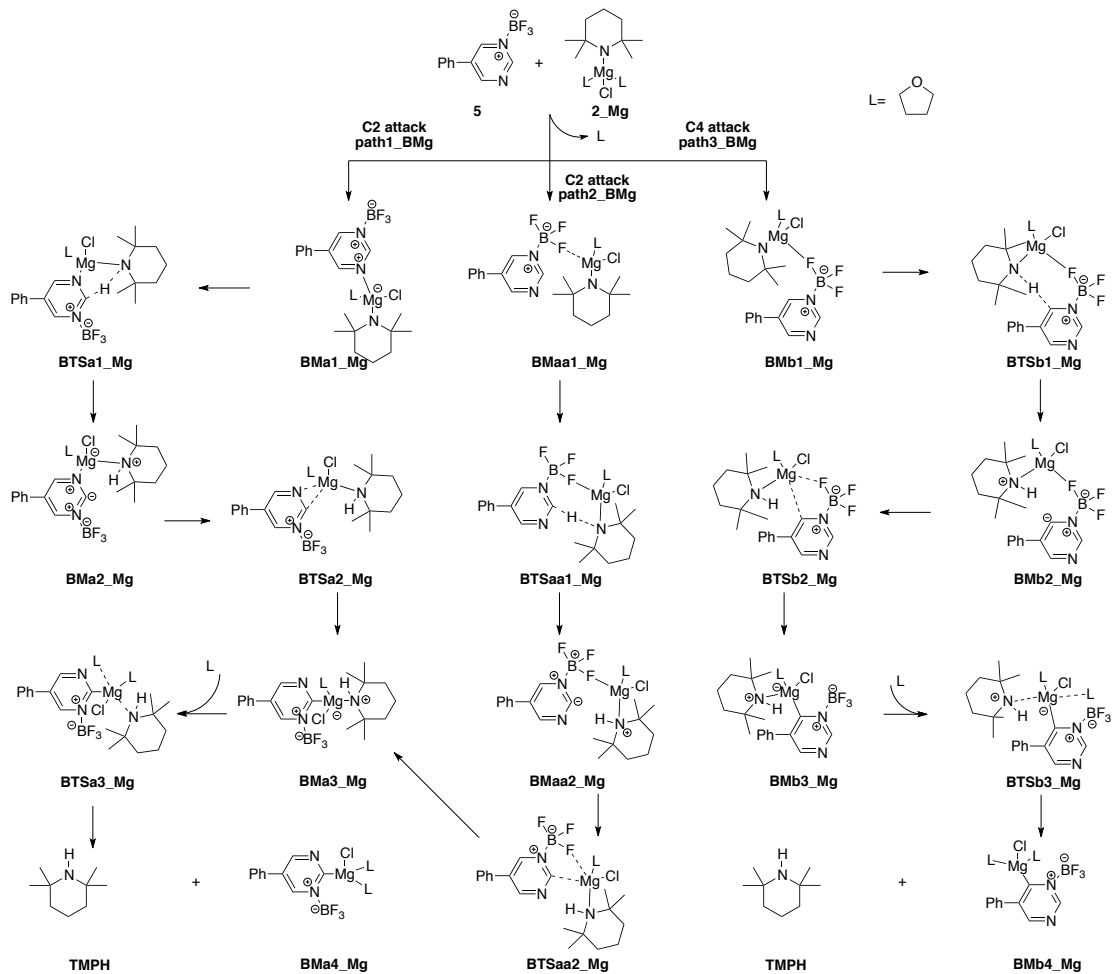
Scheme 4.6(a). Reaction of 5-phenylpyrimidine-BF₃ (**5**) with TMPZnCl·2THF activated by BF₃.

Once the Lewis acid BF₃·OEt₂ is added to reaction system, it will easily complex with 5-phenylpyrimidine (**4**) to generate BF₃-pyrimidine (**5**). Based on the results obtained from Table 4.2, BF₃ can stabilize the metallated complex when BF₃ is in neighboring position of the metal atom. In order to find how BF₃ influences the reaction, theoretical investigation is carried out.

Mechanisms for the reaction of **5** with **2_Zn** are shown in Scheme 4.6 (a). Initially the reaction of **5** with TMPZnCl·2THF generates new complex. According to the different relative positions of TMPZnCl·2THF and **5**, the three intermediates **BMA1_Zn**, **BMaa1_Zn** and **BMb1_Zn** are formed. These intermediates will lead to two different products, C2 metalation of pyrimidine **BMa4_Zn** and C4 position metalated pyrimidine **BMB4_Zn**.

In the regiosomeric complex **BMaa1_Zn**, TMP is close to the C2 position and it has a facility for C2-H bond activation in Path2_BZn through **BTsa1_Zn**. In the third reactant complex **BMb1_Zn**, TMP can easily abstract H from C4 position along reaction pathway Path3_BZn through **BTsb1_Zn**. After the deprotonation steps, zinc shifts from the N atom to the C2 position in Path1_BZn, and the last step involves the replacement of THF by TMPH. For Path2_BZn, after deprotonation, the coordination between F and Zn is broken, and zinc connects with C2. For Path3_BZn, the procedure after deprotonation is similar with that of Path2_BZn, but Zn connects with C4 instead of C2. From Scheme 4.6 (a) we can see that Path1_BZn and Path2_BZn afford C2 metalated pyrimidine, but Path3_BZn affords the C4 position metalation of of pyrimidine.

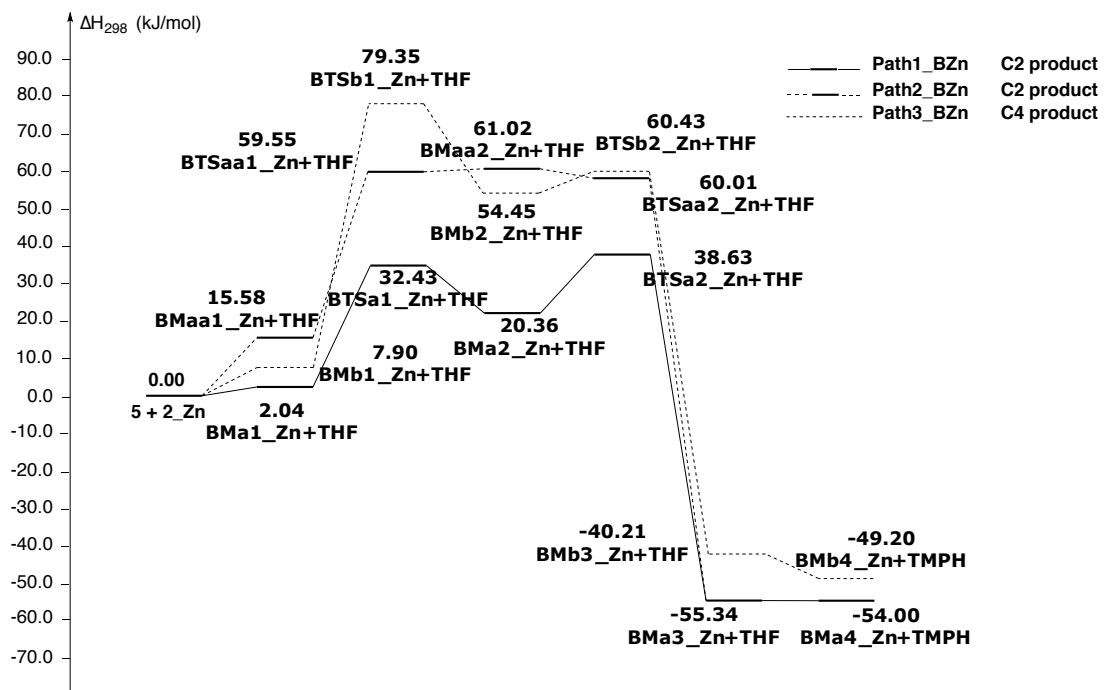
5-phenylpyrimidine (5) reacts with $\text{TMPPMgCl}\cdot\text{2THF}$



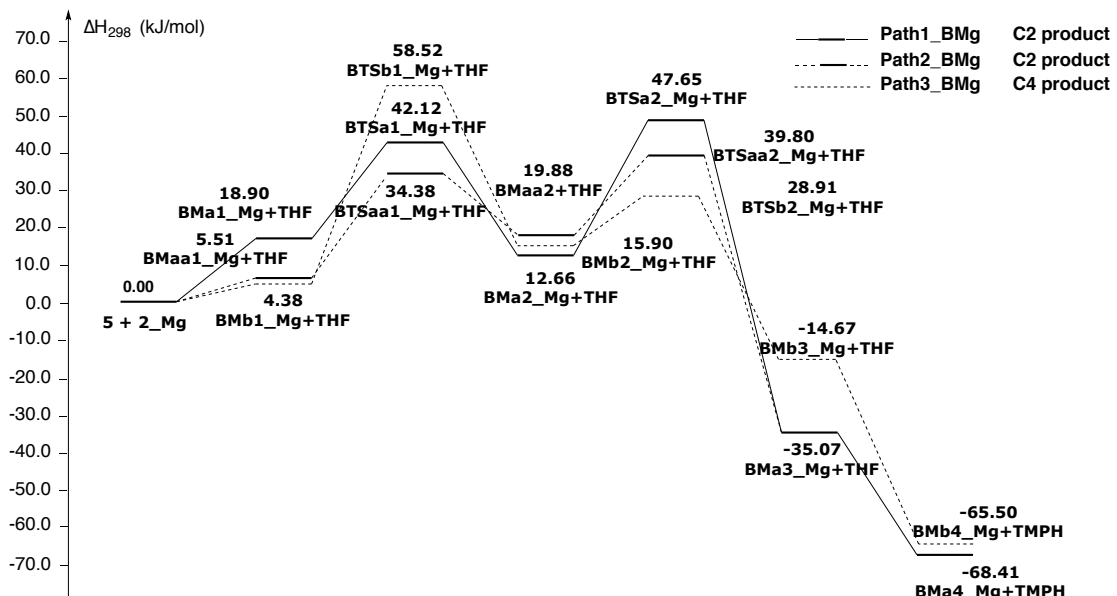
Scheme 4.6 (b). Reaction of 5-phenylpyrimidine-BF₃ (**5**) with TMPPMgCl·2THF activated by BF₃.

The mechanisms for the reaction of **5** with TMPPMgCl·2THF are similar with that of TMPZnCl·2THF. Three different reaction pathways are found with different coordination modes between **5** and TMPPMgCl·2THF. Path1_BMg starts with intermediate **BMa1_Mg**, leading to C2 metalated product. Path2_BMg starts with intermediate **BMaa1_Mg**, whereas Path3_BMg begins with intermediate **BMb1_Mg**. The difference between the three intermediates is the relative position of **5** and **2_Mg**. Starting from intermediate **BMa1_Mg**, TMP easily takes the H atom from the C2 position, followed by metalation. Similar to Path1_BMg, because TMP base is located near to the C2 position in Path2_BMg and the reaction will lead to the C2 position metalation products as well. The different intermediate **BMb1_Mg**, which has the interaction between Mg and F in BF₃ is located for Path3_BMg. The metal base can easily rotate around BF₃. In Path3_BMg, **BMb1_Mg** has the facility to activate C4-H bond, subsequently followed by the metalation step.

5-phenylpyrimidine (5) reacts with TMPZnCl·2THF



5-phenylpyrimidine (5) reacts with TMMPMgCl·2THF



Scheme 4.7. Reaction energy profiles for reaction of 5-phenylpyrimidine-BF₃ (**5**) with TMMPMetCl·2THF (Met=Zn, Mg) in THF solution at SMD/B3LYP/631SVP//B3LYP/631SVP level.

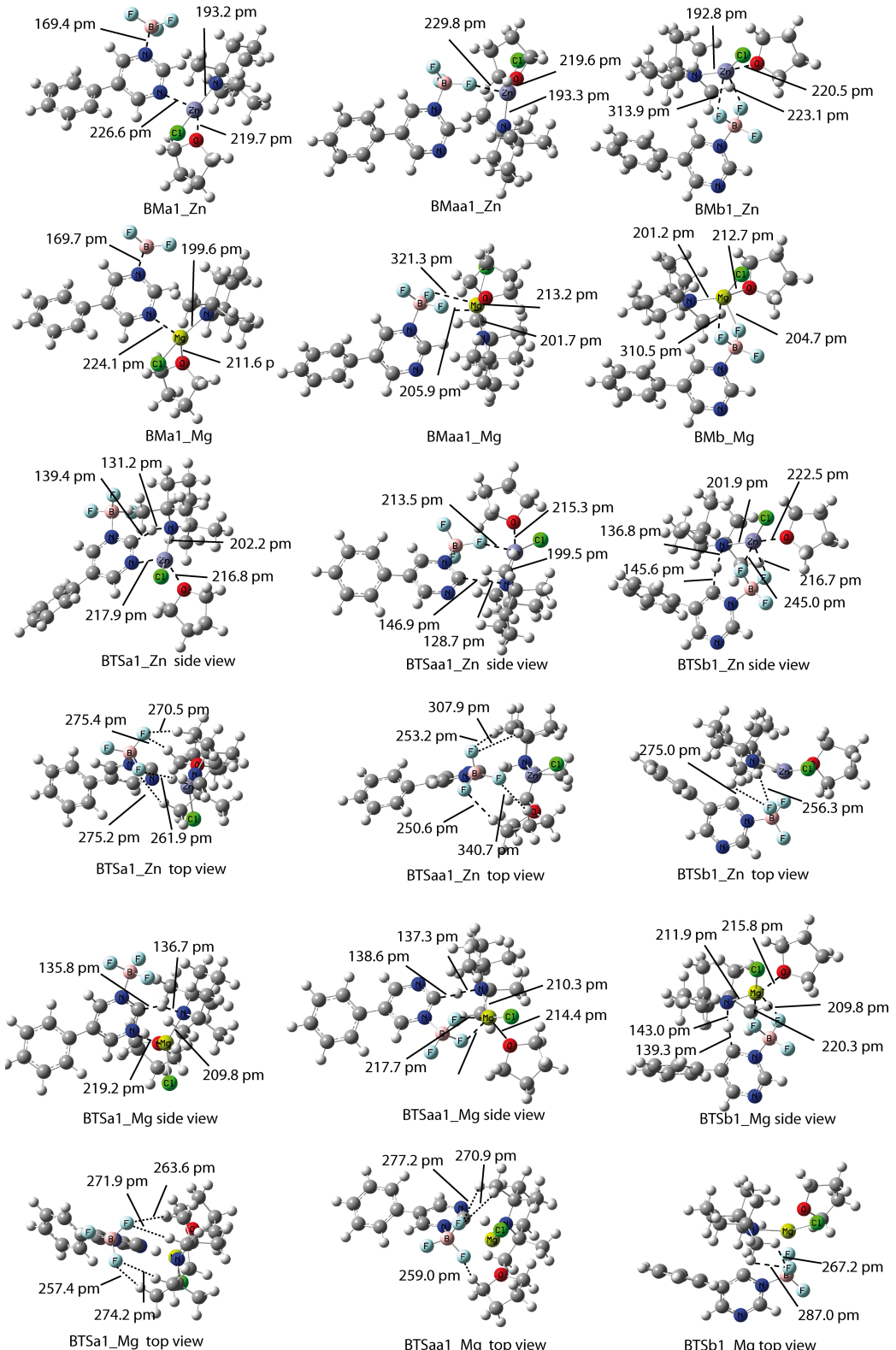


Figure 4.3. Geometries of intermediates and transition states for the reaction of 5-phenylpyrimidine-BF₃ (**5**) with TMPMetCl·2THF (Met=Zn, Mg) at B3LYP/631SVP level.

For the reaction of **5** with **2_Zn**, the total reaction energy is the energy difference between products and reactants. Reaction profiles clearly show that the reaction involving TMPZnCl·2THF is strongly exothermic reaction for three different reaction pathways. Comparing the two different products, the C2 metalation product (**BMa4_Zn**) is 4.80 kJ/mol more stable than C4 metalation product **BMb4_Zn**, and the energy difference is rather small.

Considering the reaction energy barriers, for Path1_BZn, the C2-H activation energy is 32.43 kJ/mol, and it is 6.20 kJ/mol lower than the metalation energy barrier. For Path2_BZn, the activation energy needed for deprotonation and metalation is 59.55 kJ/mol and 60.01 kJ/mol, respectively. In Path3_BZn, C4-H has been activated and the activation energy is 79.35 kJ/mol, but the energy needed for metalation in C4 is 60.43 kJ/mol. Comparing the three reaction pathways, the most energetic favorable reaction channel is Path1_BZn, leading to C2 metalation product.

Energy profile is also preformed for the reaction system involving $\text{TMPPMgCl}\cdot\text{2THF}$. In Path1_BMg, energy barriers for C2-H activation and metalation are 42.12 kJ/mol and 47.65 kJ/mol, respectively. With the same product, in Path2_BMg, the activation energies for the same steps are 34.38 kJ/mol and 39.80 kJ/mol, respectively. In order to obtain C4 magnesium-pyrimidine, activation energy needed for C4-H activation is 58.52 kJ/mol, and activation energy needed for metalation is 28.91 kJ/mol. After adding BF_3 , the reactions become strongly exothermic. Comparing the energy barriers in three reaction pathways, the most energetic favorable reaction Path is Path2_BMg leading to C2 metalation product.

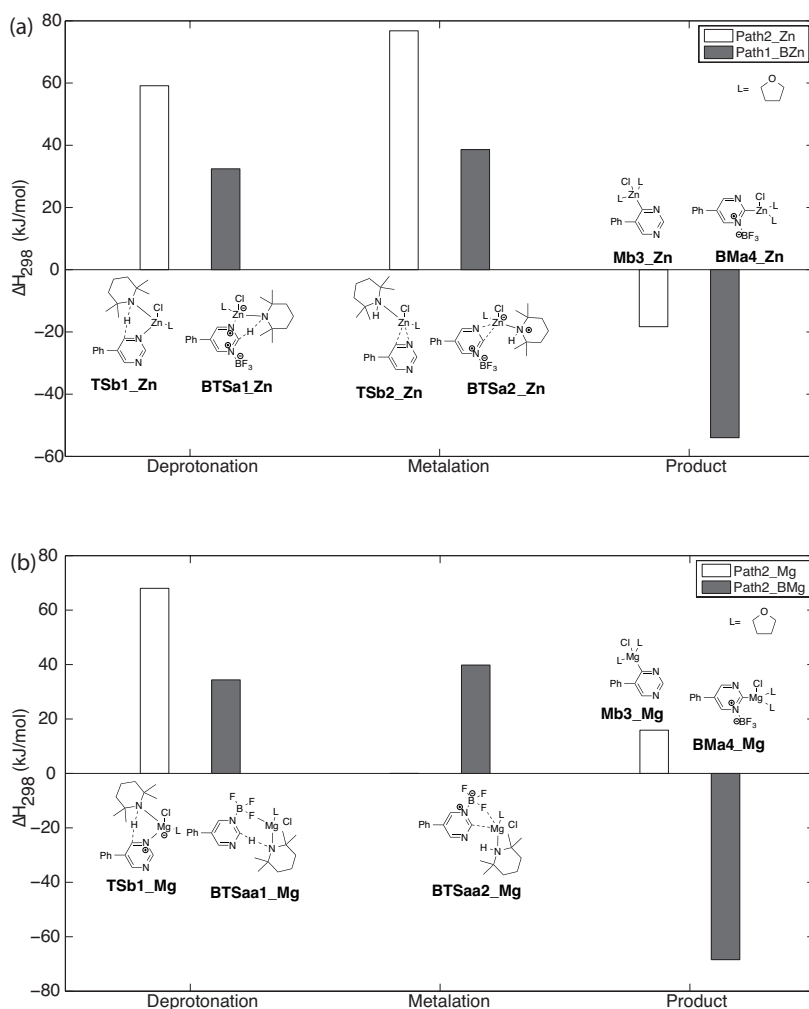


Figure 4.4. Relative energies of transition states and products at SMD/B3LYP/631SVP//B3LYP/631SVP level. (a) Energies of transition states and products for Path2_Zn and Path1_BZn. (b) Energies of transition states and products for Path2_Mg and Path2_BMg.

The energies of transition states and products in the most energetically preferred reaction pathways involving $\text{TMPPMetCl}\cdot\text{2THF}$ (Met= Zn, Mg) are collected in Figure 4.4. For the

reaction system without $\text{BF}_3\cdot\text{OEt}_2$, the main products are C4 metalated pyrimidines according to the calculation results. But the Lewis acid $\text{BF}_3\cdot\text{OEt}_2$ changes the regioselectivity. The main products are C2 metalated pyrimidines for both organozinc and organomagnesium. The relative energies show that the $\text{BF}_3\cdot\text{OEt}_2$ significantly reduces the energy barriers for the reaction involving $\text{TMPZnCl}\cdot2\text{THF}$ and $\text{TMPCMgCl}\cdot2\text{THF}$, and also stabilized the products.

4.3 Conclusions

The results of relative energy analysis of metalated pyrimidines show that when the system without $\text{BF}_3\cdot\text{OEt}_2$, the C4 metalation of pyrimidine is energetically preferred for both $\text{TMPZnCl}\cdot2\text{THF}$ and $\text{TMPCMgCl}\cdot2\text{THF}$. However, BF_3 can greatly stabilize the complex by the interaction between BF_3 and ligands. Therefore in the most stable conformer of metalated pyrimidine- BF_3 , BF_3 is in the ortho-position of metal center.

Mechanisms for the reaction of 5-phenylpyrimidine with $\text{TMPCMgCl}\cdot2\text{THF}$ ($\text{Met}=\text{Zn, Mg}$) have been studied at SMD/B3LYP/631SVP//B3LYP/631SVP level with limited experiment data available for these systems. For the reaction system without $\text{BF}_3\cdot\text{OEt}_2$, C4 metalation of pyrimidine is energetically preferred over the reaction at the C2 and C5 positions. The energy profiles indicate that the reaction without $\text{BF}_3\cdot\text{OEt}_2$ is slightly exothermic for $\text{TMPZnCl}\cdot2\text{THF}$, while the reaction is endothermic for $\text{TMPCMgCl}\cdot2\text{THF}$. The presence of $\text{BF}_3\cdot\text{OEt}_2$ changes the energy profiles dramatically. The main products with the presence of $\text{BF}_3\cdot\text{OEt}_2$ are C2 metalation of pyrimidines for both $\text{TMPZnCl}\cdot2\text{THF}$ and $\text{TMPCMgCl}\cdot2\text{THF}$. Because of the interaction between BF_3 and the ligands, the transition states and products are greatly stabilized in the pathways, which lead to C2 metalation products. Therefore, BF_3 in the reaction system can hold the reactants together to reduce the reaction barriers. These results are helpful for understanding the experiment procedure and designing catalyst system. However, the calculation results still need more experimental data for confirmation.

References

1. X.-F. Wu, H. Neumann and M. Beller, *Chem. Rev.*, 2013, **113**, 1-35.
2. M. Jaric, B. A. Haag, A. Unsinn, K. Karaghiosoff and P. Knochel, *Angew. Chem. Int. Ed.*, 2010, **49**, 5451-5455.
3. Y. Kondo, M. Shilai, M. Uchiyama and T. Sakamoto, *J. Am. Chem. Soc.*, 1999, **121**, 3539-3540.
4. S. H. Theophil Eicher, *The Chemistry of Heterocycles*, 2nd, Wiley-VCH, 2003.
5. C. O. Kappe, *Eur. J. Med. Chem.*, 2000, **35**, 1043-1052.
6. W. Xue and D. Warshawsky, *Toxicol. Appl. Pharmacol.*, 2005, **206**, 73-93.
7. D. Haas, M. Mosrin and P. Knochel, *Org. Lett.*, 2013, **15**, 6162-6165.
8. E. Negishi, A. O. King and N. Okukado, *J. Org. Chem.*, 1977, **42**, 1821-1823.
9. E. Negishi, L. F. Valente and M. Kobayashi, *J. Am. Chem. Soc.*, 1980, **102**, 3298-3299.
10. G. Wang, N. Yin and E.-i. Negishi, *Chem. Eur. J.*, 2011, **17**, 4118-4130.
11. J. E. Milne and S. L. Buchwald, *J. Am. Chem. Soc.*, 2004, **126**, 13028-13032.
12. S. Çalimsiz, M. Sayah, D. Mallik and M. G. Organ, *Angew. Chem.*, 2010, **122**, 2058-2061.
13. N. Hadei, G. T. Achonduh, C. Valente, C. J. O'Brien and M. G. Organ, *Angew. Chem. Int. Ed.*, 2011, **50**, 3896-3899.
14. O. Vechorkin, V. r. Proust and X. Hu, *J. Am. Chem. Soc.*, 2009, **131**, 9756-9766.
15. S. E. Denmark and J. Y. Choi, *J. Am. Chem. Soc.*, 1999, **121**, 5821-5822.
16. W. Lin, O. Baron and P. Knochel, *Org. Lett.*, 2006, **8**, 5673-5676.
17. A. Krasovskiy, V. Krasovskaya and P. Knochel, *Angew. Chem. Int. Ed.*, 2006, **45**, 2958-2961.
18. S. H. Wunderlich and P. Knochel, *Angew. Chem. Int. Ed.*, 2007, **46**, 7685-7688.
19. C. J. Rohbogner, G. C. Clososki and P. Knochel, *Angew. Chem. Int. Ed.*, 2008, **47**, 1503-1507.
20. A. Krasovskiy, V. Krasovskaya and P. Knochel, *Angew. Chem.*, 2006, **118**, 3024-3027.
21. S. M. Manolikakes, M. Jaric, K. Karaghiosoff and P. Knochel, *Chem. Commun.*, 2013, **49**, 2124.
22. M. Mosrin and P. Knochel, *Org. Lett.*, 2009, **11**, 1837-1840.

23. S. H. Wunderlich and P. Knochel, *Angew. Chem. Int. Ed.*, 2009, **48**, 9717-9720.
24. K. Groll, S. M. Manolikakes, X. M. du Jourdin, M. Jaric, A. Bredikhin, K. Karaghiosoff, T. Carell and P. Knochel, *Angew. Chem. Int. Ed.*, 2013, **52**, 6776-6780.
25. A. Unsinn, S. H. Wunderlich, A. Jana, K. Karaghiosoff and P. Knochel, *Chem. Eur. J.*, 2013, **19**, 14687-14696.
26. Q. Liu, Y. Lan, J. Liu, G. Li, Y.-D. Wu and A. Lei, *J. Am. Chem. Soc.*, 2009, **131**, 10201-10210.
27. N. Okukado, D. E. Vanhorn, W. L. Klima and E. I. Negishi, *Tetrahedron Lett.*, 1978, 1027-1030.
28. N. Ple, A. Turck, K. Couture and G. Queguiner, *J. Org. Chem.*, 1995, **60**, 3781-3786.
29. J. A. Casares, P. Espinet, B. Fuentes and G. Salas, *J. Am. Chem. Soc.*, 2007, **129**, 3508-3509.
30. A. O. King, N. Okukado and E.-i. Negishi, *J. Chem. Soc., Chem. Commun.*, 1977, 683.
31. E. Negishi, T. Takahashi and A. O. King, *Org. Synth.*, 1988, **66**, 67-74.
32. S. Sase, M. Jaric, A. Metzger, V. Malakhov and P. Knochel, *J Org Chem*, 2008, **73**, 7380-7382.
33. T. Thaler, B. Haag, A. Gavryushin, K. Schober, E. Hartmann, R. M. Gschwind, H. Zipse, P. Mayer and P. Knochel, *Nature Chemistry*, 2010, **2**, 125-130.
34. D. Nobuto and M. Uchiyama, *J. Org. Chem.*, 2008, **73**, 1117-1120.
35. K. Snégaroff, S. Komagawa, M. Yonehara, F. Chevallier, P. C. Gros, M. Uchiyama and F. Mongin, *J. Org. Chem.*, 2010, **75**, 3117-3120.

5 The Calculation of ^{29}Si NMR Chemical Shifts of Tetracoordinated Silicon Compounds in the Gas Phase and in Solution

5.1 Introduction

The measurement of ^{29}Si NMR chemical shifts is exceedingly helpful in elucidating the identity of silicon-containing molecular systems.^{1–13} This is not only true for stable reactants and products of well-defined transformations, but also for silicon-based species generated as transient intermediates in the course of a reaction.¹⁴ In this latter case the combination of theoretically predicted and experimentally measured ^{29}Si NMR chemical shifts is particularly helpful, as was amply demonstrated in detailed studies of, for example, silylenes¹⁵ and disilenes.¹⁶ When attempting to follow the course of base-catalyzed silylation reactions of alcohols, which constitute an important protecting group strategy in organic synthesis,^{17,18} we were confronted with the appearance of a number of silicon-based species with rather similar chemical shifts in the solution-phase ^{29}Si NMR spectra.¹⁹ With the goal of identifying a computational protocol for the accurate theoretical prediction of the respective chemical shifts in low-polarity organic solvents, we analyze here the performance of strategies based on DFT- and MP2-level calculations.^{20–27} Our particular emphasis will be on the effects of geometry optimization, methods for actual shift calculations, the modeling of solvent effects, and the evaluation of relativistic effects.

5.2 Results and Discussions

5.2.1 The Effects of Geometry Optimization

We first investigated the influence of molecular structures optimized using several computationally efficient methods on the quality of ^{29}Si chemical shifts evaluated on these structures at MP2(FULL)/IGLO-III level. These calculations were performed using SiMe_3Cl (**2**) as a model system for silyl chloride reagents used in organic synthesis. Experimentally measured chemical shifts for this system are available in selected solvents at room temperature such as benzene with $\delta(^{29}\text{Si}, \mathbf{2}) = +30.21$ ppm,²⁸ benzene-d₆ with $\delta(^{29}\text{Si}, \mathbf{2}) = +30.64$ ppm,²⁹ toluene-d₈ with $\delta(^{29}\text{Si}, \mathbf{2}) = +30$ ppm,³⁰ and CDCl_3 with $\delta(^{29}\text{Si}, \mathbf{2}) = +30.7$ ppm.³¹ It thus appears that organic solvents of intermediate polarity have only a very limited influence on the ^{29}Si chemical shift in **2**. Using microwave spectroscopy the gas phase Si–Cl bond distance in **2** has been determined in two separate studies as $r(\text{Si–Cl}, \mathbf{2}) = 202.2 \pm 5$ pm³² and 203 pm.³³ In the solid state the Si–Cl bond distance has been determined to be of comparable length at $r(\text{Si–Cl}, \mathbf{2}) = 209$ pm,³⁴ 201.0 pm (0.23 GPa and 296 K),³⁵ and 208.6 pm (0.1 MPa and 157 K).³⁶

The marked dependence of computed chemical shifts on the molecular structure is illustrated in Fig. 5.1, which displays ^{29}Si chemical shifts calculated for SiMe_3Cl (**2**) at MP2(FULL)/IGLO-III level employing structures optimized at various levels of theory in combination with the 6-31+G(d) basis set (the results obtained from MP2(FULL)/IGLO-III geometry optimizations are included as a reference). ^{29}Si chemical shifts evaluated for various points along a relaxed scan (MPW1K/6-31+G(d) structures) of the Si–Cl distance in **2** from 200 to 300 pm (solid line in Fig. 5.1) show an almost linear dependence with larger Si–Cl distances leading to systematically higher chemical shifts. This trend is also visible in the $\delta(^{29}\text{Si})$ data evaluated on molecular structures fully optimized with different methods in the gas phase (Fig. 5.1, solid circles): the shortest Si–Cl bond distances (about 208.5 pm) are obtained in MPW1K and MP2(FC) optimizations, while the other density functionals tested yield longer Si–Cl bonds reaching 211 pm obtained with the B3LYP hybrid functional. The shift values calculated for these gas phase geometries at MP2(FULL)/IGLO-III level vary by

approx. 2 ppm from +29.7 to +32.0 ppm. As detailed further below, use of the PCM solvent model for structure optimization (Fig. 5.1, empty squares) leads to systematically longer Si–Cl bonds and, correspondingly, to systematically higher $\delta(^{29}\text{Si})$ values, with larger deviations from experiment for the cases tested.

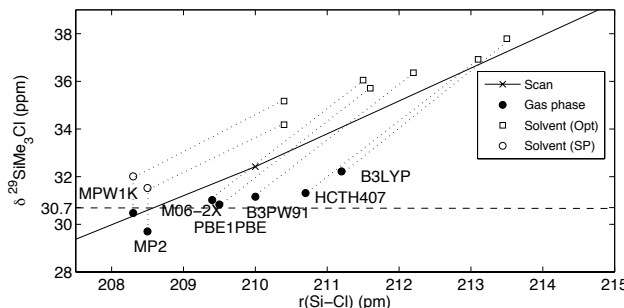


Figure 5.1. Calculated $\delta(^{29}\text{Si})$ values for SiMe_3Cl (**2**) (MP2: solid circles and PCM/MP2: empty symbols; IGLO-III basis set) using molecular structures optimized at various levels of theory using the 6-31+G(d) basis set. Dashed line: experimental value in CDCl_3 ; solid line: relaxed scan along the Si–Cl bond (gas phase, MPW1K structures). Empty circles: PCM/MP2 shifts on gas phase structures; empty squares: PCM/MP2 shifts on solution-phase geometries (all solvent calculations: CHCl_3 , UAHF radii).

We further explored whether chemical shift predictions can be improved through the use of more sophisticated basis sets in gas phase geometry optimizations for selected Pople-style and correlation consistent (cc) basis sets (Table 5.1). Use of the systematically developed cc basis sets results in a systematic decrease of Si–Cl bond distances in the order cc-pVDZ, cc-pVTZ, and cc-pVQZ, irrespective of the theoretical method used. This directly impacts the ^{29}Si chemical shift calculations performed at MP2(FULL)/IGLO-III level, where shorter Si–Cl bonds are again observed to yield lower shift values. A comparable trend is not observed for Pople-style basis sets of double- and triple-zeta quality. Among all quantum mechanical methods the MP2(FC) level is most strongly affected by these variations. Taking the MP2(FC)/cc-pVQZ structure as reference, the best agreement is observed at the MPW1K/6-31+G(d) level, which was therefore chosen for all subsequent geometry optimizations.

Table 5.1. Influence of basis set choice on the gas phase geometry optimized with various methods and the gas phase ^{29}Si chemical shift of **2** (evaluated at MP2(FULL)/IGLO-III level).

	PBE1PBE		MPW1K		M06-2X		MP2(FC)	
Basis set	r(Si–Cl) (pm)	$\delta(^{29}\text{Si})$ (ppm)	r(Si–Cl) (pm)	$\delta(^{29}\text{Si})$ (ppm)	r(Si–Cl) (pm)	$\delta(^{29}\text{Si})$ (ppm)	r(Si–Cl) (pm)	$\delta(^{29}\text{Si})$ (ppm)
6-31+G(d)	209.5	+30.84	208.3	+30.32	209.4	+31.02	208.5	+29.70
6-31+G(2d,p)	209.6	+31.81	208.5	+31.37	209.5	+31.90	210.2	+32.60
6-31++G(2d,p)	209.6	+31.82	208.5	+31.38	209.5	+31.92	210.3	+32.63
6-31++G(2df,p)	208.9	+30.90	207.8	+30.43	211.4	+34.14	208.5	+30.44
6-311++G(2d,p)	209.4	+31.82	208.3	+31.31	209.3	+31.90	209.9	+32.30
cc-pVDZ	211.2	+32.98	210.2	+32.63	211.1	+33.16	210.7	+31.83
cc-pVTZ	209.1	+31.23	208.1	+30.81	209.1	+31.39	208.6	+30.79
cc-pVQZ	208.5	+30.77	207.6	+30.36	208.5	+30.92	207.8	+30.24

5.2.2 Theoretical Methods for Chemical Shift Calculations

Chemical shift calculations at MP2(FULL)/IGLO-III level are quite challenging for larger molecular systems and an effort has therefore been made to identify more economical approaches. Table 5.2 displays ^{29}Si shift values for SiMe_3Cl (**2**) computed with selected combinations of methods and basis sets based on the MPW1K/6-31+G(d)-optimized geometry. Compared to the experimental value of $\delta(^{29}\text{Si}, \mathbf{2}) = +30.7 \text{ ppm}^{31}$ largest deviations are found for the 6-311++G(2d,2p)²⁶ basis set, while the def2-TZVP,^{37,38} cc-pVTZ,³⁹ and IGLO-III⁴⁰ triple zeta basis sets yield generally better results. The quadruple zeta pcS-3 basis set specifically developed for NMR calculations⁴¹ performs as well as IGLO-III, but its use is computationally significantly more demanding. We note that second-order perturbation theory in its canonical (MP2) or local (LMP2) variants perform best, closely followed by the HCTH407⁴² and MPW1K²⁰ hybrid functionals. Interestingly, the DF-LMP2/IGLO-III⁴³ calculations closely reproduce the much more costly MP2(FULL)/IGLO-III calculations, which we chose as reference method for ^{29}Si chemical shift calculations. The worst performer found here is clearly the M06-2X⁴⁴ functional, which responds more sensitively to the individual basis set design than any other method listed in Table 5.2. The deviations of MPW1K and HCTH407 are comparable to those of the MP2 methods and the performance of these two methods is better than that of other DFT methods tested here.

Table 5.2. Calculated $\delta(^{29}\text{Si})$ chemical shifts for **2** using different theoretical methods and basis sets^a

Method ^b	6-311++G (2d,2p)	Def2-TZVP	cc-pVDZ	cc-pVTZ	cc-pVQZ	pcS-3	IGLO-III
HCTH407	+35.00	+32.37	+32.63	+32.91	+26.37	+31.94	+31.40
B3LYP	+36.37	+34.29	+34.13	+34.14	+27.60	+33.44	+32.94
B3PW91	+36.84	+34.92	+35.31	+34.64	+28.78	+34.15	+33.66
PBE1PBE	+36.56	+34.68	+35.35	+34.83	+29.37	+33.93	+33.31
MPW1K	+34.83	+33.06	+33.89	+33.59	+28.09	+32.44	+31.88
M06-2X	+42.67	+38.10	+38.85	+31.00	+36.82	+35.64	+37.24
DF-LMP2	+33.05	+31.47	+31.36	+33.09	+29.55	+30.25	+28.40
MP2(FULL)	+33.65	+31.92	+30.71	+32.54	+28.59	+31.31	+30.32

^a Geometries optimized with MPW1K/6-31+G(d) ^b Method used for NMR chemical shift calculations.

5.2.3 Solvent effect

The experimental reference shift data for SiMe_3Cl (**2**) has been determined in apolar organic solvents such as CDCl_3 or benzene. As a first straightforward approach to account for solvent effects we performed shift calculations in combination with the polarizable continuum model (PCM) for chloroform at PCM/MP2(FULL)/IGLO-III level based on the MPW1K/6-31+G(d) gas-phase geometry, which leads to downfield shifts of the ^{29}Si signal in SiMe_3Cl (**2**) by 1.5–2.0 ppm relative to the gas phase value (+30.32 ppm), depending on the particular PCM variant employed (Table 5.3). An additional downfield shift of the same magnitude is obtained upon inclusion of the polarizable continuum also for geometry optimization at PCM/MPW1K/6-31+G(d) level owing to the elongated Si–Cl bond present in the optimized structure (Table 5.3). From a glance at the data compiled in Table 5.3 it is apparent that the

particular choice of the atomic radii used to construct the solute cavity in the PCM calculations has only a minute influence on structures and chemical shifts.

Table 5.3. Influence of continuum solvation models on ^{29}Si chemical shift calculations (PCM/MP2(FULL)/IGLO-III) for SiMe_3Cl (**2**)

	Gas-phase structure ^a r(Si-Cl) (pm)	$\delta(^{29}\text{Si})$ (ppm)	Solution-phase structure ^b r(Si-Cl) (pm)	$\delta(^{29}\text{Si})$ (ppm)
PCM(UFF)	208.4	+31.80	210.19	+34.34
PCM(UAHF)	208.4	+32.15	210.40	+35.00
PCM(UAKS)	208.4	+32.15	210.40	+35.00
SMD	208.4	+32.28	210.48	+35.22

^a Optimized at MPW1K/6-31+G(d) level. ^b Optimized in CDCl_3 with different solvation models at MPW1K/6-31+G(d) level.

A more detailed picture is presented in Fig. 5.1 above, where the PCM/MP2(FULL)/IGLO-III shift data using the gas-phase geometries (empty circles) and the solution-phase geometries (empty squares) for selected hybrid DFT methods are shown. Taking the MPW1K/6-31+G(d) gas phase geometries as an example, we can see that the PCM(UAHF)/MP2(FULL)/IGLO-III shifts are 1.7 ppm larger as compared to the gas phase MP2(FULL)/IGLO-III shifts. This is also found for all other methods used for geometry optimization. Reoptimizing the geometry of SiMe_3Cl (**2**) in the presence of the PCM reaction field leads to elongation of the Si–Cl bond, which at PCM/MPW1K/6-31+G(d) level reaches up to 210.4 pm. This geometrical change is accompanied by a downfield shift in the ^{29}Si resonance to +35.0 ppm. This is found in a very similar manner also for all other methods used for geometry optimization and we may thus conclude that the PCM continuum solvation model impacts ^{29}Si shift calculations in a significant way through changes in the molecular structure.

Effects of explicit solvation were subsequently explored for complexes of SiMe_3Cl (**2**) with one molecule of CHCl_3 . A number of minima were identified in MPW1K/6-31+G(d) geometry optimizations (Fig. 5.2). The longest Si–Cl bond with 209.5 pm (and thus the largest downfield shifted ^{29}Si signal) is found for solute–solvent complex **2_3**, in which the chlorine atom of SiMe_3Cl forms a hydrogen bond to chloroform (Table 5.4). In terms of gas phase free energies ΔG_{298} structure **2_3** is not the most stable conformer, but is 7 kJ mol^{-1} less stable than the best structure **2_1**. Due to only weak interactions between the methyl groups of **2** and chlorine atoms of the solvent molecule, the Si–Cl distance in structure **2_1** is hardly different from that of **2** alone. After Boltzmann averaging, $\delta(^{29}\text{Si})$ is only +0.18 ppm higher than the experimental result. In solution phase, the most stable structure is **2_3**. The continuum solvation model increases the Si–Cl distance and also reduces the energy gap between different conformers. With the PCM solvent model $\delta(^{29}\text{Si})$ values are 5 ppm higher than the experimental value. We thus have to conclude that, at least for model system **2**, the gas phase predictions are significantly closer to the solution phase experiment as compared to solution-phase calculations based on a combined implicit–explicit solvent model.

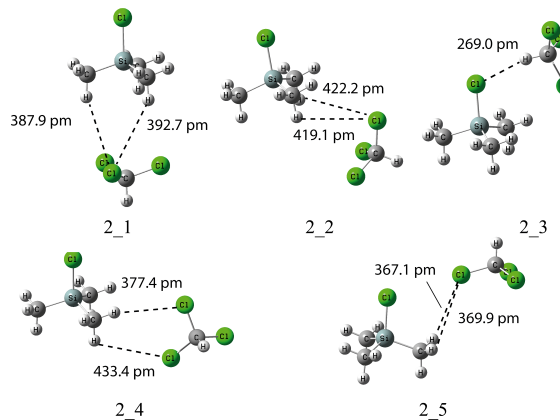


Figure 5.2. Structures of SiMe_3Cl (**2**) complexed to CHCl_3 obtained at MPW1K/6-31+G(d) level in the gas phase (dashed lines show shortest contacts between solvent and solute molecules).

Table 5.4. ^{29}Si chemical shifts for complexes **2_1 – 2_5** of SiMe_3Cl (**2**) with one chloroform molecule at MP2(FULL)/IGLO-III//MPW1K/6-31+G(d) level (bond distances are in pm, free energies ΔG_{298} are in kJ mol^{-1} and chemical shifts are in ppm)

	Gas phase			Solution phase ^a		
	r(Si-Cl)	ΔG_{298}	$\delta(^{29}\text{Si})$	r(Si-Cl)	ΔG_{298}	$\delta(^{29}\text{Si})$
2_1	208.6	0.00	+30.70	210.50	1.02	+35.09
2_2	208.6	0.99	+30.89	210.50	3.02	+35.43
2_3	209.5	7.01	+33.81	210.70	0.00	+36.24
2_4	208.5	7.44	+30.69	210.40	1.29	+35.16
2_5	208.7	7.91	+31.28	210.40	2.06	+35.06
Ave ^b			+30.88			+35.52

^a Solvent effects calculated at PCM(UAHF)/MP2(FULL)/IGLO- III//MPW1K/6-31+G(d) level.

^b $\delta(^{29}\text{Si})$ shift calculated as Boltzmann average, for detail see the Appendix for detail.

5.2.4 Spin–Orbit Corrections for Chlorosilanes

^{29}Si chemical shifts calculated at MPW1K/IGLO-III//MPW1K/6-31+G(d) level for the $\text{SiMe}_{4-x}\text{Cl}_x$ compounds show a systematic deviation between theoretically calculated and experimentally measured shift data (Fig. 5.3). That the deviations are systematic in nature can readily be seen from the good linear correlation between the actual deviation and the number of chlorine atoms (Fig. 5.3).¹⁵ The importance of heavy-atom-induced spin–orbit (SO) effects for nuclear magnetic shifts of group 14 element halides have been highlighted by several groups.^{45–50} According to these earlier reports, the experimentally observed normal halogen dependence (NHD), *i.e.* the characteristic high-field shift of the nucleus bound directly to the halogen substituents with increasing atomic number of the halogen, is mainly a result of spin–orbit effects. In these studies it was found that shifts calculated with the inclusion of SO effects agree significantly better with the experiment than their non-relativistic counterparts.

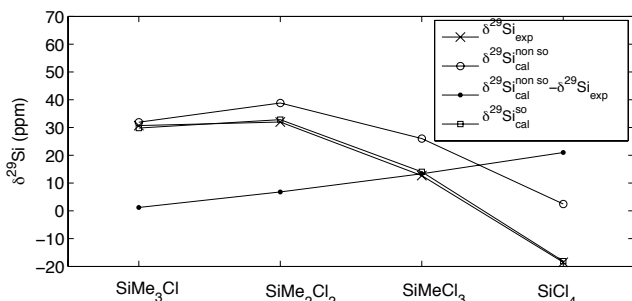


Figure. 5.3. Comparison between experimentally measured and theoretically calculated shift values at MPW1K/IGLO-III// MPW1K/6-31+G(d) level for alkylchlorosilanes $\text{SiMe}_{4-x}\text{Cl}_x$ with $x = 1-4$. SO corrections are obtained from ZORA-SO-PBE0/TZ2P single-point calculations. Geometries are obtained at MPW1K/6-31+G(d) level in gas phase.

We evaluated contributions of relativistic spin-orbit effects to the nuclear magnetic shielding constants for the series of $\text{SiMe}_{4-x}\text{Cl}_x$ compounds employing the two-component zeroth-order regular approximation (ZORA)^{51,52} formalism, as implemented in ADF. The SO correction per chloro-substituent increases monotonously from approximately -2 ppm (SiMe_3Cl) to -3 ppm for SiMe_2Cl_2 , -4 ppm for SiMeCl_3 , and -5 ppm for SiCl_4 . In line with the discussion of Kaupp *et al.* on SO-induced heavy-atom effects on NMR chemical shifts,⁴⁷ this trend can readily be explained based on the analogy to the Fermi-contact mechanism of spin-spin coupling. The increasing involvement of valence silicon s-type orbitals in the bonding orbitals to the chloro-substituents results in larger SO contributions in the series from SiMe_3Cl to SiCl_4 .⁵³ Aside from the chlorine count there is only a rather limited influence of other silicon substituents on the magnitude of the SO corrections. A SO correction of around -2 ± 0.5 ppm per chlorine substituent will thus be typical for different chloromonosilanes (see also Table 5.5). For systems with more than one conformer, Boltzmann-weighted SO corrections are close to the SO-correction for the most stable conformer.⁵⁴ This part of work is done in collaboration with Robin Panisch and Josef Heinrich Wender from Holthausen's Group.

5.2.5 ^{29}Si Chemical Shifts for Larger Molecular Systems

^{29}Si chemical shifts for a larger group of “typical” systems are collected in Table 5.5 and graphically shown in Fig. 5.4. The experiments are done by Pascal Patschinski. Already the calculation of gas phase ^{29}Si chemical shifts at MPW1K/IGLO-III//MPW1K/6-31+G(d) level provides a rather accurate agreement with experimental results obtained in low polarity organic solvents with $R^2 = 0.872$ and $MD = 2.54$ ppm (panel (a) in Fig. 5.4). The largest deviations occur for systems containing more than one chlorine atom directly attached to silicon, and inclusion of SO-corrections evaluated at ZORA-SO-PBE0/TZ2P single point level improves correlation with experiment significantly for the entire dataset to $R^2 = 0.978$ and $MD = 0.18$ ppm (compare panel (a) and (b) in Fig. 5.4). Best theoretical predictions are then obtained through shielding calculations in the presence of the PCM continuum solvation model with gas phase structures and including the SO corrections. It is remarkable to see that the correlation for this approach based on gas phase structures ($R^2 = 0.984$, $MD = 0.97$ ppm) is even slightly better as compared to the approach based on solution-phase structures with $R^2 = 0.983$ and $MD = 2.34$ ppm (compare panel (c) and (d) in Fig. 5.4). Performing the actual shielding calculations with different functionals such as HCTH407 or with the local DF-LMP2 method lead to no further systematic improvement (see Appendix for details).

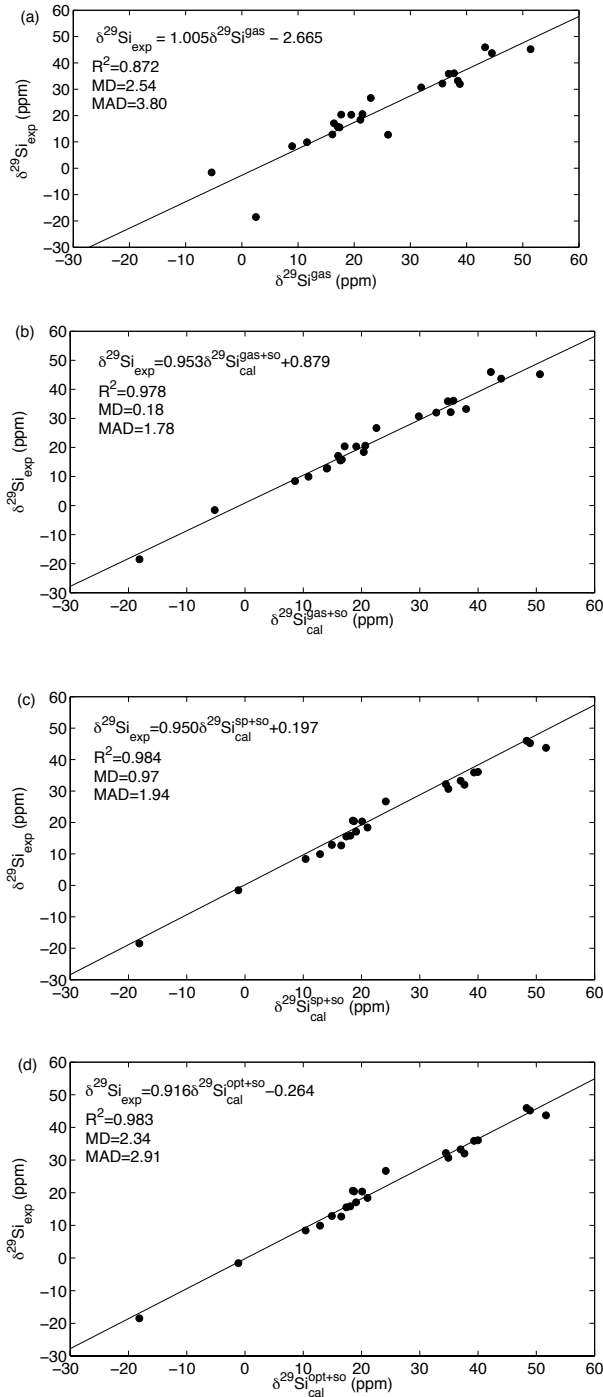


Figure. 5.4. Theoretically calculated *vs* experimentally measured ^{29}Si chemical shifts for the data set collected in Table 5.5. (a) $\delta(^{29}\text{Si})$ calculated at MPW1K/IGLO-III//MPW1K/6-31+G(d) level. (b) $\delta(^{29}\text{Si})$ calculated at MPW1K/IGLO-III(+ZORA-SO)//MPW1K/6-31+G(d). (c) $\delta(^{29}\text{Si})$ calculated at PCM(UAHF)/MPW1K/IGLO-III(+ZORA-SO)//MPW1K/6-31+G(d) level using gas phase structures. (d) $\delta(^{29}\text{Si})$ calculated at PCM(UAHF)/MPW1K/IGLO-III(+ZORA-SO)//PCM(UAHF)MPW1K/6-31+G(d) level using solution phase structures.

5.2.6 Chemical Shifts for Ion Pairs

Chemical shift calculations for the ion pair intermediates **18**, **19**, **23**, and **24** included in Table 5.5 are somewhat less accurate as compared to all other systems at the MPW1K/IGLO-III-(+ZORA-SO)//MPW1K/6-31+G(d) level. This may, in part, be due to significantly larger

solvent effects for these polar species as well as their rather large conformational flexibility. How the latter actually impacts chemical shift calculations is illustrated in detail in Fig. 5.5 for silylpyridinium ion pair **19**, whose experimentally measured ^{29}Si chemical shift amounts to +33.25 ppm in chloroform. For ion pairs, which have more than one conformer, chemical shifts are evaluated by Boltzmann averaging over individual conformers based on their relative free energies. When using gas-phase free energies the structures with the largest molecular dipole moment make the smallest contribution to the Boltzmann average due to their high relative energies (Table 5.6). In solution, however, these structures lead to the largest solvation energies: the dipole moment of conformer **19_1** is comparatively low at 10.30 D (MPW1K/6-31+G(d) level) and thus has the smallest solvation energy of -81.50 kJ mol⁻¹ (gas-phase geometry). Conformers **19_4** and **19_5** have slightly larger dipole moments and also slightly larger solvation energies around -96 kJ mol⁻¹. Conformer **19_6** has the largest dipole moment at 23.93 D, leading to a rather large solvation energy of -131.50 kJ mol⁻¹ (gas phase geometry) or -162.72 kJ mol⁻¹ (solution phase geometry). As a consequence of these variations in solvation energies, relative free energies in solution (ΔG^{opt}) are significantly smaller as compared to the gas phase. Despite these large changes in relative energies, the actual ion pair structure shows rather little change in gas-phase vs. solution-phase geometry optimization as exemplified for the Si–N bond distance (Table 5.6). This can also be stated for the electronic character of these ion pairs as characterized by the triflate ion charge, which assumes values between -0.94 and -0.96 for the best conformers **19_1** and **19_2** in gas-phase as well as in solution (Table 5.6).

Table 5.5. The ^{29}Si NMR chemical shifts of selected chemical species

System	$\delta_{\text{exp}}(\text{ppm})^{\text{a}}$	$\delta_{\text{cal}}^{\text{gas}}(\text{ppm})^{\text{b}}$	$\delta_{\text{cal}}^{\text{gas+so}}(\text{ppm})^{\text{c}}$	$\delta_{\text{cal}}^{\text{sp+so}}(\text{ppm})^{\text{d}}$	$\delta_{\text{cal}}^{\text{opt+so}}(\text{ppm})^{\text{e}}$
2	 +30.70 (CDCl ₃) ³¹	+31.92	+29.82	+31.90	+34.90
3	 -18.50 (CDCl ₃) ¹⁵	+2.49	-18.11	-18.05	-18.13
4	 -1.57 (CDCl ₃)	-5.39	-5.19	-3.01	-1.15
5	 +8.40 (C ₆ D ₆) ⁵⁵	+8.97	+8.57	+8.18	+10.41
6	 +9.91 (CDCl ₃)	+11.59	+10.79	+11.21	+12.78
7	 +12.70 (CDCl ₃)	+26.04	+14.04	+15.30	+16.53
8	 +12.86 (CDCl ₃)	+16.12	+14.42	+14.73	+15.22
9	 +15.54 (CDCl ₃)	+17.07	+16.37	+16.88	+18.16
10	 +15.80 (CDCl ₃)	+17.40	+16.60	+17.28	+18.51
11	 +17.08 (CDCl ₃)	+16.41	+16.01	+17.13	+19.06
12	 +18.42 (CDCl ₃)	+21.10	+20.40	+20.68	+21.01
13	 +20.34 (CDCl ₃)	+19.48	+19.08	+19.09	+20.10
14	 +20.39 (CDCl ₃)	+17.69	+17.09	+17.84	+18.70
15	 +20.58 (CDCl ₃)	+21.46	+20.66	+20.95	+18.51

16		+26.69 (CDCl ₃)	+22.95	+22.55	+23.36	+24.16
17		+32.00 (CDCl ₃) ³	+38.81	+32.81	+35.13	+37.66
18		+32.16 (CDCl ₃)	+35.70	+35.30	+36.18	+34.47
19		+33.25 (CDCl ₃)	+38.44	+37.94	+36.40	+37.00
20		+35.89 (CDCl ₃)	+36.81	+35.31	+37.13	+39.80
21		+36.09 (CDCl ₃)	+37.78	+35.78	+37.62	+39.98
22		+43.71 (CDCl ₃)	+44.50	+44.00	+46.55	+51.65
23		+45.21(CDCl ₃)	+51.41	+50.81	+49.83	+49.12
24		+45.96 (CDCl ₃)	+43.30	+42.70	+43.68	+48.94

^a Experimentally measured $\delta_{\text{exp}}(^{29}\text{Si})$ values for all systems. The solvent is given in parenthesis. ^b $\delta_{\text{cal}}^{\text{gas}}(^{29}\text{Si})$ chemical shift in gas phase using gas phase structure at MPW1K/IGLO-III//MPW1K/6-31+G(d) level. ^c $\delta_{\text{cal}}^{\text{gas+so}}(^{29}\text{Si})$ gas phase chemical shift with added Boltzmann-weighted SO corrections. SO corrections are obtained at ZORA-SO-PBE0/TZ2P level in gas phase. ^d $\delta_{\text{cal}}^{\text{sp+so}}(^{29}\text{Si})$ chemical shifts are calculated with PCM(UAHF)/MPW1K/IGLO-III(+ZORA-SO)//MPW1K/6-31+G(d). Boltzmann-averaged SO corrections are calculated at ZORA-SO-PBE0/TZ2P in gas phase based on gas phase structure. ^e $\delta_{\text{cal}}^{\text{opt+so}}(^{29}\text{Si})$ chemical shifts are calculated with PCM(UAHF)/MPW1K/IGLO-III//PCM/UAHF-MPW1K/6-31+G(d) level and corrected with Boltzmann-weighted SO corrections at ZORA-SO-PBE0/TZ2P level based on gas phase geometries. For more detailed information on the SO corrections see support information.

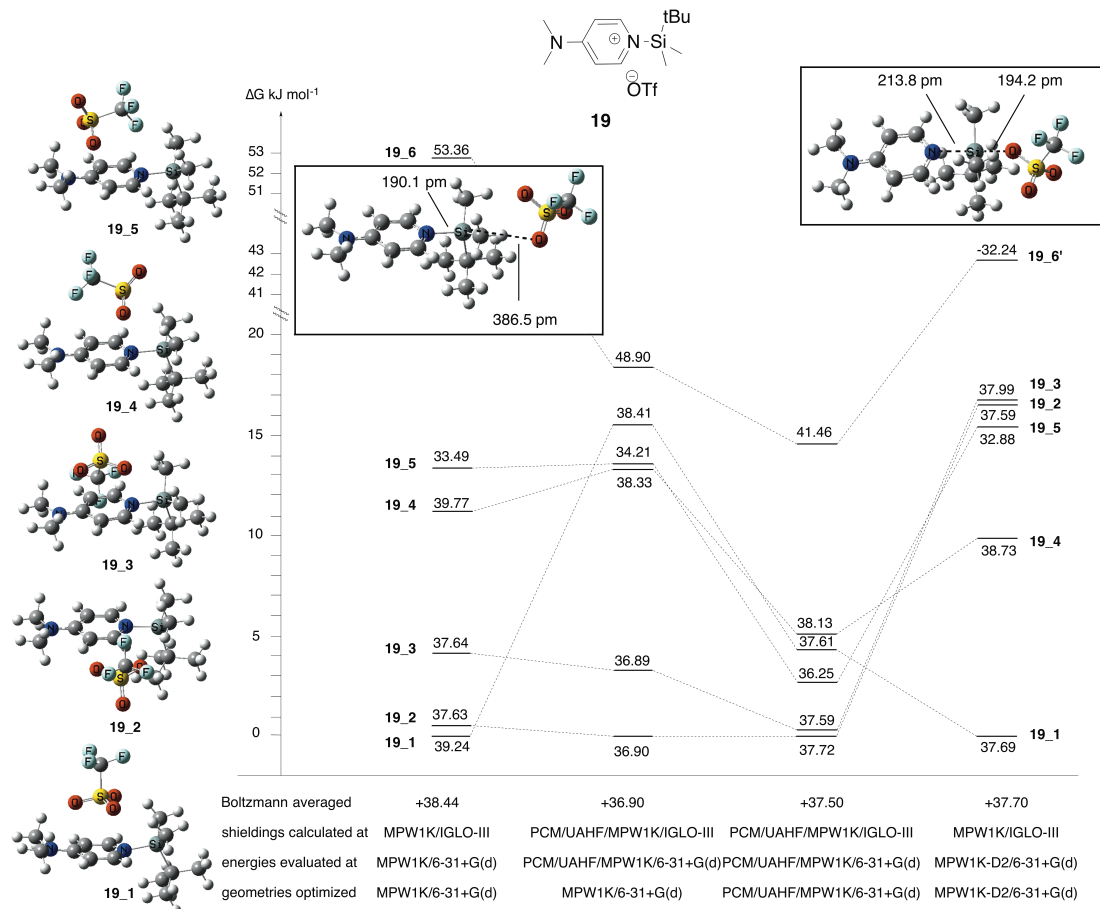


Figure 5.5. Relative free energies and chemical shifts of individual conformers of ion pair system **19** at different theory levels.

Table 5.6. Relative free energies, structural and charge parameters, and ^{29}Si chemical shifts for individual conformational isomers of ion pair **19**. Charge parameters have been obtained from the NBO analysis.⁵⁶

Level for Free Energy Calculation		19_1	19_2	19_3	19_4	19_5	19_6
MPW1K/6-31+G(d)// MPW1K/6-31+G(d)	m(Debye)	10.30	17.27	17.36	13.16	14.39	23.93
	$\Delta G(\text{kJ/mol})$	0.00	0.67	4.01	11.81	13.35	52.89
	r(Si-N) (pm)	184.3	184.9	184.9	184.7	182.9	190.1
	q(OTf)	-0.96	-0.94	-0.94	-0.95	-0.96	-0.95
	$\delta(^{29}\text{Si})$ (ppm)	+39.24	+37.63	+37.64	+39.77	+33.49	+53.36
PCM/UAHF/MPW1K/6-31+G(d)// MPW1K/6-31+G(d)	$\Delta G^{\text{sp}}_{\text{solv}}$ (kJ/mol)	-81.5	-97.65	-97.86	-95.60	-96.86	-131.50
	$\Delta G(\text{kJ mol}^{-1})$	15.54	0.00	3.13	13.20	13.47	18.23
	r(Si-N) (pm)	184.3	184.9	184.9	184.7	182.9	190.1
	q(OTf)	-0.96	-0.95	-0.95	-0.96	-0.97	-0.96
	$\delta(^{29}\text{Si})$ (ppm)	+38.41	+36.90	+36.89	+38.33	+34.21	+48.90
PCM/UAHF/MPW1K-6-31+G(d)// PCM/UAHF/MPW1K-6-31+G(d)	$\Delta G^{\text{opt}}_{\text{solv}}$ (kJ/mol)	-125.81	-119.41	-119.79	-133.05	-141.04	-162.72
	ΔG (kJ/mol)	4.31	0.00	0.29	5.10	2.69	14.51
	r(Si-N) (pm)	184.4	184.5	184.4	184.5	184.2	186.0
	q(OTf)	-0.98	-0.97	-0.97	-0.99	-0.99	-0.98
	$\delta(^{29}\text{Si})$ (ppm)	+37.61	+37.72	+37.59	+38.13	+36.25	+41.64
MPW1K-D2/6-31+G(d)// MPW1K-D2/6-31+G(d)	ΔG (kJ/mol)	0.00	16.54	16.76	9.91	15.39	42.78
	r(Si-N) (pm)	183.0	183.5	183.2	183.2	181.6	213.8
	q(OTf)	-0.95	-0.94	-0.94	-0.95	-0.95	-0.78
	$\delta(^{29}\text{Si})$ (ppm)	+37.69	+37.59	+37.99	+38.73	+32.88	-32.24

The largest effects are observed for ion pair **19_6**, whose structure also depends significantly on the chosen level of theory in the gas phase: geometry optimization at MPW1K/6-31+G(d) level leads to the structure shown as “**19_6**” in Fig. 5.5, which can be characterized as a true ion pair with a comparatively long (387 pm) distance between silicon

atom and triflate counter ion. Reoptimization with the same functional and added dispersion corrections (MPW1K-D2/6-31+G(d)) leads to a structure best described as pentacoordinated silicon intermediate (termed **19_6'**) with a much shorter Si–O (triflate) distance of 194 pm and a largely changed ^{29}Si chemical shift of -32.24 ppm.⁵⁷ More importantly, the very different chemical shift for pentacoordinate structure **19_6'** clearly supports the assignment of the experimentally detected ion pair species as systems with tetracoordinate silicon atoms. The “collapse” of the ion pair structure to a pentacoordinated intermediate upon geometry optimization at MPW1K-D2/6-31+G(d) level has only been observed for conformer **19_6** and not for any of the other (low-energy) conformers.

5.3 Conclusions

Calculated ^{29}Si chemical shifts of (chloro)organosilanes depend strongly on structural details of the respective systems. MPW1K/6-31+(d) gas phase optimizations give structures close enough to experiment for reliable NMR shielding calculations. Relativistic spin-orbit effects are large for chlorosilane systems and reliable shielding calculations thus require SO corrections for these systems. For non-halosilane systems the SO effects are rather small and ^{29}Si shift predictions are thus possible without any relativistic corrections. Solvent effects on ^{29}Si NMR chemical shifts are quite systematic, but only of moderate size, and reliable shift predictions can thus be made using gas phase geometries and, in many cases, also using gas phase shielding calculations. For the (chloro)organosilane compound family studied here MPW1K/IGLO-III(+ZORA-SO)//MPW1K/6-31+G(d) calculations are thus recommended for ^{29}Si NMR shift calculation.

Computational details

Chemical shifts of ^{29}Si containing species ($\delta(^{29}\text{Si})$) are calculated using eqn (1), where $\sigma(^{29}\text{Si}_{\text{TMS}})$ is the chemical shielding for the reference compound tetramethylsilane ($\text{Si}(\text{CH}_3)_4$, TMS, **1**) and $\sigma(^{29}\text{Si})$ is the shielding of the ^{29}Si nucleus in the compound under investigation:

$$\delta(^{29}\text{Si}) = \sigma(^{29}\text{Si}_{\text{TMS}}) - \sigma(^{29}\text{Si}) \quad (1)$$

Shieldings are calculated using the Gauge-Independent Atomic Orbital (GIAO) method.⁵⁸ Shielding values of chemicals are calculated with Gaussian 09, revision C.01⁵⁹ and MOLPRO, Version 2012.1.^{60,61}

The relativistic spin-orbit corrections to the nuclear magnetic shielding constants for ^{29}Si were calculated with the two-component zeroth-order regular approximation (ZORA)^{51,52} using the Amsterdam Density Functional (ADF 2013.01) code.⁶² The hybrid functional PBE0⁶³⁻⁶⁵ in combination with the Slater-type basis set TZ2P⁶⁶ optimized for relativistic ZORA calculations is used for these single point calculations at MPW1K/6-31+G(d) gas phase structures. The spin-orbit correction is calculated as $\delta(^{29}\text{Si})_{\text{ZORA}} - \delta(^{29}\text{Si})_{\text{non-relativistic}}$ and then Boltzmann-averaged for compounds with more than one conformer. For more details on different functionals and basis sets see the Appendix.

References

1. T. M. Alam and M. Henry, *Phys. Chem. Chem. Phys.*, 2000, **2**, 23-28.
2. C. van Wüllen, *Phys. Chem. Chem. Phys.*, 2000, **2**, 2137-2144.
3. U. Herzog, *J. Prakt. Chem.*, 2000, **342**, 379-388.
4. X. Xue and M. Kanzaki, *Phys. Chem. Miner.*, 1998, **26**, 14-30.
5. J. A. Tossell and P. Lazzeretti, *J. Chem. Phys.*, 1986, **84**, 369-374.
6. D. H. Brouwer, *J. Magn. Reson.*, 2008, **194**, 136-146.

7. D. Auer, M. Kaupp and C. Strohmann, *Organometallics*, 2004, **23**, 3647-3655.
8. C. Corminboeuf, T. Heine and J. Weber, *Chem. Phys. Lett.*, 2002, **357**, 1-7.
9. M. Profeta, F. Mauri and C. J. Pickard, *J. Am. Chem. Soc.*, 2003, **125**, 541-548.
10. J. Casanovas, F. Illas and G. Pacchioni, *Chem. Phys. Lett.*, 2000, **326**, 523-529.
11. R. Herges and F. Starck, *J. Am. Chem. Soc.*, 1996, **118**, 12752-12757.
12. J. Ambati and S. E. Rankin, *J. Phys. Chem. A*, 2010, **114**, 5279-5286.
13. T. Heine, A. Goursot, G. Seifert and J. Webert, *J. Phys. Chem. A*, 2001, **105**, 620-626.
14. A. I. Poblador-Bahamonde, R. Poteau, C. Raynaud and O. Eisenstein, *Dalton Trans.*, 2011, **40**, 11321-11326.
15. F. Meyer-Wegner, A. Nadj, M. Bolte, N. Auner, M. Wagner, M. C. Holthausen and H. W. Lerner, *Chem. Eur. J.*, 2011, **17**, 4715-4719.
16. M. Karni, Y. Apeloig, N. Takagi and S. Nagase, *Organometallics*, 2005, **24**, 6319-6330.
17. M. Sugino and Y. Ito, *Chem. Rev.*, 2000, **100**, 3221-3256.
18. R. P. Singh and J. M. Shreeve, *Tetrahedron*, 2000, **56**, 7613-7632.
19. P. Patschinski, C. Zhang, and H. Zipse, manuscript in preparation
20. B. J. Lynch, P. L. Fast, M. Harris and D. G. Truhlar, *J. Phys. Chem. A*, 2000, **104**, 4811-4815.
21. A. F. Wallace, G. V. Gibbs and P. M. Dove, *J. Phys. Chem. A*, 2010, **114**, 2534-2542.
22. A. D. Boese and N. C. Handy, *J. Chem. Phys.*, 2001, **114**, 5497.
23. V. A. Du, G. N. Stipicic and U. Schubert, *Eur. J. Inorg. Chem.*, 2011, **2011**, 3365-3373.
24. Y. Zhao, N. E. Schultz and D. G. Truhlar, *J. Chem. Theory Comput.*, 2006, **2**, 364-382.
25. Y. Zhao and D. G. Truhlar, *Theor. Chem. Acc.*, 2007, **120**, 215-241.
26. B. Maryasin and H. Zipse, *Phys. Chem. Chem. Phys.*, 2011, **13**, 5150-5158.
27. S. Sklenak, J. Dědeček, C. Li, B. Wichterlová, V. Gábová, M. Sierka and J. Sauer, *Phys. Chem. Chem. Phys.*, 2009, **11**, 1237-1247.
28. E. V. van den Berghe and G. P. van der Kelen, *J. Organomet. Chem.*, 1973, **59**, 175-187.
29. M. Tobisu, Y. Kita, Y. Ano and N. Chatani, *J. Am. Chem. Soc.*, 2008, **130**, 15982-15989.
30. K. Ohmatsu, Y. Hamajima and T. Ooi, *J. Am. Chem. Soc.*, 2012, **134**, 8794-8797.
31. B. J. Albert and H. Yamamoto, *Angew. Chem., Int. Ed.*, 2010, **49**, 2747-2749.
32. J. R. Durig, Y. S. Li and R. O. Carter, *J. Mol. Spectrosc.*, 1972, **44**, 18-31.
33. R. C. Mockler, J. H. Bailey and W. Gordy, *J. Chem. Phys.*, 1953, **21**, 1710-1713.
34. P. W. Allen and L. E. Sutton, *Acta Crystallogr.*, 1950, **3**, 46-72.
35. R. Gajda, K. Dziubek and A. Katrusiak, *Acta Crystallogr., Sect. B: Struct. Sci.*, 2006, **62**, 86-93.
36. J. Buschmann, D. Lentz, P. Luger and M. Rottger, *Acta Crystallogr. C*, 2000, **56 (Pt 1)**, 121-122.
37. F. Weigend, *Phys. Chem. Chem. Phys.*, 2006, **8**, 1057-1065.
38. F. Weigend and R. Ahlrichs, *Phys. Chem. Chem. Phys.*, 2005, **7**, 3297-3305.
39. T. H. Dunning, *J. Chem. Phys.*, 1989, **90**, 1007.
40. W. Kutzelnigg, U. Fleischer and M. Schindler, in *NMR Basic Principles and Progress*, ed. P. Diehl, E. Fluck, H. Günther, R. Kosfeld and J. Seelig, Springer, Berlin, Heidelberg, 1991, **23**, 165–262.
41. F. Jensen, *J. Chem. Theory Comput.*, 2008, **4**, 719-727.
42. A. D. Boese and N. C. Handy, *J. Chem. Phys.*, 2001, **114**, 5497-5503.
43. H.-J. Werner, F. R. Manby and P. J. Knowles, *J. Chem. Phys.*, 2003, **118**, 8149.
44. Y. Zhao and D. G. Truhlar, *Theor. Chem. Acc.*, 2008, **120**, 215-241.
45. H. Nakatsuji, T. Nakajima, M. Hada, H. Takashima and S. Tanaka, *Chem. Phys. Lett.*, 1995, **247**, 418-424.
46. T. Helgaker, S. Coriani, P. Jørgensen, K. Kristensen, J. Olsen and K. Ruud, *Chem. Rev.*, 2012, **112**, 543-631.
47. M. Kaupp, O. L. Malkina, V. G. Malkin and P. Pyykkö, *Chem. Eur. J.*, 1998, **4**, 118-126.
48. A. Bagno, M. Bonchio and J. Autschbach, *Chem. Eur. J.*, 2006, **12**, 8460-8471.
49. L. A. Truflandier, E. Brendler, J. Wagler and J. Autschbach, *Angew. Chem. Int. Ed.*, 2011, **50**, 255-259.
50. J. Autschbach, K. Sutter, L. A. Truflandier, E. Brendler and J. Wagler, *Chem. Eur. J.*, 2012, **18**, 12803-12813.
51. E. v. Lenthe, E. J. Baerends and J. G. Snijders, *J. Chem. Phys.*, 1993, **99**, 4597-4610.
52. S. K. Wolff, T. Ziegler, E. van Lenthe and E. J. Baerends, *J. Chem. Phys.*, 1999, **110**, 7689.
53. V. G. Malkin, O. L. Malkina and D. R. Salahub, *Chem. Phys. Lett.*, 1996, **261**, 335-345.

- 54.Taking ion pair system **19** as an example, the SO correction for the six different conformers shown in Fig. 5 vary from -0.3 to -0.5 ppm at ZORA-SO-PBE0/TZ2P level. After Boltzmann averaging, the SO correction amounts to -0.5 ppm, which is identical to the value of the most stable conformer **19_1** (see supporting information for details).
- 55.B. Wrackmeyer, C. Stader and H. Zhou, *Spectrochim. Acta, Part A*, 1989, **45**, 1101-1111.
- 56.NBO calculations were performed using the NBO 3.1 program as implemented in the GAUSSIAN 09.C1 package.
- 57.This type of geometry is also obtained upon geometry optimization at MP2(FC)/6-31+G(d) level.
- 58.R. Ditchfield, *Mol. Phys.*, 1974, **27**, 789-807.
- 59.M. J. Frisch, G. W. Trucks, H. B. Schlegel, G. E. Scuseria, M. A. Robb, J. R. Cheeseman, G. Scalmani, V. Barone, B. Mennucci, G. A. Petersson, H. Nakatsuji, M. Caricato, X. Li, H. P. Hratchian, A. F. Izmaylov, J. Bloino, G. Zheng, J. L. Sonnenberg, M. Hada, M. Ehara, K. Toyota, R. Fukuda, J. Hasegawa, M. Ishida, T. Nakajima, Y. Honda, O. Kitao, H. Nakai, T. Vreven, J. A. Montgomery, Jr. J. E. Peralta, F. Ogliaro, M. Bearpark, J. J. Heyd, E. Brothers, K. N. Kudin, V. N. Staroverov, T. Keith, R. Kobayashi, J. Normand, K. Raghavachari, A. Rendell, J. C. Burant, S. S. Iyengar, J. Tomasi, M. Cossi, N. Rega, J. M. Millam, M. Klene, J. E. Knox, J. B. Cross, V. Bakken, C. Adamo, J. Jaramillo, R. Gomperts, R. E. Stratmann, O. Yazyev, A. J. Austin, R. Cammi, C. Pomelli, J. W. Ochterski, R. L. Martin, K. Morokuma, V. G. Zakrzewski, G. A. Voth, P. Salvador, J. J. Dannenberg, S. Dapprich, A. D. Daniels, O. Farkas, J. B. Foresman, J. V. Ortiz, J. Cioslowski, D. J. Fox, Gaussian, Inc., Wallingford CT, 2010.
- 60.H.-J. Werner, P. J. Knowles, G. Knizia, F. R. Manby and M. Schütz, *WIREs Comput Mol Sci* 2, 2012, **2**, 242-253.
- 61.H.-J. Werner, P. J. Knowles, G. Knizia, F. R. Manby, M. Schütz, and others; see also <http://www.molpro.net>.
- 62.ADF2013, SCM, Theoretical Chemistry, Vrije Universiteit, Amsterdam, Netherlands; see also: <http://www.scm.com>.
- 63.M. Ernzerhof and G. E. Scuseria, *J. Chem. Phys.*, 1999, **110**, 5029-5036.
- 64.C. Adamo and V. Barone, *J. Chem. Phys.*, 1999, **110**, 6158-6170.
- 65.C. Adamo and V. Barone, *J. Chem. Phys.*, 1998, **108**, 664-675.
- 66.E. Van Lenthe and E. J. Baerends, *J. Comput. Chem.*, 2003, **24**, 1142-1156.

6 General Conclusions

(1) Various methods have been applied for the properties description of Lewis pairs including geometry information and complexation energy. It is a challenge to use theoretical methods for Lewis pair calculation, especially for weakly bound Lewis pairs like $\text{PH}_3\text{-BF}_3$. Relaxed scans along the P-B bond in $\text{PH}_3\text{-BF}_3$ at different theory levels produce a flat curve with a P-B bond which is more than 230 pm. Most of the theoretical methods have located one global minimum with a P-B bond length which is more than 300 pm. MPW1K and MP2 with specific basis set give two minima, and $r(\text{P-B})$ is around 220 pm and 300 pm, respectively. For both methods, minimum 1 disappeared after single point correction at CCSD(T)/cc-pVTZ level and minimum 2 is the only minimum on the relaxed scan curve.

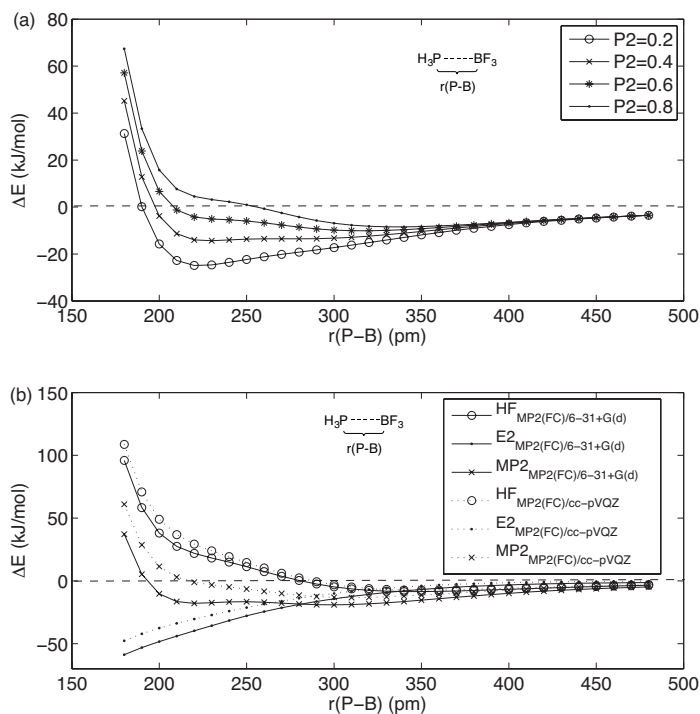


Figure 6.1.1. Relaxed scan of $r(\text{P-B})$ in $\text{PH}_3\text{-BF}_3$, $\Delta E = E_{\text{tot}}(\text{PH}_3\text{-BF}_3) - E_{\text{tot}}(\text{PH}_3) - E_{\text{tot}}(\text{BF}_3)$ (a) Variation of HF exchange in MPW1K/6-31+G(d) with $P_1=1$, $P_2+P_4=1$, $P_3=0.527$, $P_5=P_6=1$. (b) Energy contributions for MP2(FC)/6-31+G(d) and MP2(FC)/cc-pVQZ.

The results of analyzing the energy contribution of MPW1K and MP2 indicate that for MPW1K method, increasing the contribution from HF exchange energy to MPW1K energy, the global minimum shifts from minimum 1 to minimum 2 and minimum 1 vanishes gradually (Figure 6.1.1). For MP2 method, the combination of E_{HF} and E_2 affords minimum 1. All these results show that minimum 2 is the global minimum and the portion of HF exchange energy and correlation energy is the main factor which influences the bond distance between PH_3 and BF_3 . Two points extrapolation method predicts the converged $r(\text{P-B})$ is 312.5 pm and the converged complexation energy is -10.57 kJ/mol in the gas phase.

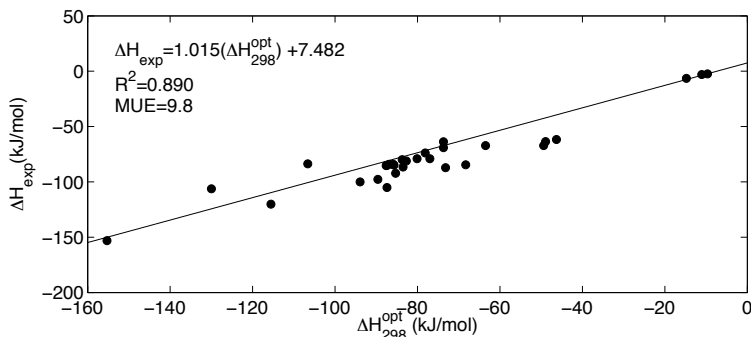
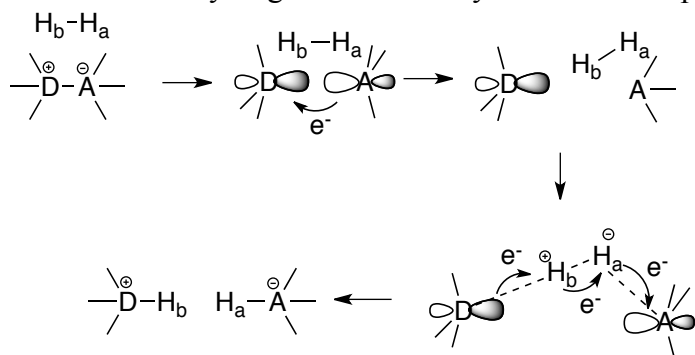


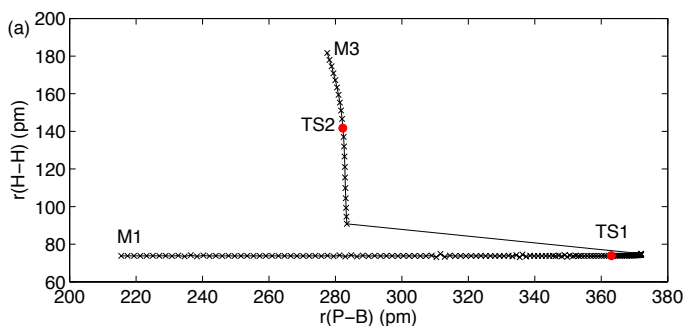
Figure 6.1.2. Calculated complexation energy correlated with experiment value at ω B97XD/6-31G(d) level.

Different theoretical methods are tested for calculations of Lewis pairs. Comparing experimental results and theoretically calculated complexation energies, it appears that ω B97XD/6-31G(d) is very well suited for Lewis pair systems (Figure 6.1.2). Except for the normal strongly bonded Lewis pairs, ω B97XD/6-31G(d) can also provide surprising reliable results for the weakly bonded Lewis pairs, which is a challenge for other methods.

(2) The mechanism of hydrogen activation by different Lewis pairs has been studied with the theoretical methods. According to the analysis of bond distance and charge distribution, the mechanism of hydrogen activation by normal Lewis pairs is suggested as follows:



Scheme 6.2.1. Reaction mechanism of hydrogen activation by normal Lewis pairs.



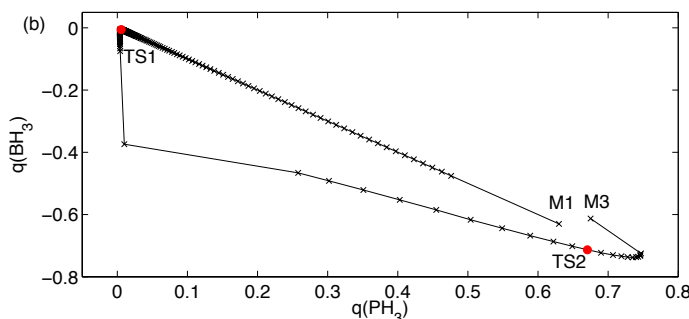
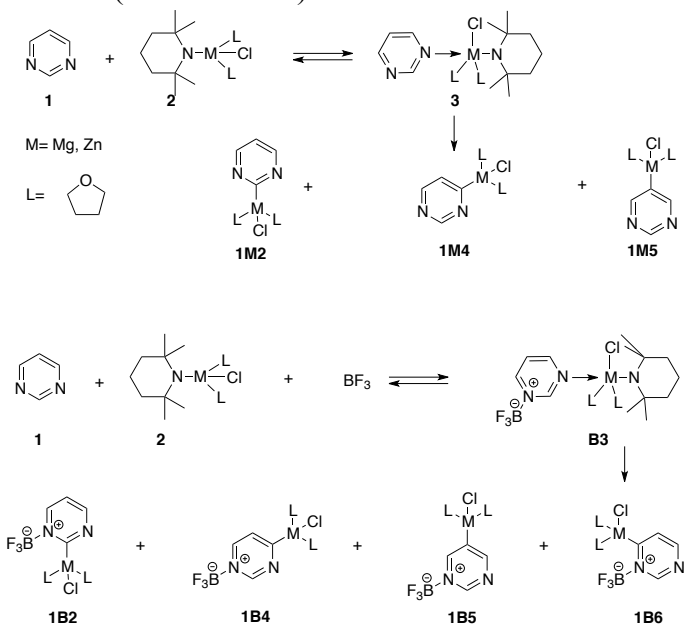


Figure 6.2.1. The reaction of H_2 with $\text{PH}_3\text{-BH}_3$. (a) $r(\text{P-B})$ vs $r(\text{H-H})$ along IRC pathway at MP2/cc-pVTZ level. (b) Charge analysis of PH_3 and BH_3 along the IRC at MP2/cc-pVTZ level.

The mechanism is the same for both the strongly bonded and the weakly bonded Lewis pairs (Figure 6.2.1). The reaction begins with the breaking of the bond between Lewis acid and Lewis base so that H_2 can enter the reaction region. During this stage the charge transfers from the Lewis acid to the Lewis base. The first stage will stop once the Lewis acid and Lewis base moieties are neutral. The next stage goes through the approaching of Lewis base to H_2 , accompanied by a charge transfer from Lewis base to Lewis acid via the H-H bond bridge. As a consequence, the hydrogen bond is split.

The reaction energy profiles show that the activation reaction of Lewis pair with hydrogen is endothermic. Comparing the activation free energies of the two steps, the second step is the rate-determining step, which includes charge donating from Lewis base to Lewis acid and H-H bond breaking. In the transition state of hydrogen bond breaking, the reaction center are non-linear, and the dihedral angles of Lewis acid and Lewis base depends on the steric effects. Since structure properties determine chemical activity, based on the eight systems studied hereby, the connection between the activation free energy of reaction and $r(\text{P-B})$ is $\Delta G_{298}^{\neq} = -3.8253 \times r(\text{P-B}) + 957.29$ with a correlation coefficient $R^2=0.835$. This formula can be used further for quantitative predictions of reaction barriers of the new systems.

(3) The relative energies of the metalation of pyrimidines are compared by theoretical methods (Scheme 6.3.1).



Scheme 6.3.1. Scheme for the reaction of pyrimidine with $\text{TMPMetCl}\cdot 2\text{THF}$ ($\text{Met}=\text{Mg, Zn}$).

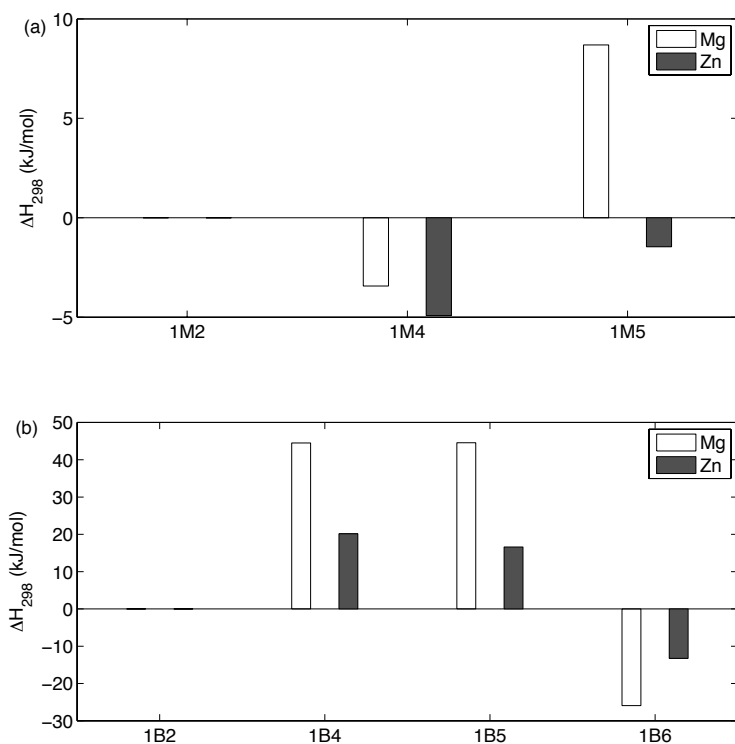
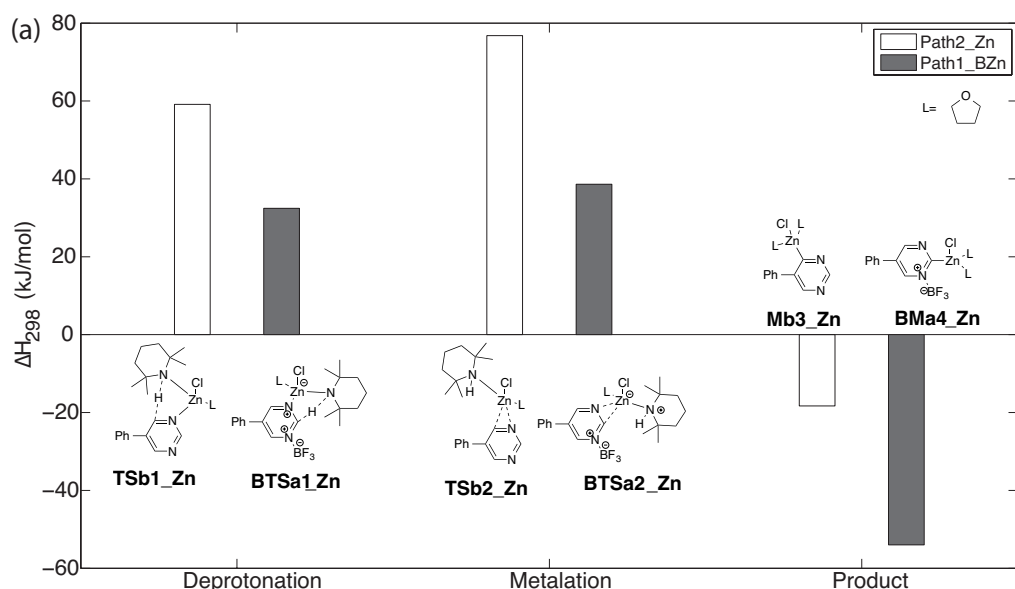


Figure 6.3.1. Relative energies of metalated pyrimidines at B3LYP/6311TZVP level.

The relative energies of metalated pyrimidines (Figure 6.3.1) show that, in the system without $\text{BF}_3\cdot\text{OEt}_2$, C4 metatlation of pyrimidines are more energetically preferred for both Mg-contained complex and Zn-contained complex. With the attachment of BF_3 , C6 metatlation product **1B6** is more energetically favorable than **1B2**, **1B4** and **1B5**. By analyzing the geometry, it is found when BF_3 is in ortho-position to the metal atom, there is a large interaction between metal atom and at least one fluorine atom of BF_3 . The coordination between metal base and BF_3 helps to stabilize the complex.

The mechanisms of the reaction of 5-phenylpyrimidine with $\text{TMPMetCl}\cdot 2\text{THF}$ (Met=Zn, Mg) are investigated and the selected information is summarized in Figure 6.3.2.



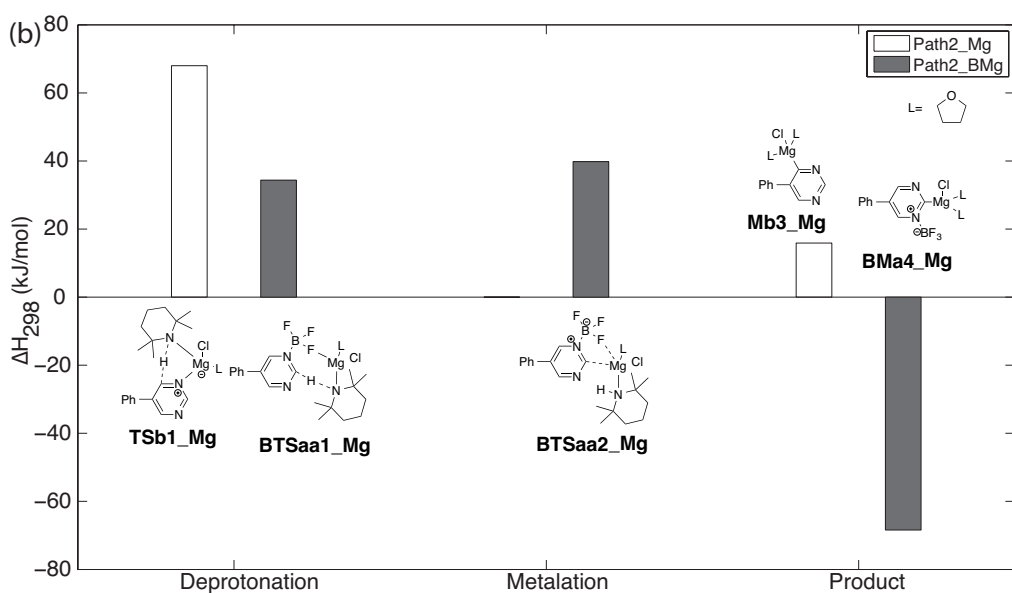


Figure 6.3.2. Relative energies of transition states and products at SMD/B3LYP /631SVP//B3LYP/631SVP level. (a) Energies of transition states and products for Path2_Zn and Path1_BZn. (b) Energies of transition states and products for Path2_Mg and Path2_BMg.

For the reaction of 5-phenylpyrimidine with $\text{TMPZnCl}\cdot\text{2THF}$, the most energetically preferred pathway is Path2_Zn, which leads to C4 metalation of pyrimidine. For the reaction of 5-phenylpyrimidine with $\text{TMPCMgCl}\cdot\text{2THF}$, the energetically preferred reaction path is Path2_Mg, which generates C4 metalated pyrimidine and the total reaction is slightly endothermic. The addition of $\text{BF}_3\cdot\text{OEt}_2$ changes the main products from C4 into C2 metalation of pyrimidines for both of $\text{TMPZnCl}\cdot\text{2THF}$ and $\text{TMPCMgCl}\cdot\text{2THF}$. For the reaction involving $\text{TMPZnCl}\cdot\text{2THF}$, the reaction occurs mainly along Path1_BZn. For the system involving $\text{TMPCMgCl}\cdot\text{2THF}$, the most energetically preferred path is Path2_BMg. Because of the interaction between BF_3 and ligands, BF_3 holds the metal base and 5-phenylpyrimidine together and as the consequence, the activation energies for Path1_BZn and Path2_BMg are greatly reduced. All the calculations are consistent with experimental observation.

(4) Theoretical methods have been tested for ^{29}Si chemical shift calculations of organosilane systems. NMR shifts are sensitive to the geometry used for NMR calculations, and it has been shown that MPW1K/6-31+(d) in the gas phase gives reliable geometry even compared with experimental results. Compared with chemical shift measured by experiment, solvent effects systematically increase ^{29}Si chemical shifts.

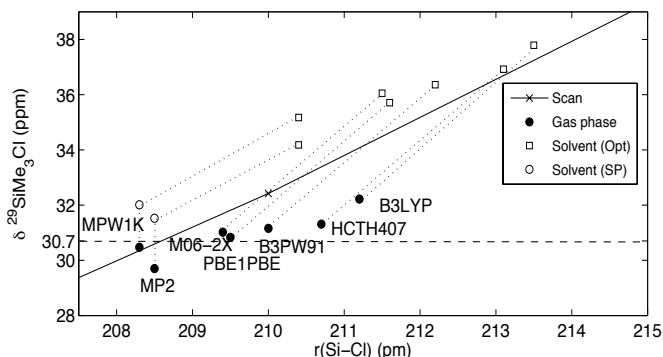


Figure 6.4.1. Calculated $\delta^{29}\text{Si}$ values for SiMe_3Cl (2) (MP2: solid circles and PCM/MP2: empty symbols; IGLO-III basis set) using molecular structures optimized at various levels of theory using the 6-31+G(d) basis set. Dashed line: experimental values in CDCl_3 ; solid line: relaxed scan along the Si-Cl bond (gas phase, MPW1K structures). Empty circles: PCM/MP2 shifts on gas phase structures; empty squares: PCM/MP2 shifts on solution-phase geometries (all solvent calculations: CHCl_3 , UAHF radii).

For the chlorosilane systems, the ^{29}Si chemical shifts have large deviations from experimental value. Relativistic spin-orbit effect (SO) is used for chemical shift corrections.

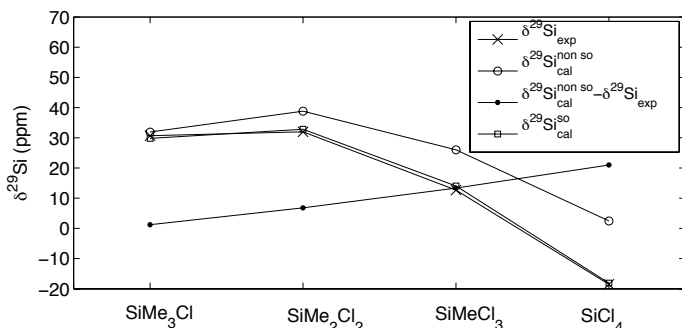


Figure 6.4.2. Comparison between experimentally measured and theoretically calculated shift values at MPW1K/IGLO-III//MPW1K/6-31+G(d) level for alkylchlorosilanes $\text{SiMe}_{4-x}\text{Cl}_x$ with $x = 1-4$. SO corrections are obtained from ZORA-SO-PBE0/TZ2P single-point calculations. Geometries are obtained at MPW1K/6-31+G(d) level in the gas phase.

SO corrections are larger for the halogen-containing system than for the non-halogen containing systems. Therefore, for chloro-substituted organosilane compounds, MPW1K/IGLO-III(+ZORA-SO)//MPW1K/6-31+G(d) is recommended for ^{29}Si NMR shift calculation; for other organosilane compounds, MPW1K/IGLO-III//MPW1K/6-31+G(d) is an accurate method to evaluate the ^{29}Si chemical shift.

7. Appendix

7.1. General Details

All calculated data (shielding values, total energies, free energies, enthalpies etc) are collected here. The quantum chemical calculations have been performed with Gaussian 09.C1¹, Molpro² and ORCA³. EDA analysis is carried out by GAMESS(US)⁴. The conformational search uses the MACROMODEL⁵.

Reference:

1. M. J. Frisch, G. W. Trucks, H. B. Schlegel, G. E. Scuseria, M. A. Robb, J. R. Cheeseman, G. Scalmani, V. Barone, B. Mennucci, G. A. Petersson, H. Nakatsuji, M. Caricato, X. Li, H. P. Hratchian, A. F. Izmaylov, J. Bloino, G. Zheng, J. L. Sonnenberg, M. Hada, M. Ehara, K. Toyota, R. Fukuda, J. Hasegawa, M. Ishida, T. Nakajima, Y. Honda, O. Kitao, H. Nakai, T. Vreven, J. A. Montgomery, Jr. J. E. Peralta, F. Ogliaro, M. Bearpark, J. J. Heyd, E. Brothers, K. N. Kudin, V. N. Staroverov, T. Keith, R. Kobayashi, J. Normand, K. Raghavachari, A. Rendell, J. C. Burant, S. S. Iyengar, J. Tomasi, M. Cossi, N. Rega, J. M. Millam, M. Klene, J. E. Knox, J. B. Cross, V. Bakken, C. Adamo, J. Jaramillo, R. Gomperts, R. E. Stratmann, O. Yazyev, A. J. Austin, R. Cammi, C. Pomelli, J. W. Ochterski, R. L. Martin, K. Morokuma, V. G. Zakrzewski, G. A. Voth, P. Salvador, J. J. Dannenberg, S. Dapprich, A. D. Daniels, O. Farkas, J. B. Foresman, J. V. Ortiz, J. Cioslowski, D. J. Fox, Gaussian, Inc., Wallingford CT, 2010.
2. H.-J. Werner, P. J. Knowles, G. Knizia, F. R. Manby, M. Schütz, and others; see <http://www.molpro.net>.
3. F. Neese, ORCA 3.0, Universitt Bonn, 2007, see http://www.mpibac.mpg.de/bac/index_en.php
4. Schmidt, M. W., Baldridge, K. K., Boatz, J. A., Elbert, S. T., Gordon, M. S., Jensen, J. H., Koseki, S., Matsunaga, N., Nguyen, K. A., Su, S., Windus, T. L., Dupuis, M. & Montgomery, J. A. (1993). J. Comput. Chem. 14, 1347-1363; see <http://www.msg.ameslab.gov/GAMESS/GAMESS.html>.
5. Schrdinger, LLC., *MacroModel* 9.7, 2009.

7.2 Calculated Data for Chapter 2

Computational detail for binding energies and geometrical characteristics of Lewis pair systems - a methodological survey

HF/6-31+G(d)	r(N-B) ()	E	H	G
NH ₃		-56.189499	-56.148724	-56.170515
BH ₃		-26.390694	-26.359251	-26.381259
NH ₃ -BH ₃	1.686	-82.614992	-82.536117	-82.563283
 (kJ/mol)		91.360000	73.890000	30.220000
B3LYP/6-31G(d)	r(N-B) ()	E	H	G
NH ₃		-56.547948	-56.509610	-56.531455
BH ₃		-26.613000	-26.582671	-26.604708
NH ₃ -BH ₃	1.669	-83.213209	-83.138169	-83.165401
 (kJ/mol)		137.210000	120.480000	76.760000
B97D/6-31+G(d)	r(N-B) ()	E	H	G
NH ₃		-56.521396	-56.483785	-56.505648
BH ₃		-26.594223	-26.564304	-26.586368
NH ₃ -BH ₃	1.707	-83.163243	-83.089940	-83.117383
 (kJ/mol)		125.040000	109.880000	66.600000
B98/6-31G(d)	r(N-B) ()	E	H	G
NH ₃		-56.524639	-56.486141	-56.507985
BH ₃		-26.597091	-26.566762	-26.588800

NH ₃ -BH ₃	1.661	-83.177270	-83.101919	-83.129101
Δ (kJ/mol)		145.820000	128.690000	84.850000
MPW1K/6-31G(d)	r(N-B) (Å)	E	H	G
NH ₃		-56.528935	-56.489358	-56.511172
BH ₃		-26.599714	-26.568958	-26.590329
NH ₃ -BH ₃	1.644	-83.187419	-83.110394	-83.137491
Δ (kJ/mol)		154.300000	136.730000	94.490000
MPW1K/6-31+G(d)	r(N-B) (Å)	E	H	G
NH ₃		-56.535293	-56.495723	-56.517540
BH ₃		-26.600665	-26.569955	-26.592363
NH ₃ -BH ₃	1.644	-83.191517	-83.114611	-83.141669
Δ (kJ/mol)		145.870000	128.470000	83.400000
M05-2X/6-31G(d)	r(N-B) (Å)	E	H	G
NH ₃		-56.538115	-56.499077	-56.520907
BH ₃		-26.594881	-26.564052	-26.586087
NH ₃ -BH ₃	1.673	-83.183917	-83.108143	-83.135344
Δ (kJ/mol)		133.690000	118.180000	74.430000
M05-2X /6-31+G(d)	r(N-B) (Å)	E	H	G
NH ₃		-56.530703	-56.491648	-56.513474
BH ₃		-26.593481	-26.562564	-26.584598
NH ₃ -BH ₃	1.672	-83.178608	-83.102687	-83.129959
Δ (kJ/mol)		142.890000	127.270000	83.720000
M06-2X/6-31+G(d)	r(N-B) (Å)	E	H	G
NH ₃		-56.520057	-56.481382	-56.503222
BH ₃		-26.586453	-26.555645	-26.577672
NH ₃ -BH ₃	1.661	-83.160572	-83.084930	-83.112059
Δ (kJ/mol)		141.940000	125.770000	81.820000
M06-2X/6-31+G(d,p)	r(N-B) (Å)	E	H	G
NH ₃		-56.528968	-56.490440	-56.512284
BH ₃		-26.588620	-26.557924	-26.579951
NH ₃ -BH ₃	1.660	-83.170163	-83.094762	-83.121932
Δ (kJ/mol)		138.040000	121.820000	77.970000
ωB97XD/6-31G(d)	r(N-B) (Å)	E	H	G
NH ₃		-56.529274	-56.490455	-56.512292
BH ₃		-26.598311	-26.568123	-26.590167
NH ₃ -BH ₃	1.658	-83.183804	-83.108070	-83.135265
Δ (kJ/mol)		147.600000	129.940000	86.130000
ωB97XD/6-31+G(d)	r(N-B) (Å)	E	H	G
NH ₃		-56.536646	-56.497846	-56.519688
BH ₃		-26.599530	-26.569420	-26.591465
NH ₃ -BH ₃	1.657	-83.188693	-83.113081	-83.140227
Δ (kJ/mol)		137.890000	120.290000	76.330000
ωB97XD/def2-TZVP	r(N-B) (Å)	E	H	G
NH ₃		-56.564337	-56.525977	-56.547816
BH ₃		-26.607955	-26.578056	-26.600095
NH ₃ -BH ₃	1.649	-83.224053	-83.149085	-83.176258
Δ (kJ/mol)		135.900000	118.280000	74.430000

	r(N-B) (Å)	E	H	G
ωB97XD/def2-TZVPP				
NH ₃		-56.567332	-56.528928	-56.550763
BH ₃		-26.608617	-26.578690	-26.600725
NH ₃ -BH ₃	1.648	-83.227437	-83.152388	-83.179593
Δ (kJ/mol)		135.180000	117.540000	73.790000
ωB97XD/cc-pVTZ	r(N-B) (Å)	E	H	G
NH ₃		-56.563338	-56.524938	-56.546771
BH ₃		-26.608391	-26.578462	-26.600497
NH ₃ -BH ₃	1.648	-83.224682	-83.149678	-83.176865
Δ (kJ/mol)		139.030000	121.500000	77.710000
MP2(FC)/aug-cc-pVDZ	r(N-B) (Å)	E	H	G
NH ₃		-56.204907	-56.366687	-56.388546
BH ₃		-26.391293	-26.456369	-26.478423
NH ₃ -BH ₃	1.667	-82.628645	-82.865499	-82.892768
Δ (kJ/mol)		85.180000	111.430000	67.740000
MP2(FC)/cc-PVTZ	r(N-B) (Å)	E	H	G
NH ₃		-56.217832	-56.414367	-56.436195
BH ₃		-26.400155	-26.482886	-26.504902
NH ₃ -BH ₃	1.649	-82.652886	-82.944846	-82.972003
Δ (kJ/mol)		91.630000	124.960000	81.140000
CCSDT/cc-PVDZ	r(N-B) (Å)	E	H	G
NH ₃		-56.365525	-56.364581	-56.387481
BH ₃		-26.479514	-26.478570	-26.501660
NH ₃ -BH ₃	1.664	-82.892595	-82.891651	-82.919874
Δ (kJ/mol)		124.860000	127.340000	80.690000
CCSDT/cc-PVTZ	r(N-B) (Å)	E	H	G
NH ₃		-56.435821	-56.434877	-56.457748
BH ₃		-26.508472	-26.507528	-26.530574
NH ₃ -BH ₃	1.655	-82.989460	-82.988516	-83.016723
Δ (kJ/mol)		118.590000	121.060000	74.570000
CCSDT/cc-PVQZ	r(N-B) (Å)	E	H	G
NH ₃		-26.515807	-26.514863	-26.537908
BH ₃		-56.455698	-56.454754	-56.477624
NH ₃ -BH ₃	1.651	-83.015321	-83.014376	-83.042587
Δ (kJ/mol)		115.040000	117.510000	71.030000
ωB97XD/cc-pvtz//ωB97XD/6-31G(d)	r(N-B) (Å)	E	Thermal correction for H	H
NH ₃		-56.563188	0.038819	-56.524369
BH ₃		-26.608365	0.030188	-26.578176
NH ₃ -BH ₃	1.658	-83.224557	0.075734	-83.148822
Δ (kJ/mol)		139.160000		121.500000
ωB97XD/def2-tzvp//ωB97XD/6-31G(d)	r(N-B) (Å)	E	Thermal correction for H	H
NH ₃		-56.564276	0.038819	-56.525457
BH ₃		-26.607944	0.030188	-26.577756
NH ₃ -BH ₃	1.658	-83.223965	0.075734	-83.148231
Δ (kJ/mol)		135.860000		118.190000
ri-scs-mp2/cc-pvtz//ωB97XD/6-31G(d)	r(N-B) (Å)	E	Thermal correction for H	H
NH ₃		-56.454630	0.038819	-56.415811

BH ₃		-26.526211	0.030188	-26.496023
NH ₃ -BH ₃	1.658	-83.030762	0.075734	-82.955027
Δ (kJ/mol)		131.070000		113.410000
ri-scs-mp2/def-tzvp//ωB97XD/6-31G(d)	r(N-B) (Å)	E	Thermal correction for H	H
NH ₃		-56.444690	0.038819	-56.405871
BH ₃		-26.517734	0.030188	-26.487545
NH ₃ -BH ₃	1.658	-83.011130	0.075734	-82.935396
Δ (kJ/mol)		127.880000		110.220000
ccsd/cbs//ωB97XD/6-31G(d)	r(N-B) (Å)	E	Thermal correction for H	H
NH ₃		-56.501978	0.038819	-56.463159
BH ₃		-26.548375	0.030188	-26.518187
NH ₃ -BH ₃	1.658	-83.101435	0.075734	-83.025701
Δ (kJ/mol)		134.120000		116.450000
HF/6-31+G(d)	r(P-B) (Å)	E	H	G
PF ₃		-639.145115	-639.131077	-639.161900
BH ₃		-26.390694	-26.359251	-26.381259
PF ₃ -BH ₃	1.933	-665.548177	-665.499015	-665.534607
Δ (kJ/mol)		32.470000	22.810000	-22.450000
B3LYP/6-31G(d)	r(P-B) (Å)	E	H	G
PF ₃		-640.956439	-640.942935	-640.974137
BH ₃		-26.613000	-26.582671	-26.604708
PF ₃ -BH ₃	1.875	-667.609518	-667.562344	-667.598318
Δ (kJ/mol)		105.230000	96.460000	51.130000
B97D/6-31+G(d)	r(P-B) (Å)	E	H	G
PF ₃		-640.824419	-640.811535	-640.843012
BH ₃		-26.594223	-26.564304	-26.586368
PF ₃ -BH ₃	1.899	-667.449070	-667.403206	-667.439634
Δ (kJ/mol)		79.890000	71.850000	26.920000
B98/6-31G(d)	r(P-B) (Å)	E	H	G
PF ₃		-640.809024	-640.795455	-640.826615
BH ₃		-26.597091	-26.566762	-26.588800
PF ₃ -BH ₃	1.881	-667.449294	-667.402037	-667.437966
Δ (kJ/mol)		113.370000	104.550000	59.210000
MPW1K/6-31G(d)	r(P-B) (Å)	E	H	G
PF ₃		-640.855645	-640.841752	-640.872748
BH ₃		-26.599714	-26.568958	-26.590329
PF ₃ -BH ₃	1.851	-667.503298	-667.455152	-667.490863
Δ (kJ/mol)		125.860000	116.680000	72.950000
MPW1K/6-31+G(d)	r(P-B) (Å)	E	H	G
PF ₃		-640.876876	-640.863224	-640.894272
BH ₃		-26.600665	-26.569955	-26.592363
PF ₃ -BH ₃	1.856	-667.517852	-667.470018	-667.505763
Δ (kJ/mol)		105.840000	96.720000	50.220000
M05-2X/6-31G(d)	r(P-B) (Å)	E	H	G
PF ₃		-640.913996	-640.900107	-640.931141
BH ₃		-26.594881	-26.564052	-26.586087
PF ₃ -BH ₃	1.862	-667.549945	-667.502056	-667.537951

Δ (kJ/mol)		107.830000	99.500000	54.410000
M05-2X /6-31+G(d)	r(P-B) (\AA)	E	H	G
PF ₃		-640.939384	-640.925772	-640.956875
BH ₃		-26.593481	-26.562564	-26.584598
PF ₃ -BH ₃	1.871	-667.568014	-667.520516	-667.556471
Δ (kJ/mol)		92.280000	84.490000	39.380000
M06-2X/6-31+G(d)	r(P-B) (\AA)	E	H	G
PF ₃		-640.845773	-640.832158	-640.863252
BH ₃		-26.586453	-26.555645	-26.577672
PF ₃ -BH ₃	1.875	-667.466957	-667.419353	-667.451579
Δ (kJ/mol)		91.180000	82.830000	37.430000
M06-2X/6-31+G(d,p)	r(P-B) (\AA)	E	H	G
PF ₃		-640.845773	-640.832158	-640.863252
BH ₃		-26.588620	-26.557924	-26.579951
PF ₃ -BH ₃	1.873	-667.469276	-667.421796	-667.457671
Δ (kJ/mol)		91.580000	83.270000	37.990000
ω B97XD/6-31G(d)	r(P-B) (\AA)	E	H	G
PF ₃		-640.856257	-640.842578	-640.873701
BH ₃		-26.598311	-26.568121	-26.590165
PF ₃ -BH ₃	1.867	-667.498718	-667.451293	-667.487147
Δ (kJ/mol)		115.920000	106.580000	61.120000
ω B97XD/6-31+G(d)	r(P-B) (\AA)	E	H	G
PF ₃		-640.881468	-640.868048	-640.899236
BH ₃		-26.599530	-26.569420	-26.591465
PF ₃ -BH ₃	1.877	-667.516164	-667.469089	-667.505021
Δ (kJ/mol)		92.330000	83.020000	37.600000
ω B97XD/def2-TZVP	r(P-B) (\AA)	E	H	G
PF ₃		-641.052831	-641.039223	-641.070224
BH ₃		-26.607955	-26.578056	-26.600095
PF ₃ -BH ₃	1.867	-667.705459	-667.658521	-667.694220
Δ (kJ/mol)		117.290000	108.280000	62.750000
ω B97XD/def2-TZVPP	r(P-B) (\AA)	E	H	G
PF ₃		-641.053124	-641.039518	-641.070520
BH ₃		-26.608617	-26.578690	-26.600725
PF ₃ -BH ₃	1.847	-667.706599	-667.659646	-667.695336
Δ (kJ/mol)		117.780000	108.800000	63.250000
ω B97XD/cc-pVTZ	r(P-B) (\AA)	E	H	G
PF ₃		-641.028979	-641.015461	-641.046512
BH ₃		-26.608391	-26.578462	-26.600497
PF ₃ -BH ₃	1.858	-667.679621	-667.632658	-667.668470
Δ (kJ/mol)		110.930000	101.700000	56.350000
ω B97XD/cc-pvtz// ω B97XD/6-31G(d)	r(P-B) (\AA)	E	Thermal correction for H	H
PF ₃		-641.0288074	0.013678	-641.015129
BH ₃		-26.60836452	0.030188	-26.578176
PF ₃ -BH ₃	1.867	-667.6790686	0.047425	-667.631644
Δ (kJ/mol)		110		100.660000
ω B97XD/def2-tzvp// ω B97XD/6-31G(d)	r(P-B) (\AA)	E	Thermal correction for H	H

PF ₃		-641.0522667	0.013678	-641.038588
BH ₃		-26.60794395	0.030188	-26.577756
PF ₃ -BH ₃	1.867	-667.7042039	0.047425	-667.656779
Δ (kJ/mol)		115.5		106.160000
ri-scs-mp2/cc-pvtz//ωB97XD/6-31G(d)	r(P-B) (Å)	E	Thermal correction for H	H
PF ₃		-640.16546	0.013678	-640.151782
BH ₃		-26.52621106	0.030188	-26.496023
PF ₃ -BH ₃	1.867	-666.7281194	0.047425	-666.680695
Δ (kJ/mol)		95.7		86.350000
ri-scs-mp2/def-tzvp//ωB97XD/6-31G(d)	r(P-B) (Å)	E	Thermal correction for H	H
PF ₃		-640.1792322	0.013678	-640.165554
BH ₃		-26.51773353	0.030188	-26.487545
PF ₃ -BH ₃	1.867	-666.7347175	0.047425	-666.687293
Δ (kJ/mol)		99.12		89.770000
ccsd/cbs//ωB97XD/6-31G(d)	r(P-B) (Å)	E	Thermal correction for H	H
PF ₃		-640.3963861	0.013678	-640.382708
BH ₃		-26.54837528	0.030188	-26.518187
PF ₃ -BH ₃	1.867	-666.9865804	0.047425	-666.939156
Δ (kJ/mol)		109.8		100.450000
HF/6-31+G(d)	r(P-B) (Å)	E	H	G
PM ₃		-459.569796	-459.442001	-459.477236
BH ₃		-26.390694	-26.359251	-26.381259
PM ₃ -BH ₃	1.967	-485.998148	-485.835366	-485.875539
Δ (kJ/mol)		98.870000	89.570000	44.750000
B3LYP/6-31G(d)	r(P-B) (Å)	E	H	G
PM ₃		-461.098424	-460.977302	-461.013212
BH ₃		-26.613000	-26.582671	-26.604708
PM ₃ -BH ₃	1.933	-487.765878	-487.610982	-487.651939
Δ (kJ/mol)		142.970000	133.920000	89.320000
B97D/6-31+G(d)	r(P-B) (Å)	E	H	G
PM ₃		-460.999059	-460.881426	-460.917861
BH ₃		-26.594223	-26.564304	-26.586368
PM ₃ -BH ₃	1.939	-487.649746	-487.498995	-487.540646
Δ (kJ/mol)		148.240000	139.850000	95.610000
B98/6-31G(d)	r(P-B) (Å)	E	H	G
PM ₃		-460.996324	-460.875451	-460.912489
BH ₃		-26.597091	-26.566762	-26.588800
PM ₃ -BH ₃	1.939	-487.651298	-487.496471	-487.537338
Δ (kJ/mol)		151.970000	142.450000	94.650000
MPW1K/6-31G(d)	r(P-B) (Å)	E	H	G
PM ₃		-461.072997	-460.948821	-460.985539
BH ₃		-26.599714	-26.568958	-26.590329
PM ₃ -BH ₃	1.913	-487.737043	-487.578553	-487.619188
Δ (kJ/mol)		168.910000	159.560000	113.740000
MPW1K/6-31+G(d)	r(P-B) (Å)	E	H	G
PM ₃		-461.076305	-460.952414	-460.989157

BH ₃		-26.600665	-26.569955	-26.592363
PM ₃ -BH ₃	1.913	-487.741238	-487.583148	-487.623778
Δ (kJ/mol)		168.740000	159.580000	110.950000
M05-2X/6-31G(d)	r(P-B) (Å)	E	H	G
PM ₃		-461.039315	-460.916417	-460.952362
BH ₃		-26.594881	-26.564052	-26.586087
PM ₃ -BH ₃	1.920	-487.691466	-487.534846	-487.575909
Δ (kJ/mol)		150.360000	142.770000	98.350000
M05-2X /6-31+G(d)	r(P-B) (Å)	E	H	G
PM ₃		-461.043639	-460.921137	-460.957124
BH ₃		-26.593481	-26.562564	-26.584598
PM ₃ -BH ₃	1.921	-487.697304	-487.541248	-487.582356
Δ (kJ/mol)		158.010000	151.090000	106.680000
M06-2X/6-31+G(d)	r(P-B) (Å)	E	H	G
PM ₃		-460.984291	-460.862607	-460.898590
BH ₃		-26.586453	-26.555645	-26.577672
PM ₃ -BH ₃	1.924	-487.629460	-487.474006	-487.515193
Δ (kJ/mol)		154.160000	146.380000	102.210000
M06-2X/6-31+G(d,p)	r(P-B) (Å)	E	H	G
PM ₃		-460.994565	-460.873464	-460.909458
BH ₃		-26.588620	-26.557924	-26.579951
PM ₃ -BH ₃	1.924	-487.642072	-487.487272	-487.528442
Δ (kJ/mol)		154.610000	146.720000	102.480000
ωB97XD/6-31G(d)	r(P-B) (Å)	E	H	G
PM ₃		-461.040808	-460.918628	-460.955270
BH ₃		-26.598311	-26.568123	-26.590167
PM ₃ -BH ₃	1.922	-487.701479	-487.545899	-487.587632
Δ (kJ/mol)		163.730000	155.290000	110.780000
ωB97XD/6-31+G(d)	r(P-B) (Å)	E	H	G
PM ₃		-461.044806	-460.922932	-460.959576
BH ₃		-26.599530	-26.569420	-26.591465
PM ₃ -BH ₃	1.922	-487.706673	-487.551526	-487.593363
Δ (kJ/mol)		163.660000	155.360000	111.120000
ωB97XD/def2-TZVP	r(P-B) (Å)	E	H	G
PM ₃		-461.117875	-460.997092	-461.033709
BH ₃		-26.607955	-26.578056	-26.600095
PM ₃ -BH ₃	1.903	-487.792055	-487.638247	-487.680161
Δ (kJ/mol)		173.870000	165.670000	121.710000
ωB97XD/def2-TZVPP	r(P-B) (Å)	E	H	G
PM ₃		-461.121679	-461.001077	-461.037160
BH ₃		-26.608617	-26.578690	-26.600725
PM ₃ -BH ₃	1.902	-487.796630	-487.642834	-487.685132
Δ (kJ/mol)		174.160000	165.580000	124.050000
ωB97XD/cc-pVTZ	r(P-B) (Å)	E	H	G
PM ₃		-461.119569	-460.998736	-461.035363
BH ₃		-26.608391	-26.578462	-26.600497
PM ₃ -BH ₃	1.911	-487.792333	-487.638568	-487.681823

Δ (kJ/mol)		169.010000	161.130000	120.680000
ω B97XD/cc-pvtz// ω B97XD/6-31G(d)	r(P-B) (\AA)	E	Thermal correction for H	H
PM ₃		-461.119339	0.122180	-460.997160
BH ₃		-26.608365	0.030188	-26.578176
PM ₃ -BH ₃	1.922	-487.792041	0.155580	-487.636461
Δ (kJ/mol)		168.920000		160.480000
ω B97XD/def2// ω B97XD/6-31G(d)	r(P-B) (\AA)	E	Thermal correction for H	H
PM ₃		-461.117566	0.122180	-460.995386
BH ₃		-26.607944	0.030188	-26.577756
PM ₃ -BH ₃	1.922	-487.791628	0.155580	-487.636047
Δ (kJ/mol)		173.590000		165.160000
ri-scs-mp2/cc-pvtz// ω B97XD/6-31G(d)	r(P-B) (\AA)	E	Thermal correction for H	H
PM ₃		-460.354095	0.122180	-460.231915
BH ₃		-26.526211	0.030188	-26.496023
PM ₃ -BH ₃	1.922	-486.938264	0.155580	-486.782684
Δ (kJ/mol)		152.170000		143.730000
ri-scs-mp2/def-tzvp// ω B97XD/6-31G(d)	r(P-B) (\AA)	E	Thermal correction for H	H
PM ₃		-460.319289	0.122180	-460.197109
BH ₃		-26.517734	0.030188	-26.487545
PM ₃ -BH ₃	1.922	-486.896662	0.155580	-486.741082
Δ (kJ/mol)		156.580000		148.150000
HF/6-31+G(d)	r(P-B) (\AA)	E	H	G
PH ₃		-342.448753	-342.418769	-342.442552
BH ₃		-26.390694	-26.359251	-26.381259
PH ₃ -BH ₃	2.021	-368.855445	-368.789544	-368.819021
Δ (kJ/mol)		42.000000	30.260000	-12.580000
B3LYP/6-31G(d)	r(P-B) (\AA)	E	H	G
PH ₃		-343.140281	-343.112206	-343.136057
BH ₃		-26.613000	-26.582671	-26.604708
PH ₃ -BH ₃	1.960	-369.786523	-369.723828	-369.753283
Δ (kJ/mol)		87.280000	76.010000	32.870000
B97D/6-31+G(d)	r(P-B) (\AA)	E	H	G
PH ₃		-343.126769	-343.098909	-343.122773
BH ₃		-26.594223	-26.564304	-26.586368
PH ₃ -BH ₃	1.970	-369.754738	-369.693103	-369.722731
Δ (kJ/mol)		88.600000	78.480000	35.680000
B98/6-31G(d)	r(P-B) (\AA)	E	H	G
PH ₃		-343.084654	-343.056502	-343.080345
BH ₃		-26.597091	-26.566762	-26.588800
PH ₃ -BH ₃	1.966	-369.718550	-369.655736	-369.685204
Δ (kJ/mol)		96.630000	85.260000	42.160000
MPW1K/6-31G(d)	r(P-B) (\AA)	E	H	G
PH ₃		-343.135431	-343.106444	-343.130261
BH ₃		-26.599714	-26.568958	-26.590329
PH ₃ -BH ₃	1.936	-369.776645	-369.712408	-369.741696
Δ (kJ/mol)		108.960000	97.160000	55.410000
MPW1K/6-31+G(d)	r(P-B) (\AA)	E	H	G

PH ₃		-343.136347	-343.107387	-343.131205
BH ₃		-26.600665	-26.569955	-26.592363
PH ₃ -BH ₃	1.936	-369.778691	-369.714612	-369.743916
Δ (kJ/mol)		109.430000	97.850000	53.420000
M05-2X/6-31G(d)	r(P-B) (Å)	E	H	G
PH ₃		-343.097543	-343.069176	-343.093016
BH ₃		-26.594881	-26.564052	-26.586087
PH ₃ -BH ₃	1.958	-369.726757	-369.663276	-369.692613
Δ (kJ/mol)		90.140000	78.890000	35.470000
M05-2X /6-31+G(d)	r(P-B) (Å)	E	H	G
PH ₃		-343.098816	-343.070473	-343.094314
BH ₃		-26.593481	-26.562564	-26.584598
PH ₃ -BH ₃	1.956	-369.729605	-369.666313	-369.695663
Δ (kJ/mol)		97.950000	87.370000	43.980000
M06-2X/6-31+G(d)	r (P-B) (Å)	E	H	G
PH ₃		-343.084424	-343.056064	-343.079893
BH ₃		-26.586453	-26.555645	-26.577672
PH ₃ -BH ₃	1.959	-369.707475	-369.644238	-369.673691
Δ (kJ/mol)		96.090000	85.400000	42.340000
M06-2X/6-31+G(d,p)	r(P-B) (Å)	E	H	G
PH ₃		-343.084424	-343.056064	-343.079893
BH ₃		-26.588620	-26.557924	-26.579951
PH ₃ -BH ₃	1.959	-369.713838	-369.650933	-369.680410
Δ (kJ/mol)		107.110000	97.000000	54.000000
ωB97XD/6-31G(d)	r(P-B) (Å)	E	H	G
PH ₃		-343.115460	-343.087050	-343.110884
BH ₃		-26.598311	-26.568123	-26.590167
PH ₃ -BH ₃	1.954	-369.751663	-369.688477	-369.717881
Δ (kJ/mol)		99.490000	87.440000	44.190000
ωB97XD/6-31+G(d)	r(P-B) (Å)	E	H	G
PH ₃		-343.116535	-343.088152	-343.111987
BH ₃		-26.599530	-26.569420	-26.591465
PH ₃ -BH ₃	1.955	-369.754147	-369.691104	-369.720520
Δ (kJ/mol)		99.980000	88.040000	44.810000
ωB97XD/def2-TZVP	r(P-B) (Å)	E	H	G
PH ₃		-343.150489	-343.122339	-343.146179
BH ₃		-26.607955	-26.578056	-26.600095
PH ₃ -BH ₃	1.927	-369.799393	-369.736873	-369.766239
Δ (kJ/mol)		107.510000	95.770000	52.420000
ωB97XD/def2-TZVPP	r(P-B) (Å)	E	H	G
PH ₃		-343.151496	-343.123340	-343.147179
BH ₃		-26.608617	-26.578690	-26.600725
PH ₃ -BH ₃	1.927	-369.801126	-369.738586	-369.767946
Δ (kJ/mol)		107.680000	95.980000	52.620000
ωB97XD/cc-pVTZ	r(P-B) (Å)	E	H	G
PH ₃		-343.153761	-343.125803	-343.149649
BH ₃		-26.608391	-26.578462	-26.600497

PH ₃ -BH ₃	1.937	-369.801774	-369.739383	-369.768784
Δ (kJ/mol)		104.030000	92.200000	48.930000
MP2(FC)/aug-cc-pVDZ	r(P-B) (Å)	E	H	G
PH ₃		-342.472064	-342.585801	-342.609667
BH ₃		-26.391286	-26.456387	-26.479480
PH ₃ -BH ₃	1.964	-368.879680	-369.074803	-369.104327
Δ (kJ/mol)		42.870000	85.630000	39.860000
MP2(FC)/cc-PVTZ	r(P-B) (Å)	E	H	G
PH ₃		-342.487456	-342.629121	-342.652954
BH ₃		-26.400155	-26.482888	-26.505941
PH ₃ -BH ₃	1.935	-368.905229	-369.148369	-369.177729
Δ (kJ/mol)		46.260000	95.460000	49.450000
CCSD(T)/cc-pVTZ	r(P-B) (Å)	E	H	G
PH ₃		-342.665504	-342.664560	-342.689448
BH ₃		-26.508472	-26.507528	-26.530574
PH ₃ -BH ₃	1.949	-369.205591	-369.204646	-369.235140
Δ (kJ/mol)		83.010000	85.480000	39.690000
MP2(FULL)/aug-cc-pvdz	r(P-B) (Å)	E	H	G
PH ₃		-342.472100	-342.594848	-342.618707
BH ₃		-26.391299	-26.458517	-26.481608
PH ₃ -BH ₃	1.958	-368.879619	-369.087468	-369.116987
Δ (kJ/mol)		42.590000	89.540000	43.770000
HF/6-31+G(d)	r(N-B) (Å)	E	H	G
NMe ₃		-173.272906	-173.137535	-173.170845
BMe ₃		-143.544525	-143.416830	-143.456814
NMe ₃ -BMe ₃	1.824	-316.820180	-316.551898	-316.597839
Δ (kJ/mol)		7.220000	-6.480000	-78.290000
B3LYP/6-31G(d)	r(N-B) (Å)	E	H	G
NMe ₃		-174.474415	-174.346925	-174.380576
BMe ₃		-144.609109	-144.487587	-144.527590
NMe ₃ -BMe ₃	1.791	-319.097808	-318.843941	-318.891251
Δ (kJ/mol)		37.500000	24.760000	-44.410000
B97D/6-31+G(d)	r(N-B) (Å)	E	H	G
NMe ₃		-174.359288	-174.235224	-174.268788
BMe ₃		-144.504113	-144.386265	-144.425865
NMe ₃ -BMe ₃	1.797	-318.893374	-318.645881	-318.692994
Δ (kJ/mol)		78.690000	64.040000	-4.360000
B98/6-31G(d)	r(N-B) (Å)	E	H	G
NMe ₃		-174.400718	-174.273294	-174.306934
BMe ₃		-144.545964	-144.424579	-144.465054
NMe ₃ -BMe ₃	1.766	-318.966346	-318.712492	-318.759244
Δ (kJ/mol)		51.630000	38.380000	-33.460000
MPW1K/6-31G(d)	r(N-B) (Å)	E	H	G
NMe ₃		-174.428770	-174.297703	-174.331187
BMe ₃		-144.574556	-144.450020	-144.490113
NMe ₃ -BMe ₃	1.731	-319.027538	-318.766931	-318.813002

Δ (kJ/mol)		63.570000	50.430000	-21.790000
MPW1K/6-31+G(d)	r(N-B) (\AA)	E	H	G
NMe ₃		-174.433382	-174.302577	-174.336068
BMe ₃		-144.578094	-144.453955	-144.492769
NMe ₃ -BMe ₃	1.728	-319.033859	-318.773744	-318.819658
Δ (kJ/mol)		58.770000	45.190000	-24.100000
M05-2X/6-31G(d)	r(N-B) (\AA)	E	H	G
NMe ₃		-174.432363	-174.302912	-174.336524
BMe ₃		-144.567292	-144.443934	-144.482411
NMe ₃ -BMe ₃	1.737	-319.034059	-318.776533	-318.822679
Δ (kJ/mol)		90.330000	77.940000	9.830000
M05-2X /6-31+G(d)	r(N-B) (\AA)	E	H	G
NMe ₃		-174.437841	-174.308742	-174.342356
BMe ₃		-144.571899	-144.449065	-144.487165
NMe ₃ -BMe ₃	1.735	-319.042657	-318.785973	-318.831932
Δ (kJ/mol)		86.430000	73.950000	6.330000
M06-2X/6-31+G(d)	r(N-B) (\AA)	E	H	G
NMe ₃		-174.380779	-174.252527	-174.286150
BMe ₃		-144.519470	-144.397190	-144.433779
NMe ₃ -BMe ₃	1.728	-318.936409	-318.680876	-318.726465
Δ (kJ/mol)		94.940000	81.810000	17.160000
M06-2X/6-31+G(d,p)	r(N-B) (\AA)	E	H	G
NMe ₃		-174.389636	-174.262052	-174.295716
BMe ₃		-144.530626	-144.409108	-144.448388
NMe ₃ -BMe ₃	1.729	-318.956061	-318.701912	-318.747580
Δ (kJ/mol)		93.990000	80.740000	9.130000
ω B97XD/6-31G(d)	r(N-B) (\AA)	E	H	G
NMe ₃		-174.418454	-174.289984	-174.323605
BMe ₃		-144.560571	-144.437951	-144.476118
NMe ₃ -BMe ₃	1.750	-319.012267	-318.755821	-318.801582
Δ (kJ/mol)		87.280000	73.210000	4.880000
ω B97XD/6-31+G(d)	r(N-B) (\AA)	E	H	G
NMe ₃		-174.423836	-174.295640	-174.329267
BMe ₃		-144.564951	-144.442810	-144.479940
NMe ₃ -BMe ₃	1.746	-319.020038	-318.763849	-318.809171
Δ (kJ/mol)		82.050000	66.690000	-0.090000
ω B97XD/def2-TZVP		E	H	G
NMe ₃		-174.483430	-174.356193	-174.389932
BMe ₃		-144.616578	-144.495230	-144.532125
NMe ₃ -BMe ₃	1.742	-319.129426	-318.875439	-318.921415
Δ (kJ/mol)		77.240000	63.050000	-1.690000
ω B97XD/def2-TZVPP	r(N-B) (\AA)	E	H	G
NMe ₃		-174.487121	-174.359815	-174.393558
BMe ₃		-144.620166	-144.498736	-144.535583
NMe ₃ -BMe ₃	1.742	-319.136610	-318.882441	-318.928379
Δ (kJ/mol)		76.990000	62.720000	-2.000000
ω B97XD/cc-pVTZ	r(N-B) (\AA)	E	H	G

NMe ₃		-174.480882	-174.353691	-174.387489
BMe ₃		-144.616002	-144.494620	-144.531295
NMe ₃ -BMe ₃	1.742	-319.126907	-318.872793	-318.918634
Δ (kJ/mol)		78.820000	64.280000	-0.390000
ωB97XD/cc-pVTZ //ωB97XD/6-31G(d)	r(N-B) (Å)	E	Thermo for H	H
NMe ₃		-174.480000	0.128470	-174.350000
BMe ₃		-144.615845	0.122620	-144.490000
NMe ₃ -BMe ₃	1.750	-319.126646	0.254489	-318.870000
Δ (kJ/mol)		79.020000		70.100000
ωB97XD/def2-TZVP //ωB97XD/6-31G(d)	r(N-B) (Å)	E	Thermo for H	H
NMe ₃		-174.480000	0.128470	-174.350000
BMe ₃		-144.616445	0.122620	-144.490000
NMe ₃ -BMe ₃	1.750	-319.129167	0.254489	-318.870000
Δ (kJ/mol)		77.250000		68.330000
ri-scs-mp2/cc-pvtz//ωB97XD/6-31G(d)	r(N-B) (Å)	E	Thermal correction for H	H
NMe ₃		-174.092426	0.128470	-173.963956
BMe ₃		-144.248512	0.122620	-144.125891
NMe ₃ -BMe ₃	1.750	-318.375194	0.254489	-318.120705
Δ (kJ/mol)		89.940000		81.020000
RI-SCS-MP2/def2-TZVP// ωB97XD/6-31G(d)	r(N-B) (Å)	E	Thermal correction for H	H
NMe ₃		-174.065294	0.128470	-173.936824
BMe ₃		-144.220541	0.122620	-144.097921
NMe ₃ -BMe ₃	1.750	-318.319151	0.254489	-318.064662
Δ (kJ/mol)		87.470000		78.550000
CCSD(T)/CBS/ ωB97XD/6-31G(d)	r(N-B) (Å)	E	Thermal correction for H	H
NMe ₃		-174.240119	0.128470	-174.111650
BMe ₃		-144.376643	0.122620	-144.254023
NMe ₃ -BMe ₃	1.750	-318.651887	0.254489	-318.397398
Δ (kJ/mol)		92.218640		83.294762
HF/6-31+G(d)	r(P-B) (Å)	E	H	G
PF ₃		-639.145115	-639.131077	-639.161900
BH ₃		-26.390694	-26.359251	-26.381259
PF ₃ -BH ₃	1.933	-665.548177	-665.499015	-665.534607
Δ (kJ/mol)		32.470000	22.810000	-22.450000
B3LYP/6-31G(d)	r(P-B) (Å)	E	H	G
PF ₃		-640.956439	-640.942935	-640.974137
BH ₃		-26.613000	-26.582671	-26.604708
PF ₃ -BH ₃	1.875	-667.609518	-667.562344	-667.598318
Δ (kJ/mol)		105.230000	96.460000	51.130000
B97D/6-31+G(d)	r(P-B) (Å)	E	H	G
PF ₃		-640.824419	-640.811535	-640.843012
BH ₃		-26.594223	-26.564304	-26.586368
PF ₃ -BH ₃	1.899	-667.449070	-667.403206	-667.439634
Δ (kJ/mol)		79.890000	71.850000	26.920000
B98/6-31G(d)	r(P-B) (Å)	E	H	G
PF ₃		-640.809024	-640.795455	-640.826615
BH ₃		-26.597091	-26.566762	-26.588800

PF ₃ -BH ₃	1.881	-667.449294	-667.402037	-667.437966
Δ (kJ/mol)		113.370000	104.550000	59.210000
MPW1K/6-31G(d)	r(P-B) (Å)	E	H	G
PF ₃		-640.855645	-640.841752	-640.872748
BH ₃		-26.599714	-26.568958	-26.590329
PF ₃ -BH ₃	1.851	-667.503298	-667.455152	-667.490863
Δ (kJ/mol)		125.860000	116.680000	72.950000
MPW1K/6-31+G(d)	r(P-B) (Å)	E	H	G
PF ₃		-640.876876	-640.863224	-640.894272
BH ₃		-26.600665	-26.569955	-26.592363
PF ₃ -BH ₃	1.856	-667.517852	-667.470018	-667.505763
Δ (kJ/mol)		105.840000	96.720000	50.220000
M05-2X/6-31G(d)	r(P-B) (Å)	E	H	G
PF ₃		-640.913996	-640.900107	-640.931141
BH ₃		-26.594881	-26.564052	-26.586087
PF ₃ -BH ₃	1.862	-667.549945	-667.502056	-667.537951
Δ (kJ/mol)		107.830000	99.500000	54.410000
M05-2X /6-31+G(d)	r(P-B) (Å)	E	H	G
PF ₃		-640.939384	-640.925772	-640.956875
BH ₃		-26.593481	-26.562564	-26.584598
PF ₃ -BH ₃	1.871	-667.568014	-667.520516	-667.556471
Δ (kJ/mol)		92.280000	84.490000	39.380000
M06-2X/6-31+G(d)	r(P-B) (Å)	E	H	G
PF ₃		-640.845773	-640.832158	-640.863252
BH ₃		-26.586453	-26.555645	-26.577672
PF ₃ -BH ₃	1.875	-667.466957	-667.419353	-667.455179
Δ (kJ/mol)		91.180000	82.830000	37.430000
M06-2X/6-31+G(d,p)	r(P-B) (Å)	E	H	G
PF ₃		-640.845773	-640.832158	-640.863252
BH ₃		-26.588620	-26.557924	-26.579951
PF ₃ -BH ₃	1.873	-667.469276	-667.421796	-667.457671
Δ (kJ/mol)		91.580000	83.270000	37.990000
ωB97XD/6-31G(d)	r(P-B) (Å)	E	H	G
PF ₃		-640.856257	-640.842578	-640.873701
BH ₃		-26.598311	-26.568121	-26.590165
PF ₃ -BH ₃	1.867	-667.498718	-667.451293	-667.487147
Δ (kJ/mol)		115.920000	106.580000	61.120000
ωB97XD/6-31+G(d)	r(P-B) (Å)	E	H	G
PF ₃		-640.881468	-640.868048	-640.899236
BH ₃		-26.599530	-26.569420	-26.591465
PF ₃ -BH ₃	1.877	-667.516164	-667.469089	-667.505021
Δ (kJ/mol)		92.330000	83.020000	37.600000
ωB97XD/def2-TZVP	r(P-B) (Å)	E	H	G
PF ₃		-641.052831	-641.039223	-641.070224
BH ₃		-26.607955	-26.578056	-26.600095
PF ₃ -BH ₃	1.849	-667.705459	-667.658521	-667.694220
Δ (kJ/mol)		117.290000	108.280000	62.750000

	r(P-B) (Å)	E	H	G
ωB97XD/def2-TZVPP				
PF ₃		-641.053124	-641.039518	-641.070520
BH ₃		-26.608617	-26.578690	-26.600725
PF ₃ -BH ₃	1.847	-667.706599	-667.659646	-667.695336
Δ (kJ/mol)		117.780000	108.800000	63.250000
ωB97XD/cc-pVTZ	r(P-B) (Å)	E	H	G
PF ₃		-641.028979	-641.015461	-641.046512
BH ₃		-26.608391	-26.578462	-26.600497
PF ₃ -BH ₃	1.858	-667.679621	-667.632658	-667.668470
Δ (kJ/mol)		110.930000	101.700000	56.350000
ωB97XD/cc-pvtz//ωB97XD/6-31G(d)	r(P-B) (Å)	E	Thermal correction for H	H
PF ₃		-641.028807	0.013678	-641.015129
BH ₃		-26.608365	0.030188	-26.578176
PF ₃ -BH ₃	1.867	-667.679069	0.047425	-667.631644
Δ (kJ/mol)		110.000000		100.660000
ωB97XD/def2-tzvp//ωB97XD/6-31G(d)	r(P-B) (Å)	E	Thermal correction for H	H
PF ₃		-641.052267	0.013678	-641.038588
BH ₃		-26.607944	0.030188	-26.577756
PF ₃ -BH ₃	1.867	-667.704204	0.047425	-667.656779
Δ (kJ/mol)		115.500000		106.160000
ri-scs-mp2/cc-pvtz//ωB97XD/6-31G(d)	r(P-B) (Å)	E	Thermal correction for H	H
PF ₃		-640.165460	0.013678	-640.151782
BH ₃		-26.526211	0.030188	-26.496023
PF ₃ -BH ₃	1.867	-666.728119	0.047425	-666.680695
Δ (kJ/mol)		95.700000		86.350000
ri-scs-mp2/def-tzvp//ωB97XD/6-31G(d)	r(P-B) (Å)	E	Thermal correction for H	H
PF ₃		-640.179232	0.013678	-640.165554
BH ₃		-26.517734	0.030188	-26.487545
PF ₃ -BH ₃	1.867	-666.734718	0.047425	-666.687293
Δ (kJ/mol)		99.120000		89.770000
ccsd/cbs//ωB97XD/6-31G(d)	r(P-B) (Å)	E	Thermal correction for H	H
PF ₃		-640.396386	0.013678	-640.382708
BH ₃		-26.548375	0.030188	-26.518187
PF ₃ -BH ₃	1.867	-666.986580	0.047425	-666.939156
Δ (kJ/mol)		109.800000		100.450000
HF/6-31+G(d)	r(P-B) (Å)	E	H	G
PM ₃		-459.5697955	-459.442001	-459.477236
BM ₃		-143.5445249	-143.41683	-143.456814
PM ₃ -BM ₃	2.081	-603.1161149	-602.85756	-602.908737
Δ (kJ/mol)		4.71	-3.34	-66.46
B3LYP/6-31G(d)	r(P-B) (Å)	E	H	G
PM ₃		-461.098424	-460.977302	-461.013212
BM ₃		-144.6091085	-144.487587	-144.52759
PM ₃ -BM ₃	2.025	-605.72032	-605.474679	-605.526769
Δ (kJ/mol)		33.57	25.7	-36.84
B97D/6-31+G(d)	r(P-B) (Å)	E	H	G
PM ₃		-460.9990591	-460.881426	-460.917861

BMe ₃		-144.5041128	-144.386265	-144.425865
PM ₃ -BMe ₃	1.998	-605.5269408	-605.28835	-605.341534
Δ (kJ/mol)		62.41	54.24	-5.76
B98/6-31G(d)	r(P-B) (Å)	E	H	G
PM ₃		-460.9963237	-460.875451	-460.912489
BMe ₃		-144.545964	-144.424579	-144.465054
PM ₃ -BMe ₃	2.028	-605.5603811	-605.31499	-605.368325
Δ (kJ/mol)		47.5	39.28	-24.2
MPW1K/6-31G(d)	r(P-B) (Å)	E	H	G
PM ₃		-461.0729968	-460.948821	-460.985539
BMe ₃		-144.5745556	-144.45002	-144.490113
PM ₃ -BMe ₃	1.988	-605.6710125	-605.41923	-605.470799
Δ (kJ/mol)		61.59	53.53	-12.74
MPW1K/6-31+G(d)	r(P-B) (Å)	E	H	G
PM ₃		-461.076305	-460.952414	-460.989157
BMe ₃		-144.578094	-144.453955	-144.492769
PM ₃ -BMe ₃	1.989	-605.677751	-605.426636	-605.479711
Δ (kJ/mol)		61.31	53.21	-5.82
M05-2X/6-31G(d)	r(P-B) (Å)	E	H	G
PM ₃		-461.0393147	-460.916417	-460.952362
BMe ₃		-144.5672915	-144.443934	-144.482411
PM ₃ -BMe ₃	1.989	-605.6328355	-605.384058	-605.436831
Δ (kJ/mol)		68.87	62.24	5.4
M05-2X /6-31+G(d)	r(P-B) (Å)	E	H	G
PM ₃		-461.0436385	-460.921137	-460.957124
BMe ₃		-144.5718986	-144.449065	-144.487165
PM ₃ -BMe ₃	1.991	-605.641643	-605.393765	-605.44754
Δ (kJ/mol)		68.54	61.86	8.54
M06-2X/6-31+G(d)	r(P-B) (Å)	E	H	G
PM ₃		-460.9842905	-460.862607	-460.89859
BMe ₃		-144.5194696	-144.39719	-144.433779
PM ₃ -BMe ₃	1.994	-605.5308256	-605.284375	-605.338096
Δ (kJ/mol)		71.06	64.53	15.04
M06-2X/6-31+G(d,p)	r(P-B) (Å)	E	H	G
PM ₃		-460.9945653	-460.873464	-460.909458
BMe ₃		-144.5306258	-144.409108	-144.448388
PM ₃ -BMe ₃	1.994	-605.5520939	-605.306801	-605.359971
Δ (kJ/mol)		70.63	63.61	5.58
ωB97XD/6-31G(d)	r(P-B) (Å)	E	H	G
PM ₃		-461.0408076	-460.918628	-460.95527
BMe ₃		-144.5605713	-144.437951	-144.476118
PM ₃ -BMe ₃	1.992	-605.6300316	-605.38258	-605.436337
Δ (kJ/mol)		75.23	68.27	12.99
ωB97XD/6-31+G(d)	r(P-B) (Å)	E	H	G
PM ₃		-461.0448064	-460.922932	-460.959576
BMe ₃		-144.5649508	-144.44281	-144.47994
PM ₃ -BMe ₃	1.994	-605.6381226	-605.39141	-605.445692

Δ (kJ/mol)		74.47	67.39	16.22
ω B97XD/def2-TZVP	r(P-B) (\AA)	E	H	G
PM ₃		-461.1178748	-460.997285	-461.033314
BMe ₃		-144.6201656	-144.498736	-144.535583
PM ₃ -BMe ₃	1.975	-605.7642057	-605.519461	-605.572639
Δ (kJ/mol)		68.7	61.54	9.82
ω B97XD/def2-TZVPP	r(P-B) (\AA)	E	H	G
PM ₃		-461.121679	-461.001077	-461.03716
BMe ₃		-144.6201656	-144.498736	-144.535583
PM ₃ -BMe ₃	1.975	-605.7715335	-605.526755	-605.580227
Δ (kJ/mol)		77.95	70.74	19.65
ω B97XD/cc-pVTZ	r(P-B) (\AA)	E	H	G
PM ₃		-461.1195693	-460.998736	-461.035363
BMe ₃		-144.6160022	-144.49462	-144.531295
PM ₃ -BMe ₃	1.985	-605.7636621	-605.51893	-605.573685
Δ (kJ/mol)		73.75	67.14	18.45
ω B97XD/cc-pvtz// ω B97XD/6-31G(d)	r(P-B) (\AA)	E	Thermal correction for H	H
PM ₃		-461.1193393	0.122179628	-460.9971597
BMe ₃		-144.6158447	0.122620268	-144.4932244
PM ₃ -BMe ₃	1.992	-605.7632561	0.247451627	-605.5158045
Δ (kJ/mol)		73.7		66.74
ω B97XD/def2// ω B97XD/6-31G(d)	r(P-B) (\AA)	E	Thermal correction for H	H
PM ₃		-461.1175655	0.122179628	-460.9953859
BMe ₃		-144.6164454	0.122620268	-144.4938251
PM ₃ -BMe ₃	1.992	-605.7637078	0.247451627	-605.5162561
Δ (kJ/mol)		77.97		71.01
ri-scs-mp2/cc-pvtz// ω B97XD/6-31G(d)	r(P-B) (\AA)	E	Thermal correction for H	H
PM ₃		-460.3540948	0.122179628	-460.2319152
BMe ₃		-144.2485116	0.122620268	-144.1258913
PM ₃ -BMe ₃	1.992	-604.6308797	0.247451627	-604.3834281
Δ (kJ/mol)		74.23		67.27
ri-scs-mp2/def-tzvp// ω B97XD/6-31G(d)	r(P-B) (\AA)	E	Thermal correction for H	H
PM ₃		-460.3192886	0.122179628	-460.197109
BMe ₃		-144.220541	0.122620268	-144.0979208
PM ₃ -BMe ₃	1.992	-604.569778	0.247451627	-604.3223264
Δ (kJ/mol)		78.63		71.67
HF/6-31+G(d)	r(P-B) (\AA)	E	H	G
PM ₃		-459.5697955	-459.442001	-459.477236
BF ₃		-323.2089338	-323.191411	-323.220182
PM ₃ -BF ₃	2.092	-782.7923686	-782.64533	-782.69294
Δ (kJ/mol)		35.81	31.29	-11.76
B3LYP/6-31G(d)	r(P-B) (\AA)	E	H	G
PM ₃		-461.098424	-460.977302	-461.013212
BF ₃		-324.5532218	-324.536227	-324.56579
PM ₃ -BF ₃	2.096	-785.6703606	-785.530535	-785.579406
Δ (kJ/mol)		49.14	44.65	1.06
B97D/6-31+G(d)	r(P-B) (\AA)	E	H	G

PM ₃		-460.9990591	-460.881426	-460.917861
BF ₃		-324.4083486	-324.392031	-324.421074
PM ₃ -BF ₃	2.086	-785.4317677	-785.295959	-785.345553
Δ (kJ/mol)		63.96	59.08	17.38
B98/6-31G(d)	r(P-B) (Å)	E	H	G
PM ₃		-460.9963237	-460.875451	-460.912489
BF ₃		-324.4461325	-324.429088	-324.45865
PM ₃ -BF ₃	2.109	-785.4629328	-785.323153	-785.371981
Δ (kJ/mol)		53.76	48.87	2.21
MPW1K/6-31G(d)	r(P-B) (Å)	E	H	G
PM ₃		-461.0729968	-460.948821	-460.985539
BF ₃		-324.4491316	-324.431771	-324.461263
PM ₃ -BF ₃	2.060	-785.5473851	-785.404083	-785.452389
Δ (kJ/mol)		66.31	61.68	14.67
MPW1K/6-31+G(d)	r(P-B) (Å)	E	H	G
PM ₃		-461.076305	-460.952414	-460.989157
BF ₃		-324.4670829	-324.44994	-324.47946
PM ₃ -BF ₃	2.055	-785.5719365	-785.429115	-785.477396
Δ (kJ/mol)		74.95	70.26	23.05
M05-2X/6-31G(d)	r(P-B) (Å)	E	H	G
PM ₃		-461.0393147	-460.916417	-460.952362
BF ₃		-324.5353615	-324.518102	-324.54763
PM ₃ -BF ₃	2.071	-785.5991083	-785.457617	-785.507298
Δ (kJ/mol)		64.15	60.64	19.18
M05-2X /6-31+G(d)	r(P-B) (Å)	E	H	G
PM ₃		-461.0436385	-460.921137	-460.957124
BF ₃		-324.556645	-324.539638	-324.569203
PM ₃ -BF ₃	2.056	-785.6280415	-785.487148	-785.536559
Δ (kJ/mol)		72.88	69.24	26.86
M06-2X/6-31+G(d)	r(P-B) (Å)	E	H	G
PM ₃		-460.9842905	-460.862607	-460.89859
BF ₃		-324.4698488	-324.452876	-324.481795
PM ₃ -BF ₃	2.072	-785.479127	-785.339053	-785.388366
Δ (kJ/mol)		65.61	61.88	20.95
M06-2X/6-31+G(d,p)	r(P-B) (Å)	E	H	G
PM ₃		-460.9945653	-460.873464	-460.909458
BF ₃		-324.4698485	-324.452876	-324.48245
PM ₃ -BF ₃	2.071	-785.4897083	-785.350181	-785.399385
Δ (kJ/mol)		66.41	62.59	19.63
ωB97XD/6-31G(d)	r(P-B) (Å)	E	H	G
PM ₃		-461.0408076	-460.918628	-460.95527
BF ₃		-324.4641582	-324.447148	-324.476707
PM ₃ -BF ₃	2.071	-785.530577	-785.389959	-785.43959
Δ (kJ/mol)		67.24	63.49	19.99
ωB97XD/6-31+G(d)	r(P-B) (Å)	E	H	G
PM ₃		-461.0448064	-460.922932	-460.959576
BF ₃		-324.4848377	-324.468089	-324.497687

PM ₃ -BF ₃	2.062	-785.5590766	-785.41902	-785.468508
Δ (kJ/mol)		77.28	73.51	29.52
ωB97XD/def2-TZVP	r(P-B) (Å)	E	H	G
PM ₃		-461.1178748	-460.997285	-461.033314
BF ₃		-324.617982	-324.601146	-324.630715
PM ₃ -BF ₃	2.070	-785.7621495	-785.623211	-785.672986
Δ (kJ/mol)		69.03	65.06	23.52
ωB97XD/def2-TZVPP	r(P-B) (Å)	E	H	G
PM ₃		-461.121679	-461.001077	-461.03716
BF ₃		-324.617982	-324.601152	-324.630722
PM ₃ -BF ₃	2.070	-785.7660304	-785.627114	-785.677364
Δ (kJ/mol)		69.23	65.34	24.89
ωB97XD/cc-pVTZ	r(P-B) (Å)	E	H	G
PM ₃		-461.1195693	-460.998736	-461.035363
BF ₃		-324.5992523	-324.582384	-324.611944
PM ₃ -BF ₃	2.079	-785.7441826	-785.605063	-785.65615
Δ (kJ/mol)		66.59	62.86	23.22
ωB97XD/cc-pvtz//ωB97XD/6-31G(d)	r(P-B) (Å)	E	Thermal correction for H	H
PM ₃		-461.1193393	0.122179628	-460.9971597
BF ₃		-324.5992083	0.017010233	-324.5821981
PM ₃ -BF ₃	2.071	-785.7437345	0.140617962	-785.6031166
Δ (kJ/mol)		66.13		62.38
ωB97XD/def2//ωB97XD/6-31G(d)	r(P-B) (Å)	E	Thermal correction for H	H
PM ₃		-461.1175655	0.122179628	-460.9953859
BF ₃		-324.6179571	0.017010233	-324.6009468
PM ₃ -BF ₃	2.071	-785.7616725	0.140617962	-785.6210546
Δ (kJ/mol)		68.66		64.91
ri-scs-mp2/cc-pvtz//ωB97XD/6-31G(d)	r(P-B) (Å)	E	Thermal correction for H	H
PM ₃		-460.3540948	0.122179628	-460.2319152
BF ₃		-324.1409627	0.017010233	-324.1239525
PM ₃ -BF ₃	2.071	-784.5147896	0.140617962	-784.3741717
Δ (kJ/mol)		51.81		48.06
ri-scs-mp2/def-tzvp//ωB97XD/6-31G(d)	r(P-B) (Å)	E	Thermal correction for H	H
PM ₃		-460.3192886	0.122179628	-460.197109
BF ₃		-324.1525787	0.017010233	-324.1355685
PM ₃ -BF ₃	2.071	-784.4940323	0.140617962	-784.3534143
Δ (kJ/mol)		58.19		54.44
CCSD(T)/CBS//wB97XD/6-31G(d)	r(P-B) (Å)	E	Thermal correction for H	H
PM ₃		-460.504990	0.122180	-460.382810
BF ₃		-324.340399	0.017010	-324.323388
PM ₃ -BF ₃	2.071	-784.869429	0.140618	-784.728812
Δ (kJ/mol)		63.12		59.37

PH₃-BF₃ geometry and energy parameters

MIM1	H(PH ₃)	H(BF ₃)	H(PH ₃ -BF ₃)	ΔH(kJ/mol)	r(P-B) (Å)
MPW1K/6-31+G(d)	-343.107374	-324.449954	-667.560417	-8.11	2.291
MPW1K/6-31+G(d,p)	-343.112444	-324.449955	-667.565392	-7.86	2.288
MPW1K/6-311+G(d,p)	-343.136335	-324.52936	-667.66973	-10.59	2.266

MPW1K/6-311++G(2d,2p)	-343.140419	-324.545125	-	-	-
MPW1K/cc-pVDZ	-343.128533	-324.444573	-	-	-
MPW1K/cc-pVTZ	-343.145151	-324.564602	-	-	-
MPW1K/cc-pVQZ	-343.149851	-324.593094	-	-	-
MPW1K/aug-cc-pVDZ	-343.130462	-324.466585	-667.601404	-11.44	2.238
MPW1K/aug-cc-pVTZ	-343.145587	-324.568803	-	-	-
MPW1K/aug-cc-pVQZ	-343.149996	-324.594163	-	-	-
MP2(FC)/6-31+G(d)	-342.524503	-323.788244	-666.317679	-12.95	2.203
MP2(FC)/6-31+G(d,p)	-342.551238	-323.788242	-666.343482	-10.51	2.219
MP2(FC)/6-31+G(2d,2p)	-342.572711	-323.897237	-	-	-
MP2(FC)/6-311++G(d,p)	-342.584497	-323.967276	-	-	-
MP2(FC)/6-311++G(2d,2p)	-342.601238	-324.048616	-	-	-
MP2(FC)/ cc-pVDZ	-342.576679	-323.822102	-	-	-
MP2(FC)/ cc-pVTZ	-342.629127	-324.149481	-	-	-
MP2(FC)/ cc-pVQZ	-342.645984	-324.252865	-	-	-
MP2(FC)/ aug-cc-pVDZ	-342.58582	-323.89022	-666.479395	-8.81	2.272
MP2(FC)/ aug-cc-pVTZ	-342.632912	-324.172038	-	-	-
MP2(Full)/ 6-31+G(d)	-342.535746	-323.802189	-666.343533	-14.70	2.196
MP2(Full)/ 6-31+G(d,p)	-342.563466	-323.802189	-666.370349	-12.32	2.208
MP2(Full)/6-311++G(d,p)	-342.708928	-324.041916	-666.754321	-9.13	2.288
MP2(Full)/6-311++G(2d,2p)	-342.736686	-324.13146	-	-	-
MP2(Full)/ cc-pVDZ	-342.584393	-323.830626	-	-	-
MP2(Full)/ cc-pVTZ	-342.673299	-324.201916	-	-	-
MP2(Full)/ cc-pVQZ	-342.699722	-324.372683	-	-	-
MP2(Full)/ aug-cc-pVDZ	-342.594863	-323.900674	-666.499931	-11.54	2.247
MP2(Full)/ aug-cc-pVTZ	-342.681468	-324.232258	-	-	-
MP2(Full)/ aug-cc-pVQZ	-342.703007	-324.384707	-	-	-
SCS-MP2(FC)/6-31+G(d)	-342.5285109	-323.7521342	-666.2831912	-6.68	2.232
SCS-MP2(FC)/6-31+G(d,p)	-342.5577413	-323.7521342	-666.3117496	-4.92	2.248
SCS-MP2(FC)/cc-pVTZ	-342.639155	-324.1239102	-	-	-
SCS-MP2(FC)/aug-cc-pVDZ	-342.5933239	-323.8624234	-	-	-
SCS-MP2(FULL)/6-31+G(d)	-342.5350251	-323.759742	-666.2978906	-8.20	2.219
SCS-MP2(FULL)/6-31+G(d,p)	-342.5650486	-323.7599582	-666.3272592	-5.91	2.231
SCS-MP2(FULL)/cc-pVTZ	-342.6806141	-324.17671	-	-	-
SCS-MP2(FULL)/aug-cc-pVDZ	-342.6016722	-323.8720164	-	-	-
SCS-MP2(FC)/def2-SVP	-342.4768611	-323.5216546	-	-	-
SCS-MP2(FC)/def2-TZVP	-342.6224348	-324.1355857	-	-	-
SCS-MP2(FC)/def2-QZVP	-342.6600346	-324.2342394	-	-	-
CCSD(T)/cc-pVDZ	-342.609773	-323.838859	-	-	-
CCSD(T)/cc-pVTZ	-342.66456	-324.173827	-	-	-
CCSD(T)/cc-pVQZ	-342.680052	-324.276367	-	-	-

MIM2	H(PH ₃)	H(BF ₃)	H(PH ₃ -BF ₃)	ΔH(kJ/mol)	r(P-B) (Å)
MPW1K/6-31+G(d)	-343.107374	-324.449954	-667.560334	2.886	-7.89
MPW1K/6-31+G(d,p)	-343.112444	-324.449955	-667.565299	2.896	-7.61
MPW1K/6-311+G(d,p)	-343.136335	-324.52936	-	-	-
MPW1K/6-311++G(2d,2p)	-343.140419	-324.545125	-667.68858	2.889	-7.97
MPW1K/cc-pVDZ	-343.128533	-324.444573	-667.576594	2.775	-9.16
MPW1K/cc-pVTZ	-343.145151	-324.564602	-667.712322	2.995	-6.74
MPW1K/cc-pVQZ	-343.149851	-324.593094	-667.745005	3.035	-5.41
MPW1K/aug-cc-pVDZ	-343.130462	-324.466585	-	-	-
MPW1K/aug-cc-pVTZ	-343.145587	-324.568803	-667.716829	2.982	-6.40
MPW1K/aug-cc-pVQZ	-343.149996	-324.594163	-667.746186	3.029	-5.32

MP2(FC)/6-31+G(d)	-342.524503	-323.788244	-666.319064	2.984	-16.59
MP2(FC)/6-31+G(d,p)	-342.551238	-323.788242	-666.344467	3.018	-13.09
MP2(FC)/6-31+G(2d,2p)	-342.572711	-323.897237	-666.473674	3.089	-9.78
MP2(FC)/6-311++G(d,p)	-342.584497	-323.967276	-666.556615	3.075	-12.71
MP2(FC)/6-311++G(2d,2p)	-342.601238	-324.048616	-666.653825	3.081	-10.43
MP2(FC)/ cc-pVDZ	-342.576679	-323.822102	-666.401717	3.169	-7.71
MP2(FC)/ cc-pVTZ	-342.629127	-324.149481	-666.782718	3.090	-10.79
MP2(FC)/ cc-pVQZ	-342.645984	-324.252865	-666.902013	3.087	-8.31
MP2(FC)/ aug-cc-pVDZ	-342.58582	-323.89022	-666.480656	3.041	-12.12
MP2(FC)/ aug-cc-pVTZ	-342.632912	-324.172038	-666.808961	3.056	-10.53
MP2(Full)/ 6-31+G(d)	-342.535746	-323.802189	-666.343773	2.963	-15.33
MP2(Full)/ 6-31+G(d,p)	-342.563466	-323.802189	-666.371047	2.992	-14.16
MP2(Full)/6-311++G(d,p)	-342.708928	-324.041916	-666.755844	3.064	-13.13
MP2(Full)/6-311++G(2d,2p)	-342.736686	-324.13146	-666.872355	3.064	-11.05
MP2(Full)/ cc-pVDZ	-342.584393	-323.830626	-666.418179	3.155	-8.30
MP2(Full)/ cc-pVTZ	-342.673299	-324.201916	-666.879618	3.059	-11.56
MP2(Full)/ cc-pVQZ	-342.699722	-324.372683	-667.075769	3.083	-8.83
MP2(Full)/ aug-cc-pVDZ	-342.594863	-323.900674	-666.50083	3.001	-13.90
MP2(Full)/ aug-cc-pVTZ	-342.681468	-324.232258	-666.920261	2.947	-17.16
MP2(Full)/ aug-cc-pVQZ	-342.703007	-324.384707	-667.075771	3.027	-10.36
SCS-MP2(FC)/6-31+G(d)	-342.5285109	-323.7521342	-666.2858674	3.083	-13.71
SCS-MP2(FC)/6-31+G(d,p)	-342.5577413	-323.7521342	-666.3148043	3.106	-12.94
SCS-MP2(FC)/cc-pVTZ	-342.639155	-324.1239102	-666.7654913	3.205	-6.37
SCS-MP2(FC)/aug-cc-pVDZ	-342.5933239	-323.8624234	-666.4594826	3.136	-9.81
SCS-MP2(FULL)/6-31+G(d)	-342.5350251	-323.759742	-666.300424	3.071	-14.85
SCS-MP2(FULL)/6-31+G(d,p)	-342.5650486	-323.7599582	-666.3301558	3.094	-13.52
SCS-MP2(FULL)/cc-pVTZ	-342.6806141	-324.17671	-666.8610153	3.137	-9.69
SCS-MP2(FULL)/aug-cc-pVDZ	-342.6016722	-323.8720164	-666.4780097	3.099	-11.35
SCS-MP2(FC)/def2-SVP	-342.4768611	-323.5216546	-666.000641	3.246	-5.58
SCS-MP2(FC)/def2-TZVP	-342.6224348	-324.1355857	-666.7605147	3.183	-6.55
SCS-MP2(FC)/def2-QZVP	-342.6600346	-324.2342394	-666.8968788	3.189	-6.84
CCSD(T)/cc-pVDZ	-342.609773	-323.838859	-666.451379	3.170	-7.21
CCSD(T)/cc-pVTZ	-342.66456	-324.173827	-666.842368	3.139	-10.45
CCSD(T)/cc-pVQZ	-342.680052	-324.276367	-666.960432	3.129	-10.54

Relaxed scan of $\text{PH}_3\text{-BF}_3$ at CCSD(T)(BSSE)/cc-pVTZ//MPW1K/6-31+G(d) level

	MPW1K/6-31+G(d)	CCSD(T)/cc-pVTZ//MPW1K/6-31+G(d)
PH_3	-343.136347	-342.692372
BF_3	-324.467083	-324.190890

	MPW1K/6-31+G(d)	MPW1K/6-31+G(d)	CCSD(T)/cc-pVTZ// MPW1K	CCSD(T)/cc-pVTZ// MPW1K
R(P-B) (\AA) (pm)	E($\text{PH}_3\text{-BF}_3$) (AU)	E(PH_3BF_3) - E(PH_3) - E(BF_3) (kJ/mol)	E($\text{PH}_3\text{-BF}_3$) (AU)	BSSE (kJ/mol)
180	-667.585533	46.99	-666.854753	14.17
190	-667.597902	14.51	-666.867775	12.59
200	-667.604293	-2.27	-666.874985	11.20
210	-667.607182	-9.85	-666.878855	9.99
220	-667.608198	-12.52	-666.880981	8.93
230	-667.608369	-12.97	-666.882341	8.00
240	-667.608277	-12.73	-666.883455	7.19

250	-667.608191	-12.50	-666.884519	6.48
260	-667.608185	-12.48	-666.885549	5.85
270	-667.608235	-12.62	-666.886473	5.28
280	-667.608291	-12.76	-666.887224	4.77
290	-667.608311	-12.82	-666.887768	4.31
300	-667.608272	-12.71	-666.888102	3.89
310	-667.608169	-12.44	-666.888249	3.51
320	-667.608010	-12.02	-666.888241	3.17
330	-667.607807	-11.49	-666.888115	2.85
340	-667.607574	-10.88	-666.887903	2.55
350	-667.607320	-10.21	-666.887635	2.27
360	-667.607055	-9.52	-666.887333	2.01
370	-667.606790	-8.82	-666.887016	1.77
380	-667.606538	-8.16	-666.886697	1.54
390	-667.606300	-7.54	-666.886387	1.34
400	-667.606074	-6.94	-666.886093	1.15
410	-667.605857	-6.37	-666.885817	0.98
420	-667.605655	-5.84	-666.885561	0.84
430	-667.605470	-5.36	-666.885332	0.71
440	-667.605302	-4.92	-666.885123	0.60
450	-667.605147	-4.51	-666.884934	0.51
460	-667.605004	-4.13	-666.884766	0.44
470	-667.604872	-3.79	-666.884616	0.37
480	-667.604753	-3.47	-666.884482	0.32

Relaxed scan at CCSD(T)(BSSE)/cc-pVTZ//MPW1K/aug-cc-pVDZ level

	MPW1K/aug-cc-pvDZ	CCSD(T)/cc-pVTZ//MPW1K
PH ₃	-343.158753	-342.692429
BF ₃	-324.483505	-324.190951

R(P-B) (Å) (pm)	MPW1K	MPW1K	CCSD(T) //	CCSD(T) //
			MPW1K	MPW1K
180	-667.6268319	40.50	-666.854714	14.14
190	-667.638944	8.70	-666.867733	12.57
200	-667.6450328	-7.28	-666.874938	11.18
210	-667.6476327	-14.11	-666.878803	9.97
220	-667.6483989	-16.12	-666.880937	8.92
230	-667.6483593	-16.02	-666.882313	8.00
240	-667.6480863	-15.30	-666.883449	7.20
250	-667.6478391	-14.65	-666.884540	6.49
260	-667.6476832	-14.24	-666.885592	5.86
270	-667.6475896	-14.00	-666.886532	5.30
280	-667.6475059	-13.78	-666.887296	4.79
290	-667.6473917	-13.48	-666.887847	4.32
300	-667.6472297	-13.05	-666.888187	3.90
310	-667.6470204	-12.50	-666.888337	3.52

320	-667.6467724	-11.85	-666.888332	3.17
330	-667.6464972	-11.13	-666.888207	2.85
340	-667.6462066	-10.37	-666.887996	2.55
350	-667.6459094	-9.59	-666.887728	2.27
360	-667.6456131	-8.81	-666.887426	2.01
370	-667.6453275	-8.06	-666.887109	1.77
380	-667.6450613	-7.36	-666.886791	1.54
390	-667.6448142	-6.71	-666.886480	1.34
400	-667.644581	-6.10	-666.886182	1.15
410	-667.6443639	-5.53	-666.885908	0.98
420	-667.6441659	-5.01	-666.885654	0.84
430	-667.6439875	-4.54	-666.885423	0.71
440	-667.6438285	-4.12	-666.885214	0.60
450	-667.6436847	-3.75	-666.885026	0.51
460	-667.6435533	-3.40	-666.884858	0.43
470	-667.6434343	-3.09	-666.884708	0.37
480	-667.6433278	-2.81	-666.884574	0.32

Relaxed scan of $\text{PH}_3\text{-BF}_3$ at CCSD(T)(BSSE)/cc-pVTZ//MP2(FC)/6-31+G(d) level

	MP2(FC)/ 6-31+G(d)	CCSD(T)/cc-pVTZ//MP2//6-31+G(d)
PH_3	-342.553374	-342.692348
BF_3	-323.804985	-324.190286

	MP2	MP2	CCSD(T // MP2	CCSD(T)// MP2
R(P-B) (\AA) (pm)	E($\text{PH}_3\text{-BF}_3$) (AU)	E(PH_3BF_3)-E(PH_3)-E(BF_3) (kJ/mol)	E($\text{PH}_3\text{-BF}_3$) (AU)	BSSE (kJ/mol)
180	-666.3442067	37.16	-666.853893	14.13
190	-666.3563313	5.32	-666.866874	12.56
200	-666.3622793	-10.29	-666.874020	11.18
210	-666.3646442	-16.50	-666.877855	9.96
220	-666.3651706	-17.88	-666.879988	8.91
230	-666.364983	-17.39	-666.881387	7.98
240	-666.3647239	-16.71	-666.882567	7.18
250	-666.3646646	-16.55	-666.883709	6.47
260	-666.3648257	-16.98	-666.884805	5.85
270	-666.3651058	-17.71	-666.885776	5.29
280	-666.365383	-18.44	-666.886556	4.78
290	-666.3655686	-18.93	-666.887116	4.32
300	-666.3656197	-19.06	-666.887459	3.91
310	-666.3655302	-18.83	-666.887610	3.53
320	-666.3653164	-18.27	-666.887604	3.18
330	-666.365005	-17.45	-666.887478	2.86
340	-666.3646254	-16.45	-666.887266	2.56
350	-666.3642047	-15.35	-666.886996	2.28
360	-666.363766	-14.19	-666.886693	2.02
370	-666.3633275	-13.04	-666.886374	1.77
380	-666.3629029	-11.93	-666.886055	1.55

390	-666.3625004	-10.87	-666.885724	1.34
400	-666.3621281	-9.89	-666.885431	1.15
410	-666.3617873	-9.00	-666.885158	0.99
420	-666.3614784	-8.19	-666.884905	0.84
430	-666.3612005	-7.46	-666.884675	0.71
440	-666.3609512	-6.80	-666.884466	0.61
450	-666.3607277	-6.22	-666.884278	0.51
460	-666.3605269	-5.69	-666.884110	0.44
470	-666.3603458	-5.22	-666.883960	0.37
480	-666.3601817	-4.78	-666.883827	0.32

Relaxed scan of $\text{PH}_3\text{-BF}_3$ at CCSD(T)(BSSE)/cc-pVTZ//MP2(FC)/aug-cc-pVDZ level

	MP2(FC)/ aug-cc-pVDZ	CCSD(T)/cc-pVTZ//MP2//aug-cc-pVDZ
PH_3	-342.614054	-342.692387
BF_3	-323.906698	-324.189104

	MP2	MP2	CCSD(T // MP2	CCSD(T) // MP2
R(P-B) (\AA) (pm)	E($\text{PH}_3\text{-BF}_3$) (AU)	E(PH_3BF_3)-E(PH_3)-E(BF_3) (kJ/mol)	E($\text{PH}_3\text{-BF}_3$) (AU)	BSSE (kJ/mol)
180	-666.5033365	45.72	-666.8527321	14.07
190	-666.5159769	12.54	-666.8655703	12.51
200	-666.522291	-4.04	-666.8727703	11.14
210	-666.5249574	-11.04	-666.8765905	9.94
220	-666.5257589	-13.15	-666.8787181	8.89
230	-666.5258187	-13.30	-666.8801279	7.98
240	-666.5257654	-13.16	-666.8813311	7.18
250	-666.5258631	-13.42	-666.8825042	6.48
260	-666.5261373	-14.14	-666.8836289	5.86
270	-666.5265	-15.09	-666.8846234	5.3
280	-666.5268449	-16.00	-666.8854209	4.79
290	-666.5270965	-16.66	-666.8859928	4.33
300	-666.5272191	-16.98	-666.886344	3.91
310	-666.5272082	-16.95	-666.8865	3.53
320	-666.5270775	-16.61	-666.8864967	3.18
330	-666.5268486	-16.01	-666.8863714	2.86
340	-666.5265458	-15.21	-666.8861588	2.56
350	-666.5261919	-14.28	-666.8858883	2.28
360	-666.5258074	-13.27	-666.8855838	2.02
370	-666.5254096	-12.23	-666.8852638	1.77
380	-666.5250124	-11.19	-666.8849424	1.54
390	-666.5246255	-10.17	-666.8846174	1.33
400	-666.5242588	-9.21	-666.8843235	1.15
410	-666.5239159	-8.31	-666.8840483	0.98
420	-666.5235995	-7.48	-666.8837944	0.84
430	-666.5233106	-6.72	-666.8835626	0.71
440	-666.5230489	-6.03	-666.8833528	0.6
450	-666.5228132	-5.41	-666.8831642	0.51

460	-666.5226017	-4.86	-666.8829953	0.43
470	-666.5224124	-4.36	-666.8828446	0.37
480	-666.5222433	-3.92	-666.8827105	0.32

Varies HF exchange energy of PH₃-BF₃ in MPW1K/6-31+G(d,_s) level with P₁=1, P₂+P₄=1, P₃=0.527, P₅=P₆=1.

Etot	P ₂ = 0.2	P ₂ = 0.4	P ₂ = 0.6	P ₂ = 0.8
BF ₃	-323.766173	-324.380649	-325.00010	-325.624105
PH ₃	-342.696308	-343.082188	-343.46974	-343.858929
r(P-B) (Å) (pm)	P ₂ = 0.2	P ₂ = 0.4	P ₂ = 0.6	P ₂ = 0.8
180	-666.450570	-667.445631	-668.448081	-669.457372
190	-666.462415	-667.457942	-668.460762	-669.470333
200	-666.468479	-667.464300	-668.467326	-669.477033
210	-666.471147	-667.467168	-668.470327	-669.480107
220	-666.471952	-667.468163	-668.471456	-669.481328
230	-666.471873	-667.468304	-668.471786	-669.481814
240	-666.471453	-667.468174	-668.471915	-669.482179
250	-666.470979	-667.468041	-668.472103	-669.482668
260	-666.470544	-667.467986	-668.472400	-669.483301
270	-666.470161	-667.467986	-668.472759	-669.483995
280	-666.469793	-667.467993	-668.473110	-669.484660
290	-666.469434	-667.467966	-668.473393	-669.485222
300	-666.469053	-667.467886	-668.473584	-669.485666
310	-666.468652	-667.467747	-668.473679	-669.485966
320	-666.468244	-667.467558	-668.473691	-669.486153
330	-666.467826	-667.467329	-668.473632	-669.486245
340	-666.467415	-667.467077	-668.473518	-669.486255
350	-666.467007	-667.466804	-668.473361	-669.486202
360	-666.466618	-667.466524	-668.473179	-669.486098
370	-666.466249	-667.466248	-668.472980	-669.485967
380	-666.465913	-667.465986	-668.472780	-669.485822
390	-666.465607	-667.465741	-668.472586	-669.485667
400	-666.465325	-667.465508	-668.472397	-669.485511
410	-666.465063	-667.465289	-668.472209	-669.485350
420	-666.464825	-667.465083	-668.472029	-669.485190
430	-666.464615	-667.464895	-668.471859	-669.485033
440	-666.464426	-667.464726	-668.471702	-669.484886
450	-666.464257	-667.464570	-668.471558	-669.484748
460	-666.464101	-667.464426	-668.471421	-669.484617
470	-666.463960	-667.464294	-668.471294	-669.484496
480	-666.463833	-667.464173	-668.471178	-669.484380

HF, E2 and MP2 energy analysis of Relaxed scan at MP2(FC)/6-31+G(d) level

	HF in MP2 (AU)	E2 in MP2 (AU)	MP2 (AU)
BF ₃	-323.206841	-0.598144	-323.804985
PH ₃	-342.448552	-0.104822	-342.553374
r(P-B) (Å) (pm)	HF in MP2 (AU)	E2 in MP2 (AU)	MP2 (AU)
180	-665.618836	-0.725371	-666.344207
190	-665.633131	-0.723200	-666.356331
200	-665.640904	-0.721375	-666.362279
210	-665.644919	-0.719725	-666.364644
220	-665.647047	-0.718123	-666.365171
230	-665.648437	-0.716546	-666.364983

240	-665.649713	-0.715011	-666.364724
250	-665.651094	-0.713571	-666.364665
260	-665.652556	-0.712270	-666.364826
270	-665.653986	-0.711120	-666.365106
280	-665.655276	-0.710107	-666.365383
290	-665.656358	-0.709210	-666.365569
300	-665.657210	-0.708410	-666.365620
310	-665.657835	-0.707695	-666.365530
320	-665.658259	-0.707058	-666.365316
330	-665.658512	-0.706493	-666.365005
340	-665.658628	-0.705997	-666.364625
350	-665.658640	-0.705565	-666.364205
360	-665.658576	-0.705190	-666.363766
370	-665.658458	-0.704870	-666.363328
380	-665.658306	-0.704597	-666.362903
390	-665.658127	-0.704374	-666.362500
400	-665.657949	-0.704180	-666.362128
410	-665.657768	-0.704020	-666.361787
420	-665.657590	-0.703889	-666.361478
430	-665.657419	-0.703782	-666.361200
440	-665.657257	-0.703694	-666.360951
450	-665.657105	-0.703623	-666.360728
460	-665.656964	-0.703563	-666.360527
470	-665.656834	-0.703512	-666.360346
480	-665.656715	-0.703467	-666.360182

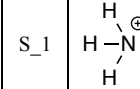
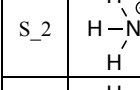
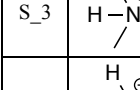
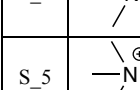
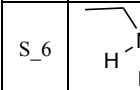
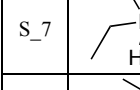
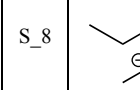
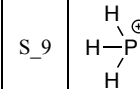
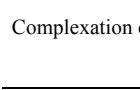
HF, E2 and MP2 energy analysis of Relaxed scan at MP2(FC)/cc-pVQZ level

	HF in MP2 (AU)	E2 in MP2 (AU)	MP2 (AU)
BF ₃	-323.352457	-0.917348	-324.269805
PH ₃	-342.492509	-0.181930	-342.674439
r(P-B) (Å) (pm)	HF in MP2 (AU)	E2 in MP2 (AU)	MP2 (AU)
180	-665.803556	-1.117472	-666.921027
190	-665.817989	-1.115328	-666.933317
200	-665.826276	-1.113591	-666.939867
210	-665.830952	-1.112166	-666.943118
220	-665.833807	-1.110854	-666.944661
230	-665.835845	-1.109629	-666.945474
240	-665.837624	-1.108466	-666.946091
250	-665.839359	-1.107369	-666.946728
260	-665.841061	-1.106347	-666.947408
270	-665.842659	-1.105405	-666.948063
280	-665.844069	-1.104546	-666.948615
290	-665.845242	-1.103773	-666.949014
300	-665.846159	-1.103086	-666.949245
310	-665.846833	-1.102483	-666.949316
320	-665.847294	-1.101960	-666.949254
330	-665.847578	-1.101512	-666.949090
340	-665.847722	-1.101130	-666.948852
350	-665.847761	-1.100807	-666.948568
360	-665.847722	-1.100536	-666.948259
370	-665.847631	-1.100310	-666.947941
380	-665.847505	-1.100121	-666.947626

390	-665.847358	-1.099965	-666.947323
400	-665.847208	-1.099827	-666.947035
410	-665.847048	-1.099719	-666.946768
420	-665.846890	-1.099631	-666.946521
430	-665.846738	-1.099558	-666.946296
440	-665.846592	-1.099499	-666.946091
450	-665.846456	-1.099450	-666.945906
460	-665.846329	-1.099410	-666.945739
470	-665.846212	-1.099378	-666.945590
480	-665.846105	-1.099352	-666.945456

EDA analysis

EDA analysis (without BSSE) at ω B97XD/6-31G(d) level.

		E^{ES}	E^{EX}	E^{REP}	E^{POL}	E^{DISP}	E_{decomp}	$E^{DEF}_{(base)}$	$E^{DEF}_{(acid)}$	E_{ccomp}
S_1		10912.78	-108.41	645.87	-11605.71	-46.22	-201.7	0.48	53.3	147.91
S_2		26566.36	-118.09	735.98	-27281.04	-53.23	-150.02	0.58	63.01	86.43
S_3		31775.98	-117.32	751.68	-32519.47	-61.15	-170.28	2.02	69.38	98.88
S_4		37007.85	-111.73	731.5	-37738.78	-69.13	-180.3	4.28	77.93	98.09
S_5		42251.94	-104.2	692.43	-42945.21	-76.44	-181.47	8.36	85.20	87.91
S_6		36995.05	-116.17	752.38	-37742.18	-64.47	-175.39	10.7	71.46	93.23
S_7		47441.59	-113.53	747.78	-48191.78	-72.52	-188.46	18.1	79.76	90.6
S_8		57940.56	-98.79	667.83	-58608.46	-82.66	-181.52	22.88	93.77	64.88
S_9		44949.61	-1.26	53.99	-45006.24	-12.99	-16.89	0.3	1.68	14.91

Complexation energy of Lewis pair at different theory level.

	$r(N-B)$ (Å)	E_{tot}^a	ΔH^b	ΔG^c	ΔH_{sp}^d	$q(N)^e$	$q(B)^f$	$d(B)^g$	$d(P)^h$
S_01	130.08	165.8	147.60	129.95	86.14	106.36	0.355	-0.355	132.5
S_02	57.57	169.2	86.17	73.75	20.23	63.79	0.336	-0.336	133.7
S_03	73.86	168.8	98.83	85.94	25.37	84.10	0.332	-0.332	131.5
S_04	47.77	200.2	57.47	49.42	-8.59	67.24	0.666	-0.666	130.9
S_05	73.77	175.0	87.28	73.21	4.88	87.29	0.304	-0.304	126.0
S_06	75.36	169.1	93.10	80.13	17.85	79.05	0.331	-0.331	130.7
S_07	68.29	170.5	89.97	77.00	13.43	79.05	0.318	-0.318	128.3
S_08	41.87	180.2	63.99	48.75	89.96	63.52	0.303	-0.303	123.0
S_09	4.61	379.9	15.42	9.67	-22.43	2.52	-0.001	0.001	178.4
S_10	10.05	371.8	16.61	11.05	-22.82	2.99	0.001	-0.001	177.8
S_11	12.98	429.7	20.36	14.78	-28.05	6.51	0.006	-0.006	176.8

S_12	36.43	200.5	54.45	46.28	-13.24	61.69	0.654	-0.654	131.3
S_13	39.57	221.3	42.70	37.46	-8.19	73.87	0.496	-0.496	132.6
S_14	49.99	186.7	115.92	106.58	61.12	83.76	0.708	-0.708	136.6
S_15	54.39	171.5	86.82	73.74	9.37	69.15	0.329	-0.329	128.6
S_16	61.55	211.5	46.03	41.10	-2.82	47.85	0.444	-0.444	136.7
S_17	68.96	199.2	75.23	68.27	12.99	84.48	0.694	-0.694	129.7
S_18	72.26	169.1	96.61	83.69	20.33	79.97	0.330	-0.330	130.8
S_19	72.93	169.3	95.30	82.70	20.44	81.05	0.330	-0.330	128.7
S_20	73.65	167.2	93.66	83.53	27.08	86.66	0.321	-0.321	128.4
S_21	75.95	169.9	99.50	85.71	23.78	84.78	0.331	-0.331	131.2
s_22	77.58	168.4	100.52	87.44	25.50	85.12	0.331	-0.331	131.1
S_24	78.34	168.7	100.12	86.90	23.60	84.11	0.332	-0.331	131.2
S_25	79.13	207.1	67.24	63.48	19.98	67.21	0.490	-0.490	134.3
S_26	80.64	170.8	97.66	85.31	26.76	92.18	0.321	-0.321	128.4
S_27	82.27	170.2	102.21	89.59	28.94	97.72	0.319	-0.319	128.0
S_28	83.48	172.7	100.16	87.41	15.93	105.10	0.304	-0.304	125.1
S_29	85.54	169.1	106.05	95.32	31.12	103.06	0.319	-0.319	129.2
S_30	94.12	167.5	133.25	115.46	50.02	120.20	0.324	-0.324	130.0
S_31	178.36	192.2	163.73	155.30	110.79	153.15	0.699	-0.699	131.5

^aΔEtot calculated at ωB97XD/6-31G(d) level. ^bΔH calculated at ωB97XD/6-31G(d) level. ^c ΔG calculated at ωB97XD/6-31G(d) level. ^d MP2(FC)/6-31+G(2d,p)//ωB97XD/6-31G(d) level. ^e NBO charge of base moiety. ^f NBO charge of acid moiety. ^g d(B) dihedral angle of acid moiety. ^h dihedral angle of base moiety.

7.3 Calculated Data for Chapter 3

Computational detail for the reactivity of Lewis pairs for hydrogen activation

For the reaction profile calculated here using the formula

$$\Delta H_{298} = H(\text{interesting species}) - H(\text{Lewis pair}) - H(H_2) \quad (1)$$

$$\Delta G_{298} = G(\text{interesting species}) - G(\text{Lewis pair}) - G(H_2) \quad (2)$$

PH₃-BH₃

ωB97XD/cc-pVTZ	H (hartree)	G(hartree)	ΔH (kJ/mol)	ΔG (kJ/mol)
PH₃	-343.125803	-343.149649	-	-
BH₃	-26.578467	-26.601539	-	-
PH₃-BH₃	-369.739383	-369.768784	-	-
H₂	-1.163172	-1.177964	-	-
1M1	-370.902143	-370.939309	1.08	19.53
1TS1	-370.867674	-370.908820	91.58	99.58
1M2	-370.874042	-370.913183	74.86	88.12
1TS2	-370.830238	-370.861894	189.87	222.78
1M3	-370.832100	-370.864668	184.98	215.50

MP2(FC)/cc-pVTZ	H (hartree)	G(hartree)	ΔH (kJ/mol)	ΔG (kJ/mol)
PH₃	-342.629121	-342.652962	-	-
BH₃	-26.482888	-26.505941	-	-
PH₃-BH₃	-369.148369	-369.177729	-	-
H₂	-1.151033	-1.165811	-	-
1M1	-370.298834	-370.337383	1.49	16.17
1TS1	-370.262909	-370.307610	95.81	94.33
1M2	-370.267308	-370.308823	84.26	91.15
1TS2	-370.224040	-370.255619	197.86	230.84
1M3	-370.226227	-370.258469	192.12	223.35

PH₃-BF₃

ω B97XD/cc-pVTZ	H (hartree)	G(hartree)	ΔH (kJ/mol)	ΔG (kJ/mol)
PH₃	-343.125803	-343.149649	-	-
BF₃	-324.582384	-324.611944	-	-
PH₃-BF₃	-667.711638	-667.754429	-	-
H₂	-1.163172	-1.177964	-	-
2M1	-668.873890	-668.923377	2.42	23.67
2M2	-668.871370	-668.920604	9.03	30.95
2TS2	-668.814838	-668.853211	157.46	207.89
2M2	-668.819258	-668.858201	145.85	194.79
MP2(FC)/cc-pVTZ	H (hartree)	G(hartree)	ΔH (kJ/mol)	ΔG (kJ/mol)
PH₃	-342.62913	-342.65296	-	-
BF₃	-324.14948	-324.17902	-	-
PH₃-BF₃	-666.78178	-666.82482	-	-
H₂	-1.15103	-1.16581	-	-
2M1	-667.93222	-667.98465	1.55	15.72
2M2	-667.92935	-667.98190	9.09	22.93
2TS2	-667.86937	-667.90781	166.57	217.47
2M2	-667.87635	-667.91561	148.23	196.98
PM_e₃-BF₃				
ω B97XD/cc-pVTZ	H (hartree)	G(hartree)	ΔH (kJ/mol)	ΔG (kJ/mol)
PM_e₃	-460.99874	-461.03536	-	-
BF₃	-324.58238	-324.61194	-	-
PM_e₃-BF₃	-785.60523	-785.65709	-	-
H₂	-1.16317	-1.17796	-	-
3M1	-786.76771	-786.82255	1.80	32.83
3TS2	-786.72103	-786.77189	124.36	165.85
3M3	-786.72911	-786.77978	103.16	145.12
MP2(FC)/cc-pVTZ	H (hartree)	G(hartree)	ΔH (kJ/mol)	ΔG (kJ/mol)
PM_e₃	-460.222961	-460.258763	-	-
BF₃	-324.149481	-324.179022	-	-
PM_e₃-BF₃	-784.393630	-784.442424	-	-
H₂	-1.151033	-1.165811	-	-
3M1	-785.544543	-785.602845	0.32	14.15
3TS2	-785.493819	-785.544858	133.49	166.40
3M3	-785.504152	-785.555295	106.36	138.99
PPh₃-BF₃				
ω B97XD/cc-pVTZ	H (hartree)	G(hartree)	ΔH (kJ/mol)	ΔG (kJ/mol)
PPh₃	-1036.003487	-1036.063992	-	-
BF₃	-324.582384	-324.611944	-	-
PPh₃-BF₃	-1360.604806	-1360.676341	-	-
H₂	-1.163177	-1.177970	-	-
4M1	-1361.771807	-1361.851583	-10.04	7.16
4M2	-1361.752796	-1361.835211	39.87	50.15
4TS2	-1361.724295	-1361.801868	114.70	137.69

4M3	-1361.733246	-1361.808980	91.20	119.02
PM_e₃-BH₃				
ωB97XD/cc-pVTZ	H (hartree)	G(hartree)	ΔH (kJ/mol)	ΔG (kJ/mol)
PM_e₃	-460.998736	-461.035363	-	-
BH₃	-26.578467	-26.601539	-	-
PM_e₃-BH₃	-487.638568	-487.681823	-	-
H₂	-1.163172	-1.177964	-	-
5M1	-488.801325	-488.849823	1.09	26.16
5TS1	-488.743140	-488.793653	153.85	173.63
5M2	-488.751100	-488.798633	132.96	160.56
5TS2	-488.739906	-488.784587	162.35	197.44
5M3	-488.739220	-488.783697	164.15	199.77
PM_e₃-BMe₃				
ωB97XD/cc-pVTZ	H (hartree)	G(hartree)	ΔH (kJ/mol)	ΔG (kJ/mol)
PM_e₃	-460.998736	-461.035363	-	-
BMe₃	-144.494620	-144.531295	-	-
PM_e₃-BMe₃	-605.518874	-605.572843	-	-
H₂	-1.163172	-1.177964	-	-
6M1	-606.680762	-606.738470	3.37	32.39
TS1	-606.660839	-606.724255	55.68	69.71
6M2	-606.659703	-606.722975	58.66	73.07
6TS2	-606.614344	-606.667452	177.75	218.85
6M3	-606.624301	-606.679880	151.61	186.22
PF₃-BH₃				
ωB97XD/cc-pVTZ	H (hartree)	G(hartree)	ΔH (kJ/mol)	ΔG (kJ/mol)
PF₃	-641.015461	-641.046512	-	-
BH₃	-26.578459	-26.600494	-	-
PF₃-BH₃	-667.632658	-667.668470	-	-
H₂	-1.163177	-1.177970	-	-
7M1	-668.794505	-668.836457	3.49	26.21
7M2	-668.762848	-668.809229	86.61	97.70
7TS2	-668.712337	-668.749729	219.22	253.91
7M3	-668.737573	-668.777418	152.97	181.22
PH₃-BMe₃				
ωB97XD/cc-pVTZ	H (hartree)	G(hartree)	ΔH (kJ/mol)	ΔG (kJ/mol)
PH₃	-343.125803	-343.149649	-	-
BMe₃	-144.494620	-144.531295	-	-
PH-BMe₃	-487.620907	-487.663545	-	-
H₂	-1.163172	-1.177964	-	-
8M1	-488.782793	-488.831428	3.38	26.47
8MP2	-488.783789	-488.837078	0.76	11.63
8TS2	-488.696897	-488.740807	228.90	264.39
8MP3	-488.723163	-488.767823	159.93	193.46

7.4 Calculated Data for Chapter 4

Computational detail for theoretical studies on regioselective functionalization of pyrimidines

Relative energy of metalated pyrimidine at different theory level.

B3LYP/631SVP	E(hartree)	H(hartree)	G(hartree)	ΔE (kJ/mol)	ΔH (kJ/mol)	ΔG (kJ/mol)
1M2_Mg	-1389.006586	-1388.679865	-1388.756025	0.00	0.00	0.00
1M4_Mg	-1389.008347	-1388.681189	-1388.757678	-4.62	-3.48	-4.34
1M5_Mg	-1389.004570	-1388.677194	-1388.753912	5.29	7.01	5.55
B3LYP/631TZVP	E(hartree)	H(hartree)	G(hartree)	ΔE (kJ/mol)	ΔH (kJ/mol)	ΔG (kJ/mol)
1M2_Mg	-1389.083840	-1388.757217	-1388.832696	0.00	0.00	0.00
1M4_Mg	-1389.085169	-1388.758034	-1388.836005	-3.49	-2.15	-8.69
1M5_Mg	-1389.082848	-1388.755517	-1388.831629	2.60	4.46	2.80
B3LYP/6311TZVP	E(hartree)	H(hartree)	G(hartree)	ΔE (kJ/mol)	ΔH (kJ/mol)	ΔG (kJ/mol)
1M2_Mg	-1389.291436	-1388.966245	-1389.041765	0.00	0.00	0.00
1M4_Mg	-1389.293061	-1388.967553	-1389.044464	-4.27	-3.43	-7.09
1M5_Mg	-1389.288566	-1388.962937	-1389.039692	7.53	8.69	5.44
B3LYP/631SVP	E(hartree)	H(hartree)	G(hartree)	ΔE (kJ/mol)	ΔH (kJ/mol)	ΔG (kJ/mol)
1M2_Zn	-2968.117454	-2967.790624	-2967.866098	0.00	0.00	0.00
1M4_Zn	-2968.119210	-2967.792131	-2967.871464	-4.61	-3.96	-14.09
1M5_Zn	-2968.116736	-2967.789686	-2967.867991	1.89	2.46	-4.97
B3LYP/631TZVP	E(hartree)	H(hartree)	G(hartree)	ΔE (kJ/mol)	ΔH (kJ/mol)	ΔG (kJ/mol)
1M2_Zn	-2968.374231	-2968.047574	-2968.124262	0.00	0.00	0.00
1M4_Zn	-2968.376139	-2968.049108	-2968.126561	-5.01	-4.03	-6.04
1M5_Zn	-2968.375258	-2968.048103	-2968.125655	-2.70	-1.39	-3.66
B3LYP/6311TZVP	E(hartree)	H(hartree)	G(hartree)	ΔE (kJ/mol)	ΔH (kJ/mol)	ΔG (kJ/mol)
1M2_Zn	-2968.582964	-2968.257990	-2968.335449	0.00	0.00	0.00
1M4_Zn	-2968.585181	-2968.259865	-2968.338866	-5.82	-4.92	-8.97
1M5_Zn	-2968.583970	-2968.258547	-2968.337950	-2.64	-1.46	-6.57

Relative energy of metalated BF_3 -pyrimidine at different theory level.

B3LYP/631SVP	E(hartree)	H(hartree)	G(hartree)	ΔE (kJ/mol)	ΔH (kJ/mol)	ΔG (kJ/mol)
1B2_Mg	-1713.618445	-1713.272704	-1713.356172	0.00	0.00	0.00
1B4_Mg	-1713.597722	-1713.251105	-1713.338702	54.41	56.71	45.87
1B5_Mg	-1713.598185	-1713.251296	-1713.337881	53.19	56.21	48.02
1B6_Mg	-1713.628728	-1713.282217	-1713.364917	-27.00	-24.98	-22.96
B3LYP/6311TZVP	E(hartree)	H(hartree)	G(hartree)	ΔE (kJ/mol)	ΔH (kJ/mol)	ΔG (kJ/mol)
1B2_Mg	-1714.002816	-1713.658887	-1713.742644	0.00	0.00	0.00
1B4_Mg	-1713.986692	-1713.641943	-1713.729351	42.33	44.49	34.90
1B5_Mg	-1713.986819	-1713.641918	-1713.729314	42.00	44.55	35.00
1B6_Mg	-1714.013239	-1713.668758	-1713.752202	-27.37	-25.92	-25.09
B3LYP/631SVP	E(hartree)	H(hartree)	G(hartree)	ΔE (kJ/mol)	ΔH (kJ/mol)	ΔG (kJ/mol)
1B2_Zn	-3292.713777	-3292.367768	-3292.452618	0.00	0.00	0.00
1B4_Zn	-3292.706385	-3292.360012	-3292.448763	19.41	20.36	10.12
1B5_Zn	-3292.708247	-3292.361571	-3292.448622	14.52	16.27	10.49
1B6_Zn	-3292.722084	-3292.375648	-3292.460606	-21.81	-20.69	-20.97
B3LYP/6311TZVP	E(hartree)	H(hartree)	G(hartree)	ΔE (kJ/mol)	ΔH (kJ/mol)	ΔG (kJ/mol)
1B2_Zn	-3293.283153	-3292.939182	-3293.023509	0.00	0.00	0.00
1B4_Zn	-3293.275973	-3292.931510	-3293.020620	18.85	20.14	7.59
1B5_Zn	-3293.277475	-3292.932857	-3293.022090	14.91	16.61	3.73
1B6_Zn	-3293.288694	-3292.944237	-3293.029629	-14.55	-13.27	-16.07

Path1_Mg: the reaction of 5-phenylprimidine and TMPMgCl·2THF in THF solution

Energy of reactant, intermediates and products in the reaction of 5-phenylprimidine (**4**) with TMPMgCl·2THF in THF solution at SMD/B3LYP/631SVP// B3LYP/631SVP level.

	E _{gas} ^a (hartree)	H _{gas} ^a (hartree)	G _{gas} ^a (hartree)	ΔH ^b (kJ/mol)	E _{solv} ^c (hartree)	H _{solv} ^d (hartree)	ΔH ^e (kJ/mol)
4	-1533.867784	-1533.341214	-1533.428326		-1533.884709	-1533.358139	
2_Mg	-495.382792	-495.214879	-495.259061	0.00	-495.393411	-495.225498	0.00
TS1_Mg	-2029.251725	-2028.556070	-2028.665449	0.06	-2029.273408	-2028.577753	15.45
M1_Mg	-1796.793556	-1796.222259	-1796.319638	2.25	-1796.818006	-1796.246710	2.19
THF	-232.456038	-232.332978	-232.368086		-232.459153	-232.336093	
TSa1_Mg	-1796.760212	-1796.193758	-1796.288789	77.08	-1796.784723	-1796.218269	76.86
THF	-232.456038	-232.332978	-232.368086		-232.459153	-232.336093	
Ma2_Mg	-1796.788263	-1796.215390	-1796.310888	20.28	-1796.810966	-1796.238093	24.81
THF	-232.456038	-232.332978	-232.368086		-232.459153	-232.336093	
TSa3_Mg	-2029.238649	-2028.545212	-2028.654367	28.57	-2029.262963	-2028.569525	37.05
Ma3_Mg	-1620.066296	-1619.654015	-1619.741151	10.09	-1620.089916	-1619.677635	9.12
TMPH	-409.180801	-408.898234	-408.944954		-409.185095	-408.902528	

^aThe value is obtained at B3LYP/631G(d, p)/SVP level. ^bReaction enthalpies is defined as $\Delta H = H_{\text{gas}}(\text{interesting species}) - \Delta H_{\text{gas}}(\mathbf{4}) - \Delta H_{\text{gas}}(\mathbf{2_Mg})$ (kJ/mol). ^cThe solvent effect is calculated at SMD/B3LYP/631SVP//B3LYP/631SVP level in THF solution. ^d $H_{\text{solv}} = E_{\text{solv}} + (H_{\text{gas}} - E_{\text{tot}})$. ^e $\Delta H = H_{\text{solv}}(\text{interesting species}) - \Delta H_{\text{solv}}(\mathbf{4}) - \Delta H_{\text{solv}}(\mathbf{2_Mg})$ (kJ/mol).

Path2_Mg: the reaction of 5-phenylprimidine and TMPMgCl·2THF in THF solution

Energy of reactent, intermediates and products in the reaction of 5-phenylprimidine (**4**) with TMPZnCl·2THF in THF solution at SMD/B3LYP/631SVP// B3LYP/631SVP level

	E _{gas} ^a (hartree)	H _{gas} ^a (hartree)	G _{gas} ^a (hartree)	ΔH ^b (kJ/mol)	E _{solv} ^c (hartree)	H _{solv} ^d (hartree)	ΔH ^e (kJ/mol)
4	-1533.867784	-1533.341214	-1533.428326		-1533.88471	-1533.35814	
2_Mg	-495.382792	-495.214879	-495.259061	0.00	-495.39341	-495.22550	0.00
TS1_Mg	-2029.251725	-2028.556070	-2028.665449	0.06	-2029.27341	-2028.57775	15.45
M1_Mg	-1796.793556	-1796.222259	-1796.319638	2.25	-1796.81801	-1796.24671	2.19
THF	-232.456038	-232.332978	-232.368086		-232.45915	-232.33609	
TSb1_Mg	-1796.765968	-1796.199061	-1796.293070	63.15	-1796.78856	-1796.22165	67.98
THF	-232.456038	-232.332978	-232.368086		-232.45915	-232.33609	
Mb2_Mg	-1796.791317	-1796.218153	-1796.312273	13.03	-1796.81268	-1796.23951	21.08
THF	-232.456038	-232.332978	-232.368086		-232.45915	-232.33609	
TSb3_Mg	-2029.245631	-2028.548589	-2028.657536	19.70	-2029.26739	-2028.57035	34.89
Mb3_Mg	-1620.061974	-1619.649523	-1619.735445	21.89	-1620.08751	-1619.67506	15.88
TMPH	-409.180801	-408.898234	-408.944954		-409.18509	-408.90253	

^aThe value is obtained at B3LYP/631G(d, p)/SVP level. ^bReaction enthalpies is defined as $\Delta H = H_{\text{gas}}(\text{interesting species}) - \Delta H_{\text{gas}}(\mathbf{4}) - \Delta H_{\text{gas}}(\mathbf{2_Mg})$ (kJ/mol). ^cThe solvent effect is calculated at SMD/B3LYP/631SVP//B3LYP/631SVP level in THF solution. ^d $H_{\text{solv}} = E_{\text{solv}} + (H_{\text{gas}} - E_{\text{tot}})$. ^e $\Delta H = H_{\text{solv}}(\text{interesting species}) - \Delta H_{\text{solv}}(\mathbf{4}) - \Delta H_{\text{solv}}(\mathbf{2_Mg})$ (kJ/mol)

Path1_Zn: the reaction of 5-phenylprimidine and TMPZnCl·2THF in THF solution

Energy of reactent, intermediates and products in the reaction of 5-phenylprimidine (**4**) with TMPZnCl·2THF in THF solution at SMD/B3LYP/631SVP// B3LYP/631SVP level

	E _{gas} ^a (hartree)	H _{gas} ^a (hartree)	G _{gas} ^a (hartree)	ΔH ^b (kJ/mol)	E _{solv} ^c (hartree)	H _{solv} ^d (hartree)	ΔH ^e (kJ/mol)
4	-495.382792	-495.214879	-495.259061		-495.393411	-495.225498	
2_Zn	-3112.971185	-3112.444419	-3112.530837	0.00	-3112.985313	-3112.458548	0.00
TS1_Zn	-3608.350664	-3607.654822	-3607.767539	11.75	-3608.372023	-3607.676181	20.65
M1_Zn	-3375.900440	-3375.329065	-3375.426948	-7.21	-3375.923523	-3375.352148	-11.01
THF	-232.456038	-232.332978	-232.368086		-232.459153	-232.336093	
TSa1_Zn	-3375.864493	-3375.297872	-3375.393758	74.69	-3375.888401	-3375.321780	68.71
THF	-232.456038	-232.332978	-232.368086		-232.459153	-232.336093	
Ma1_Zn	-3375.867473	-3375.296127	-3375.391837	79.27	-3375.894085	-3375.322739	66.20
THF	-232.456038	-232.332978	-232.368086		-232.459153	-232.336093	
TSa2_Zn	-3375.860967	-3375.289867	-3375.385612	95.71	-3375.886317	-3375.315217	85.95
THF	-232.456038	-232.332978	-232.368086		-232.459153	-232.336093	
Ma2_Zn	-3375.906219	-3375.333057	-3375.429160	-17.69	-3375.927547	-3375.354384	-16.89
THF	-232.456038	-232.332978	-232.368086		-232.459153	-232.336093	
TSa3_Zn	-3608.357847	-3607.661522	-3607.774405	-5.84	-3608.380013	-3607.683688	0.94

Ma3_Zn	-3199.176504	-3198.764031	-3198.850637	-7.79	-3199.198089	-3198.785616	-10.76
TMPH	-409.180801	-408.898234	-408.944954		-409.185095	-408.902528	

^aThe value is obtained at B3LYP/631G(d, p)/SVP level. ^bReaction enthalpies is defined as $\Delta H = H_{\text{gas}}(\text{interesting species}) - \Delta H_{\text{gas}}(\mathbf{4}) - \Delta H_{\text{gas}}(\mathbf{2_Zn})$ (kJ/mol). ^cThe solvent effect is calculated at SMD/B3LYP/631SVP//B3LYP/631SVP level in THF solution. ^d $H_{\text{solv}} = E_{\text{solv}} + (H_{\text{gas}} - E_{\text{tot}})$. ^e $\Delta H = H_{\text{solv}}(\text{interesting species}) - \Delta H_{\text{solv}}(\mathbf{4}) - \Delta H_{\text{solv}}(\mathbf{2_Zn})$ (kJ/mol).

Path2_Zn: the reaction of 5-phenylprimidine and TMPZnCl·2THF in THF solution

Energy of reactant, intermediates and products in the reaction of 5-phenylprimidine (**4**) with TMPZnCl·2THF in THF solution at SMD/B3LYP/631SVP// B3LYP/631SVP level

	E _{gas} ^a (hartree)	H _{gas} ^a (hartree)	G _{gas} ^a (hartree)	ΔH ^b (kJ/mol)	E _{solv} ^c (hartree)	H _{solv} ^d (hartree)	ΔH ^e (kJ/mol)
4	-495.382792	-495.214879	-495.259061		-495.393411	-495.225498	
2_Zn	-3112.971185	-3112.444419	-3112.530837	0.00	-3112.985313	-3112.458548	0.00
TS1	-3608.350664	-3607.654822	-3607.767539	11.75	-3608.372023	-3607.676181	20.65
M1_Zn	-3375.900440	-3375.329065	-3375.426948	-7.21	-3375.923523	-3375.352148	-11.01
THF	-232.456038	-232.332978	-232.368086		-232.459153	-232.336093	
TSb1_Zn	-3375.871022	-3375.304061	-3375.399395	58.44	-3375.892393	-3375.325432	59.13
THF	-232.456038	-232.332978	-232.368086		-232.459153	-232.336093	
Mb1_Zn	-3375.876576	-3375.304475	-3375.400366	57.35	-3375.899841	-3375.327740	53.07
THF	-232.456038	-232.332978	-232.368086		-232.459153	-232.336093	
TSb2_Zn	-3375.866600	-3375.295089	-3375.390569	82.00	-3375.890210	-3375.318699	76.80
THF	-232.456038	-232.332978	-232.368086		-232.459153	-232.336093	
Mb2_Zn	-3375.908019	-3375.334528	-3375.429505	-21.55	-3375.927808	-3375.354317	-16.71
THF	-232.456038	-232.332978	-232.368086		-232.459153	-232.336093	
TSb3_Zn	-3608.357501	-3607.660748	-3607.771259	-3.81	-3608.379044	-3607.682292	4.60
Mb3_Zn	-3199.179413	-3198.766863	-3198.852994	-15.23	-3199.201040	-3198.788490	-18.31
TMPH	-409.180801	-408.898234	-408.944954		-409.185095	-408.902528	

^aThe value is obtained at B3LYP/631G(d, p)/SVP level. ^bReaction enthalpies is defined as $\Delta H = H_{\text{gas}}(\text{interesting species}) - \Delta H_{\text{gas}}(\mathbf{4}) - \Delta H_{\text{gas}}(\mathbf{2_Zn})$ (kJ/mol). ^cThe solvent effect is calculated at SMD/B3LYP/631SVP//B3LYP/631SVP level in THF solution. ^d $H_{\text{solv}} = E_{\text{solv}} + (H_{\text{gas}} - E_{\text{tot}})$. ^e $\Delta H = H_{\text{solv}}(\text{interesting species}) - \Delta H_{\text{solv}}(\mathbf{4}) - \Delta H_{\text{solv}}(\mathbf{2_Zn})$ (kJ/mol).

Path1_BMg for the reaction of 5-phenylprimidine and TMPMgCl·2THF involving BF₃·OEt₂ in THF solution

Energy of reactant, intermediates and products in the reaction of 5-phenylprimidine (**4**) and TMPZnCl·2THF involving BF₃·OEt₂ in THF solution at SMD/B3LYP/631SVP// B3LYP/631SVP level.

	E _{gas} ^a (hartree)	H _{gas} ^a (hartree)	G _{gas} ^a (hartree)	ΔH ^b (kJ/mol)	E _{solv} ^c (hartree)	H _{solv} ^d (hartree)	ΔH ^e (kJ/mol)
5	-819.964488	-819.777265	-819.832692		-819.984610	-819.797388	
2_Mg	-1533.867784	-1533.341214	-1533.428326	0.00	-1533.884709	-1533.358139	0.00
BMa1_Mg	-2121.370502	-2120.779889	-2120.887192	14.73	-2121.402848	-2120.812235	18.90
THF	-232.456038	-232.332978	-232.368086		-232.459153	-232.336093	
BTsA1_Mg	-2121.356295	-2120.770053	-2120.874388	40.56	-2121.389631	-2120.803390	42.12
THF	-232.456038	-232.332978	-232.368086		-232.459153	-232.336093	
BMa2_Mg	-2121.376204	-2120.783973	-2120.891945	4.01	-2121.406843	-2120.814612	12.66
THF	-232.456038	-232.332978	-232.368086		-232.459153	-232.336093	
BTsA2_Mg	-2121.367920	-2120.777228	-2120.878721	21.72	-2121.391979	-2120.801287	47.65
THF	-232.456038	-232.332978	-232.368086		-232.459153	-232.336093	
BMa3_Mg	-2121.397865	-2120.805788	-2120.911748	-53.26	-2121.424869	-2120.832792	-35.07
THF	-232.456038	-232.332978	-232.368086		-232.459153	-232.336093	
BMa4_Mg	-1944.682794	-1944.251186	-1944.344389	-81.24	-1944.710664	-1944.279056	-68.41
TMPH	-409.180801	-408.898234	-408.944954		-409.185095	-408.902528	

^aThe value is obtained at B3LYP/631G(d, p)/SVP level. ^bReaction enthalpies is defined as $\Delta H = H_{\text{gas}}(\text{interesting species}) - \Delta H_{\text{gas}}(\mathbf{5}) - \Delta H_{\text{gas}}(\mathbf{2_Mg})$ (kJ/mol). ^cThe solvent effect is calculated at SMD/B3LYP/631SVP//B3LYP/631SVP level in THF solution. ^d $H_{\text{solv}} = E_{\text{solv}} + (H_{\text{gas}} - E_{\text{tot}})$. ^e $\Delta H = H_{\text{solv}}(\text{interesting species}) - \Delta H_{\text{solv}}(\mathbf{5}) - \Delta H_{\text{solv}}(\mathbf{2_Mg})$ (kJ/mol).

Path2_BMg: the reaction of 5-phenylprimidine and TMPMgCl·2THF involving BF₃·OEt₂ in THF solution

Energy of reactant, intermediates and products in the reaction of 5-phenylprimidine (**4**) and TMPZnCl·2THF involving BF₃·OEt₂ in THF solution at SMD/B3LYP/631SVP// B3LYP/631SVP level.

	E _{gas} ^a (hartree)	H _{gas} ^a (hartree)	G _{gas} ^a (hartree)	ΔH ^b (kJ/mol)	E _{solv} ^c (hartree)	H _{solv} ^d (hartree)	ΔH ^e (kJ/mol)
5	-819.964488	-819.777265	-819.832692		-819.984610	-819.797388	
2_Mg	-1533.867784	-1533.341214	-1533.428326	0.00	-1533.884709	-1533.358139	0.00
BMa1_Mg	-2121.370502	-2120.779889	-2120.887192	14.73	-2121.407948	-2120.817335	5.51
THF	-232.456038	-232.332978	-232.368086		-232.459153	-232.336093	
BTsaa1_Mg	-2121.366456	-2120.780817	-2120.882788	12.30	-2121.391979	-2120.806340	34.38
THF	-232.456038	-232.332978	-232.368086		-232.459153	-232.336093	
BMa2_Mg	-2121.377092	-2120.785900	-2120.888569	-1.05	-2121.403053	-2120.811861	19.88
THF	-232.456038	-232.332978	-232.368086		-232.459153	-232.336093	
BTsaa2_Mg	-2121.367920	-2120.777228	-2120.878721	21.72	-2121.394967	-2120.804275	39.80
THF	-232.456038	-232.332978	-3699.979472		-232.459153	-232.336093	
BMa3_Mg	-2121.397865	-2120.805788	-2120.911794	-53.26	-2121.424869	-2120.832792	-35.07
THF	-232.456038	-232.332978	-232.368086		-232.459153	-232.336093	
BMa4_Mg	-1944.682794	-1944.251186	-1944.344389	-81.24	-1944.710664	-1944.279056	-68.41
TMPH	-409.180801	-408.898234	-408.944954		-409.185095	-408.902528	

^aThe value is obtained at B3LYP/631G(d, p)/SVP level. ^b Reaction enthalpies is defined as ΔH = H_{gas}(interesting species) - ΔH_{gas}(**5**) - ΔH_{gas}(**2_Mg**) (kJ/mol). ^cThe solvent effect is calculated at SMD/B3LYP/631SVP//B3LYP/631SVP level in THF solution. ^dH_{solv} = E_{solv} + (H_{gas} - E_{tot}). ^eΔH=H_{solv}(interesting species) - ΔH_{solv}(**5**) - ΔH_{solv}(**2_Mg**) (kJ/mol).

Path3_BMg: the reaction of 5-phenylprimidine and TMPMgCl·2THF involving BF₃·OEt₂ in THF solution

Energy of reactent, intermediates and products in the reaction of 5-phenylprimidine (**4**) and TMPZnCl·2THF involving BF₃·OEt₂ in THF solution at SMD/B3LYP/631SVP// B3LYP/631SVP level.

	E _{gas} ^a (hartree)	H _{gas} ^a (hartree)	G _{gas} ^a (hartree)	ΔH ^b (kJ/mol)	E _{solv} ^c (hartree)	H _{solv} ^d (hartree)	ΔH ^e (kJ/mol)
5	-819.964488	-819.777265	-819.832692		-819.984610	-819.797388	
2_Mg	-1533.867784	-1533.341214	-1533.428326	0.00	-1533.884709	-1533.358139	0.00
BMb1_Mg	-2121.377228	-2120.787135	-2120.892251	-4.29	-2121.407860	-2120.817767	4.38
THF	-232.456038	-232.332978	-232.368086		-232.459153	-232.336093	
BTsB1_Mg	-2121.359302	-2120.773590	-2120.876424	31.27	-2121.382857	-2120.797145	58.52
THF	-232.456038	-232.332978	-232.368086		-232.459153	-232.336093	
BMb2_Mg	-2121.380648	-2120.788802	-2120.891310	-8.67	-2121.405225	-2120.813378	15.90
THF	-232.456038	-232.332978	-232.368086		-232.459153	-232.336093	
BTsB2_Mg	-2121.373389	-2120.782276	-2120.882975	8.47	-2121.399534	-2120.808422	28.91
THF	-232.456038	-232.332978	-3699.979472		-232.459153	-232.336093	
BMb3_Mg	-2121.399309	-2120.806846	-2120.910351	-56.04	-2121.417484	-2120.825021	-14.67
THF	-232.456038	-232.332978	-232.368086		-232.459153	-232.336093	
BMb4_Mg	-1944.685730	-1944.253951	-1944.347175	-88.50	-1944.709728	-1944.277949	-65.50
TMPH	-409.180801	-408.898234	-408.944954		-409.185095	-408.902528	

^aThe value is obtained at B3LYP/631G(d, p)/SVP level. ^b Reaction enthalpies is defined as ΔH = H_{gas}(interesting species) - ΔH_{gas}(**5**) - ΔH_{gas}(**2_Mg**) (kJ/mol). ^cThe solvent effect is calculated at SMD/B3LYP/631SVP//B3LYP/631SVP level in THF solution. ^dH_{solv} = E_{solv} + (H_{gas} - E_{tot}). ^eΔH=H_{solv}(interesting species) - ΔH_{solv}(**5**) - ΔH_{solv}(**2_Mg**) (kJ/mol).

Path1_BZn for the reaction of 5-phenylprimidine and TMPZnCl·2THF involving BF₃·OEt₂ in THF solution

Energy of reactent, intermediates and products in the reaction of 5-phenylprimidine (**4**) and TMPZnCl·2THF involving BF₃·OEt₂ in THF solution at SMD/B3LYP/631SVP// B3LYP/631SVP level.

	E _{gas} ^a (hartree)	H _{gas} ^a (hartree)	G _{gas} ^a (hartree)	ΔH ^b (kJ/mol)	E _{solv} ^c (hartree)	H _{solv} ^d (hartree)	ΔH ^e (kJ/mol)
5	-819.964488	-819.777265	-819.832692		-819.984610	-819.797388	
2_Zn	-3112.971185	-3112.444419	-3112.530837	0.00	-3112.985313	-3112.458548	0.00
BMa1_Zn	-3700.478004	-3699.887296	-3699.995821	3.70	-3700.509773	-3699.919065	2.04
THF	-232.456038	-232.332978	-232.368086		-232.459153	-232.336093	
BTsaa1_Zn	-3700.461262	-3699.874839	-3699.979472	36.41	-3700.493914	-3699.907491	32.43
THF	-232.456038	-232.332978	-232.368086		-232.459153	-232.336093	
BMa2_Zn	-3700.467864	-3699.876320	-3699.982595	32.52	-3700.503630	-3699.912086	20.36
THF	-232.456038	-232.332978	-232.368086		-232.459153	-232.336093	

BTSa2_Zn	-3700.464535	-3699.873442	-3699.977868	40.08	-3700.496222	-3699.905128	38.63
THF	-232.456038	-232.332978	-3699.979472		-232.459153	-232.336093	
BMa3_Zn	-3700.498429	-3699.905751	-3700.010221	-44.75	-3700.533596	-3699.940919	-55.34
THF	-232.456038	-232.332978	-232.368086		-232.459153	-232.336093	
BMa4_Zn	-3523.780137	-3523.348501	-3523.442750	-65.77	-3523.805610	-3523.373974	-54.00
TMPH	-409.180801	-408.898234	-408.944954		-409.185095	-408.902528	

^aThe value is obtained at B3LYP/631G(d, p)/SVP level. ^b Reaction enthalpies is defined as $\Delta H = H_{\text{gas}}(\text{interesting species}) - \Delta H_{\text{gas}}(\mathbf{5}) - \Delta H_{\text{gas}}(\mathbf{2_Zn})$ (kJ/mol). ^cThe solvent effect is calculated at SMD/B3LYP/631SVP//B3LYP/631SVP level in THF solution. ^d $H_{\text{solv}} = E_{\text{solv}} + (H_{\text{gas}} - E_{\text{tot}})$. ^e $\Delta H = H_{\text{solv}}(\text{interesting species}) - \Delta H_{\text{solv}}(\mathbf{5}) - \Delta H_{\text{solv}}(\mathbf{2_Zn})$ (kJ/mol).

Path2_BZn for the reaction of 5-phenylprimidine and TMPZnCl·2THF involving $\text{BF}_3 \cdot \text{OEt}_2$ in THF solution

Energy of reactent, intermediates and products in the reaction of 5-phenylprimidine (**4**) and TMPZnCl·2THF involving $\text{BF}_3 \cdot \text{OEt}_2$ in THF solution at SMD/B3LYP/631SVP// B3LYP/631SVP level.

	E _{gas} ^a (hartree)	H _{gas} ^a (hartree)	G _{gas} ^a (hartree)	ΔH ^b (kJ/mol)	E _{solv} ^c (hartree)	H _{solv} ^d (hartree)	ΔH ^e (kJ/mol)
5	-819.964488	-819.777265	-819.832692		-819.984610	-819.797388	
2_Zn	-3112.971185	-3112.444419	-3112.530837	0.00	-3112.985313	-3112.458548	0.00
BMaa1_Zn	-3700.475443	-3699.884680	-3699.991135	10.57	-3700.504672	-3699.913909	15.58
THF	-232.456038	-232.332978	-232.368086		-232.459153	-232.336093	
BTaa1_Zn	-3700.456946	-3699.870805	-3699.973674	47.00	-3700.483302	-3699.897160	59.55
THF	-232.456038	-232.332978	-232.368086		-232.459153	-232.336093	
BMaa2_Zn	-3700.461620	-3699.870845	-3699.975815	46.89	-3700.487341	-3699.896566	61.11
THF	-232.456038	-232.332978	-232.368086		-232.459153	-232.336093	
BTaa2_Zn	-3700.459104	-3699.868703	-3699.970847	52.52	-3700.487386	-3699.896985	60.01
THF	-232.456038	-232.332978	-3699.979472		-232.459153	-232.336093	
BMa3_Zn	-3700.498429	-3699.905751	-3700.010221	-44.75	-3700.533596	-3699.940919	-55.34
THF	-232.456038	-232.332978	-232.368086		-232.459153	-232.336093	
BMa4_Zn	-3523.780137	-3523.348501	-3523.442750	-65.77	-3523.805610	-3523.373974	-54.00
TMPH	tmpf	-409.180801	-408.898234	-408.944954		-409.185095	-408.902528

^aThe value is obtained at B3LYP/631G(d, p)/SVP level. ^b Reaction enthalpies is defined as $\Delta H = H_{\text{gas}}(\text{interesting species}) - \Delta H_{\text{gas}}(\mathbf{5}) - \Delta H_{\text{gas}}(\mathbf{2_Zn})$ (kJ/mol). ^cThe solvent effect is calculated at SMD/B3LYP/631SVP//B3LYP/631SVP level in THF solution. ^d $H_{\text{solv}} = E_{\text{solv}} + (H_{\text{gas}} - E_{\text{tot}})$. ^e $\Delta H = H_{\text{solv}}(\text{interesting species}) - \Delta H_{\text{solv}}(\mathbf{5}) - \Delta H_{\text{solv}}(\mathbf{2_Zn})$ (kJ/mol).

Path3_BZn for the reaction of 5-phenylprimidine and TMPZnCl·2THF involving $\text{BF}_3 \cdot \text{OEt}_2$ in THF solution

Energy of reactent, intermediates and products in the reaction of 5-phenylprimidine (**4**) and TMPZnCl·2THF involving $\text{BF}_3 \cdot \text{OEt}_2$ in THF solution at SMD/B3LYP/631SVP// B3LYP/631SVP level.

	E _{gas} ^a (hartree)	H _{gas} ^a (hartree)	G _{gas} ^a (hartree)	ΔH ^b (kJ/mol)	E _{solv} ^c (hartree)	H _{solv} ^d (hartree)	ΔH ^e (kJ/mol)
5	-819.964488	-819.777265	-819.832692		-819.984610	-819.797388	
2_Zn	-3112.971185	-3112.444419	-3112.530837	0.00	-3112.985313	-3112.458548	0.00
BMb1_Zn	-3700.477142	-3699.886736	-3699.993752	5.17	-3700.507240	-3699.916834	7.90
THF	-232.456038	-232.332978	-232.368086		-232.459153	-232.336093	
BTsb1_Zn	-3700.452380	-3699.866289	-3699.969109	58.86	-3700.475709	-3699.889618	79.35
THF	-232.456038	-232.332978	-232.368086		-232.459153	-232.336093	
BMb2_Zn	-3700.465767	-3699.873970	-3699.977248	38.69	-3700.490900	-3699.899102	54.45
THF	-232.456038	-232.332978	-232.368086		-232.459153	-232.336093	
BTsb2_Zn	-3700.456905	-3699.865907	-3699.967918	59.86	-3700.487822	-3699.896824	60.43
THF	-232.456038	-232.332978	-3699.979472		-232.459153	-232.336093	
BMb3_Zn	-3700.495654	-3699.903344	-3700.010605	-38.43	-3700.527466	-3699.935156	-40.21
THF	-232.456038	-232.332978	-232.368086		-232.459153	-232.336093	
BMb4_Zn	-3523.779274	-3523.347373	-3523.439941	-62.81	-3523.804050	-3523.372149	-49.20
TMPH	-409.180801	-408.898234	-408.944954		-409.185095	-408.902528	

^aThe value is obtained at B3LYP/631G(d, p)/SVP level. ^b Reaction enthalpies is defined as $\Delta H = H_{\text{gas}}(\text{interesting species}) - \Delta H_{\text{gas}}(\mathbf{5}) - \Delta H_{\text{gas}}(\mathbf{2_Zn})$ (kJ/mol). ^cThe solvent effect is calculated at SMD/B3LYP/631SVP//B3LYP/631SVP level in THF solution. ^d $H_{\text{solv}} = E_{\text{solv}} + (H_{\text{gas}} - E_{\text{tot}})$. ^e $\Delta H = H_{\text{solv}}(\text{interesting species}) - \Delta H_{\text{solv}}(\mathbf{5}) - \Delta H_{\text{solv}}(\mathbf{2_Zn})$ (kJ/mol).

7.5 Calculated Data for Chapter 5

Computational detail for the calculation of ^{29}Si NMR chemical shifts of tetracoordinated silicon compounds in the gas phase and in solution

Solvent effect

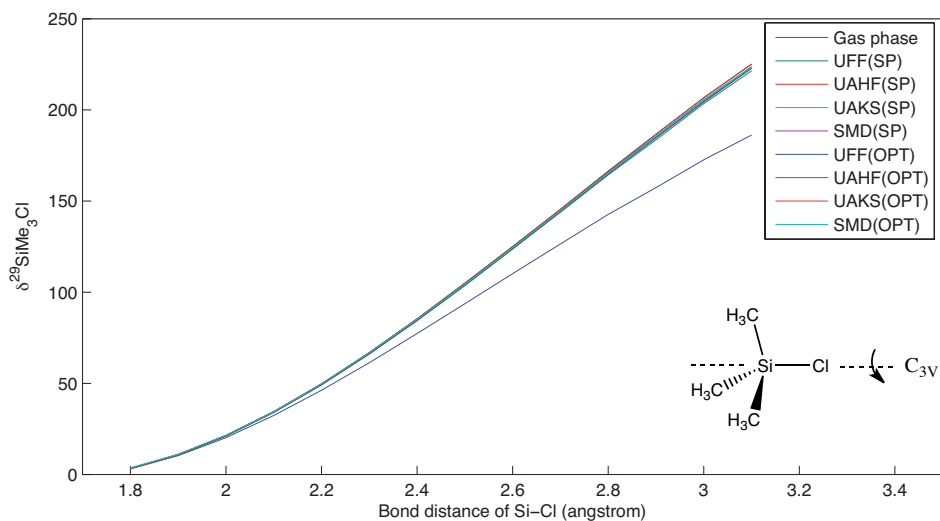


Figure 7.5.1. Calculated $\delta(^{29}\text{Si})$ values for SiMe_3Cl at various levels of theory.

Chemical shifts are sensitive to the Si-Cl bond length in gas phase and solution phase. For solvent effects (covered by an implicit solvent model), PCM with different atomic radii have similar results (Figure 7.5.1). Compared to the gas phase, chemical shifts are always higher in solution phase. The structures in gas phase and solution phase have no big influence on chemical shift calculations.

The results in Table 7.5.1 have been obtained in gas phase and in the presence of the PCM continuum solvation model for complexes of **2** with one chloroform molecule.

Table 7.5.1. $\delta(^{29}\text{Si})$ for **2** complexed to one chloroform molecule weighted by ΔG_{298} and ΔH_{298} in gas phase at MP2(FULL)/IGLO-III//MPW1K/6-31+G(d) level.

	r(Si-Cl) (pm)	ΔG (kJ/mol)	$\delta(^{29}\text{Si})$ (ppm) (Weighted by ΔG)	ΔH (kJ/mol)	$\delta(^{29}\text{Si})$ (ppm) (Weighted by ΔH)
2 1	208.6	0.0	30.7	3.8	30.7
2 2	208.6	1.0	30.9	2.0	30.9
2 3	209.5	7.0	33.8	0.0	33.8
2 4	208.5	7.4	30.7	7.3	30.7
2 5	208.7	7.9	31.3	5.4	31.3
SUM			30.88		32.47

Table 7.5.2. $\delta(^{29}\text{Si})$ for **2** complexed to one chloroform molecule weighted by ΔG_{298} and ΔH_{298} in solution phase at PCM/UAHF/MP2(FULL)/IGLO-III//PCM/UAHF/MPW1K/6-31+G(d) level.

	r(Si-Cl) (pm)	ΔG (kJ/mol)	$\delta(^{29}\text{Si})$ (ppm) (Weighted by ΔG)	ΔH (kJ/mol)	$\delta(^{29}\text{Si})$ (ppm) (Weighted by ΔH)
2 1	210.5	1.02	35.09	0.00	35.09
2 2	210.5	3.02	35.43	5.49	35.43
2 3	210.7	0.00	36.24	3.67	36.24
2 4	210.4	2.06	35.06	6.05	35.06
2 5	210.4	1.29	35.16	5.66	35.16
SUM			35.52		35.29

$\delta(^{29}\text{Si})$ values are dependent on the relative energy taken for Boltzmann averaging.

Table 7.5.3. Calculated $\delta(^{29}\text{Si})$ chemical shifts for SiMe_3Cl (**2**) using different theoretical methods and basis sets^a

Methods ^b	6-31+G(d)	6-311++G(2d,2p)	cc-pVDZ	cc-pVTZ	cc-pVQZ	Def2-TZVP	IGLO-III	MAD ^b
HCTH407	+33.99	+35.00	+32.63	+32.91	+26.37	+32.37	+31.40	+2.63
B3LYP	+34.22	+36.37	+34.13	+34.14	+27.60	+34.29	+32.94	+3.57
B3PW91	+35.41	+36.84	+35.31	+34.64	+28.78	+34.92	+33.66	+4.07
PBE1PBE	+35.38	+36.56	+35.35	+34.83	+29.37	+34.68	+33.31	+3.89
MPW1K	+34.18	+34.83	+33.89	+33.59	+28.09	+33.06	+31.88	+2.83
M06-2X	+32.89	+42.67	+38.85	+31.00	+36.82	+38.10	+37.24	+6.10
DF-LMP2	+31.39	+33.05	+31.36	+33.09	+29.55	+31.47	+28.40	+1.47
MP2(FULL)	+32.28	+33.65	+30.71	+32.54	+28.59	+31.92	+30.32	+1.44
MAD ^c	+3.02	+5.42	+3.33	+2.64	+2.83	+3.15	+2.36	-

^aThe geometries are optimized with MPW1K/6-31+G(d) ^bDifferent methods are used for calculate NMR chemical shifts. ^cMean absolute deviation MAD=1/nΣ|X_{cal}-X_{exp}|

Table 7.5.3 shows the basis sets effects on chemical shift calculation. MAD of triple zeta Pople basis sets has biggest MAD 5.42 compared with other basis sets. MAD with double zeta Pople basis sets is 3.02 close to triple zeta Ahlrichs basis set.

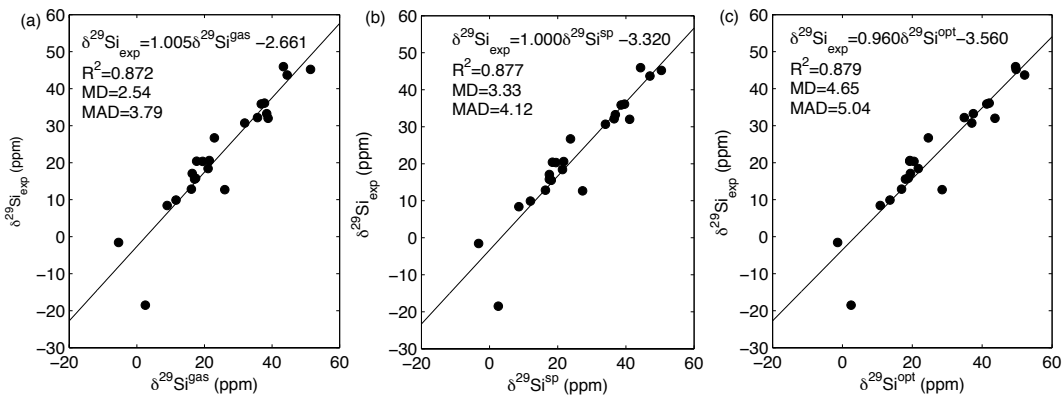


Figure 7.5.2. Comparison between experimentally measured and theoretically calculated shift values. (a) MPW1K/IGLO-III// MPW1K/6-31+G(d). (b) PCM/UAHF/MPW1K/IGLO-III// MPW1K/6-31+G(d). (c) PCM/UAHF/MPW1K/IGLO-III//PCM/UAHF/MPW1K/6-31+G(d).

For the systems chosen in this publication, the correlations between calculation and experiment have no significant change in gas phase and solution phase. But the MAD value in gas phase is smaller than in solution phase. Therefore, solvent effects have no big influence on chemical shift calculations.

Table 7.5.4. The influence of scaling factor alpha on ²⁹Si of SiMe₃Cl chemical shifts in PCM.

Alpha	Bond distance of Si-Cl (pm) ^a	δ(²⁹ Si) (ppm) ^b
1.0	211.0	+35.71
1.1(default)	210.4	+35.17
1.2	209.9	+33.54
1.4	209.4	+32.66
1.6	209.1	+31.97
1.8	208.9	+31.58
2.0	208.7	+31.21
Bondi(Alpha=1.1)	210.8	+36.10
Pauling(Alpha=1.1)	214.4	+36.65

^aThe structures are optimized with PCM model (Radii=UAHF, CDCl₃) at MPW1K/6-31+G(d) level. ^b Chemical shifts are calculated with MP2/IGLO-III.

With PCM, the scaling factor of atomic radii (UAHF) defined the solvent exclusive surface, which is used for calculating electrostatic energy. Table 7.5.4 shows that with an increasing scaling factor, bond distance of Si-Cl and shifts will decrease. Compared with gas phase results, δ(²⁹Si) in solution is higher than the experimental value.

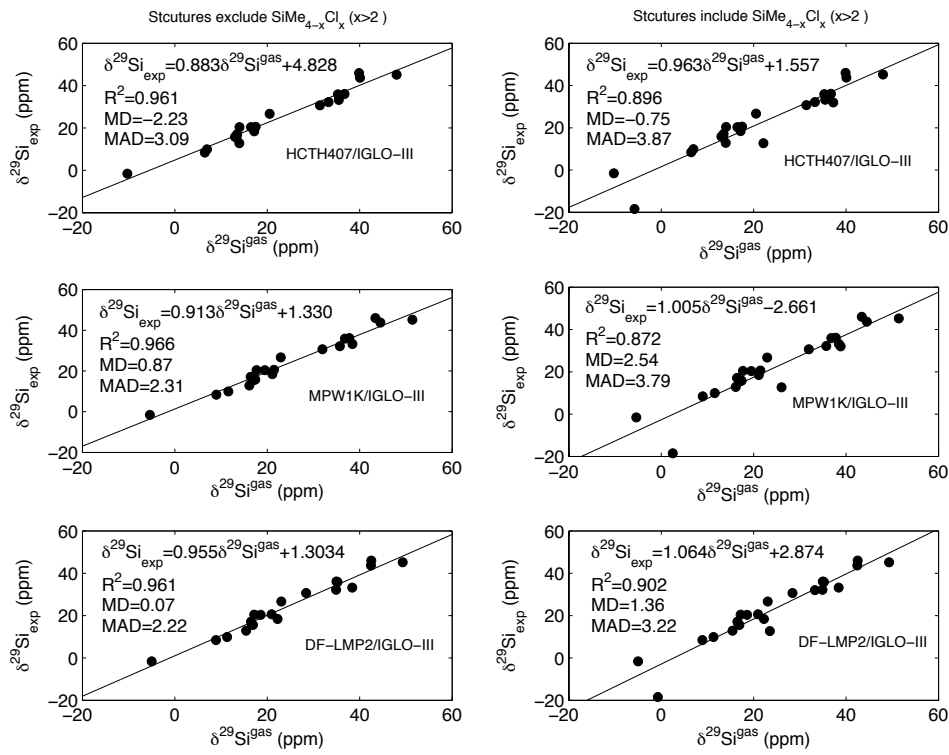


Figure 7.5.3. Influence of $\delta^{29}\text{Si}$ of $\text{SiMe}_{4-x}\text{Cl}_x (x > 2)$ on correlation at different theory levels.

For the total systems chosen in Table 7.5.5, deviations become big once systems contain more than one Si-Cl bond. For SiCl_3 the deviation is -20.99 ppm at MPW1K/IGLO-III//MPW1K/6-31+G(d) level. The deviation is reduced to +1.22 ppm in SiMe_3Cl . pcS-n basis set effects for NMR calculation are following:

pcS-n basis sets for $\delta^{29}\text{SiMe}_{4-x}\text{Cl}_x$

pcS-n methods are designed for nuclear magnetic shielding constants calculation,¹ this basis set are used for $\text{SiMe}_{4-x}\text{Cl}_x$ system.

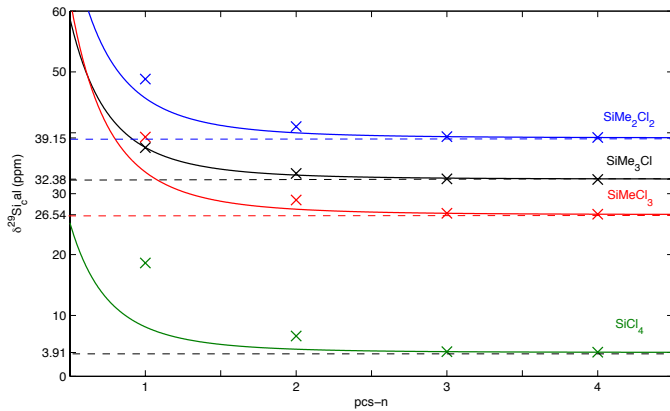


Figure 7.5.5. Chemical shifts extrapolation (from MPW1K/pcS-3 to MPW1K/pcS-4) for $\text{SiMe}_{4-x}\text{Cl}_x$ by using $y=a+b/(x+0.5)^4$. Geometries are optimized with MPW1K/6-31+G(d).

Table 7.5.5. pcS-n basis sets effects for $\delta(\text{SiMe}_{4-x}\text{Cl}_x)$.

	SiMe_3Cl	SiMe_2Cl_2	SiMeCl_3	SiCl_4
exp	+30.70	+32.00	+12.70	-18.50
MPW1K/pcs1//MPW1K/6-31+G(d)	+37.57	+48.83	+39.30	+18.61
MPW1K/pcs2//MPW1K/6-31+G(d)	+33.32	+41.02	+28.96	+6.62
MPW1K/pcs3//MPW1K/6-31+G(d)	+32.44	+39.37	+26.78	+4.05
MPW1K/pcs4//MPW1K/6-31+G(d)	+32.33	+39.23	+26.63	+3.96
MPW1K/CBS//MPW1K/6-31+G(d)	+32.38	+39.15	+26.54	+3.91

MPW1K/IGLO-III//MPW1K/6-31+G(d)	+31.92	+38.81	+26.04	+1.97
DF-LMP2/IGLO-III//MPW1K/6-31+G(d)	+28.41	+33.25	+23.51	-0.74

MPW1K/CBS: extrapolate from MPW1K/pcS-3 to MPW1K/pcS-4 by using $y=a+b/(x+0.5)^4$.

The results with the MPW1K method get close to experiment while the basis set is changing from pcS-1 to pcS-4. The two point extrapolation formula from Jan Martin² is used as extrapolation method. The deviation of MPW1K/CBS//MPW1K/6-31+G(d) is slightly higher than the deviation at MPW1K/IGLO-III level, which indicates that the IGLO-III basis set can give better results than pcS-n basis sets at the same theory level. Using the IGLO-III basis set, the deviation at DF-LMP2 theory level is smaller than at MPW1K theory level. Therefore, DF-LMP2/IGLO-III is the best-suited method for ²⁹Si chemical shifts calculations.

Effects of Spin-Orbit correction

Methods

NMR chemical shifts were calculated with the NMR program module of ADF 2013.01.^{3,4} The contributions of relativistic spin-orbit effects to the nuclear magnetic shielding constants were included with the two-component zeroth-order regular approximation (ZORA)^{5,6} formalism, as implemented in ADF. All applied Slater-type basis sets, optimized for relativistic ZORA calculations, were taken from the internal basis set library of ADF 2013.01.⁷ A series of representative hybrid and GGA exchange-correlation functionals commonly in use was included in our study, the hybrid functionals mPW1K,⁸ B1PW91,⁹ PBE0,¹⁰⁻¹² B3LYP¹³ as well as the GGA models PBE,¹⁴ OPBE¹⁵ and OP86.^{16,17} ²⁹Si NMR chemical shifts are reported relative to tetramethylsilane ($\delta^{29}\text{Si}(\text{TMS}) = 0$). Solvent effects have been taken into account with the conductor-like screening model (COSMO)¹⁸ as implemented in ADF 2013.01 with the parameters epsilon=4.8, radius=3.17 (both for the solvent CHCl₃), cav0=1.321¹⁹ and cav1=0.0067639¹⁹.

Introduction

The importance of heavy-atom induced spin-orbit (SO) effects for nuclear magnetic shifts of group 14 elements halides have been highlighted by several groups.²⁰⁻²² According to these early reports, the experimentally observed normal halogen dependence (NHD), i.e. the characteristic high-field shift of the nucleus bound directly to the halogen substituents with increasing atomic number of the halogen, is mainly a result of the spin-orbit effect. In these studies it was found that shifts calculated with the inclusion of SO effects agree significantly better with the experiment than their non-relativistic counterparts.

Recently, Chernyshev and Krivdin²³ have investigated the ²⁹Si NMR chemical shifts of selected silanes, which included the series of chlorohydrosilanes SiH_{4-n}Cl_n (n=1-4) as well as halosilanes SiX₄ (X=Br, I), using the Amsterdam Density Functional (ADF) code. Based on the results of their initial benchmark study, in which the performance of three common hybrid functionals was evaluated, they confirmed the necessity of the inclusion of SO effects for an accurate prediction of NMR chemical shifts of halosilanes. The authors have identified the functionals PBE0 and B1PW91 (mean square error 3 ppm for 27 compounds) along with a triple- ζ Slater-type basis set (TZP) as the preferred methods.

Results and Discussions

Amongst the group of silanes, which are subject of the present study, specifically the accurate prediction of NMR chemical shifts of chlorosilanes at the HCTH407/IGLO-III level of theory was found to be problematic. In order to provide an explanation for this issue, we performed calculations with the inclusion of relativistic SO effects using the zeroth-order regular approximation (ZORA) implemented in the program package ADF.

Our results clearly demonstrate that ²⁹Si shifts of a series of four representative alkylchlorosilanes, a class of compounds not reported by Chernyshev and Krivdin,²³ can be predicted with almost quantitative accuracy (MaxE < -1.7 ppm) if SO effects are included (Table 7.5.6). In contrast, the non-relativistic shifts differ significantly from the experimental values (Figure 7.5.3). For all methods, SO contributions result in a high-field shift compared to the non-relativistic values.

Table 7.5.6. ²⁹Si NMR chemical shifts of alkylchlorosilanes.

	SiMe ₃ Cl	SiMe ₂ Cl ₂	SiMeCl ₃	SiCl ₄	MAE ^b
$\delta^{29}\text{Si}_{\text{expt}}$	30.7	32.0	12.7	-18.5	
functional ^a					
mPW1K	basis set				
	DZP	25.6	25.8	4.0	-30.8
	TZ2P	27.6	30.6	11.9	-18.8
	QZ4P	31.4	35.6	16.5	-13.8
B1PW91	DZP	27.5	27.7	5.0	-31.8
	TZ2P	28.9	32.3	13.0	-19.5
	QZ4P	32.4	37.0	17.2	-15.1
PBE0	DZP	27.9	28.3	5.8	-30.8
	TZ2P	29.0	32.5	13.2	-19.2
	QZ4P	32.6	37.3	17.6	-14.8
B3LYP	DZP	27.1	26.8	3.5	-34.3
	TZ2P	28.8	31.7	11.8	-21.7
	QZ4P	31.4	35.0	14.9	-18.1
PBE	DZP	29.8	30.5	5.9	-34.8
	TZ2P	32.3	35.8	14.8	-21.2
	QZ4P	33.2	37.5	16.9	-19.2
OPBE	DZP	28.2	28.8	5.4	-33.2
	TZ2P	31.1	33.4	13.9	-20.4
	QZ4P	30.2	33.4	14.0	-19.1
OP86	DZP	28.1	28.6	5.0	-33.8
	TZ2P	31.2	34.1	13.6	-20.9
	QZ4P	30.3	33.5	13.8	-19.7

^a All calculated chemical shifts include the SO correction. ^b MAE: mean absolute error. Shown is the MAE of the deviation from the experimental chemical shift.

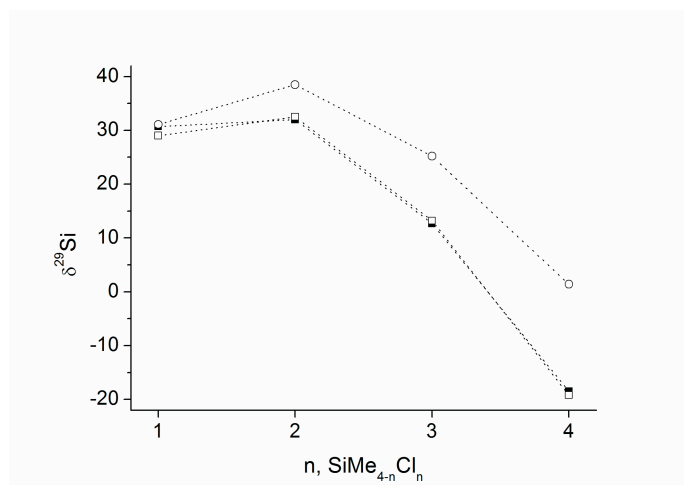


Figure 7.5.5. Comparison of experimental $\delta^{29}\text{Si}$ (filled rectangles), non-relativistic $\delta^{29}\text{Si}$ (hollow circles) and SO corrected $\delta^{29}\text{Si}$ (hollow rectangles) for a series of alkylchlorosilanes $\text{SiMe}_{4-n}\text{Cl}_n$.

If SO effects are included, the majority of tested GGA and hybrid exchange-correlation functionals shows an excellent to fair agreement with the experimental chemical shifts, if used in combination with the triple- ζ TZ2P and the quadruple- ζ QZ4P basis set, while shifts calculated with the small DZP basis set show significant deviations. Furthermore, the increasing deviation with an increasing number of chloro-substituents indicates the inadequacy of the small basis set for the calculation of NMR chemical shifts.

The mean absolute error calculated with the hybrid models mPW1K, B1PW91 and PBE0 (B3LYP being an exception) are lowest for the triple- ζ basis set, while it increases with increasing basis set size, which is obviously an effect of error compensation. In contrast, the errors calculated for the GGA models employing the OPTX exchange functional decrease with increasing basis set size. A significant part of this trend is due to the influence of the quality of the calculated shift for SiCl_4 on the statistical error. Apparently, basis set convergence for silanes with a smaller number of chloro-substituents has been reached for TZ2P, while converged shifts for perchlorinated silanes require larger basis sets such as QZ4P.

However, the best performing methods are ZORA-SO-PBE0/TZ2P (MAE = 0.9 ppm, MaxE = -1.7 ppm) and ZORA-SO-B1PW91/TZ2P (MAE = 0.9 ppm, MaxE = -1.8 ppm).

A closer examination of the calculated chemical shifts obtained at the ZORA-SO-PBE0/TZ2P level reveals an increasing SO correction from SiMe_3Cl ($\text{SO}_{\text{corr}} = -2.1$ ppm) to SiCl_4 ($\text{SO}_{\text{corr}} = -20.6$ ppm), i.e. with the increasing number of chloro-substituents (Figure 7.5.1). We furthermore note the non-additivity of the SO corrections. The SO correction per chloro-substituent increases monotonously from approximately 2 ppm (SiMe_3Cl), 3 ppm for SiMe_2Cl_2 , 4 ppm for SiMeCl_3 , to 5 ppm for SiCl_4 . As first stated by Kaupp et al.,²² this trend can be readily explained based on the analogy to the Fermi-contact mechanism of spin-spin coupling. The increasing involvement of valence s orbitals of the Si atoms in the bonding orbitals to the chloro-substituents results in larger SO contributions in the series from SiMe_3Cl to SiCl_4 .

Spin-Orbit correction for other structures

Table 7.5.7. Theoretically Calculated and Experimentally Measured ^{29}Si Chemical Shifts together with Calculated Spin-orbit Corrections of Selected Organosilanes.^a Values are given in ppm.

Index	System	Conformer	ZORA-SO-PBE0/TZ2P ^a	$\text{SO}_{\text{corr}}^{\text{b}}$	Experiment ^c
2		1	29.0	-2.1	+30.70 (CDCl ₃)
3		1	-19.2	-20.6	-18.50 (CDCl ₃)
4		1	-6.8	0.2	-1.57 (CDCl ₃)
5		1	8.8	-0.4	+8.40 (C ₆ D ₆) ²⁴
6		1	12.6	-0.7	
6		2	11.1	-0.8	
6		Boltz. av.	11.7	-0.8	+9.91 (CDCl ₃)
7		1	13.2	-12.0	+12.70 (CDCl ₃)
8		1	16.2	-1.7	+12.86 (CDCl ₃)
9		1	18.6	-0.7	

9		2	18.7	-0.8	
9		3	18.6	-0.7	
9		4	17.7	-0.8	
9		5	17.8	-0.8	
9		6	17.4	-0.8	
9		7	18.4	-0.8	
9		8	18.4	-0.8	
9		9	17.9	-0.7	
9		10	18.5	-0.7	
9		11	18.3	-0.8	
9		12	18.7	-0.8	
9		13	18.0	-0.8	
9	Boltz. av.		18.3	-0.7	+15.54 (CDCl ₃)
10		1	18.6	-0.8	
10		2	18.1	-0.7	
10	Boltz. av.		18.5	-0.8	+15.80 (CDCl ₃)
11		1	17.3	-0.4	+17.08 (CDCl ₃)
12		1	23.5	-0.7	
12		2	22.1	-0.7	
12		3	22.1	-0.7	
12		4	23.0	-0.7	
12		5	21.7	-0.7	
12		6	23.5	-0.7	
12		7	22.0	-0.5	
12		8	18.2	-0.8	
12		9	17.3	-0.7	
12		10	17.7	-0.7	
12	Boltz. av.		22.4	-0.7	+18.42 (CDCl ₃)
13		1	20.0	-0.4	+20.34 (CDCl ₃)
14		1	18.4	-0.6	+20.39 (CDCl ₃)
15		1	22.8	-0.8	
15		2	23.9	-0.9	
15		3	23.7	-0.7	
15		4	25.1	-0.7	
15		5	25.1	-0.7	
15		6	23.3	-0.6	
15		7	23.6	-0.8	
15		8	23.8	-0.6	
15		9	25.0	-0.6	
15		10	21.1	-0.7	
15		11	25.2	-0.6	
15	Boltz. av.		23.1	-0.8	+20.58 (CDCl ₃)
16		1	24.5	-0.4	
16		2	21.9	-0.6	
16	Boltz. av.		24.5	-0.4	+26.69 (CDCl ₃)
17		1	32.5	-6.0	+32.00(CDCl ₃) ²⁶
18		1	38.0	-0.4	
18		2	32.8	-0.5	
18		3	40.4	-0.5	
18		4	39.6	-0.4	
18		5	52.5	-0.5	
18	Boltz. av.		37.2	-0.4	+32.16(CDCl ₃)
19		1	41.2	-0.5	
19		2	39.8	-0.5	
19		3	39.8	-0.5	
19		4	42.0	-0.3	
19		5	35.2	-0.4	
19		6	55.8	-0.4	
19	Boltz. av.		40.5	-0.5	+33.25(CDCl ₃)
20		1	34.0	-1.5	
20		2	35.9	-1.5	
20		3	32.6	-1.4	
20		4	34.5	-1.4	
20		5	34.3	-1.5	

20		6	30.4	-1.6	
20		7	34.5	-1.6	
20		Boltz. av.	34.5	-1.5	+35.89(CDCl ₃)
21		1	36.2	-2.0	+36.09 (CDCl ₃)
22		1	46.2	-0.5	
22		2	46.3	-0.5	
22		Boltz. av.	46.2	-0.5	+43.71 (CDCl ₃)
23		1	53.8	-0.6	
23		2	54.0	-0.6	
23		3	52.8	-0.6	
23		4	52.8	-0.6	
23		5	57.3	-0.7	
23		6	52.2	-0.7	
23		7	49.4	-0.3	
23		8	48.7	-0.7	
23		Boltz. av.	53.6	-0.6	+45.21(CDCl ₃)
24		1	44.8	-0.6	
24		2	43.8	-0.6	
24		3	44.9	-0.6	
24		4	43.5	-0.6	
24		5	45.2	-0.8	
24		6	43.3	-0.8	
24		7	56.4	-0.6	
24		Boltz. av.	44.5	-0.6	+45.96(CDCl ₃)

^a All geometries are obtained at MPW1K/6-31+G(d) level, shifts include relativistic spin-orbit effects using the ZORA formalism. Boltzmann averaged values are calculated in the same way as the ones in the “tables of ²⁹Si shielding number” (see below). ^b the spin-orbit correction is calculated as $\delta_{\text{ZORA}} - \delta_{\text{NR}}$. ^c For experimental details see the corresponding supplementary material.

Table 7.5.7 shows the influence of different conformers on the chemical shifts and spin-orbit corrections. The differences between shifts can be relatively large, especially for ion pairs (e.g. deviation of 14.6 ppm between **19_1** and **19_6**), whereas the influence on the spin-orbit corrections is only small (maximum deviation of 0.4 ppm for **23_6** and **23_7**). So one may just calculate the spin-orbit correction for the most stable isomer, because the deviation between this value and the Boltzmann averaged one is not exceeding 0.1 ppm (at least for the above systems, which only have relatively low SO corrections).

The influence of solvent effects (calculated with COSMO) on spin-orbit corrections is depicted in Table 7.5.8. The differences between the values are of the same magnitude as the ones for different conformers. Therefore, the influence of solvation is also negligible.

Table 7.5.8. Theoretically Calculated Spin-orbit Corrections (Influence of Solvent Effects) of a small Selection of Organosilanes.^a Values are given in ppm.

Index	System	SO _{corr} ^{gas}	SO _{corr} ^{sp}	SO _{corr} ^{opt}
2		-6.0	-5.8	-5.9
11		-0.4	-0.4	-0.6
24		-0.6	-0.7	-0.8

^a The spin-orbit corrections for the conformer 1 is calculated as $\delta_{\text{ZORA}} - \delta_{\text{NR}}$. SO_{corr}^{gas}: ZORA-SO-PBE0/TZ2P//MPW1K/6-31+G(d). SO_{corr}^{sp}: COSMO/ZORA-SO-PBE0/TZ2P//MPW1K/6-31+G(d). SO_{corr}^{opt}: COSMO/ZORA-SO-PBE0/TZ2P//PCM/UHAF-MPW1K/6-31+G(d).

Tables 7.5.9-7.5.14 display the results for the non-relativistic shifts (δ_{NR}), the spin-orbit corrected shifts (δ_{ZORA}), the spin-orbit corrections (SO_{corr}) and the deviations from experiment (Δ_{expt}) for a number of exchange-correlation functionals and basis sets (DZP, TZ2P, QZ4P). Tables S4-S6 show the results for the non-relativistic isotropic shielding constants (σ_{NR}) and the spin-orbit corrected isotropic shielding constants (σ_{ZORA}).

Table 7.5.9. ²⁹Si NMR chemical shifts calculated for several exchange-correlation functionals employing the DZP basis set. Values are given in ppm.

		SiMe ₃ Cl	SiMe ₂ Cl ₂	SiMeCl ₃	SiCl ₄
XC functional mPW1K	δ_{expt}	30.7	32.0	12.7	-18.5
	$\delta_{\text{NR}}^{\text{a}}$	28.9	32.7	17.2	-8.5
	$\delta_{\text{ZORA}}^{\text{b}}$	25.6	25.8	4.0	-30.8
	SO _{corr} ^c	-3.3	-6.9	-13.2	-22.3
B1PW91	$\Delta_{\text{expt}}^{\text{d}}$	-5.1	-6.2	-8.7	-12.3
	$\delta_{\text{NR}}^{\text{a}}$	30.4	34.8	18.6	-8.7
	$\delta_{\text{ZORA}}^{\text{b}}$	27.5	27.7	5.0	-31.8
	SO _{corr} ^c	-2.9	-7.1	-13.6	-23.1
PBE0	$\Delta_{\text{expt}}^{\text{d}}$	-3.2	-4.3	-7.7	-13.3
	$\delta_{\text{NR}}^{\text{a}}$	30.7	35.3	19.3	-7.8

	$\delta_{\text{ZORA}}^{\text{b}}$	27.9	28.3	5.8	-30.8
	$\delta_{\text{SO corr}}^{\text{c}}$	-2.8	-7.0	-13.5	-23.0
	$\Delta_{\text{expt}}^{\text{d}}$	-2.8	-3.7	-6.9	-12.3
B3LYP	$\delta_{\text{NR}}^{\text{a}}$	30.0	34.2	17.8	-9.6
	$\delta_{\text{ZORA}}^{\text{b}}$	27.1	26.8	3.5	-34.3
	$\delta_{\text{SO corr}}^{\text{c}}$	-2.9	-7.4	-14.3	-24.7
	$\Delta_{\text{expt}}^{\text{d}}$	-3.6	-5.2	-9.2	-15.8
PBE	$\delta_{\text{NR}}^{\text{a}}$	32.6	37.8	20.1	-10.2
	$\delta_{\text{ZORA}}^{\text{b}}$	29.8	30.5	5.9	-34.8
	$\delta_{\text{SO corr}}^{\text{c}}$	-2.8	-7.3	-14.2	-24.6
	$\Delta_{\text{expt}}^{\text{d}}$	-0.9	-1.5	-6.8	-16.3
OPBE	$\delta_{\text{NR}}^{\text{a}}$	30.7	35.2	17.7	-12.1
	$\delta_{\text{ZORA}}^{\text{b}}$	28.2	28.8	5.4	-33.2
	$\delta_{\text{SO corr}}^{\text{c}}$	-2.5	-6.4	-12.3	-21.1
	$\Delta_{\text{expt}}^{\text{d}}$	-2.5	-3.2	-7.3	-14.7
OP86	$\delta_{\text{NR}}^{\text{a}}$	30.7	35.1	17.5	-12.3
	$\delta_{\text{ZORA}}^{\text{b}}$	28.1	28.6	5.0	-33.8
	$\delta_{\text{SO corr}}^{\text{c}}$	-2.6	-6.5	-12.5	-21.5
	$\Delta_{\text{expt}}^{\text{d}}$	-2.6	-3.4	-7.7	-15.3

^a δ_{NR} : non-relativistic $\delta^{29}\text{Si}$ vs. TMS, ^b δ_{ZORA} : $\delta^{29}\text{Si}$ including relativistic spin-orbit effects using the ZORA formalism, ^c $\delta_{\text{SO corr}}$: the spin-orbit correction is calculated as $\delta_{\text{ZORA}} - \delta_{\text{NR}}$, ^d Δ_{expt} : the deviation of calculated $\delta^{29}\text{Si}$ from experimental values is calculated as $\delta_{\text{ZORA}} - \delta_{\text{expt}}$.

Table 7.5.10. ^{29}Si NMR chemical shifts calculated for several exchange-correlation functionals employing the TZ2P basis set. Values are given in ppm.

	δ_{expt}	SiMe_3Cl 30.7	SiMe_2Cl_2 32.0	SiMeCl_3 12.7	SiCl_4 -18.5
XC functional	δ_{expt}				
	$\delta_{\text{NR}}^{\text{a}}$	29.4	36.4	23.5	0.9
	$\delta_{\text{ZORA}}^{\text{b}}$	27.6	30.6	11.9	-18.8
	$\delta_{\text{SO corr}}^{\text{c}}$	-1.8	-5.8	-11.6	-19.7
mPW1K	$\Delta_{\text{expt}}^{\text{d}}$	-3.1	-1.4	-0.8	-0.3
	$\delta_{\text{NR}}^{\text{a}}$	31.0	38.4	25.1	1.2
	$\delta_{\text{ZORA}}^{\text{b}}$	28.9	32.3	13.0	-19.5
	$\delta_{\text{SO corr}}^{\text{c}}$	-2.1	-6.1	-12.1	-20.7
B1PW91	$\Delta_{\text{expt}}^{\text{d}}$	-1.8	0.3	0.3	-1.0
	$\delta_{\text{NR}}^{\text{a}}$	31.1	38.5	25.2	1.4
	$\delta_{\text{ZORA}}^{\text{b}}$	29.0	32.5	13.2	-19.2
	$\delta_{\text{SO corr}}^{\text{c}}$	-2.1	-6.0	-12.0	-20.6
PBE0	$\Delta_{\text{expt}}^{\text{d}}$	-1.7	0.5	0.5	-0.7
	$\delta_{\text{NR}}^{\text{a}}$	31.0	38.2	20.4	0.6
	$\delta_{\text{ZORA}}^{\text{b}}$	28.8	31.7	11.8	-21.7
	$\delta_{\text{SO corr}}^{\text{c}}$	-2.2	-6.5	-8.6	-22.3
B3LYP	$\Delta_{\text{expt}}^{\text{d}}$	-1.9	-0.3	-0.9	-3.2
	$\delta_{\text{NR}}^{\text{a}}$	31.0	43.0	28.4	1.8
	$\delta_{\text{ZORA}}^{\text{b}}$	32.3	35.8	14.8	-21.2
	$\delta_{\text{SO corr}}^{\text{c}}$	-2.9	-7.2	-13.6	-23.0
PBE	$\Delta_{\text{expt}}^{\text{d}}$	1.6	3.8	2.1	-2.7
	$\delta_{\text{NR}}^{\text{a}}$	35.2	39.9	25.6	-0.7
	$\delta_{\text{ZORA}}^{\text{b}}$	32.3	33.4	13.9	-20.4
	$\delta_{\text{SO corr}}^{\text{c}}$	-2.9	-6.5	-11.7	-19.7
OPBE	$\Delta_{\text{expt}}^{\text{d}}$	0.4	1.4	1.2	-1.9
	$\delta_{\text{NR}}^{\text{a}}$	33.8	40.5	25.5	-0.8
	$\delta_{\text{ZORA}}^{\text{b}}$	31.1	34.1	13.6	-20.9
	$\delta_{\text{SO corr}}^{\text{c}}$	-2.7	-6.4	-11.9	-20.1
OP86	$\Delta_{\text{expt}}^{\text{d}}$	0.5	2.1	0.9	-2.4

^a δ_{NR} : non-relativistic $\delta^{29}\text{Si}$ vs. TMS, ^b δ_{ZORA} : $\delta^{29}\text{Si}$ including relativistic spin-orbit effects using the ZORA formalism, ^c $\delta_{\text{SO corr}}$: the spin-orbit correction is calculated as $\delta_{\text{ZORA}} - \delta_{\text{NR}}$, ^d Δ_{expt} : the deviation of calculated $\delta^{29}\text{Si}$ from experimental values is calculated as $\delta_{\text{ZORA}} - \delta_{\text{expt}}$.

Table 7.5.11. ^{29}Si NMR chemical shifts calculated for several exchange-correlation functionals employing the QZ4P basis set. Values are given in ppm.

	δ_{expt}	SiMe_3Cl 30.7	SiMe_2Cl_2 32.0	SiMeCl_3 12.7	SiCl_4 -18.5
XC functional	δ_{expt}				
	$\delta_{\text{NR}}^{\text{a}}$	33.2	40.8	28.2	7.1
	$\delta_{\text{ZORA}}^{\text{b}}$	31.4	35.6	16.5	-13.8
	$\delta_{\text{SO corr}}^{\text{c}}$	-1.8	-5.2	-11.7	-20.9
mPW1K	$\Delta_{\text{expt}}^{\text{d}}$	0.7	3.6	3.8	4.7

B1PW91	$\delta_{\text{NR}}^{\text{a}}$	34.3	42.4	29.3	6.6
	$\delta_{\text{ZORA}}^{\text{b}}$	32.4	37.0	17.2	-15.1
	$\text{SO}_{\text{corr}}^{\text{c}}$	-1.9	-5.4	-12.1	-21.7
	$\Delta_{\text{expt}}^{\text{d}}$	1.7	5.0	4.5	3.4
PBE0	$\delta_{\text{NR}}^{\text{a}}$	34.6	42.8	29.8	7.0
	$\delta_{\text{ZORA}}^{\text{b}}$	32.6	37.3	17.6	-14.8
	$\text{SO}_{\text{corr}}^{\text{c}}$	-2.0	-5.5	-12.2	-21.8
	$\Delta_{\text{expt}}^{\text{d}}$	1.9	5.3	4.9	3.7
B3LYP	$\delta_{\text{NR}}^{\text{a}}$	33.4	40.8	27.9	5.4
	$\delta_{\text{ZORA}}^{\text{b}}$	31.4	35.0	14.9	-18.1
	$\text{SO}_{\text{corr}}^{\text{c}}$	-2.0	-5.8	-13.0	-23.5
	$\Delta_{\text{expt}}^{\text{d}}$	0.7	3.0	2.2	0.4
PBE	$\delta_{\text{NR}}^{\text{a}}$	35.4	43.7	29.8	3.8
	$\delta_{\text{ZORA}}^{\text{b}}$	33.2	37.5	16.9	-19.2
	$\text{SO}_{\text{corr}}^{\text{c}}$	-2.2	-6.2	-12.9	-23.0
	$\Delta_{\text{expt}}^{\text{d}}$	2.5	5.5	4.2	-0.7
OPBE	$\delta_{\text{NR}}^{\text{a}}$	32.0	38.7	24.9	0.1
	$\delta_{\text{ZORA}}^{\text{b}}$	30.2	33.4	14.0	-19.1
	$\text{SO}_{\text{corr}}^{\text{c}}$	-1.8	-5.3	-10.9	-19.2
	$\Delta_{\text{expt}}^{\text{d}}$	-0.5	1.4	1.3	-0.6
OP86	$\delta_{\text{NR}}^{\text{a}}$	32.1	38.8	24.9	-0.1
	$\delta_{\text{ZORA}}^{\text{b}}$	30.3	33.5	13.8	-19.7
	$\text{SO}_{\text{corr}}^{\text{c}}$	-1.8	-5.3	-11.1	-19.6
	$\Delta_{\text{expt}}^{\text{d}}$	-0.4	1.5	1.1	-1.2

^a δ_{NR} : non-relativistic $\delta^{29}\text{Si}$ vs. TMS, ^b δ_{ZORA} : $\delta^{29}\text{Si}$ including relativistic spin-orbit effects using the ZORA formalism, ^c SO_{corr} : the spin-orbit correction is calculated as $\delta_{\text{ZORA}} - \delta_{\text{NR}}$, ^d Δ_{expt} : the deviation of calculated $\delta^{29}\text{Si}$ from experimental values is calculated as $\delta_{\text{ZORA}} - \delta_{\text{expt}}$.

Table 7.5.12. ^{29}Si NMR isotropic shielding constants calculated for several exchange-correlation functionals employing the DZP basis set. Values are given in ppm.

XC functional		SiMe_3Cl	SiMe_2Cl_2	SiMeCl_3	SiCl_4	TMS
mPW1K	$\sigma_{\text{NR}}^{\text{a}}$	319.6	315.8	331.3	357.0	348.5
	$\sigma_{\text{ZORA}}^{\text{b}}$	332.0	331.8	353.6	388.4	357.6
B1PW91	$\sigma_{\text{NR}}^{\text{a}}$	307.9	303.5	319.7	347.0	338.3
	$\sigma_{\text{ZORA}}^{\text{b}}$	319.7	319.5	342.2	379.0	347.2
PBE0	$\sigma_{\text{NR}}^{\text{a}}$	308.8	304.2	320.2	347.3	339.5
	$\sigma_{\text{ZORA}}^{\text{b}}$	320.6	320.2	342.7	379.3	348.5
B3LYP	$\sigma_{\text{NR}}^{\text{a}}$	294.4	290.2	306.6	334.0	324.4
	$\sigma_{\text{ZORA}}^{\text{b}}$	306.3	306.6	329.9	367.7	333.4
PBE	$\sigma_{\text{NR}}^{\text{a}}$	291.3	286.1	303.8	334.1	323.9
	$\sigma_{\text{ZORA}}^{\text{b}}$	303.0	302.3	326.9	367.6	332.8
OPBE	$\sigma_{\text{NR}}^{\text{a}}$	322.3	317.8	335.3	365.1	353.0
	$\sigma_{\text{ZORA}}^{\text{b}}$	333.6	333.0	356.4	395.0	361.8
OP86	$\sigma_{\text{NR}}^{\text{a}}$	319.9	315.5	333.1	362.9	350.6
	$\sigma_{\text{ZORA}}^{\text{b}}$	331.3	330.8	354.4	393.2	359.4

^a σ_{NR} : non-relativistic $\sigma^{29}\text{Si}$, ^b σ_{ZORA} : $\sigma^{29}\text{Si}$ including relativistic spin-orbit effects using the ZORA formalism.

Table 7.5.13. ^{29}Si NMR isotropic shielding constants calculated for several exchange-correlation functionals employing the TZ2P basis set. Values are given in ppm.

XC functional		SiMe_3Cl	SiMe_2Cl_2	SiMeCl_3	SiCl_4	TMS
mPW1K	$\sigma_{\text{NR}}^{\text{a}}$	339.3	332.3	345.2	367.8	368.7
	$\sigma_{\text{ZORA}}^{\text{b}}$	349.8	346.8	365.5	396.2	377.4
B1PW91	$\sigma_{\text{NR}}^{\text{a}}$	325.5	318.1	331.4	355.3	356.5
	$\sigma_{\text{ZORA}}^{\text{b}}$	336.0	332.6	351.9	384.4	364.9
PBE0	$\sigma_{\text{NR}}^{\text{a}}$	325.9	318.5	331.8	355.6	357
	$\sigma_{\text{ZORA}}^{\text{b}}$	336.5	333.0	352.3	384.7	365.5
B3LYP	$\sigma_{\text{NR}}^{\text{a}}$	308.4	301.2	319.0	338.8	339.4
	$\sigma_{\text{ZORA}}^{\text{b}}$	319.0	316.1	336.0	369.5	347.8
PBE	$\sigma_{\text{NR}}^{\text{a}}$	304.9	297.1	311.7	338.3	340.1
	$\sigma_{\text{ZORA}}^{\text{b}}$	315.3	311.8	332.8	368.8	347.6

OPBE	$\sigma_{\text{NR}}^{\text{a}}$	343.8	337.7	352.0	378.3	377.6
	$\sigma_{\text{ZORA}}^{\text{b}}$	353.9	351.6	371.1	405.4	385.0
OP86	$\sigma_{\text{NR}}^{\text{a}}$	340.8	334.2	349.2	375.5	374.7
	$\sigma_{\text{ZORA}}^{\text{b}}$	350.9	348.0	368.5	403.0	382.1

^a σ_{NR} : non-relativistic $\sigma^{29}\text{Si}$, ^b σ_{ZORA} : $\sigma^{29}\text{Si}$ including relativistic spin-orbit effects using the ZORA formalism.

Table 7.5.14. ^{29}Si NMR isotropic shielding constants calculated for several exchange-correlation functionals employing the QZ4P basis set. Values are given in ppm.

XC functional		SiMe_3Cl	SiMe_2Cl_2	SiMeCl_3	SiCl_4	TMS
mPW1K	$\sigma_{\text{NR}}^{\text{a}}$	320.9	313.3	325.9	347.0	354.1
	$\sigma_{\text{ZORA}}^{\text{b}}$	330.3	326.1	345.2	375.5	361.7
B1PW91	$\sigma_{\text{NR}}^{\text{a}}$	308.2	300.1	313.2	335.9	342.5
	$\sigma_{\text{ZORA}}^{\text{b}}$	317.6	313.0	332.8	365.1	350.0
PBE0	$\sigma_{\text{NR}}^{\text{a}}$	308.1	299.9	312.9	335.7	342.7
	$\sigma_{\text{ZORA}}^{\text{b}}$	317.5	312.8	332.5	364.9	350.1
B3LYP	$\sigma_{\text{NR}}^{\text{a}}$	292.4	285.0	297.9	320.4	325.8
	$\sigma_{\text{ZORA}}^{\text{b}}$	301.9	298.3	318.4	351.4	333.3
PBE	$\sigma_{\text{NR}}^{\text{a}}$	289.7	281.4	295.3	321.3	325.1
	$\sigma_{\text{ZORA}}^{\text{b}}$	299.9	295.6	316.2	352.3	333.1
OPBE	$\sigma_{\text{NR}}^{\text{a}}$	324.7	318.0	331.8	356.6	356.7
	$\sigma_{\text{ZORA}}^{\text{b}}$	334.4	331.2	350.6	383.7	364.6
OP86	$\sigma_{\text{NR}}^{\text{a}}$	321.5	314.8	328.7	353.7	353.6
	$\sigma_{\text{ZORA}}^{\text{b}}$	331.3	328.1	347.8	381.3	361.6

^a σ_{NR} : non-relativistic $\sigma^{29}\text{Si}$, ^b σ_{ZORA} : $\sigma^{29}\text{Si}$ including relativistic spin-orbit effects using the ZORA formalism

We also note that during the course of this work it has been found that the variance of geometry optimization (with standard options) in the Gaussian 09 program package can lead to deviations of ^{29}Si NMR shielding constants of up to 0.2 ppm. This is due to the higher geometry sensitivity of NMR parameters compared to the total energy.

Tables of ^{29}Si Shielding Number

When more than a single conformer merits consideration, chemical shifts are reported as an average over a Boltzmann-weighted population of conformers according to Boltzmann average: The NMR calculation for species at MPW1K/IGLO-III//MPW1K/6-31+G(d) level in gas phase and solution phase:

$$f_i = e^{\frac{G_{\min} - G_i}{kT}}$$

f : Boltzmann factor

$$k = 8.314 \text{ } JK^{-1} \text{ } mol^{-1}$$

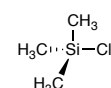
$$T = 298.15 \text{ } K$$

$$\delta^{29}\text{Si}_{\text{boltz}} = \sum \frac{f_i}{\sum f_i} \delta^{29}\text{Si}_i$$

$\delta^{29}\text{Si}_i$: chemical shift of individual conformer

$\delta^{29}\text{Si}_{\text{boltz}}$: Boltzmann averaged chemical shift

The following table is the detail of species in Table 5.5



MPW1K/IGLO-III//MPW1K/6-31+G(d)

2	δ^{gas}
Gas	31.92

PCM/UAHF/MPW1K/IGLO-III//MPW1K/6-31+G(d)

2	$\delta^{\text{sp}}_{\text{CDCl}_3}$
sp	34.00

PCM/UAHF/MPW1K/IGLO-III// PCM/UAHF/MPW1K/6-31+G(d)

2	$\delta^{\text{opt}}_{\text{CDCl}_3}$
Opt	37.00

DF-LMP2/IGLO-III//MPW1K/6-31+G(d)

2	δ^{gas}
Gas	28.41

HCTH407/IGLO-III//MPW1K/6-31+G(d)

2	δ^{gas}
Gas	31.40



MPW1K/IGLO-III//MPW1K/6-31+G(d)

3	δ^{gas}
Gas	2.49

PCM/UAHF/MPW1K/IGLO-III// MPW1K/6-31+G(d)

3	$\delta^{\text{sp}}_{\text{CDCl}_3}$
sp	2.55

PCM/UAHF/MPW1K/IGLO-III// PCM/UAHF/MPW1K/6-31+G(d)

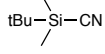
3	$\delta^{\text{opt}}_{\text{CDCl}_3}$
Opt	2.47

DF-LMP2/IGLO-III//MPW1K/6-31+G(d)

3	δ^{gas}
Gas	-0.74

HCTH407/IGLO-III//MPW1K/6-31+G(d)

3	δ^{gas}
Gas	-5.77



MPW1K/IGLO-III//MPW1K/6-31+G(d)

4	NMR
Gas	-5.39

PCM/UAHF/MPW1K/IGLO-III// MPW1K/6-31+G(d)

4	NMR
sp	-3.21

PCM/UAHF/MPW1K/IGLO-III// PCM/UAHF/MPW1K/6-31+G(d)

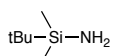
4	NMR
Opt	-1.35

DF-LMP2/IGLO-III//MPW1K/6-31+G(d)

4	NMR
Gas	-5.00

HCTH407/IGLO-III//MPW1K/6-31+G(d)

4	NMR
Gas	-10.26



MPW1K/IGLO-III//MPW1K/6-31+G(d)

5	δ^{gas}
Gas	8.97

PCM/UAHF/MPW1K/IGLO-III// MPW1K/6-31+G(d)

5	δ^{gas}
sp	8.58

PCM/UAHF/MPW1K/IGLO-III// PCM/UAHF/MPW1K/6-31+G(d)

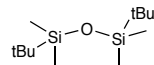
5	δ^{gas}
Opt	10.81

DF-LMP2/IGLO-III//MPW1K/6-31+G(d)

5		δ^{gas}
Gas	sicn 01	8.92

HCTH407/IGLO-III//MPW1K/6-31+G(d)

5		δ^{gas}
Gas	sicn 01	6.47



MPW1K/IGLO-III//MPW1K/6-31+G(d)

gas	ΔG_{gas} kJ/mol	NMR MPW1K/IGLO-III in gas phase	Boltzmann weighted factor	δ^{gas}
6_1	1.36	11.83	0.37	4.34
6_2	0.00	11.45	0.63	7.25
SUM			1.00	11.59

PCM/UAHF/MPW1K/IGLO-III//MPW1K/6-31+G(d)

sp	$\Delta G^{\text{sp}}_{\text{CDCl}_3}$ kJ/mol	NMR UAHF-MPW1K/IGLO-III	Boltzmann weighted factor	$\delta^{\text{sp}}_{\text{CDCl}_3}$
6_1	0.77	12.29	0.42	5.20
6_2	0.00	11.81	0.58	6.81
SUM			1.00	12.01

PCM/UAHF/MPW1K/IGLO-III// PCM/UAHF/MPW1K/6-31+G(d)

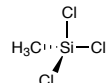
opt	$\Delta G^{\text{opt}}_{\text{CDCl}_3}$ kJ/mol	NMR UAHF-MPW1K/IGLO-III	Boltzmann weighted factor	$\delta^{\text{opt}}_{\text{CDCl}_3}$
6_1	0.00	13.22	0.52	6.85
6_2	0.18	13.97	0.48	6.73
SUM			1.00	13.58

DF-LMP2/IGLO-III//MPW1K/6-31+G(d)

gas	ΔG_{gas} kJ/mol	NMR DF-LMP2/IGLO-III in gas phase	Boltzmann weighted factor	δ^{gas}
6_1	0.37	11.85	0.37	4.34
6_2	0.63	10.99	0.63	6.96
SUM			1.00	11.31

HCTH407/IGLO-III//MPW1K/6-31+G(d)

gas	ΔG_{gas} kJ/mol	NMR HCTH407/IGLO-III in gas phase	Boltzmann weighted factor	δ^{gas}
6_1	1.36	7.67	0.37	2.81
6_2	0.00	6.57	0.63	4.16
SUM			1.00	6.97



MPW1K/IGLO-III//MPW1K/6-31+G(d)

7	δ^{gas}
Gas	26.04

PCM/UAHF/MPW1K/IGLO-III//MPW1K/6-31+G(d)

7	$\delta^{\text{sp}}_{\text{CDCl}_3}$
sp	27.30

PCM/UAHF/MPW1K/IGLO-III// PCM/UAHF/MPW1K/6-31+G(d)

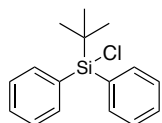
7	$\delta^{\text{opt}}_{\text{CDCl}_3}$
Opt	28.53

DF-MP2/IGLO-III//MPW1K/6-31+G(d)

7	δ^{gas}
Gas	23.51

HCTH407/IGLO-III//MPW1K/6-31+G(d)

7	δ^{gas}
Gas	22.10



MPW1K/IGLO-III//MPW1K/6-31+G(d)

8	δ^{gas}
Gas	16.12

PCM/UAHF/MPW1K/IGLO-III//MPW1K/6-31+G(d)

8	$\delta^{\text{sp}}_{\text{CDCl}_3}$
sp	16.43

PCM/UAHF/MPW1K/IGLO-III// PCM/UAHF/MPW1K/6-31+G(d)

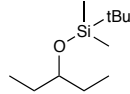
8	$\delta^{\text{opt}}_{\text{CDCl}_3}$
Opt	16.92

DF-MP2/IGLO-III//MPW1K/6-31+G(d)

8	δ^{gas}
Gas	15.45

HCTH407/IGLO-III//MPW1K/6-31+G(d)

8	δ^{gas}
Gas	13.96



MPW1K/IGLO-III//MPW1K/6-31+G(d)

gas	ΔG_{gas} kJ/mol	NMR MPW1K/IGLO-III in gas phase	Boltzmann weighted factor	δ^{gas}
9_1	0.00	16.99	0.41	6.94
9_2	2.36	17.21	0.16	2.72
9_3	2.53	17.41	0.15	2.56
9_4	4.26	16.62	0.07	1.22
9_5	5.57	16.52	0.04	0.71
9_6	5.66	16.52	0.04	0.69
9_7	6.07	17.53	0.04	0.62
9_8	6.09	17.58	0.03	0.61
9_9	7.01	17.02	0.02	0.41
9_10	8.15	17.36	0.02	0.26
9_11	8.39	16.90	0.01	0.23
9_12	11.37	17.74	0.00	0.07
9_13	14.70	17.16	0.00	0.02
SUM			1.00	17.07

PCM/UAHF/MPW1K/IGLO-III//MPW1K/6-31+G(d)

sp	$\Delta G^{\text{sp}}_{\text{CDCl}_3}$ kJ/mol	NMR UAHF-MPW1K/IGLO-III	Boltzmann weighted factor	$\delta^{\text{sp}}_{\text{CDCl}_3}$
9_1	0.00	17.50	0.44	7.73
9_2	3.20	17.57	0.12	2.14
9_3	2.57	17.92	0.16	2.81
9_4	4.64	17.26	0.07	1.17
9_5	5.95	16.88	0.04	0.68
9_6	6.34	17.03	0.03	0.58
9_7	6.57	18.19	0.03	0.57
9_8	6.55	18.24	0.03	0.57
9_9	6.63	17.73	0.03	0.54
9_10	7.82	18.05	0.02	0.34
9_11	7.63	17.54	0.02	0.36
9_12	12.59	18.06	0.00	0.05
9_13	13.19	18.03	0.00	0.04
SUM			1.00	17.58

PCM/UAHF/MPW1K/IGLO-III// PCM/UAHF/MPW1K/6-31+G(d)

opt	$\Delta G^{\text{opt}}_{\text{CDCl}_3}$ kJ/mol	NMR UAHF-MPW1K/IGLO-III	Boltzmann weighted factor	$\delta^{\text{opt}}_{\text{CDCl}_3}$
9_1	0.00	18.71	0.37	6.86
9_2	2.66	18.85	0.13	2.36

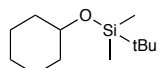
9_3	1.51	19.17	0.20	3.83
9_4	4.13	18.47	0.07	1.28
9_5	6.39	18.04	0.03	0.50
9_6	6.88	17.92	0.02	0.41
9_7	5.21	19.37	0.04	0.87
9_8	5.20	19.38	0.05	0.87
9_9	5.07	19.14	0.05	0.91
9_10	8.08	19.30	0.01	0.27
9_11	7.51	18.94	0.02	0.34
9_12	7.51	18.70	0.02	0.33
9_13	14.01	19.38	0.00	0.02
SUM			1.00	18.86

DF-LMP2/IGLO-III//MPW1K/6-31+G(d)

gas	ΔG_{gas} kJ/mol	NMR DF-LMP2/IGLO-III in gas phase	Boltzmann weighted factor	δ^{gas}
9_1	0.00	16.67	0.41	6.81
9_2	2.36	16.88	0.16	2.67
9_3	2.53	16.86	0.15	2.48
9_4	4.26	16.45	0.07	1.20
9_5	5.57	16.21	0.04	0.70
9_6	5.66	16.15	0.04	0.67
9_7	6.07	17.03	0.04	0.60
9_8	6.09	17.07	0.03	0.60
9_9	7.01	16.49	0.02	0.40
9_10	8.15	17.02	0.02	0.26
9_11	8.39	16.48	0.01	0.23
9_12	11.37	17.33	0.00	0.07
9_13	14.70	16.65	0.00	0.02
SUM			1.00	16.70

HCTH407/IGLO-III//MPW1K/6-31+G(d)

gas	ΔG_{gas} kJ/mol	NMR HCTH407/IGLO-III in gas phase	Boltzmann weighted factor	δ^{gas}
9_1	0.00	12.88	0.41	5.26
9_2	2.36	13.21	0.16	2.09
9_3	2.53	13.48	0.15	1.99
9_4	4.26	12.38	0.07	0.90
9_5	5.57	12.58	0.04	0.54
9_6	5.66	12.57	0.04	0.52
9_7	6.07	13.56	0.04	0.48
9_8	6.09	13.60	0.03	0.48
9_9	7.01	12.87	0.02	0.31
9_10	8.15	13.12	0.02	0.20
9_11	8.39	12.82	0.01	0.18
9_12	11.37	13.71	0.00	0.06
9_13	14.70	13.19	0.00	0.01
SUM			1.00	13.01



MPW1K/IGLO-III//MPW1K/6-31+G(d)

gas	ΔG_{gas} kJ/mol	NMR MPW1K/IGLO-III in gas phase	Boltzmann weighted factor	δ^{gas}
10_1	0.00	17.45	0.80	13.92
10_2	3.40	17.20	0.20	3.48
SUM			1.00	17.40

PCM/UAHF/MPW1K/IGLO-III//MPW1K/6-31+G(d)

sp	$\Delta G^{\text{sp}}_{\text{CDCl}_3}$ kJ/mol	NMR UAHF-MPW1K/IGLO-III	Boltzmann weighted factor	$\delta^{\text{sp}}_{\text{CDCl}_3}$
10_1	0.00	18.09	0.76	13.75
10_2	2.86	18.05	0.24	4.33
SUM			1.00	18.08

PCM/UAHF/MPW1K/IGLO-III//PCM/UAHF/MPW1K/6-31+G(d)

opt	$\Delta G^{\text{opt}}_{\text{CDCl}_3}$ kJ/mol	NMR UAHF-MPW1K/IGLO-III	Boltzmann weighted factor	$\delta^{\text{opt}}_{\text{CDCl}_3}$
10_1	0.00	19.33	0.93	18.03
10_2	6.52	19.02	0.07	1.28
SUM			1.00	19.31

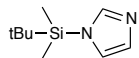
DF-LMP2/IGLO-III//MPW1K/6-31+G(d)

gas	ΔG_{gas} kJ/mol	NMR DF-LMP2/IGLO-III in gas phase	Boltzmann weighted factor	δ^{gas}
-----	--------------------------------	-----------------------------------	---------------------------	-----------------------

10_1	0.00	16.91	0.80	13.49
10_2	3.40	16.81	0.20	3.40
SUM			1.00	16.89

HCTH407/IGLO-III//MPW1K/6-31+G(d)

gas	ΔG_{gas} kJ/mol	NMR HCTH407/IGLO-III in gas phase	Boltzmann weighted factor	δ^{gas}
10_1	0.00	13.43	0.80	10.72
10_2	3.40	13.02	0.20	2.63
SUM			1.00	13.35



MPW1K/IGLO-III//MPW1K/6-31+G(d)

11	NMR
Gas	16.41

PCM/UAHF/MPW1K/IGLO-III//MPW1K/6-31+G(d)

11	NMR
sp	17.53

PCM/UAHF/MPW1K/IGLO-III// PCM/UAHF/MPW1K/6-31+G(d)

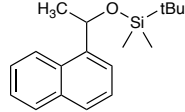
11	NMR
Opt	19.46

DF-LMP2/IGLO-III//MPW1K/6-31+G(d)

11	δ^{gas}
Gas	16.47

HCTH407/IGLO-III//MPW1K/6-31+G(d)

11	δ^{gas}
Gas	13.51



MPW1K/IGLO-III//MPW1K/6-31+G(d)

gas	ΔG_{gas} kJ/mol	NMR MPW1K/IGLO-III in gas phase	Boltzmann weighted factor	δ^{gas}
12_1	0.00	21.83	0.31	6.73
12_2	0.07	20.71	0.30	6.20
12_3	0.41	20.70	0.26	5.41
12_4	4.79	20.98	0.04	0.94
12_5	5.13	20.61	0.04	0.80
12_6	5.78	22.04	0.03	0.66
12_7	7.68	21.43	0.01	0.30
12_8	12.48	17.19	0.00	0.03
12_9	14.86	16.43	0.00	0.01
12_10	16.88	16.09	0.00	0.01
SUM			1.00	21.10

PCM/UAHF/MPW1K/IGLO-III//MPW1K/6-31+G(d)

sp	$\Delta G^{\text{sp}}_{\text{CDCl}_3}$ kJ/mol	NMR UAHF-MPW1K/IGLO-III	Boltzmann weighted factor	$\delta^{\text{sp}}_{\text{CDCl}_3}$
12_1	0.00	22.27	0.33	7.24
12_2	0.03	20.94	0.32	6.72
12_3	0.37	20.93	0.28	5.86
12_4	7.48	21.11	0.02	0.34
12_5	5.59	21.12	0.03	0.72
12_6	7.80	22.29	0.01	0.31
12_7	10.16	21.79	0.01	0.12
12_8	11.01	17.84	0.00	0.07
12_9	16.20	16.84	0.00	0.01
12_10	18.90	16.24	0.00	0.00
SUM			1.00	21.38

PCM/UAHF/MPW1K/IGLO-III// PCM/UAHF/MPW1K/6-31+G(d)

opt	$\Delta G^{\text{opt}}_{\text{CDCl}_3}$ kJ/mol	NMR UAHF-MPW1K/IGLO-III	Boltzmann weighted factor	$\delta^{\text{opt}}_{\text{CDCl}_3}$
12_1	22.44	4.59	0.07	1.50
12_2	21.64	0.01	0.42	9.15
12_3	21.64	0.00	0.42	9.18

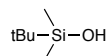
12_4	21.70	7.61	0.02	0.43
12_5	22.07	5.93	0.04	0.85
12_6	22.31	8.08	0.02	0.36
12_7	22.21	10.49	0.01	0.14
12_8	19.17	12.41	0.00	0.05
12_9	17.28	13.26	0.00	0.03
12_10	16.64	16.65	0.00	0.01
SUM			1.00	21.71

DF-LMP2/IGLO-III//MPW1K/6-31+G(d)

Gas	ΔG_{gas} kJ/mol	NMR DF-LMP2/IGLO-III in gas phase	Boltzmann weighted factor	δ^{gas}
12_1	0.00	20.77	0.31	6.41
12_2	0.07	19.92	0.30	5.96
12_3	0.41	19.92	0.26	5.21
12_4	4.79	20.43	0.04	0.91
12_5	5.13	19.69	0.04	0.77
12_6	5.78	20.91	0.03	0.63
12_7	7.68	20.34	0.01	0.28
12_8	12.48	16.20	0.00	0.03
12_9	14.86	15.58	0.00	0.01
12_10	16.88	15.57	0.00	0.01
SUM			1.00	20.22

HCTH407/IGLO-III//MPW1K/6-31+G(d)

Gas	ΔG_{gas} kJ/mol	NMR HCTH407/IGLO-III in gas phase	Boltzmann weighted factor	δ^{gas}
12_1	0.00	17.88	0.31	5.51
12_2	0.07	16.83	0.30	5.04
12_3	0.41	16.81	0.26	4.40
12_4	4.79	17.17	0.04	0.77
12_5	5.13	16.28	0.04	0.63
12_6	5.78	18.27	0.03	0.55
12_7	7.68	17.07	0.01	0.24
12_8	12.48	13.83	0.00	0.03
12_9	14.86	13.79	0.00	0.01
12_10	16.88	13.10	0.00	0.00
SUM			1.00	17.18



MPW1K/IGLO-III//MPW1K/6-31+G(d)

13	δ^{gas}
Gas	19.48

PCM/UAHF/MPW1K/IGLO-III//MPW1K/6-31+G(d)

13	$\delta^{\text{sp}}_{\text{CDCl}_3}$
sp	19.49

PCM/UAHF/MPW1K/IGLO-III//PCM/UAHF/MPW1K/6-31+G(d)

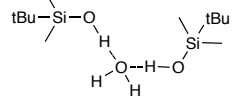
13	$\delta^{\text{opt}}_{\text{CDCl}_3}$
Opt	20.50

DF-LMP2/IGLO-III//MPW1K/6-31+G(d)

13	δ^{gas}
Gas	18.56

HCTH407/IGLO-III//MPW1K/6-31+G(d)

13	δ^{gas}
Gas	16.49



MPW1K/IGLO-III//MPW1K/6-31+G(d)

14	δ^{gas}
Gas	17.69

PCM/UAHF/MPW1K/IGLO-III//MPW1K/6-31+G(d)

14	$\delta^{\text{sp}}_{\text{CDCl}_3}$
14	17.69

sp	18.44
----	-------

PCM/UAHF/MPW1K/IGLO-III// PCM/UAHF/MPW1K/6-31+G(d)

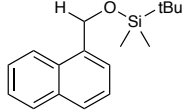
14	$\delta^{\text{opt}}_{\text{CDCl}_3}$
Opt	19.30

DF-LMP2/IGLO-III//MPW1K/6-31+G(d)

14	δ^{gas}
Gas	17.19

HCTH407/IGLO-III//MPW1K/6-31+G(d)

14	δ^{gas}
Gas	14.02



MPW1K/IGLO-III//MPW1K/6-31+G(d)

gas	ΔG_{gas} kJ/mol	NMR MPW1K/IGLO-III in gas phase	Boltzmann weighted factor	δ^{gas}
15_1	0.00	20.87	0.59	δ^{gas}
15_2	4.61	22.27	0.09	2.05
15_3	5.15	22.36	0.07	1.65
15_4	5.53	22.98	0.06	1.46
15_5	6.00	22.97	0.05	1.20
15_6	6.35	21.73	0.05	0.99
15_7	7.10	20.89	0.03	0.70
15_8	7.71	21.90	0.03	0.58
15_9	8.83	23.44	0.02	0.39
15_10	12.06	19.82	0.00	0.09
15_11	14.04	23.00	0.00	0.05
SUM			1.00	21.46

PCM/UAHF/MPW1K/IGLO-III//MPW1K/6-31+G(d)

sp	$\Delta G^{\text{sp}}_{\text{CDCl}_3}$ kJ/mol	NMR UAHF-MPW1K/IGLO-III	Boltzmann weighted factor	$\delta^{\text{sp}}_{\text{CDCl}_3}$
15_1	0.00	21.30	0.68	14.56
15_2	5.87	22.58	0.06	1.45
15_3	5.07	22.96	0.09	2.03
15_4	7.13	23.46	0.04	0.91
15_5	7.60	23.46	0.03	0.75
15_6	8.58	22.02	0.02	0.47
15_7	8.61	21.16	0.02	0.45
15_8	7.75	22.49	0.03	0.67
15_9	10.60	24.01	0.01	0.23
15_10	10.47	20.53	0.01	0.21
15_11	15.67	23.48	0.00	0.03
SUM			1.00	21.75

PCM/UAHF/MPW1K/IGLO-III// PCM/UAHF/MPW1K/6-31+G(d)

opt	$\Delta G^{\text{opt}}_{\text{CDCl}_3}$ kJ/mol	NMR UAHF-MPW1K/IGLO-III	Boltzmann weighted factor	$\delta^{\text{opt}}_{\text{CDCl}_3}$
15_1	0.00	22.28	0.68	15.23
15_2	9.65	23.29	0.01	0.32
15_3	7.02	24.02	0.04	0.97
15_4	11.69	24.00	0.01	0.15
15_5	11.69	24.00	0.01	0.15
15_6	8.61	22.49	0.02	0.48
15_7	9.64	23.29	0.01	0.33
15_8	6.70	23.26	0.05	1.06
15_9	9.64	23.29	0.01	0.33
15_10	11.27	22.16	0.01	0.16
15_11	11.68	24.01	0.01	0.15
SUM			0.86	19.31

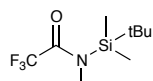
DF-LMP2/IGLO-III//MPW1K/6-31+G(d)

gas	ΔG_{gas} kJ/mol	NMR DF-LMP2/IGLO-III in gas phase	Boltzmann weighted factor	δ^{gas}
15_1	0.00	20.60	0.59	12.15
15_2	4.61	21.02	0.09	1.93
15_3	5.15	21.46	0.07	1.58
15_4	5.53	22.24	0.06	1.41
15_5	6.00	22.24	0.05	1.17
15_6	6.35	20.54	0.05	0.93

15_7	7.10	20.59	0.03	0.69
15_8	7.71	21.47	0.03	0.56
15_9	8.83	22.72	0.02	0.38
15_10	12.06	19.24	0.00	0.09
15_11	14.04	22.27	0.00	0.05
SUM			1.00	20.94

HCTH407/IGLO-III//MPW1K/6-31+G(d)

gas	ΔG_{gas} kJ/mol	NMR HCTH407/IGLO-III in gas phase	Boltzmann weighted factor	δ^{gas}
15_1	0.00	16.71	0.59	9.86
15_2	4.61	19.07	0.09	1.75
15_3	5.15	18.44	0.07	1.36
15_4	5.53	19.02	0.06	1.21
15_5	6.00	19.00	0.05	1.00
15_6	6.35	18.45	0.05	0.84
15_7	7.10	16.96	0.03	0.57
15_8	7.71	17.49	0.03	0.46
15_9	8.83	19.41	0.02	0.32
15_10	12.06	15.49	0.00	0.07
15_11	14.04	19.06	0.00	0.04
SUM			1.00	17.48



MPW1K/IGLO-III//MPW1K/6-31+G(d)

	ΔG kJ/mol	NMR ppm	Boltzmann weighted factor	δ^{gas}
16_1	0.00	22.97	0.99	22.76
16_2	11.58	20.65	0.01	0.19
SUM			1.00	22.95

PCM/UAHF/MPW1K/IGLO-III//MPW1K/6-31+G(d)

sp	ΔG kJ/mol	NMR ppm	Boltzmann weighted factor	$\delta^{\text{sp}}_{\text{CDCl}_3}$
16_1	0.00	23.80	0.98	23.41
16_2	10.11	21.10	0.02	0.35
SUM		23.80	1.00	23.76

PCM/UAHF/MPW1K/IGLO-III// PCM/UAHF/MPW1K/6-31+G(d)

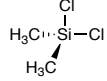
opt	ΔG kJ/mol	NMR ppm	Boltzmann weighted factor	$\delta^{\text{sp}}_{\text{CDCl}_3}$
16_1	0.00	24.66	0.98	24.25
16_2	10.53	21.74	0.01	0.31
SUM			1.00	24.56

DF-LMP2/IGLO-III//MPW1K/6-31+G(d)

Gas	ΔG kJ/mol	NMR ppm	Boltzmann weighted factor	δ^{gas}
16_1	0.00	23.08	0.99	22.86
16_2	11.58	21.01	0.01	0.19
SUM			1.00	23.06

HCTH407/IGLO-III//MPW1K/6-31+G(d)

Gas	ΔG kJ/mol	NMR ppm	Boltzmann weighted factor	δ^{gas}
16_1	0.00	20.52	0.99	20.33
16_2	11.58	18.48	0.01	0.17
SUM			1.00	20.50



MPW1K/IGLO-III//MPW1K/6-31+G(d)

17	δ^{gas}
Gas	38.81

PCM/UAHF/MPW1K/IGLO-III//MPW1K/6-31+G(d)

17	$\delta^{\text{sp}}_{\text{CDCl}_3}$
sp	41.13

PCM/UAHF/MPW1K/IGLO-III// PCM/UAHF/MPW1K/6-31+G(d)

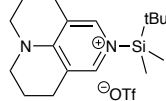
17	$\delta^{\text{opt}}_{\text{CDCl}_3}$
Opt	43.66

DF-LMP2/IGLO-III//MPW1K/6-31+G(d)

17	δ^{gas}
Gas	33.25

HCTH407/IGLO-III//MPW1K/6-31+G(d)

17	δ^{gas}
Gas	37.21



MPW1K/IGLO-III//MPW1K/6-31+G(d)

gas	ΔG_{gas} kJ/mol	NMR MPW1K/IGLO-III in gas phase	Boltzmann weighted factor	δ^{gas}
18_1	0.00	36.47	0.84	30.75
18_2	4.18	31.53	0.16	4.93
18_3	19.92	38.73	0.00	0.01
18_4	20.58	37.61	0.00	0.01
18_5	59.15	50.04	0.00	0.00
SUM			1.00	35.70

PCM/UAHF/MPW1K/IGLO-III//MPW1K/6-31+G(d)

sp	$\Delta G^{\text{sp}}_{\text{CDCl}_3}$ kJ/mol	NMR UAHF-MPW1K/IGLO-III	Boltzmann weighted factor	$\delta^{\text{sp}}_{\text{CDCl}_3}$
18_1	3.66	35.90	0.15	5.44
18_2	6.07	32.02	0.06	1.83
18_3	5.22	37.09	0.08	2.99
18_4	0.00	36.44	0.66	24.18
18_5	6.56	45.49	0.05	2.14
SUM			1.00	36.58

PCM/UAHF/MPW1K/IGLO-III// PCM/UAHF/MPW1K/6-31+G(d)

opt	$\Delta G^{\text{opt}}_{\text{CDCl}_3}$ kJ/mol	NMR UAHF-MPW1K/IGLO-III	Boltzmann weighted factor	$\delta^{\text{opt}}_{\text{CDCl}_3}$
18_1	0.00	35.10	0.60	21.00
18_2	2.71	33.29	0.20	6.68
18_3	5.45	36.08	0.07	2.40
18_4	3.85	35.48	0.13	4.49
18_5	10.75	38.23	0.01	0.30
SUM			1.00	34.87

DF-LMP2/IGLO-III//MPW1K/6-31+G(d)

gas	ΔG_{gas} kJ/mol	NMR DF-LMP2/IGLO-III in gas phase	Boltzmann weighted factor	δ^{gas}
18_1	0.00	35.57	0.84	29.99
18_2	4.18	31.22	0.16	4.88
18_3	19.92	38.87	0.00	0.01
18_4	20.58	37.35	0.00	0.01
18_5	59.15	50.06	0.00	0.00
SUM			1.00	34.89

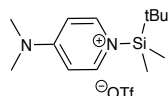
HCTH407/IGLO-III//MPW1K/6-31+G(d)

gas	ΔG_{gas} kJ/mol	NMR HCTH407/IGLO-III in gas phase	Boltzmann weighted factor	δ^{gas}
18_1	0.00	34.23	0.84	28.86
18_2	4.18	28.14	0.16	4.40
18_3	19.92	35.72	0.00	0.01
18_4	20.58	34.83	0.00	0.01
18_5	59.15	46.67	0.00	0.00
SUM			1.00	33.28

Parameters of individual conformers of 18

		18_1	18_2	18_3	18_4	18_5
MPW1K/6-31+G(d)	ΔG (kJ/mol)	0.00	4.18	19.92	20.58	59.15
	r(Si-N) (pm)	183.3	183.0	184.9	184.6	189.2
	q(OTf)	-0.96	-0.96	-0.94	-0.94	-0.95
	NMR (ppm)	36.47	31.53	38.73	37.61	50.04
MPW1K/6-31+G(d)+sp	ΔG (kJ/mol)	3.66	6.07	5.22	0.00	6.56
	r(Si-N) (pm)	183.3	183.0	184.9	184.6	189.2
	q(OTf)	-0.96	-0.96	-0.95	-0.95	-0.96
	NMR (ppm)	35.90	32.02	37.09	36.44	45.49
PCM/UAHF/MPW1K/6-31+G(d)	ΔG (kJ/mol)	0.00	2.71	5.45	3.85	10.75

	r(Si-N) (pm)	183.4	183.3	184.0	184.0	185.0
	q(OTf)	-0.98	-0.98	-0.98	-0.98	-0.99
	NMR (ppm)	35.10	33.29	36.08	35.48	38.23
MPW1K-D2/6-31+G(d)	ΔG (kJ/mol)	0.00	4.96	4.95	31.04	62.69
	r(Si-N) (pm)	182.2	181.7	181.7	183.0	209.5
	q(OTf)	-0.94	-0.95	-0.95	-0.94	-0.79
	NMR (ppm)	34.43	29.68	29.70	35.33	-35.03



MPW1K/IGLO-III//MPW1K/6-31+G(d)

gas	ΔG _{gas} kJ/mol	NMR MPW1K/IGLO-III in gas phase	Boltzmann weighted factor	δ _{gas}
19_1	0.00	39.24	0.51	19.88
19_2	0.67	37.63	0.39	14.53
19_3	4.01	37.64	0.10	3.78
19_4	11.81	39.77	0.00	0.17
19_5	13.35	33.49	0.00	0.08
19_6	52.89	53.36	0.00	0.00
SUM			1.00	38.44

PCM/UAHF/MPW1K/IGLO-III//MPW1K/6-31+G(d)

sp	ΔG ^{SP} _{CDCl3} kJ/mol	NMR UAHF-MPW1K/IGLO-III	Boltzmann weighted factor	δ ^{SP} _{CDCl3}
19_1	15.54	38.41	0.00	0.06
19_2	0.00	36.90	0.77	28.49
19_3	3.13	36.89	0.22	8.07
19_4	13.20	38.33	0.00	0.14
19_5	13.47	34.21	0.00	0.12
19_6	18.23	48.90	0.00	0.02
SUM			1.00	36.90

PCM/UAHF/MPW1K/IGLO-III// PCM/UAHF/MPW1K/6-31+G(d)

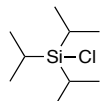
opt	ΔG ^{opt} _{CDCl3} kJ/mol	NMR UAHF-MPW1K/IGLO-III	Boltzmann weighted factor	δ ^{opt} _{CDCl3}
19_1	4.31	37.61	0.07	2.61
19_2	0.00	37.72	0.39	14.88
19_3	0.29	37.59	0.35	13.20
19_4	5.10	38.13	0.05	1.93
19_5	2.69	36.25	0.13	4.83
19_6	14.51	41.64	0.00	0.05
SUM				37.50

DF-LMP2/IGLO-III//MPW1K/6-31+G(d)

gas	ΔG _{gas} kJ/mol	NMR DF-LMP2/IGLO-III in gas phase	Boltzmann weighted factor	δ _{gas}
19_1	0.00	0.00	0.51	19.67
19_2	0.67	0.67	0.39	14.65
19_3	4.01	4.01	0.10	3.81
19_4	11.81	11.81	0.00	0.17
19_5	13.35	13.35	0.00	0.08
19_6	52.89	52.89	0.00	0.00
SUM			1.00	38.39

HCTH407/IGLO-III//MPW1K/6-31+G(d)

gas	ΔG _{gas} kJ/mol	NMR HCTH407/IGLO-III in gas phase	Boltzmann weighted factor	δ _{gas}
19_1	0.00	36.70	0.51	18.59
19_2	0.67	34.17	0.39	13.20
19_3	4.01	34.24	0.10	3.44
19_4	11.81	37.31	0.00	0.16
19_5	13.35	30.55	0.00	0.07
19_6	52.89	50.17	0.00	0.00
SUM				35.46



MPW1K/IGLO-III//MPW1K/6-31+G(d)

gas	ΔG_{gas} kJ/mol	NMR MPW1K/IGLO-III in gas phase	Boltzmann weighted factor	δ^{gas}
20_1	0.00	36.51	0.59	21.58
20_2	1.77	37.96	0.29	11.00
20_3	5.86	35.13	0.06	1.96
20_4	7.42	36.47	0.03	1.08
20_5	8.41	36.20	0.02	0.72
20_6	10.26	33.07	0.01	0.31
20_7	12.09	36.30	0.00	0.16
SUM			1.00	36.81

PCM/UAHF/MPW1K/IGLO-III//MPW1K/6-31+G(d)

sp	$\Delta G^{\text{sp}}_{\text{CDCl}_3}$ kJ/mol	NMR UAHF-MPW1K/IGLO-III	Boltzmann weighted factor	$\delta^{\text{sp}}_{\text{CDCl}_3}$
20_1	0.00	38.38	0.61	23.54
20_2	2.15	39.78	0.26	10.27
20_3	5.35	37.38	0.07	2.65
20_4	7.72	38.13	0.03	1.04
20_5	8.87	37.89	0.02	0.65
20_6	10.26	35.14	0.01	0.34
20_7	12.80	38.24	0.00	0.13
SUM			1.00	38.63

PCM/UAHF/MPW1K/IGLO-III// PCM/UAHF/MPW1K/6-31+G(d)

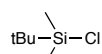
opt	$\Delta G^{\text{opt}}_{\text{CDCl}_3}$ kJ/mol	NMR UAHF-MPW1K/IGLO-III	Boltzmann weighted factor	$\delta^{\text{opt}}_{\text{CDCl}_3}$
20_1	6.98	40.30	0.05	1.87
20_2	0.00	41.71	0.78	32.42
20_3	5.77	39.99	0.08	3.03
20_4	7.01	40.31	0.05	1.85
20_5	7.93	39.78	0.03	1.26
20_6	9.44	37.26	0.02	0.64
20_7	12.29	40.17	0.01	0.22
SUM			1.00	41.30

DF-LMP2/IGLO-III//MPW1K/6-31+G(d)

gas	ΔG_{gas} kJ/mol	NMR DF-LMP2/IGLO-III in gas phase	Boltzmann weighted factor	δ^{gas}
20_1	0.00	34.82	0.59	20.58
20_2	1.77	36.43	0.29	10.56
20_3	5.86	33.56	0.06	1.87
20_4	7.42	35.31	0.03	1.04
20_5	8.41	35.08	0.02	0.70
20_6	10.26	31.92	0.01	0.30
20_7	12.09	34.64	0.00	0.16
SUM			1.00	35.21

HCTH407/IGLO-III//MPW1K/6-31+G(d)

gas	ΔG_{gas} kJ/mol	NMR HCTH407/IGLO-III in gas phase	Boltzmann weighted factor	δ^{gas}
20_1	0.00	34.86	0.59	20.61
20_2	1.77	36.64	0.29	10.62
20_3	5.86	33.35	0.06	1.86
20_4	7.42	35.18	0.03	1.04
20_5	8.41	35.29	0.02	0.70
20_6	10.26	31.64	0.01	0.30
20_7	12.09	36.11	0.00	0.16
SUM			1.00	35.28



MPW1K/IGLO-III//MPW1K/6-31+G(d)

21	δ^{gas}
Gas	37.78

PCM/UAHF/MPW1K/IGLO-III//MPW1K/6-31+G(d)

21	$\delta^{\text{sp}}_{\text{CDCl}_3}$
sp	39.62

PCM/UAHF/MPW1K/IGLO-III// PCM/UAHF/MPW1K/6-31+G(d)

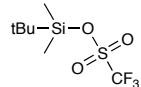
21	$\delta^{\text{opt}}_{\text{CDCl}_3}$
Opt	41.98

DF-LMP2/IGLO-III//MPW1K/6-31+G(d)

21	δ^{gas}
Gas	34.97

HCTH407/IGLO-III//MPW1K/6-31+G(d)

21	δ_{gas}
Gas	36.71



MPW1K/IGLO-III//MPW1K/6-31+G(d)

gas	ΔG_{gas} kJ/mol	NMR MPW1K/IGLO-III in gas phase	Boltzmann weighted factor	δ_{gas}
22_1	0.00	44.47	0.51	22.47
22_2	0.05	44.54	0.49	22.03
SUM			1.00	44.50

PCM/UAHF/MPW1K/IGLO-III//MPW1K/6-31+G(d)

sp	$\Delta G^{\text{sp}}_{\text{CDCl}_3}$ kJ/mol	NMR UAHF-MPW1K/IGLO-III	Boltzmann weighted factor	$\delta^{\text{sp}}_{\text{CDCl}_3}$
22_1	0.00	47.05	0.51	23.77
22_2	0.05	47.05	0.49	23.28
SUM			1.00	47.05

PCM/UAHF/MPW1K/IGLO-III// PCM/UAHF/MPW1K/6-31+G(d)

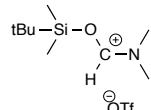
opt	$\Delta G^{\text{opt}}_{\text{CDCl}_3}$ kJ/mol	NMR UAHF-MPW1K/IGLO-III	Boltzmann weighted factor	$\delta^{\text{opt}}_{\text{CDCl}_3}$
22_1	0.01	51.66	0.50	26.05
22_2	0.00	51.66	0.51	26.10
SUM			1.01	52.15

DF-LMP2/IGLO-III//MPW1K/6-31+G(d)

	ΔG_{gas} kJ/mol	NMR DF-LMP2/IGLO-III in gas phase	Boltzmann weighted factor	δ_{gas}
22_1	0.00	42.43	0.51	21.44
22_2	0.05	42.50	0.49	21.02
SUM			1.00	42.46

HCTH407/IGLO-III//MPW1K/6-31+G(d)

	ΔG_{gas} kJ/mol	NMR HCTH407/IGLO-III in gas phase	Boltzmann weighted factor	δ_{gas}
22_1	0.00	40.01	0.51	20.22
22_2	0.05	40.07	0.49	19.82
SUM			1.00	40.04



MPW1K/IGLO-III//MPW1K/6-31+G(d)

gas	ΔG_{gas} kJ/mol	NMR MPW1K/IGLO-III in gas phase	Boltzmann weighted factor	δ_{gas}
23_1	0.00	51.64	0.50	25.89
23_2	3.06	51.91	0.15	7.59
23_3	3.17	50.36	0.14	7.02
23_4	3.20	50.37	0.14	6.94
23_5	6.08	55.15	0.04	2.38
23_6	7.35	49.94	0.03	1.29
23_7	11.69	47.72	0.00	0.21
23_8	13.95	46.82	0.00	0.08
SUM			1.00	51.41

PCM/UAHF/MPW1K/IGLO-III//MPW1K/6-31+G(d)

sp	$\Delta G^{\text{sp}}_{\text{CDCl}_3}$ kJ/mol	NMR UAHF-MPW1K/IGLO-III	Boltzmann weighted factor	$\delta^{\text{sp}}_{\text{CDCl}_3}$
23_1	0.00	50.21	0.38	19.00
23_2	4.19	50.09	0.07	3.50
23_3	2.21	49.38	0.16	7.68
23_4	2.24	49.38	0.15	7.58
23_5	1.42	52.77	0.21	11.28
23_6	7.35	48.80	0.02	0.95
23_7	11.31	47.37	0.00	0.19
23_8	10.38	46.63	0.01	0.27
SUM			1.00	50.43

PCM/UAHF/MPW1K/IGLO-III// PCM/UAHF/MPW1K/6-31+G(d)

opt	$\Delta G^{\text{opt}}_{\text{CDCl}_3}$ kJ/mol	NMR UAHF-MPW1K/IGLO-III	Boltzmann weighted factor	$\delta^{\text{opt}}_{\text{CDCl}_3}$
23_1	1.22	50.08	0.17	8.65
23_2	5.36	49.98	0.03	1.63
23_3	0.00	49.50	0.28	13.97
23_4	0.07	49.52	0.27	13.58

23_5	1.50	50.88	0.15	7.82
23_6	8.37	49.21	0.01	0.47
23_7	5.81	48.39	0.03	1.31
23_8	4.40	47.85	0.05	2.29
SUM			1.00	49.72

DF-LMP2/IGLO-III//MPW1K/6-31+G(d)

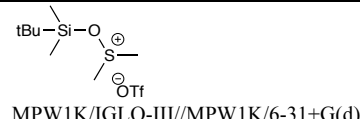
gas	ΔG_{gas} kJ/mol	NMR DF-LMP2/IGLO-III in gas phase	Boltzmann weighted factor	δ_{gas}
23_1	0.00	49.41	0.50	24.77
23_2	3.06	49.92	0.15	7.29
23_3	3.17	48.41	0.14	6.75
23_4	3.20	48.41	0.14	6.67
23_5	6.08	52.68	0.04	2.27
23_6	7.35	48.17	0.03	1.25
23_7	11.69	45.40	0.00	0.20
23_8	13.95	44.74	0.00	0.08
SUM			1.00	49.29

HCTH407/IGLO-III//MPW1K/6-31+G(d)

gas	ΔG_{gas} kJ/mol	NMR HCTH407/IGLO-III in gas phase	Boltzmann weighted factor	δ_{gas}
23_1	0.00	48.35	0.50	24.24
23_2	3.06	48.41	0.15	7.07
23_3	3.17	46.65	0.14	6.51
23_4	3.20	46.65	0.14	6.42
23_5	6.08	52.25	0.04	2.26
23_6	7.35	46.16	0.03	1.19
23_7	11.69	44.36	0.00	0.20
23_8	13.95	43.36	0.00	0.08
SUM			1.00	47.98

Parameters of individual conformers of **23**

		23_1	23_2	23_3	23_4	23_5	23_6	23_7	23_8
MPW1K/6-31+G(d)	ΔG (kJ/mol)	0.00	3.06	3.17	3.20	6.08	7.35	11.69	13.95
	r(Si-O) (pm)	175.4	175.5	175.2	175.2	176.7	175.5	175.0	174.9
	q(OTf)	-0.92	-0.92	-0.93	-0.93	-0.92	-0.92	-0.93	-0.94
	NMR (ppm)	51.64	51.91	50.36	50.37	55.15	49.94	47.72	46.82
MPW1K/6-31+G(d)+sp	ΔG (kJ/mol)	0.00	4.19	2.21	2.24	1.42	7.35	11.31	10.38
	r(Si-O) (pm)	175.4	175.5	175.2	175.2	176.7	175.5	175.0	174.9
	q(OTf)	-0.94	-0.93	-0.94	-0.94	-0.94	-0.94	-0.94	-0.95
	NMR (ppm)	50.21	50.09	49.38	49.38	52.77	48.8	47.37	46.63
PCM/UAHF/MPW1K/6-31+G(d)	ΔG (kJ/mol)	1.22	5.36	0.00	0.07	1.50	8.37	5.81	4.4
	r(Si-O) (pm)	175.2	175.1	175.0	175.0	175.9	175.2	175.2	175.1
	q(OTf)	-0.97	-0.97	-0.97	-0.97	-0.96	-0.97	-0.98	-0.98
	NMR (ppm)	50.08	49.98	49.50	49.52	50.88	49.21	48.39	47.85
MPW1K-D2/6-31+G(d)	ΔG (kJ/mol)	0.00	4.63	3.89	3.90	4.68	7.49	13.38	12.04
	r(Si-O) (pm)	174.9	174.9	175.0	175.0	174.9	174.9	174.5	174.6
	q(OTf)	-0.91	-0.90	-0.93	-0.93	-0.90	-0.92	-0.91	-0.92
	NMR (ppm)	51.34	51.02	51.09	51.12	51.01	50.11	48.43	49.65



gas	ΔG_{gas} kJ/mol	NMR MPW1K/IGLO-III in gas phase	Boltzmann weighted factor	δ_{gas}
24_1	0.00	43.85	0.55	24.19
24_2	2.50	42.34	0.20	8.52
24_3	3.51	42.94	0.13	5.75
24_4	5.18	42.37	0.07	2.89
24_5	6.57	43.57	0.04	1.69
24_6	11.19	41.59	0.01	0.25
24_7	32.77	53.49	0.00	0.00
SUM			1.00	43.30

PCM/UAHF/MPW1K/IGLO-III//MPW1K/6-31+G(d)

sp	$\Delta G_{\text{CDCl}_3}^{\text{sp}}$ kJ/mol	NMR UAHF-MPW1K/IGLO-III	Boltzmann weighted factor	$\delta_{\text{CDCl}_3}^{\text{sp}}$
24_1	0.00	44.66	0.55	24.48
24_2	2.29	43.74	0.22	9.52
24_3	3.76	43.88	0.12	5.28
24_4	6.19	43.62	0.05	1.97
24_5	6.57	44.48	0.04	1.72
24_6	7.20	43.76	0.03	1.31
24_7	25.96	53.62	0.00	0.00
SUM			1.00	44.28

PCM/UAHF/MPW1K/IGLO-III// PCM/UAHF/MPW1K/6-31+G(d)

opt	$\Delta G_{\text{CDCl}_3}^{\text{opt}}$ kJ/mol	NMR UAHF-MPW1K/IGLO-III	Boltzmann weighted factor	$\delta_{\text{CDCl}_3}^{\text{opt}}$
24_1	0.00	49.41	0.79	38.98
24_2	5.09	50.22	0.10	5.08
24_3	8.74	49.81	0.02	1.15
24_4	8.87	49.48	0.02	1.09
24_5	8.20	50.41	0.03	1.46
24_6	7.68	49.74	0.04	1.77
24_7	19.85	54.43	0.00	0.01
SUM			1.00	49.54

DF-LMP2/IGLO-III//MPW1K/6-31+G(d)

	ΔG_{gas} kJ/mol	NMR DF-LMP2/IGLO-III in gas phase	Boltzmann weighted factor	δ_{gas}
24_1	0.00	42.69	0.55	23.55
24_2	2.50	41.93	0.20	8.44
24_3	3.51	42.81	0.13	5.74
24_4	5.18	41.85	0.07	2.86
24_5	6.57	43.28	0.04	1.68
24_6	11.19	41.09	0.01	0.25
24_7	32.77	52.10	0.00	0.00
SUM			1.00	42.51

HCTH407/IGLO-III//MPW1K/6-31+G(d)

gas	ΔG_{gas} kJ/mol	NMR HCTH407/IGLO-III in gas phase	Boltzmann weighted factor	δ_{gas}
24_1	0.00	40.44	0.55	22.31
24_2	2.50	39.04	0.20	7.86
24_3	3.51	39.33	0.13	5.27
24_4	5.18	39.07	0.07	2.67
24_5	6.57	40.13	0.04	1.56
24_6	11.19	38.73	0.01	0.23
24_7	32.77	51.73	0.00	0.00
SUM			1.00	39.89

Parameters of individual conformer 24.

		24_1	24_2	24_3	24_4	24_5	24_6	24_7
MPW1K/6-31+G(d)	ΔG (kJ/mol)	0.00	2.50	3.51	5.18	6.57	11.19	32.77
	r(Si-O) (pm)	173.5	173.2	173.3	173.1	173.6	172.7	175.0
	q(OTf)	-0.91	-0.91	-0.90	-0.90	-0.91	-0.89	-0.93
	NMR (ppm)	43.85	42.34	42.94	42.37	43.57	41.59	53.49
MPW1K/6-31+G(d)+sp	ΔG (kJ/mol)	0.00	2.29	3.76	6.19	6.57	7.2	25.96
	r(Si-O) (pm)	173.5	173.2	173.3	173.1	173.6	172.7	175.0
	q(OTf)	-0.93	-0.92	-0.92	-0.92	-0.93	-0.91	-0.94
	NMR (ppm)	44.66	43.74	43.88	43.62	44.48	43.76	53.62
PCM/UAHF/MPW1K/6-31+G(d)	ΔG (kJ/mol)	0.00	5.09	8.74	8.87	8.20	7.68	19.85
	r(Si-O) (pm)	174.9	175.0	174.8	174.8	175.0	174.9	175.5
	q(OTf)	-0.96	-0.96	-0.96	-0.96	-0.96	-0.96	-0.97
	NMR (ppm)	49.41	50.22	49.81	49.48	50.41	49.74	54.43
MPW1K-D2/6-31+G(d)	ΔG (kJ/mol)	4.24	7.63	3.53	0.00	4.24	13.61	29.15
	r(Si-O) (pm)	173.1	172.6	173.0	172.8	173.2	172.0	174.5
	q(OTf)	-0.91	-0.90	-0.90	-0.90	-0.91	-0.89	-0.93
	NMR (ppm)	43.17	43.26	42.72	42.85	42.67	41.42	53.52

Curriculum Vitae

Name: Cong Zhang

Date of birth: 31st, May, 1984

Place of birth: Xuchang, P. R. China

Nationality: Chinese

Marital status: Unmarried

Working Experience

LMU Munich	2010–Present, System administrator for HPC Cluster, LMU Administering LINUX based high performance computing (HPC) cluster in the research group of Prof. Dr. H. Zipse. Installation of scientific softwares.
LMU Munich	2013, Teaching Assistant (T.A.) LMU

Education

Ph. D. Candidate 2010–2014.09, Ludwig Maximilian University, Munich
Department of Chemistry, Adviser: Prof. Hendrik Zipse.

Masters of Science 2007–2010, Zheng Zhou University, Henan
Department of Chemistry, Adviser: Prof. MingSheng Tang

Bachelor of Science 2003-2007, Zheng Zhou University, Henan
Department of Chemistry, Adviser: Prof. MingSheng Tang

Skills

Shell-scripting, Unix systems, Scientific softwares (Gaussian, Molpro, ORCA, Schrödinger Suite), LATEX, C++(BASIC)

List of Publications

- 1 C. Zhang, P. Patschinski, D. S. Stephenson, R. Panisch, J. Wender, M. Holthausen and H. Zipse “The Calculation of ²⁹Si NMR Chemical Shifts of Tetracoordinated Silicon Compounds in the Gas Phase and in Solution” *Phys. Chem. Chem. Phys.* 2014, **16**, 16642–16650.
- 2 P. Patschinski, C. Zhang and H. Zipse “The Lewis Base-Catalyzed Silylation of Alcohols — A Mechanistic Analysis”, *J. Org. Chem. ASAP*, DOI: 10.1021/jo5016568.
- 3 S. Seel, T. Thaler, K. Takatsu, C. Zhang, H. Zipse, B. F. Straub, P. Mayer, P. Knochel, “Highly Diastereoselective Arylations of Substituted Piperidines”. *J. Am. Chem. Soc.* 2011, **133**, 4774 – 4777.
- 4 D. H. Wei, Y. Y. Zhu, C. Zhang, and M. S. Tang. “A DFT Study on Enantioselective Synthesis of Aza-β-lactams via NHC-catalyzed [2 + 6] Cycloaddition of Ketenes with Diazenedicarboxylates”. *J. Mol. Catal. A: Chem.* 2011, **334**, 108–115.

- 5 C. Zhang, Y. Y. Zhu, D. H. Wei, and M. S. Tang. “Theoretical Study on the Reaction Mechanism between 6-Benzyl-6-azabicyclo[2.2.1]hept-2-ene and Benzoyl Isocyanate to Urea and Isourea”. *J. Phys. Chem. A* 2010, **114**, 2913–2919.